SVENSKA GEOFYSISKA FÖRENINGEN

VOLUME 5, NUMBER 4 **Tellus** NOVEMBER 1953

A QUARTESLY JOURNAL OF GEOPHYSICS

Identification of Sunspots

By H. ALFVÉN, Royal Institute of Technology, Stockholm

(Manuscript received June 6, 1953)

Abstract

According to the magneto-hydrodynamic theory of sunspots there should be a correlation between the spots on one hemisphere during a certain cycle and spots on the opposite hemisphere during the following cycle. This has been statistically confirmed by Galvenius and Wold, and by Whittle. It is pointed out that *individual* sunspot groups may be reproduced at the opposite hemisphere during the following cycle. An analysis of the sunspots between $-4°$ and $+4°$ seems to support this conclusion, and a number of sunspots are "identified" as being produced by the same original disturbance in the solar core.

1. Magneto-hydrodynamic theory of sunspots

In the magneto-hydrodynamic theory of sunspots a rather complicated mechanism must be postulated by which the sunspot producing whirl-rings should originate in the solar core[1]. The relatively small latitude displacement of sunspots shows that the plane of the rings must be parallel to the magnetic field. The difference in magnetic polarity between the northern and the southern hemispheres indicates that the spots occurring during a certain cycle at the northern hemisphere cannot have originated at the same time as the spots of the southern hemisphere during the same cycle. This leads to the conclusion that the magnetic lines of force must pass *two* activity regions in the solar core, one to the north and one to the south of the equatorial plane (cf. Fig. 1). The production of a disturbance e.g. in the northern region gives rise to magneto-hydrodynamic waves which about 40 years later appear on the surface of the northern hemisphere and produce sunspots. The same disturbance, however, also proceeds southwards and passes the southern activity region, where it becomes amplified, and finally reaches the surface of the southern hemisphere where it produces sunspots. These spots appear about 11 years after the spots due to the same original disturbance have appeared at the northern hemisphere.

2. Statistical confirmation

Although a mechanism of about this kind seems to be an inevitable consequence of the magneto-hydrodynamic theory, it is obvious that such a complicated mechanism could not be accepted without very strong empirical confirmation. The first direct support of the theory was obtained by an analysis of the latitude distribution of sunspots on the northern hemisphere, compared with the corre-

[1] Alfvén (1948). Summarized in Cosmical Electrodynamics, Oxford 1950. Other theories of sunspots have recently been proposed by Walén and Schwartzschild. Waléns earlier papers (Ark. f. mat., astr. o. fysik 30 A, No 15; 31 B No 3 1944) are reviewed in Cosmical Electrodynamics. The later development of his ideas, with which the present author is not in agreement, are published in Ark. f. mat., astr. o. fysik 33 A No 18, 1946, and On the vibratory rotation of the sun, Lindståhls, Stockholm 1949. Schwarzschild's contribution was presented at the Solar physics conference in Florence 1952.

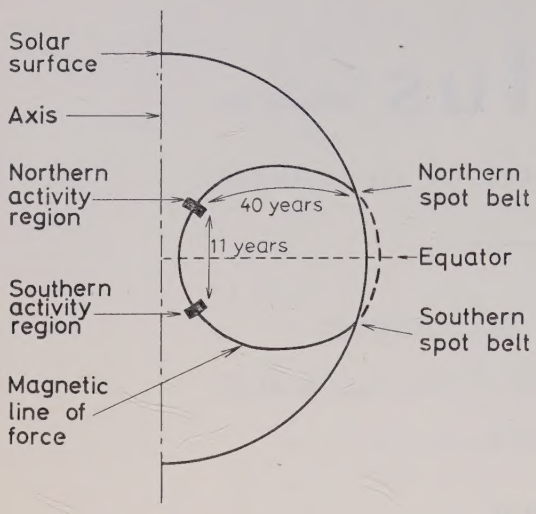

Fig. 1. Magnetic field within the sun. Meridional projection.

sponding distribution of the southern hemisphere 11 years later (ALFVÉN, 1948). According to the theory these patterns should be similar because the sunspots of one hemisphere have the same origin as sunspots of the other hemisphere 11 years later. A statistical investigation by GALVENIUS and WOLD (1948) showed that the similarity of the patterns was statistically significant.

Next confirmation was obtained by WHITTLE (1954) who investigated the correlation between the time series of spots in the latitude belts 16°—20° at the northern and at the southern hemisphere. He was able to demonstrate in a very convincing way that there exists a correlation between the two hemispheres of the kind required by the theory.

3. Possible methods for spot correlation

The statistical correlation between the two hemispheres which consequently has been demonstrated in two independent ways, gives a strong support to the general lines of the magneto-hydrodynamic theory. There could no longer be any doubt that the spot activity on one hemisphere is coupled with the activity on the other hemisphere during next cycle. So far it has only been demonstrated that there is a statistical connection and this may be due to some factor which in a general way regulates the activity. It is also possible, however, that there is a much more direct connection between the spots of the opposite hemispheres. The most extreme case would be that *each individual spot on one hemisphere is directly connected with a certain spot on the other hemisphere one cycle later.* The purpose of the present paper is to investigate whether such a connection exists. The work was started as soon as WHITTLE had got his positive results and inspired by this.

Suppose that a disturbance in e.g. the northern activity region of the solar core produces a whirl ring. This moves out along the magnetic lines of force to the surface and appears as a spot A_N in the northern hemisphere. The same disturbance also produces a wave which moves through the core, passes the southern activity region, where it may be in part amplified and in part reflected, and finally reaches the surface and produces a spot A_S on the southern hemisphere one cycle later. The problem is: how could we identify the spots A_N and A_S as being caused by the same original disturbance. There are two different possibilities:

1. Identification by position. The two spots should occur at the two intersections with the solar surface of the same magnetic line of force with a time difference corresponding to the time of travel through the core (which is of the order 11 years). If we could find that point of the southern hemisphere which is interconnected by a line of force through the interior with a certain point of the northern hemisphere we could study whether spots at these two points preferably occur with a certain time interval (of the order 11 years).

2. Identification by structure. The two spots which originate from the same disturbance in the solar core may have some similarity in structure. For example, their size, life time, or proper motion, may be correlated in some way.

4. Regularity of solar magnetic field

The identification by position would be easy if we knew the shape of the magnetic field inside the sun. This is not the case: We could, however, make a reasonable guess about it under the condition that it is rather regular. On the other hand if the solar field is very irregular, we have little hope to succeed. The first question to discuss is whether we should

expect the field in the sun's interior to be regular or not.

At first sight there seems to be an overwhelming probability that the solar field is very irregular. Zeeman effect measurements of the surface field indicate an irregular structure and strong variations from one day to next. (Whether Zeeman effect measurements of weak fields are reliable at all is still an open question (ALFVÉN, 1951). Further the structure of the corona, which probably is governed to a considerable extent by the magnetic field, indicates a variable and irregular structure. These arguments are not decisive, however, because what is important is the regularities of the "general" field in which the magneto-hydrodynamic waves proceed. This could be thought of as the time average of the actual field. It is superimposed by a variable field which the waves carry with them. Hence the irregularities and rapid changes of the actual magnetic field are quite consistent with a regular general magnetic field.

Further, the magnetic lines of force pass at least two layers, which according to current solar models should be turbulent, *viz.* in the core and in the photosphere. This seems to exclude the possibility of a regular field. Again it must be observed that the field of interest is the time average. A turbulence should be described as a series of waves travelling in the general field, but it does not contradict the assumption of a regular general field.

Having thus found that there is no decisive argument *against* a regular field we shall now examine the arguments in favour of it. According to Ferraro's theorem all parts of a certain line of force must in average rotate with equal angular velocity. As the sun has a non-uniform rotation it is likely that this brings with it that the rotational axis and the magnetic axis must coincide (although this has not been rigidly proved). If the solar magnetic field is of Cowling's decaying type it is quite reasonable that it is very regular because at the decay all irregularities should disappear rapidly. LUNDQUIST has discussed the shape of "magneto-hydrostatic fields" which can exist in a liquid medium without producing a hydrodynamic motion (LUNDQUIST, 1951). Such fields are in general "twisted". If the sun's general field is of this type it is quite reasonable that it should be regular but "twisted", i. e.

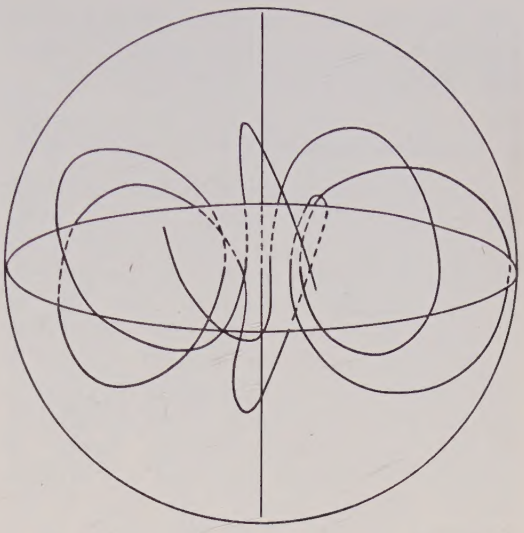

Fig. 2. Twisted magnetic field.

the field has a longitudinal component, so that a magnetic line of force intersects the surface at two points which do not have the same longitude. In fact, there is no reason to suppose that the longitude difference between the northern and the southern intersections with the solar surface should be zero. It is important to observe that Fig. 1 shows only the *projection* of a line of force on the meridional plane. The real shape is obtained if we rotate this plane around the axis when we proceed along the line of force. The spiral structure of a line of force is shown in Fig. 2.

Cowling has shown that a general magnetic field cannot be sustained if it is regular and symmetrical. The models by ELSASSER (1946, 1947), BULLARD (1949), and others are rather complicated and irregular. A regular field which does not decay systematically (counted over very long periods) is compatible with a model proposed some time ago, which assumes a decaying field, at intervals reinforced by a "convulsion" (ALFVÉN, 1950).

The irregularities and disturbances of the general field according to the mentioned models need not necessarily affect the lines of force which intersect the solar surface. They can very well be confined to the lines of force which altogether are hidden in the sun's interior.

Hence theoretical considerations rather sup-

port the view that the general field may be regular and symmetrical but possibly twisted. The conclusions are not decisive, however.

5. Empirical arguments for a regular field

There are quite a few empirical arguments for a regular field. During a certain cycle bipolar sunspots have a certain polarity at the northern hemisphere and the opposite polarity at the southern hemisphere. The line of division is the equator. Only very seldom does a spot of the "northern" polarity proceed as much as one degree to the south of the equator, and vice versa(WALDMEIER). Even independent of the magneto-hydrodynamic theory of sunspots this indicates that there is a division line in magnetic respect very close to the rotational equator. With this theory as a background we must suppose that waves with a certain polarity reach the northern hemisphere exactly down to the equator, and that waves of opposite polarity reach the southern hemisphere. Hence the magnetic equator must almost coincide with the rotational equator.

A second argument is obtained from the sunspot progression curve. According to the theory this curve should be given purely by the geometry of the field (Cosm. El. p. 118). The fact that the progression curve is very well reproduced during all the sunspot cycles, which have been studied, speaks in favour of a regular magnetic field.

Our third—and most important—argument is derived from the correlation between the spottedness pattern of the two hemispheres. An excess of sunspots at a certain latitude of one hemisphere is connected with a corresponding excess at the same latitude of the opposite hemisphere during next cycle. Judging from Fig. 5.16 in Cosmical Electrodynamics there is an agreement between the corresponding latitudes within a few degrees. This can only be interpreted in such a way that magnetic lines of force intersecting one hemisphere at a certain latitude, appear at the other hemisphere at the same latitude.

The accuracy can also be judged from the fact that if the spottednes is plotted as a function of the latitude with latitude intervals of 2°, the correlation is poor, but if the curves are smoothed with the weight 1:3:5:3:1 a good correlation is obtained. This indicates that the accuracy by which a certain latitude is connected with the corresponding latitude of the other hemisphere is a few degrees.

A further confirmation of the regularity of the solar field is given by WHITTLE's analysis. The fact that the time series of 16°—20° north is correlated with the series of 16°—20° south shows that lines of force must connect these belts in a regular way.

The first ZEEMAN effect measurements of the general magnetic field indicated an angle of 5° between the magnetic and rotational axes. It is now generally agreed that the accuracy was insufficient to establish this, and there is no later confirmation. ABETTI has made an interesting study of the shape of the magnetic field near the poles as found from the structure of the corona (ABETTI, 1952). The difference between the magnetic pole and the heliographic pole which he finds refers to the instant structure of the field and not to the time average, which is what we discuss.

6. Identification by position

Our survey has shown that it is likely that magnetic lines of force of the general field intersect the two hemispheres at the same latitudes. Hence one of the necessary conditions for a sunspot identification by position is given. On the other hand we do not know the difference in longitude between the two "ends" of a line of force, so we must introduce this quantity as an unknown parameter. It should be kept in mind that the period of the solar rotation is not very well known. Further the rotation is non-uniform. Hence it is difficult to keep account of the longitudes.

We must now ascertain how an attempt to identify sunspots should be made in order to have some chance of success.

The regularity of the magnetic field is probably best near the equator. This is indicated by the fact that the equator strictly separates spots of different polarities(WALDMEIER). The pattern analysis discussed above (ALFVÉN, 1948) which refers to latitudes in the range 10°—30° does not give a higher accuracy than a few degrees for the correspondence in latitude.

The non-uniform rotation introduces a difficulty into the analysis. Suppose that a disturbance travels along a line of force which intersects the solar surface at latitude φ and

another disturbance travels along a line of force through $\varphi + \triangle\varphi$. Suppose further that at a certain time the two disturbances have the same longitude. A certain time t later a longitude difference $\triangle\lambda$ will be produced by the non-uniform rotation. Adopting for the rotational velocity ω NEWTON's formula

$$\omega = \omega_0 - \omega' \sin^2 \varphi$$

we find

$$\triangle\lambda = \omega' t \left[\sin^2 (\varphi + \triangle\varphi) - \sin^2 \varphi\right]$$
$$\approx \omega' t \sin 2\varphi \cdot \triangle\varphi$$

Putting $t = 4{,}000$ days and $\omega' = 2.8$ degrees per day we find

$$\triangle\lambda = 195 \sin 2\varphi \cdot \triangle\varphi$$

where $\triangle\varphi$ as well as $\triangle\lambda$ is expressed in degrees. It is unlikely that we can find or even define the latitude of a sunspot group within less than a couple of degrees. Putting $\triangle\varphi = 2°$ we find that $\triangle\lambda \geq 90°$ unless $\varphi < 7°$. This means that for latitudes higher than 7° the uncertainty in longitude becomes more than 90° after one solar cycle. Consequently the possibility of identifying spots by their longitude becomes small unless we confine ourselves to very low latitudes.

There is also a third argument for choosing low latitudes, *viz.* that the number of sunspots is relatively small near the equator. This should make an eventual identification more unambiguous.

7. Construction of spot diagrams for the equatorial belt

Hence we confine the analysis to a small belt near the equator. All spot groups which in Greenwich "General Catalogue of Sunspots" or "Ledgers of groups of sunspots" are listed as having a mean latitude $0 < \varphi < 4°$ or $0 > \varphi > -4°$ are selected. For each cycle and hemisphere a diagram is plotted with the time "First seen" as abscissa and "Mean position of group, longitude" as ordinate. If the "Mean Area, corrected for foreshortening, whole spot" is less than 50 the spot group is represented by a dot. Larger spots are marked by the symbols shown in Fig. 3. The longitude is iterated in order to show the pattern even near 360°. A recurrent spot appears in the diagram as two dots close together.

8. Comparison between the patterns

According to the magneto-hydrodynamic theory of sunspots there is a possibility that the patterns of opposite hemispheres during the two consecutive cycles should be similar. In order to investigate whether this is the case we should compare e.g. the diagram 15 S (for the southern hemisphere during the 15th cycle) with 14 N and 16 N. Further we should compare 15 N with 14 S and 16 S. When comparing the diagrams we do not know *a priori* how the diagrams should be placed in longitude because the solar magnetic field may be twisted around the axis as discussed in § 4. Further it is difficult to keep account of the longitudes especially with regard to the non-uniform rotation. Hence the longitude displacement of two diagrams is arbitrary.

The exact time difference between a spot on one hemisphere and the opposite one is also unknown *a priori*, but it should be of the same order as the sunspot period, say in general between 10 and 12 years.

For the comparison we take the two diagrams (which have been plotted on transparent paper) and place one on the top of the other in such a way that one of the biggest spots of one diagram coincides with one of the biggest spots of the other diagram. If in this position most of the spots coincide the diagrams are judged to be similar.

9. The sequence 13 S—14 N—15 S—16 N—17 S

A comparison between the patterns is most unarbitrary when there are only a few spot-groups, and these form a distinct pattern. This makes it reasonable to start with the diagrams 15 S and 16 N. The biggest spot groups during 15 S occur in 1919 and at the end of 1922. In 16 N there is no big spot group later than 1932. Let us see whether it is possible to identify the spot group of 1932 as being caused by the same disturbance as the spot group of 1922. The difference in time between the two spot groups is about $9^1/_2$ years, the difference in longitude about 50°. If we place the two diagrams 15 S and 16 N on top of each other we find that the medium size spot group in 1921 falls close to the spot group of 1931. A series of spot groups in 1919 and 1920 could very well be of the same origin as a similar series in 1929 and 1930. So far we have only considered large

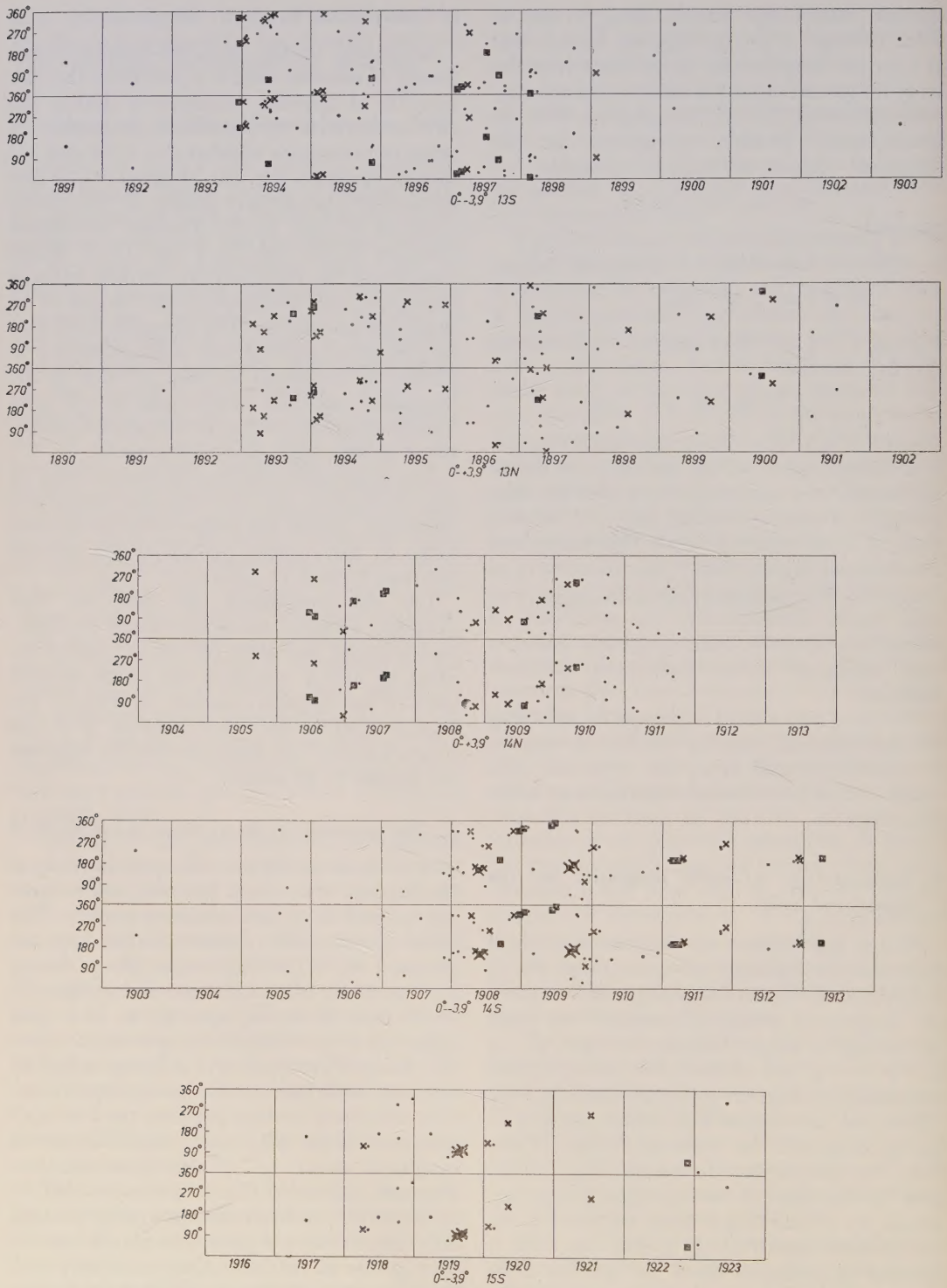

Fig. 3. Spot groups with $[\varphi] < 4°$ during the cycles 13—17 in the northern (N) and southern (S) hemisphere.

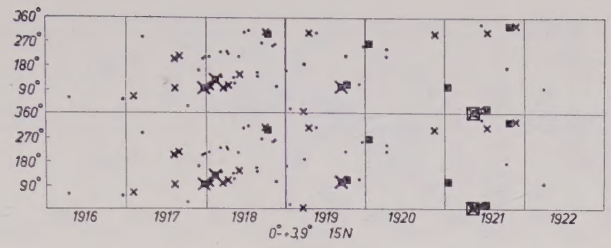

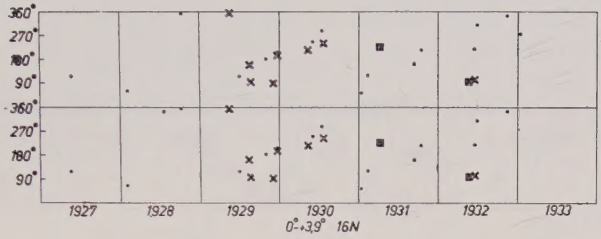

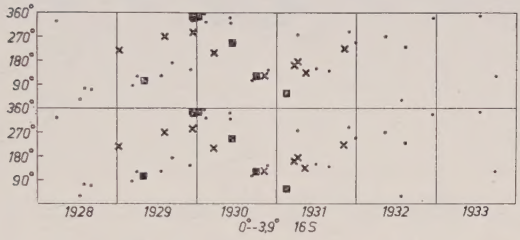

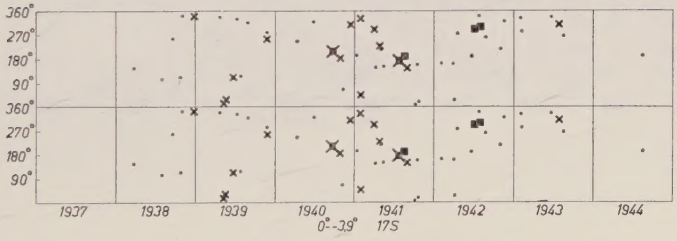

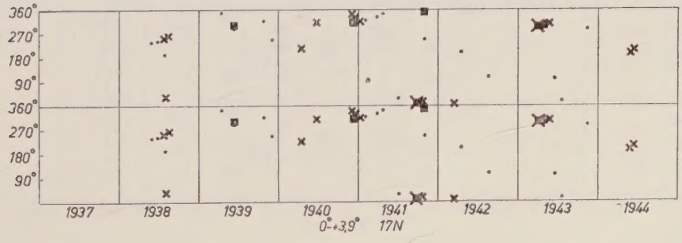

● Area 50. × Area 50—150. ■ Area 150—500. & Area 500—

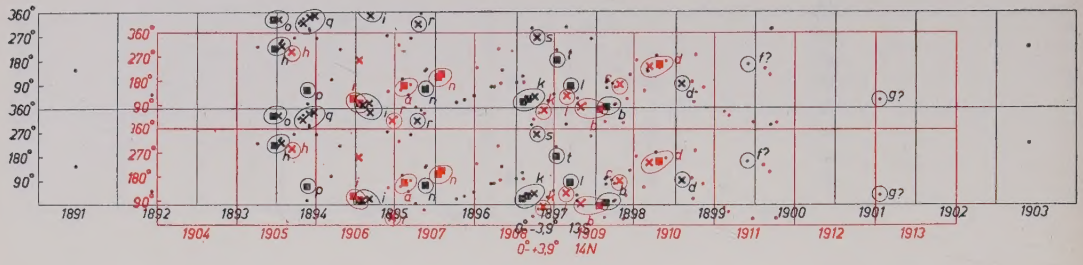

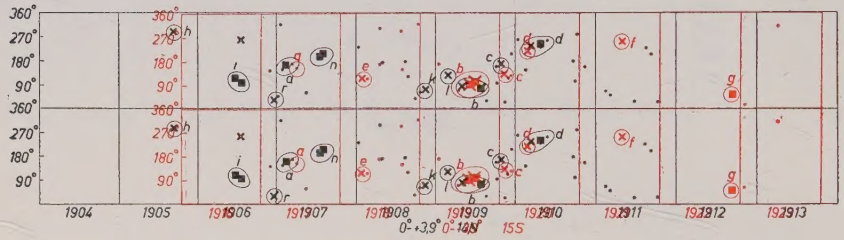

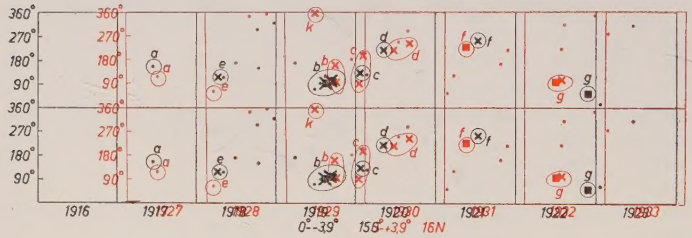

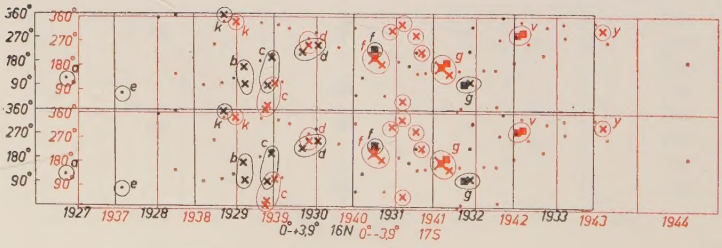

Fig. 4. Comparison between the diagrams of fig. 3. The northern hemisphere is black, the southern hemisphere

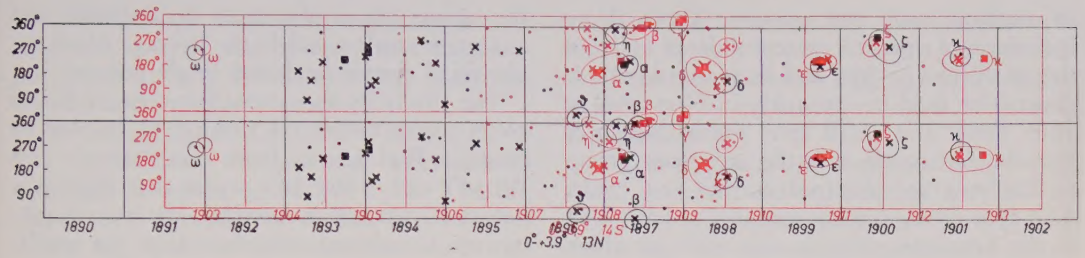

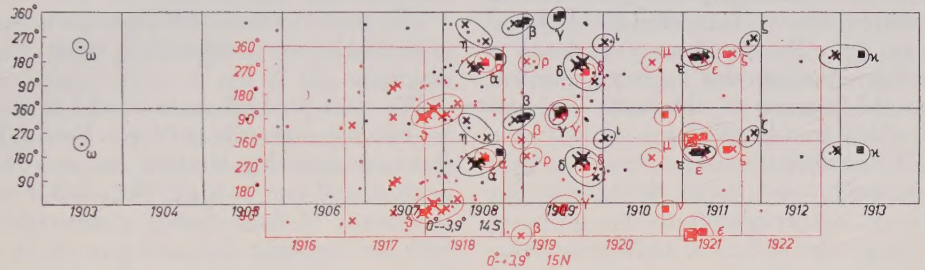

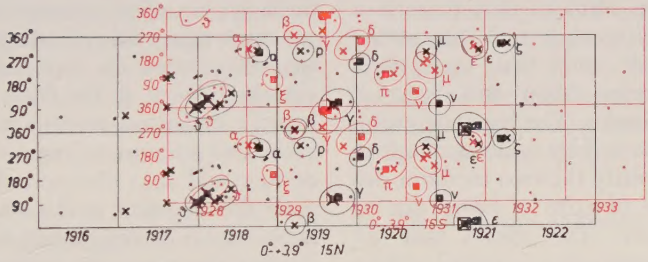

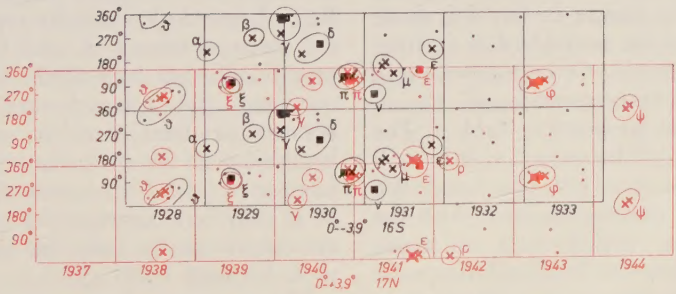

red. The diagrams are placed in the positions indicated by the values of A and T given in Table 2.

or medium size spot groups. There is no indication of a general correspondence between the small spot groups, and these should not in general be used in our analysis. However, in 1917 there is a small spot group which is remarkable because it is the only spot group in that year and it introduces the new cycle. This spot group corresponds in a notable way to the first spot group in the cycle 16 which occurs in 1927. In the same way the first medium size spot group in 15 S, which occurs in the beginning of 1918 corresponds to a small spot group in the beginning of 1928.

The result of the comparison is shown in Fig. 4 where cycle 15 S is marked by black and 16 N by red. The diagrams are placed in such a relative position that the best agreement between the patterns is obtained. The spot groups which are identified are marked by a letter. The identifications a, e, f, and g seem to be unambiguous. In all these cases one group in 15 S corresponds to one group in 16 N. The groups 15 S e and 16 N g are recurrent and as they appear during two consecutive solar rotations they are marked by two dots in the diagram.

The identifications b, c, and d are perhaps more doubtful. It is obvious that there is a general spot activity in 1919 and 1920 at the longitude 100°—250° and that there is a similar activity during 1929 and 1930 at corresponding longitudes. The big spot group in 1919 was accompanied by some small spots. It is tempting to identify the two medium size spots in the middle of 1929 as being due to the same disturbance. This means that we identify what we could call a "cluster" of spot groups with another "cluster" or single group. Such clusters are b, c, and d in 16 N, identified with the cluster b and the spots c and d in 15 S. The group marked k in the middle of 1929 might belong to the cluster b, but it is more likely that it should be considered as a group with no correspondence. Of course we could not expect *all* spots to be reproduced.

The identifications are listed in Table 1. The difference in time $\triangle T$ between a spot in 15 S and its reproduction in 16 N is calculated. We shall call $\triangle T$ the *reproduction time*. Also the longitude difference and latitude difference are given. For clusters the weighted means are used, where the weight of the groups in a cluster is put equal to the spotted surface. In the figures the displacement in longitude and in time is made equal to the average of all the identified cluster (inclusive single groups).

The similarity in pattern between 15 S and 16 N seems to be too striking to be due to chance. We know from GALVENIUS' and WOLD's and WHITTLE's papers that there is a statistical correlation between the two hemispheres. Combined with these facts our results give more support to the general lines of the magneto-hydrodynamic theory. Of course it would be highly desirable to calculate the statistical significance of the similarity between the patterns.

The positive result of this comparison makes it desirable to compare all other pairs of diagrams.

We next proceed to 16 N and 17 S. There are two big clusters in 16 N, *viz.* f and g. In 17 S there are three big clusters, one in 1940, one in 1941, and one in 1942. The relative time of appearance of these clusters agrees rather well with the sequence d, f, and g in 16 N, but if the diagram is placed in such a way that the clusters of 1940 and 1941 coincide with d and f there is a disagreement in longitude of 125° between g and the cluster of 1942. Further there are no other clusters coinciding. Hence we must reject this identification and suppose that the cluster of 1942 (called "v") has no correspondence, in the same way as the group k in 16 N has no correspondence in 15 S.

In next attempt we assume that the clusters of 1940 and 1941 correspond to f and g. If we place the diagrams in this way (Fig. 4) we find in 17 S spots corresponding to k and d in 16 N. Further there are two spots which correspond to the cluster c. As there seems to be no way to obtain a better correspondence between the patterns of 16 N and 17 S we accept these identifications. In 16 N there are five clusters (k, c, d, f, and g) which are reproduced. There are three clusters a, e, and b which are not reproduced, but two of them consist of only one small spot each and were discussed earlier because of their peculiar situation in the beginning of the cycle. In 17 S there is one large spot (v) which is new. (The last spot in 16 N may be a correspondence.) Further there are now some medium size spots (y and five spots between f and g).

The agreement between 16 N and 17 S is not so striking as between 15 S and 16 N. The

identification of 16 N d, f, and g with 17 S f, g, and v could not be altogether ruled out but is definitely less convincing than the identification we have accepted.

As the spot material for the next cycle is not yet available we proceed backwards in time and compare 14 N and 15 S. The big cluster 15 S b could correspond either to one of the big spots in 1906 and 1907 or to one of the big spots in 1909 and 1910. According to the first alternative we could identify b, c, and d with the three big spots in 1906 and 1907. No other identifications are obtained in this way, and the reproduction time becomes as large as 13 years. The second alternative is shown in Fig. 4. The clusters 1909 and 1910 are identified with b, c, and d. The small spot a is considered as a reminiscence of one of the big cluster of 1907. No identification of e, f, and g is obtained. Hence this alternative is only slightly better than the first one. It leaves us, however, with a more reasonable value (10 years) of the reproduction time.

As is evident from the comparison 15 S—16 N the clusters b, c and d form one big region of sunspots and the division of it into clusters is somewhat arbitrary. The comparison 14 N—15 S shows that the corresponding region of sunspots is found in 1909—1910, but the subdivision into clusters is somewhat arbitrary. An identification of 15 S b, c, and d with 14 N m, b, and c is not ruled out although less probable than the identification which we have accepted.

Comparing 13 S and 14 N we find in both cases two maxima of spot activity (1894—1895 and 1897 in 13 S and 1906—1907 and 1909—1910 in 14 N) separated by about one year (1896 and 1908), of low activity. During the two maxima of 13 S the spots have a rather even distribution in longitude so that the pattern is not very distinct. The identification shown in Fig. 4 is no doubt the best one but it is not absolutely convincing because it leaves us with quite a few unreproduced clusters.

The treatment of the sunspot material has not yet been extended more backwards in time. We have thus treated the whole sequence 13 S—14 N—15 S—16 N—17 S. There is no cluster which can be followed the whole way through the sequence. Our identifications depend to a considerable extent on the spot region which in 13 S is represented by k, l, and b with an extension to d. This is reproduced in 14 N by k, l, b, c, and d. In 15 S and 16 N the same region consists of b, c, and d, whereas it fades out in 17 S with c and d as the only representatives.

A new region of spots appears in 15 S with f and g, which are reproduced in 16 N. By being the only spots in the later parts of each cycle they are very valuable as identity marks. There are no signs at all of f and g in 14 N. Going to 13 S, however, we find in 1901 one single small spot which ends the cycle. This has the same position as a predecessor of g should have, so a genetical connection is possible. (The fact that no corresponding spot is observed in 14 N does not contradict this because there may have been one on the sun's backside.) There is also a possible correspondence to f in 13 S. The spots f and g develop further in 17 S where a number of new spots are created between them. Two new big groups v and y appear in the late part of 17 S.

In 13 S there is an extended spot region from o and h to n and r. This is also prominent in 14 N but it dies away in 15 S. The only remnant is the small spot a which even survives to 16 N.

Consequently in the sequence 13 S—14 N—15 S—16 N—17 S there is a tendency for spot regions to form in the late part of a cycle, proceed to the middle of the cycle where they develop their greatest intensity and finally die at the beginning of the cycle.

10. The sequence 13 N—14 S—15 N—16 S—17 N

We shall now make the same analysis for the sequence 13 N—14 S—15 N—16 S—17 N.

In 13 N there is a number of spots in 1893 and 1894. After a lull in 1895 and 1896 there comes a long train of clusters α, δ, ε, ζ, all at about the same longitude. Our earlier results indicate that the first spot of the cycle are in general not very well reproduced, so we should primarily try to find a correspondence to α, δ, ε, and ζ. A similar long train is found in 14 S. This leads to the identification shown by fig. 4. A cluster 14 S $\varkappa$ seems to correspond to the last small spot in 13 N. Further, at about the same time as α appears there is a number of spots also at other longitudes. An identification of the spots η and β seems possible. The small spots in 1905, 1906 and

Table 1. Comparison between the diagrams

CYCLE 13 N								CYCLE 14 S									
No.	First seen	φ lat.	λ long.	A Area	Dur. Days		Remarks	No.	First seen	φ lat.	λ long.	A Area	Dur. Days		Remarks	ΔT	$\Delta\lambda$	$\Delta\varphi$
23511	1891 Nov. 20	3.5	265	33	6	ω		5037	1903 May 21	2.1	229	12	1	ω		11^y+182^d	$-36°$	$-1°.4$
4415	1896 Aug. 21	2.2	28	130	7	ϑ	No corresp.	6406	1908 Apr. 18	2.9	308	59	12					
								6482	July 17	1.9	249	134	9					
4536	1897 Febr. 27	2.2	352	146	12	η		Mean	June 19	2.2	267	193		η		11^y+112^d	$-85°$	0.0
								6427	May 7	2.8	156	71	5					
								6441	» 29	3.0	144	562	10					
4560	Apr. 4	3.3	224	364	13			6464	June 23	2.9	154	108	12					
4573	May 1	3.6	232	148	12			6525	Sept. 10	2.5	183	215	13					
Mean	Apr. 12	3.4	226	512		α		Mean	June 23	2.9	155	956		α		11^y+72^d	$-71°$	-0.5
								6571	Nov. 21	1.8	312	53	4					
								6589	Dc. 25	2.7	320	336	6					
								6602	1909 Jan. 14	2.9	326	192	13					
4576	May 20	1.6	1	71	8	β		Mean	Dec. 29	2.7	321	581		β		11^y+223^d	$-40°$	$+1.1$
								6676	June 4	2.7	339	280	7					
								6686	» 25	1.2	347	167	12					
								Mean	June 12	2.1	343	447		γ	No corresp.			
								6723	Sept. 5	2.3	156	667	10					
								6734	Oct. 1	0.9	166	554	10					
								6778	Nov. 27	3.4	97	61	8					
4759	1898 July 22	1.9	162	81	5	δ		Mean	Sept. 20	1.7	158	1282		δ		11^y+60^d	$-4°$	-0.2
								6805	1910 Jan. 10	3.9	245	134	12	ι	No corresp.			
								6928	1911 Febr. 26	1.5	195	193	10					
								6937	Mar. 28	1.7	192	152	10					
								6942	Apr. 21	1.8	202	139	13					
4879	1899 Sept. 26	3.1	215	58	6	ε		Mean	Mar. 22	1.6	196	484		ε		11^y+117^d	$-19°$	-1.5
4931	1900 June 15	3.6	326	183	10													
4938	Aug. 11	0.6	291	62	3													
Mean	June 26	2.8	317	245		ζ		6972	Nov. 21	2.0	263	140	12	ζ		11^y+148^d	$-54°$	-1.8
								7005	1912 Dec. 12	1.8	202	136	11					
								7006	» 12	1.7	196	115	7					
								7015	1913 Apr. 5	1.9	205	229	3					
4957	1901 July 8	2.1	266	4	1	$\varkappa$	Last spot	Mean	Febr. 4	1.8	202	480		$\varkappa$		11^y+211^d	$-64°$	-0.3
															Mean	11^y+148^d	$-47°$	$-0°.6$

CYCLE 13 S								CYCLE 14 N								ΔT	$\Delta\lambda$	$\Delta\varphi$
No.	First seen	φ lat.	λ long.	A Area	Dur. Days		Remarks	No.	First seen	φ lat.	λ long.	A Area	Dur. Days		Remarks			
3305	1893 Dec. 13	0.7	330	268	13													
3352	1894 Jan. 9	2.0	335	135	12													
Mean	Dec. 22	1.1	332	403		o												
3318	1893 Dec. 21	3.5	221	331	10													
3367	1894 Jan. 24	3.1	233	184	5													
Mean	Jan. 2	3.4	225	515		h		5655	1905 Sept. 7	2.3	286	96	12	h		11^y+248^d	$+61°$	$-1°.1$
3528	May 18	3.9	68	262	12	p	No corresp.											
3498	Apr. 29	3.8	318	85	13													
3546	May 31	0.6	342	62	6													
3583	June 21	1.1	348	57	10													
Mean	May 23	2.1	334	204		q	No corresp.											
3888	1895 Jan. 31	3.0	14	139	4													
3924	Mar. 1	3.7	23	67	2			5892	1906 June 21	3.9	111	155	10					
3929	» 4	3.0	—13	91	2			5924	July 18	3.4	96	188	13					
Mean	Febr. 16	3.2	8	297		i		Mean	July 6	3.6	103	343		i		11^y+140^d	$+95°$	$+0.4$
4192	Oct. 6	2.1	314	137	6	r		6047	Dec. 15	2.4	32	76	4	r		11^y+70^d	$+78°$	$+0.3$
								6117	1907 Febr. 17	3.6	163	265	12	a	No corresp.			
								6211	July 2	3.5	194	379	11					
								6230	Aug. 5	3.3	204	161	4					
4221	Nov. 14	2.7	72	239	13	n		Mean	July 12	3.4	197	540		n		11^y+240^d	$+125°$	$+0.7$
4517	1897 Jan. 28	2.3	23	246	12													
4532	Febr. 23	0.7	34	288	13													
4549	Mar. 22	2.1	41	76	11													
Mean	Febr. 16	1.5	30	610		k		6567	1908 Nov. 13	3.3	75	73	12	k		11^y+270^d	$+45°$	$+1.8$
4556	Apr. 1	3.2	262	122	13	s	No corresp.											
4590	June 28	3.6	179	196	13	t	No corresp.											
4620	Sept. 3	3.7	82	255	7	l		6632	1909 Febr. 26	3.3	125	145	12	l		11^y+176^d	$+43°$	-0.4
								6665	Apr. 30	1.9	83	72	5					
								6700	July 24	2.8	76	152	4					
4695	1898 Febr. 17	0.6	3	153	10	b		Mean	June 26	2.5	78	224		b		11^y+129^d	$+75°$	$+1.9$
								6753	Oct. 25	1.6	169	148	13	c	No corresp.			
								6825	1910 Mar. 8	2.5	236	58	7					
								6842	Apr. 29	1.9	242	169	12					
4837	1899 Jan. 30	2.0	91	68	7	d		Mean	Apr. 16	2.1	240	227		d		11^y+76^d	$+149°$	$+0.1$
4893	Nov. 25	1.5	163	11	3	f	No corresp.											
4958	1901 July 22	1.6	32	9	3	g	No corresp.											
															Mean	$\mathbf{11^y+169^d}$	$\mathbf{+84°}$	$\mathbf{+0°.5}$

CYCLE 14 N								CYCLE 15 S								ΔT	$\Delta\lambda$	$\Delta\varphi$
No.	First seen	φ lat.	λ long.	A Area	Dur. Days		Remarks	No.	First seen	φ lat.	λ long.	A Area	Dur. Days		Remarks			
6117	1907 Febr. 17	3.6	163	265	13	a		8117	1917 June 14	3.2	155	30	7	a		$10^{y}+117^{d}$	$-8°$	$-0°.4$
6211	July 2	3.5	194	379	11													
6230	Aug. 5	3.3	204	161	4													
Mean	July 12	3.4	197	540		n	No corresp.											
6567	1908 Nov. 13	3.3	75	73	12	k	No corresp.	8489	1918 Apr. 8	1.0	119	113	12	e	No corresp.			
6632	1909 Febr. 26	3.3	125	145	12	l	No corresp.											
6665	Apr. 30	1.9	83	72	5			9007	1919 Aug. 14	2.8	94	764	12					
6700	July 24	2.8	76	152	4			9030	Sept. 8	1.8	105	427	13					
Mean	June 26	2.5	78	224		b		Mean	Aug. 23	2.4	98	1191		b		$10^{y}+58^{d}$	$+20°$	-0.1
6753	Oct. 25	1.6	169	148	13	c		9112	1920 Jan. 24	2.9	133	60	9	c		$10^{y}+91^{d}$	$-36°$	$+1.3$
6825	1910 Mar. 8	2.5	236	58	7													
6842	Apr. 29	1.9	242	169	12													
Mean	Apr. 16	2.1	240	227		d		9173	May 7	3.8	220	56	6	d		$10^{y}+21^{d}$	$-20°$	$+1.7$
								9377	1921 Aug. 11	0.5	253	75	8	f	No corresp.			
								9482	1922 Nov. 28	3.0	50	235	13	g	No corresp.			
															Mean	$10^{y}+72^{d}$	$-11°$	$+0°.6$

CYCLE 14 S								CYCLE 15 N								ΔT	$\Delta\lambda$	$\Delta\varphi$
No.	First seen	φ lat.	λ long.	A Area	Dur. Days		Remarks	No.	First seen	φ lat.	λ long.	A Area	Dur. Days		Remarks			
6406	1908 Apr. 18	2.9	308	59	12	η	No corresp.	8374	1917 Dec. 21	2.6	92	527	13					
								8406	1918 Jan. 17	2.4	97	87	7					
								8433	Febr. 11	3.6	125	730	13					
								8464	Mar. 15	3.0	96	73	9					
								8492	Apr. 12	3.1	101	81	9					
								8552	May 31	3.4	143	77	10					
6427	May 7	2.8	156	71	5			Mean	Febr. 2	3.1	111	1575		ϑ	No corresp.			
6441	» 29	3.0	144	562	10													
6464	June 23	2.9	154	108	12			8703	Oct. 8	1.2	296	358	6					
6525	Sept. 10	2.5	183	215	13			8727	» 28	0.6	304	91	13					
Mean	June 23	2.9	155	956		α		Mean	Oct. 12	1.1	298	449		α		$10^y + 111^d$	$+142°$	$-1°.8$
6482	July 17	1.9	249	134	9	λ												
6571	Nov. 21	1.8	312	53	4													
6589	Dec. 25	2.7	320	336	6													
6602	1909 Jan. 14	2.9	326	192	13													
Mean	Dec. 29	2.7	321	581		β		8859	1919 Mar. 17	2.6	4	62	4	β		$10^y + 78^d$	$+43°$	-0.1
								8881	Apr. 13	2.3	304	95	10	ϱ	No corresp.			
6676	June 4	2.7	339	280	7			9031	Sept. 8	1.6	102	526	13					
6686	» 25	1.2	347	167	12			9047	Oct. 5	2.2	106	359	13					
Mean	June 12	2.1	343	447		γ		Mean	Sept. 19	1.8	104	885		γ		$10^y + 99^d$	$+121°$	-0.3
6723	Sept. 5	2.3	156	667	10													
6734	Oct. 1	0.9	166	556	10													
6778	Nov. 27	3.4	97	61	8													
Mean	Sept. 20	1.6	146	1284		δ		9102	1920 Jan. 11	2.0	261	219	13	δ		$10^y + 123^d$	$+115°$	$+0.4$
								9262	Nov. 12	1.6	297	114	4	μ	No corresp.			
								9286	1921 Jan. 12	3.2	102	164	13	ν	No corresp.			
6805	1910 Jan. 10	3.9	245	134	12		No corresp.	9334	May 8	0.5	3	1324	14					
6928	1911 Febr. 26	1.5	195	193	10			9345	June 4	0.8	15	138	12					
6937	Mar. 28	1.7	192	152	10			9360	» 30	3.7	21	264	13					
6942	Apr. 21	1.8	202	139	13			9369	July 8	2.6	308	56	8					
Mean	Mar. 22	1.6	196	484		ε		Mean	May 19	1.1	16	1782		ε		$10^y + 58^d$	$+180°$	-0.5
								9397	Oct. 22	3.9	327	387	12					
								9400	Nov. 17	3.8	332	104	13					
6972	Nov. 21	2.0	263	140	12	ζ		Mean	Oct. 28	3.9	328	491		ζ		$10^y - 24^d$	$+65°$	$+1.9$
7005	1912 Dec. 12	1.8	202	136	11													
7006	» 12	1.7	196	115	7													
7015	1913 Apr. 5	1.9	205	229	3													
Mean	Febr. 4	1.8	202	480		$\varkappa$	No corresp.								**Mean**	$10^y + 74^d$	$+111°$	$-0°.1$

CYCLE 15 S								CYCLE 16 N								ΔT	$\Delta\lambda$	$\Delta\varphi$
No.	First seen	φ lat.	λ long.	A Area	Dur. Days		Remarks	No.	First seen	φ lat.	λ long.	A Area	Dur. Days		Remarks			
8117	1917 June 14	3.2	155	30	7	a	Only spot this year	10299	1927 May 18	3.1	117	24	7	a	Only spot this yar	$10^y -27^d$	$-38°$	$-0°.1$
8489	1918 Apr. 8	1.0	119	113	12													
8519	May 5	0.6	116	49	10													
Mean	Apr. 16	0.8	118	162		e	Biggest spot this year	10514	1928 Febr. 3	1.6	59	13	2	e	Only spot this half-year	$10^y -72^d$	$-59°$	$+0.8$
								10928	1929 May 6	3.3	349	71	12	k	No corresp.			
9007	1919 Aug. 14	2.8	94	764	12			11018	Aug. 10	3.6	154	113	10					
9030	Sept. 8	1.8	105	427	13			11027	» 15	2.7	84	60	8/9					
Mean	Aug. 23	2.4	98	1191		b		Mean	Aug. 12	3.3	130	173		b		$10^y -11^d$	$+32°$	$+0.9$
								11125	Dec. 11	3.2	82	56	4					
								11144	» 22	3.9	188	142	10					
9112	1920 Jan. 24	2.9	133	60	9	c		Mean	Dec. 19	3.7	158	198		c		$10^y -36^d$	$+25°$	$+0.8$
								11235	1930 May 11	2.2	208	85	7					
								11274	July 24	2.0	239	67	11					
9173	May 7	3.8	220	56	6	d		Mean	June 13	2.1	222	152		d		$10^y +37^d$	$+2°$	-1.7
9377	1921 Aug. 11	0.5	253	75	8	f		11381	1931 Apr. 7	3.2	223	179	3	f		$10^y -126^d$	$-30°$	$+2.7$
								11491	1932 May 20	3.6	95	314	13					
								11497	June 16	0.4	101	142	12					
9482	1922 Nov. 28	3.0	50	235	13	g		Mean	May 28	2.6	97	456		g		$10^y -184^d$	$+47°$	-0.4
															Mean	$10^y -60^d$	$-3°$	$+0°.4$

CYCLE 15 N									CYCLE 16 S									ΔT	$\Delta\lambda$	$\Delta\varphi$
No.	First seen	φ lat.	λ long.	A Area	Dur. Days		Remarks		No.	First seen	φ lat.	λ long.	A Area	Dur. Days		Remarks				
8374	1917 Dec. 21	2.6	92	527	13															
8406	1918 Jan. 17	2.4	97	87	7															
8433	Febr. 11	3.6	125	730	13				10560	1928 Mar. 25	2.3	—34	8	6						
8464	Mar. 15	3.0	96	73	9				10666	July 12	3.8	32	30	6						
8492	Apr. 12	3.1	101	81	9				10693	Aug. 2	3.8	74	20	5						
8552	May 31	3.4	143	77	10				10729	Sept. 3	1.0	71	32	5						
Mean	Febr. 2	3.1	111	1575			ϑ		Mean	July 26	2.7	49	90			ϑ		$10^{y}+174^{d}$	$-62°$	$-0°.4$
8703	Oct. 8	1.2	296	358	6															
8727	» 28	0.6	304	91	13															
Mean	Oct. 12	1.1	297	449			α		10837	1929 Jan. 7	1.1	216	60	4		α		$10^{y}+87^{d}$	$-81°$	0.0
									10922	Apr. 29	1.5	104	295	11		ξ	No corresp.			
8859	1919 Mar. 17	2.6	4	62	4		β		11010	Aug. 4	2.4	270	66	4		β		$10^{y}+140^{d}$	$-94°$	-0.2
8881	Apr. 13	2.3	304	95	10		ϱ	No corresp.												
									11122	Dec. 10	3.5	347	379	13						
									11127	» 12	2.6	338	365	11						
9031	Sept. 8	1.6	102	526	13				11130	» 15	3.9	287	106	12						
9047	Oct. 5	2.2	106	359	13				11159	1930 Jan. 8	2.3	347	350	11						
Mean	Sept. 19	1.8	104	885			γ		Mean	Dec. 20	2.9	340	1200			γ		$10^{y}+92^{d}$	$-124°$	$+1.1$
									11207	Mar. 16	1.2	211	52	8						
									11255	June 6	0.3	246	178	6						
9102	1920 Jan. 11	2.0	261	219	13		δ		Mean	May 18	0.5	238	230			δ		$10^{y}+127^{d}$	$-23°$	-1.5
									11307	Sept. 26	3.0	118	161	12						
									11320	Nov. 2	2.9	123	52	2						
									Mean	Oct. 5	3.0	119	213			π	No corresp.			
									11370	1931 Mar. 17	3.6	163	135	12						
									11378	Apr. 1	3.3	172	132	13						
									11392	May 6	1.0	133	56	7						
9262	Nov. 12	1.6	297	114	4		μ		Mean	Apr. 1	3.0	161	323			μ		$10^{y}+140^{d}$	$-136°$	$+1.4$
9286	1921 Jan. 12	3.2	102	164	13		ν		11358	Febr. 15	3.8	57	268	12		ν		$(10^{y}+34^{d})$	$(-45°)$	$(+0.6)$
9334	May 8	0.5	3	1324	14															
9345	June 4	0.8	15	138	12															
9360	» 30	3.7	21	264	13															
9369	July 8	2.6	—52	56	8															
Mean	May 19	1.1	5	1782			ε		11444	Nov. 3	0.6	223	62	10		ε		$10^{y}+168^{d}$	$-142°$	-0.7
9397	Oct. 22	3.9	327	387	12															
9400	Nov. 17	3.8	332	104	13															
Mean	Oct. 28	3.9	328	491			ζ	No corresp.									**Mean**	$10^{y}+133^{d}$	$-95°$	$0°.0$

CYCLE 16 N								CYCLE 17 S								ΔT	$\Delta\lambda$	$\Delta\varphi$
No.	First seen	φ lat.	λ long.	A Area	Dur. Days		Remarks	No.	First seen	φ lat.	λ long.	A Area	Dur. Days		Remarks			
10928	1929 May 6	3.3	349	71	12	k		13124	1938 Dec. 24	2.6	341	144	13	k		10^y—133^d	— 8°	—0°.7
11018	Aug. 10	3.6	154	113	10													
11027	» 15	2.7	84	60	8/9													
Mean	Aug. 12	3.3	130	173		b	No corresp.											
								13268	1939 May 7	2.8	11	86	11					
11125	Dec. 11	3.2	82	56	4			13275	» 12	1.1	19	68	6					
11144	» 22	3.9	188	142	10			13331	June 23	3.4	119	90	11					
Mean	Dec. 19	3.7	158	198		c		Mean	May 26	2.5	50	244		c		10^y—207^d	— 108°	— 1.2
11235	1930 May 11	2.2	208	85	7													
11274	July 24	1.9	239	67	11													
Mean	June 13	2.1	222	152		d		13479	Nov. 24	2.0	253	71	12	d		10^y—201^d	+ 31°	— 0.1
								13711	1940 Sept. 21	3.6	207	409	13					
								13729	Oct. 24	2.6	181	92	9					
11381	1931 Apr. 7	3.2	223	179	3	f		Mean	Sept. 27	3.4	202	501		f		10^y—192^d	— 21°	+ 0.2
								13771	Dec. 12	3.9	307	52	4		No corresp.			
								13799	1941 Jan. 28	1.4	333	95	9		No corresp.			
								13801	Jan. 29	1.8	44	56	4		No corresp.			
								13839	Apr. 1	1.4	291	62	2		No corresp.			
								13849	Apr. 26	0.6	227	135	13		No corresp.			
								13904	July 21	3.7	173	498	13					
11491	May 20	3.6	95	314	13			13919	Aug. 16	3.6	186	298	13					
11497	June 16	0.4	101	142	12			13927	Aug. 29	2.2	147	61	2					
Mean	May 28	2.6	97	456		g		Mean	Aug. 1	3.6	176	857		g		10^y—300^d	+ 79°	+ 1.0
								14074	1942 July 4	3.1	292	330	10					
								14080	» 28	2.0	299	161	13					
								Mean	July 12	2.7	294	491		v	No corresp.			
								14162	1943 July 24	1.8	306	77	6	y	No corresp.			
															Mean	10^y—207^d	+ 5°	—0°.2

CYCLE 16 S								CYCLE 17 N								ΔT	$\Delta\lambda$	$\Delta\varphi$
No.	First seen	φ lat.	λ long.	A Area	Dur. Days		Remarks	No.	First seen	φ lat.	λ long.	A Area	Dur. Days		Remarks			
10560	1928 Mar. 25	2.4	—34	8	6													
10666	July 12	3.8	32	30	6													
10693	Aug. 2	3.8	74	20	5			12927	1938 July 20	3.7	249	128	13					
10729	Sept. 3	1.0	71	32	5			12966	Aug. 15	2.6	262	99	12					
Mean	July 26	2.7	49	90		ϑ		Mean	July 31	3.2	255	227		ϑ		$10^{y}+5^{d}$	$+206°$	$+0°.5$
10837	1929 Jan. 7	1.1	216	60	4	α	No corresp.	12952	Aug. 5	3.9	33	124	13		No corresp.			
10922	Apr. 29	1.5	104	295	11	ξ		13317	1939 June 9	3.4	298	162	11	ξ		$10^{y}+40^{d}$	$+194°$	$+1.9$
11010	Aug. 4	2.4	270	66	4		No corresp.											
11122	Dec. 10	3.5	347	379	13													
11127	» 12	2.6	338	365	11													
11130	» 12	3.9	287	106	12													
11159	1930 Jan. 8	2.3	347	350	11													
Mean	Dec. 20	2.9	340	1200		γ		13586	1940 Apr. 19	0.8	225	77	3	γ		$10^{y}+120^{d}$	$+245°$	-2.1
11207	Mar. 16	1.2	211	52	8													
11255	June 6	0.3	246	178	6													
Mean	May 18	0.5	238	230		δ	No corresp.	13636	June 24	2.5	308	76	12		No corresp.			
								13758	Dec. 3	1.2	342	89	11					
								13767	» 9	1.0	306	195	8					
11307	Sept. 26	3.0	118	161	12			13772	» 13	2.2	324	147	3					
11320	Nov. 2	2.9	123	52	2			13792	1941 Jan. 9	1.6	315	100	4					
Mean	Oct. 5	3.0	119	213		π		Mean	Dec. 15	1.5	319	531		π		$10^{y}+71^{d}$	$+200°$	-1.5
11358	1931 Febr. 15	3.8	57	268	12	ν	No corresp.											
11370	Mar. 17	3.6	163	135	12													
11378	Apr. 1	3.3	172	132	13													
11392	May 6	1.0	133	56	7			13948	Sept. 26	1.4	9	541	13					
Mean	Apr. 1	3.0	161	323		μ	No corresp.	13959	Oct. 23	0.6	14	64	10					
								13962	» 31	3.8	—14	235	7					
11444	Nov. 3	0.6	223	62	10	ε		Mean	Oct. 8	2.0	0.3	840		ε		$10^{y}-26^{d}$	$+140°$	$+2.4$
								14023	1942 Mar. 13	2.5	5	83	9		No corresp.			
								14148	1943 Mar. 31	2.4	297	477	13					
								14152	Apr. 27	1.0	300	171	13					
								14157	May 24	3.8	305	50	11					
								Mean	Apr. 10	2.2	298	698		φ	No corresp.			
								14196	1944 May 29	0.7	197	132	5					
								14198	June 16	1.7	206	71	13					
								Mean	June 4	1.0	200	203		ψ	No corresp.			
															Mean	$10^{y}+42^{d}$	$+197°$	$+0°.2$

1907 seem not to correspond to the activity in 13 N during 1893—94 but the first small spots ω of each cycle agrees very well. Upon the whole the similarity 13 N—14 S is satisfactory.

Proceeding to 15 N we recognize easily the long train α, δ, ε, ζ. The cluster γ which was born in 14 S is very well reproduced. An identification of 14 S β, which is also a new-born spot, with a spot in 15 N is indicated. The clusters ε and ζ have grown but there is no correspondence of $\varkappa$. New-born clusters are μ and ν. Further there is a strong activity in the beginning of the cycle, especially a cluster 15 N ϑ containing two very big and four medium groups. There is no correspondence to this in 14 S but the cluster 13 N ϑ coincides with it.

The comparison 15 N—16 S is more difficult. The long train has been dissolved. The biggest cluster in 16 S occurs at Christmas 1929. This could obviously not be identified with the biggest cluster ε in 15 N because this would give a reproduction time of only 8.5 years. An identification with the second biggest cluster γ seems to be acceptable (fig. 4). The clusters α, β, γ, δ, μ and possibly ν are reproduced in a reasonable way. Of the big cluster ε only one medium group remains, and ζ is not reproduced. The big cluster ϑ may be reproduced by four small spots which start the cycle. A new cluster is ξ.

In 17 N the prevailing feature is again a long train of spots, even longer than in 13 N and 14 S. The best identification seems to be to associate this with ϑ—ξ—π—ε (fig. 4) This means that α, β, δ, and ν have died and two new clusters φ and ψ have been born.

In the "Greek sequence" 13N—14 S—15 N—16 S—17 N, which we have now examined, some clusters have a remarkably long duration. In fact, ϑ, δ, and ε have persisted during the whole time (with an interruption for ϑ in 14 S). If 17 N is placed on top of 13 N these three clusters are easily brought to coincide. If all the five diagrams 13 N—14 S—15 N—16 S—17 N are placed on top of each other these three clusters are in about the same place in all of them.

11. Correlation between the two sequences

We have found a good correlation within the "Latin sequence" 13 S—14 N—15 S—16 N—17 S and also within the "Greek sequence" 13 N—14 S—15 N—16 S—17 N. It is of interest to see whether these series are interconnected. A comparison of the type $(n, N) — (n+1, N)$ or $(n, S) — (n+1, S)$ or of the type $(nN) — (nS)$ shows in may cases some degree of similarity.

12. Check of identifications

First check: comparison of non-related patterns

It is of decisive importance to investigate whether the pattern similarities which we have found are significant or not. It is quite possible that two patterns are judged to be similar even if there is no real correlation between them. The first way to check this is to compare diagrams which we do not expect theoretically to be similar. A difficulty is that if there exists a correlation between the two sequences, all diagrams without exception ought to show some correlation. In order to compare diagrams with as small theoretical correlation as possible we should choose them from different sequences, and with as long a time interval as possible. Hence we select the four pairs 13 N—16 N, 14 N—17 N, 13 S—16 S, and 14 S—17 S as material for our check comparison. Proceeding in the same way as earlier we place the biggest spot of one diagram on the top of one of the biggest spots of the other diagram.

The comparison shows that 13 S and 16 S gives a not too bad similarity, 13 S t, l, b, and d forming a pattern similar to 16 S γ, δ, π, ε. In the three other cases no similarity at all could be traced.

The negative result in three cases indicates that it is probable that our earlier identifications are significant but the fact that in one case a similarity could be found which mainly must be accidental, shows that our method is not quite without danger. Hence other checks are highly desirable.

13. Second check: Calculation of the "twist" of the magnetic field

Our second check is of physical character and concerned with the calculation of the twist of the magnetic field (see § 4).

Suppose that the magnetic field is twisted in such a way that a magnetic line of force which

intersects the southern hemisphere at the longitude λ_S arrives to the northern hemisphere at the longitude

$$\lambda_N = \lambda_S + \Theta \quad \ldots\ldots\ldots \quad (1)$$

where Θ is a constant which we shall call the *twist*. Suppose further that a disturbance travels along a certain line of force and reaches the southern hemisphere during the cycle n at the longitude λ_S^n. The same disturbance reaches the northern hemisphere during the cycle $n+1$ after a time interval $T_{S,n}^{N,n+1}$ (the reproduction time). If the latitude at which the spots occur rotates with the angular velocity ω_d in comparison to the latitude to which the heliographic longitude determination refers, the longitude at the northern hemisphere is

$$\lambda_N^{n+1} = \lambda_S^n + \Theta + \omega_d T_{S,n}^{N,n+1} \quad \ldots\ldots \quad (2)$$

Consider another disturbance which reaches the northern hemisphere at longitude λ_N^n during cycle n and the southern hemisphere at longitude λ_S^{n+1} during next cycle.

In a similar way we obtain

$$\lambda_S^{n+1} = \lambda_N^n - \Theta + \omega_d T_{N,n}^{S,n+1} \quad \ldots\ldots \quad (3)$$

where $T_{N,n}^{S,n+1}$ is the reproduction time of the disturbance. We put

$$\Lambda_{N,n}^{S,n+1} = \lambda_S^{n+1} - \lambda_N^n \quad \ldots\ldots\ldots \quad (4)$$

and

$$\Lambda_{S,n}^{N,n+1} = \lambda_N^{n+1} - \lambda_S^n \quad \ldots\ldots\ldots \quad (5)$$

The quantities Λ are the longitude differences which are found empirically at the comparison between the diagrams. Subtracting (3) from (2) we obtain

$$\Theta = \frac{1}{2}(\Lambda_{S,n}^{N,n+1} - \Lambda_{N,n}^{S,n+1}) - \frac{1}{2}\omega_d \triangle T \quad (6)$$

with $\triangle T = T_{S,n}^{N,n+1} - T_{N,n}^{S,n+1}$

We do not know ω_d with certainty. We do not even know whether it is constant. In fact, some of the results of the present analysis indicate that this is not the case. The differential rotation is usually computed from the systematic longitude drifts of sunspots which for our latitude belt is 5° per solar rotation, corresponding to $\frac{1}{2}\omega_d = 0.09$ degrees/day. From the point of view of the magneto-hydrodynamic theory of sunspots it is conceivable that systematic drifts may be caused also by other effects than a differential rotation. However, all these problems will be reserved for a later analysis. In view of the uncertainty we shall here calculate Θ in two ways, *viz.* by neglecting the second term in (6) and by including this term. The latter value will be referred to as Θ_{corr}.

Table 2 shows the values of Θ calculated with and without the second term. The constancy of Θ is remarkable. In fact, without correction it varies only within the relatively narrow limits 46° and 96°. The excessive agreement between the corrected values is of course only a numerical coincidence. As mean we obtain

$$\Theta = 66° \pm m\ 180°$$

where m is an integer.

The constancy of Θ gives a strong support for our identifications. In fact, if we accept all identifications except one, we could calculate the relative longitude position Λ for this one from (6). The position would agree with what we have found within an error of less than about 45°. This shows that in no case a serious error can have been made when fixing the relative longitude position of the diagrams.

14. Third check: Correlation between reproduction time and the length of the solar cycle

Having thus shown that the identifications must be correct in longitude, it remains to investigate whether there is any possibility to check the values of the reproduction time. It could be suspected that there should be a positive correlation between this and the length of the solar cycle. In fact, if sunspots are reproduced after a certain time T we should expect that this quantity regulates the length of the solar cycle. It is obviously not the only factor of importance, because as we have seen not all spots are reproduced. There is a general tendency that spots in the beginning of a cycle are not very well reproduced and that new spots are born at the end of the cycle.

Table 2 shows a comparison between the average of $T_{N,n}^{S,n+1}$ and $T_{S,n}^{N,n+1}$ and the length of the solar cycle (= time difference between two sunspot maxima). The correlation is obviously positive. This is satisfactory, but on the other hand the correlation is not good

Table 2. Results of the comparison.

Cycle	$\Lambda^{S,n+1}_{N,n}$	$\Lambda^{N,n+1}_{S,n}$	Θ	$\Theta_{corr.}$	$T^{S,n+1}_{N,n}$	$T^{N,n+1}_{S,n}$	ΔT	T_{mean}	Diff. sunspot max.
13—14	— 47°	+ 84°	66°	64°	11^y 148^d	11^y 169^d	21^d	11^y 159^d	12.9
14—15	— 11°	+ 111°	62°	62°	10^y 72^d	10^y 74^d	2^d	10^y 73^d	10.6
15—16	— 95°	— 3°	46°	63°	10^y 133^d	9^y 305^d	— 193^d	10^y 36^d	10.8
16—17	+ 5°	+ 197°	96°	74°	9^y 158^d	10^y 42^d	249^d	9^y 283^d	9.0
		Mean	**68°**	**66°**					

enough to give an accurate check of our values of the reproduction time.

15. Identification by structure

In § 3 it was pointed out that it may be possible to identify two spots as produced by the same original disturbance by discovering some peculiar property which is common to both. If for example a sunspot whirl ring makes a certain angle with the magnetic field, this may cause correlated proper motions of one spot of the northern hemisphere and the corresponding spot of the southern hemisphere.

This could preferably be checked by comparing the proper motions of spots which we have identified by their position. Simple spots like f and g are especially suited for this. A preliminary analysis indicates that there may be a correlation between the proper motions, but the problem must be studied much more carefully before any definite conclusions can be reached.

16. Spots at higher latitudes

The whole analysis has so far been confined to the latitude belt 4° S—4° N. An extension to higher latitudes is very desirable. It seems relatively easy to proceed up to 6° or may be even 8° by the same method, but when we approach the maximum belt at 10°—15° the number of spots gets so large, that it is impossible to distinguish distinct patterns. It will be necessary to develop other methods of identification before a real attack towards higher latitudes could be launched. If the identification by structure succeeds, the problem will be easier.

It is of interest to note that the survival of spot groups during several cycles which was found in §§ 9 and 10 is in good agreement with earlier results concerning the latitude pattern of spottedness (cf. Cosmical Electrodynamics p. 138). The latitude distribution for cycle 14 is very similar to that of cycle 15 and 16, and there is also a definite resemblance for cycle 12. These results refer to higher latitudes (10°—30°) and indicate that the persistency of spots may be a general phenomenon.

17. Theoretical conclusions

The reproduction of sunspots which has been found here is well explicable according to the magneto-hydrodynamic theory of sunspots. A wave which reaches e.g. the southern activity region becomes in part amplified, and in part reflected. The reflected wave goes to the northern activity region where the same phenomenon occurs and a reflected wave is sent out to the southern region. This can be repeated several times.

In the theory it was assumed that when a whirl ring passes an activity region it usually gives rise to a series of reflected whirl rings. None, or one, or many of these may survive the destruction by damping and other causes, and finally give rise to new spots. The activity regions were thought to consist of the upper parts of the convective core and to be rather thick, perhaps a few tenths of the size of the core.

This idea of the activity regions is well reconcilable with the present results except that the activity regions cannot be very thick. A sunspot group may be reproduced next cycle by a cluster of groups, a single group, or not at all. If it is reproduced by a cluster of groups the spread in time of the spots of the cluster is a measure of the thickness of the activity region, where they are produced. Suppose that a wave pulse with the velocity V passes a region with thickness D in which it may be partially reflected anywhere. The difference in time t between pulses reflected at the beginning and at the end of the region is

$$t = 2D/V$$

In our case t represents the maximum spread in time within a cluster. Judging from the diagrams it is reasonable to put $t = 10^6$ sec. (≈ 4 months). The velocity V is likely to be of the order 60 cm/sec (Cosmical Electrodynamics p. 100). This gives $3 \cdot 10^7$ cm which is only 0.004 of the solar radius.

Consequently the activity region is so thin that it more resembles a surface of discontinuity, which should have the property of reflecting and amplifying waves passing it. The existence of such a surface is hardly reconcilable with current solar models. GAMOW (1945) and REIZ (1948, 1949) have discussed a model in which the energy is released in a spherical shell. It is conceivable that magneto-hydrodynamic waves passing such an energy producing shell should be reflected and amplified in the way our results require. The possibility to construct a solar model of this type should be seriously discussed. When we learn to correlate more closely the appearance and structure of sunspots with the phenomena in the solar core by which the spots originate, sunspots data will give us valuable information concerning the interior of the sun.

I wish to thank Dr. N. HERLOFSON for numerous discussions. Mrs. B.-M. HOLMLIN has kindly extracted the sunspots data from the catalogues and Mr. WITT has prepared the diagrams.

REFERENCES

ABETTI, G.: Solar Physics Conference, Florence 1952.
— Sul Luogo Probabile dei Poli Magnetici Solari, Accademia Nazionale dei Lincei, 269—276, 1953.
ALFVÉN, H.: Magneto-Hydrodynamic Waves and Sunspots III, Ark. f. Mat., Astr. o. Fysik **34 A**, 23, 1948. Compare also Cosmical Electrodynamics, p. 138, Oxford 1950.
— The Impossibility of Determining the Sun's General Magnetic Field by Zeeman Effect Measurements, Nature **168**, 1036, 1951.
— On the Zeeman Effect Measurements of the Sun's General Magnetic Field, Ark. f. Fysik **4**, 24, 1952.
— Discussion of the Origin of the Terrestrial and Solar Magnetic Fields. Tellus **2**, 74, 1950.
BULLARD, E. C.: The Magnetic Field within the Earth, Proc. Roy. Soc. **A 197**, 433, 1949.
CRITCHFIELD, C. L., and GAMOW, G.: The Shell-Source Stellar Model, Astrophys. J. **98**, 244, 1939.
ELSASSER, W. M.: Induction Effects in Terrestrial Magnetism. Theory Part I, Phys. Rev. **69**, 106, 1946.
— Induction Effects in Terrestrial Magnetism. The Secular Variation. Part II, Phys. Rev. **70**, 202, 1946.
ELSASSER, W. M.: Induction Effects in Terrestrial Magnetism. Electric Modes Part III. Phys. Rev. **72**, 821, 1947.
GALVENIUS, I. and WOLD, H.: Statistical Tests of H. Alfvén's Theory of Sunspots, Ark. f. Mat., Astr. o. Fysik **34 A**, 24, 1948.
GAMOW, G.: Nuclear Energy Sources and Stellar Evolution, Phys. Rev. **53**, 595, 1938.
— The Red Giant Stage of Stellar Evolution, Phys. Rev. **67**, 120, 1945.
LUNDQUIST, S.: On the Stability of Magneto-Hydrostatic Fields, Phys. Rev. **83**, 307, 1951.
REIZ, A.: A composite Giant Star Model with Isothermal Core, Ann. d'Astroph. **10**, 301, 1947.
— A Composite Giant Star Model with Isothermal Core, Danske Vid. Selsk. **25**, 1, 1948.
— A Composite Giant Star Model with Isothermal Core. Second note. Ark. f. Astronomi **1**, 2, 1949.
WALDMEIER, M.: Ergebnisse der Sonnenforschung, p. 144, Leipzig 1941.
WHITTLE, P.: Astrophys. J. (In the Press) 1954.

A Critical Examination of Theories of Charge Generation in Thunderstorms

By B. J. MASON, Imperial College, London

(Manuscript received May 2, 1953)

Abstract

A concise review is presented of the more important features of the meteorological and electrical behaviour of thunderstorms from which the main conditions to be fulfilled by any satisfactory theory of charge generation, are enumerated. The various theories are then examined, as far as possible from a quantitative point of view, in the light of these requirements. None is found to be entirely satisfactory. It is concluded that the mechanism which most accords with the observed facts is the charge generation and separation which, according to the results of laboratory experiments, will be associated with the growth of graupel pellets in the supercooled region of the thundercloud.

1. Introduction

During the last forty years, at least eight different mechanisms for the generation of electricity in thunderclouds have achieved prominence in the literature. Too often theories have been formulated without sufficient regard to all the available experimental data on the behaviour of thunderstorms, and rarely have they been examined for *quantitative* agreement with these data. Any satisfactory theory must show quantitatively how charge can be created and separated at the rate required by the measurements of the electric field-change and the frequency of lightning discharges and must conform with known facts about the meteorological and electrical structure of the cloud, its life-history and the nature and time-scale of the precipitation processes.

2. The Electrical and Meteorological Behaviour of a Thunderstorm

(a) *The Life Cycle of a Thunderstorm*

The investigations made during the Thunderstorm Project (see BYERS and BRAHAM, 1950), indicate that a thunderstorm consists of one or more identifiable units or *cells* which are localized regions of pronounced convective, microphysical and electrical activity. The life of an individual cell can be divided into three stages, depending on the direction and magnitude of the vertical air currents. The cumulus, or growing stage is characterized by the existence of an updraught throughout the cell; the mature stage by the presence of both updraughts and downdraughts, at least in the lower part of the cell, the onset of lightning activity and the appearance of precipitation below cloud base; the dissipating stage by weak downdraughts prevailing throughout the cell with marked reduction in the intensity of precipitation and electrical activity.

The duration of the cumulus stage reckoned from the time of initial detection of the radar echo, which appears soon after the visible cloud top extends above the 0° C level, is between 10 and 15 minutes. The mature stage, during which most of the precipitation is released, lasts for 15 to 30 minutes. The duration of the dissipating stage, measured to the time when vertical motions inside the

cloud become insignificant, is of the order 30 minutes. Thus the life of one cell occupies about one hour, but the duration of the radar echo and its associated electrical activity may be confined to a period of less than 30 minutes. The larger, more persistent thunderstorms which may last for several hours probably result from the activation of a group of cells. Successive centres develop in turn and more than one may be active simultaneously.

(b) *The Meteorological Structure of a Thunderstorm*

Most of our information on the structure of the thunderstorm again comes from the data of the Thunderstorm Project and from the observations made at the Observatory on the Zugspitze (altitude 10,000 feet) and reported by KUETTNER (1950).

In the early stages, the incipient thundercloud grows rapidly in the vertical and is characterized throughout its volume by updraughts whose magnitude was 7 m/sec. on average in the storms investigated by the Thunderstorm Project, but values of 15 m/sec. are not uncommon and may be appreciably exceeded. The horizontal dimensions of the cell, as first detected by radar, may be only 0.5 km with the top extending only about 1 km above the 0° C level. Thereafter, the visible cloud top may grow rapidly towards the – 30° C isotherm, or even higher. Byers and Braham report observations which indicated that within the updraught region of a single cell there was more than one locality of strong vertical ascent; that these regions were separated in space or time, or both; and that they resulted in the development of individual cloud columns appearing as turrets at the summit of the visible cloud. Kuettner also quotes evidence for this sub-division of a cell, the smaller units having horizontal dimensions of 100 m to 1 km, i.e. about one-tenth those of the cell. They often occur at different positions relative to the centre of the cloud and successive turrets often penetrate to greater heights than their predecessors. These subcells may perhaps be identified with the "bubbles" which are regarded by SCORER and LUDLAM (1953) as the fundamental units in the structure of cumulus; a succession of rising bubbles would confer on the updraught something of the pulsating nature mentioned by BYERS and BRAHAM and by WORKMAN and HOLZER (1942).

The last-mentioned authors state that, in the early stages of cloud development, the water particles are small but their size continually increases with time. Later, as the cloud top reaches colder regions, larger particles of snow, graupel and rain appear but continue to be carried upwards by the updraught which may now be typically 1.5 km in diameter. The greatest concentration of hydrometeors occurs at and above the 0° C level. The size and concentration of the precipitation elements continue to increase until they can no longer be supported by the existing updraught and they then begin to fall relative to the earth. At about the same time, strong downdraughts appear in the lower part of the cell, particularly in the region where precipitation is falling. This marks the onset of the mature stage of the cell during which it attains its maximum height and may reach the tropopause; the horizontal dimensions of the radar echo may now lie between 5 and 14 km at the base, tapering off towards the top. There may still be strong local updraughts particularly in the upper parts of the cloud where the average velocities are about 10 m/sec., but on occasions may exceed 30 m/sec. Precipitation elements consist mainly of raindrops below, and snow or graupel particles above, but hail may occur in some cells, particularly those containing exceptionally strong updraughts. The mature stage is gradually transformed into the final dissipating stage in which the whole cell contains air moving downwards or almost at rest. Precipitation continues to fall for some time but gradually diminishes in intensity and ceases.

Kuettner presents some very valuable information on the nature of hydrometeors found in thunderstorms; his observations being made on a mountain top immersed in the cloud are more reliable and clear-cut than those made from aircraft. He reports that solid precipitation elements were predominant in the greater part of the thundercloud, being found on 93 % of the occasions, while raindrops were present in only 21 % of the clouds. Kuettner states that graupel (including snow pellets and soft hail) was the most frequent form of hydrometeor, being present on 75 % of occasions; large hail was relatively rare and

was, by no means, a necessary event in thunderclouds. Snow crystals prevailed during the later periods of a storm when the precipitation became more steady and moderate in character and the lightning activity diminished.

Both Kuettner and Workman and Reynolds (1950 a) state that a necessary condition for the development of thunderstorms on the Zugspitze and in New Mexico respectively, is that the cloud base should be warmer than 0° C. Furthermore, Workman and Reynolds state that the first lightning flash occurs only when the top of radar echo approaches the – 30° C level; Byers and Braham say that the top of the echo must be colder than – 20° C. Workman and Holzer (1942) report no lightning from clouds of depth less than 5 km.

(c) *The Electrical Structure of a Thunderstorm*

From his measurements on the change of the electric field at the ground during lightning activity and the variation in the sign of the field-change with distance from the storm, Wilson (1920) deduced that the thundercloud has a bipolar structure with a positive charge situated above a negative charge. Wilson's conclusions have been amply confirmed by similar measurements by Workman, Holzer and Pelsor (1942) in New Mexico, who found some evidence which pointed to the upper charge-centre being displaced in the direction of motion relative to the lower negative centre (this is to be expected in the presence of a wind-shear). The positive and negative charge centres were, on average, 2.5 km and 4 km respectively, above cloud base, but probably only in the early stages; Workman and Reynolds (1950 a) report that as the storm progresses, the positive centre moves upwards while the negative centre appears to remain fixed in the zone of heavy precipitation.

Malan and Schonland (1951 a, b), from a study of the electric-field changes in the intervals between successive strokes of lightning flashes to earth, conclude that the negative charge which is involved in such a flash is contained in a nearly vertical column, which, on occasion, may be 6 km long, the temperature at its base being not much below 0° C and its top frequently reaching the – 40° C level. Their techniques allow determination of the heights of the charges involved in separate strokes; the results obtained from five different methods agree in indicating that successive strokes tap progressively higher and higher regions of the negative column, the average increase in height per stroke being about 0.7 km. The first stroke appears to originate from near the – 5° C level, while later strokes may extend upwards by more than another 5 km. Malan and Schonland also report that, in their South African thunderstorms, 65 % of the first strokes of flashes to earth have type β leaders indicating that there is a positive space-charge below the base of the main negative column. The discharge of the negative column to earth may therefore, in many cases, be triggered off by the strong field between the positive pocket and the bottom of the negative column.

Wormell (1953) has made similar investigations but finds that on 75 % of occasions there is no appreciable change of field during the *j* portion of the stroke, i.e. although there is a transport of charge, the electric moment is not changing. This indicates that in 75 % of the multi-stroke flashes to earth around Cambridge, England, the negatively charged regions in the cloud which are discharged by successive strokes, are all sensibly at the same height. In the remaining 25 % of cases the form of the field change indicates that the heights of these regions increases for successive strokes as found by Malan and Schonland.

The most direct information on the electrical structure of a cumulonimbus comes from measurements of the electric field made from balloons and aircraft. The pioneer work was carried out at Kew by Simpson and Scrase (1937) and Simpson and Robinson (1941), who used the altielectrograph on a balloon to determine the sign of the vertical component of the electric field as a function of height and also to obtain an estimate of its magnitude. The records established beyond reasonable doubt that the upper part of a thundercloud is positively charged and most of the lower part negatively charged. In 7 of 13 different storms there was also evidence of one or more localised regions in the base of the cloud containing positive charge. The upper positive charge was usually associated with temperatures below – 20° C, and always below – 10° C. The temperature at the negative charge centre was below 0° C in 13 out of 15 cases while

the lower positive charge, in 5 cases out of 7, was at temperatures above 0° C. Simpson and Robinson stated that their results could be represented schematically by a thunderstorm model with an upper charge of + 24 coulombs distributed in a spherical volume of 2 km radius centred at a height of 6 km (– 30° C), a negative charge of – 20 C in a sphere of radius 1 km centered at a height of 3 km (– 8° C) and a charge of + 4 C in a sphere of radius 0.5 km centred at 1.5 km (+ 1.5° C). Thus, the upper positive charge and the bulk of the negative charge were in regions where the temperature was below 0° C. Similar results regarding the charge distribution have been reported by CHAPMAN (1950) who used a radiosonde device, the observations being telemetered to the ground. The negative charge centres for 7 storms were reported to lie with 0.5° C of the 0° C isotherm.

The results of these balloon investigations, while of great value in establishing the general features of the charge distribution, cannot be regarded as very reliable for giving the temperatures of the charge centres and the actual magnitudes of the electric field, because it seems probable that on the majority of occasions, the balloon missed the electrical centre of the storm; in fact 15 % of Simpson's useful ascents came to a violent end in a rapidly increasing field. The fields reported by Simpson et al, barely exceeded 100 V/cm while the largest field recorded by Chapman was 210 V/cm; these are to be compared with values of 1,300 V/cm, and on one occasion, 3,400 V/cm measured by GUNN (1948) from an aircraft. The last named author encountered the most intense fields near the 0° C level.

KUETTNER (1950), from his observations on the Zugspitze, finds that the lower positive charge has a horizontal extent generally less than 1 km and is accurately centred at the 0° C level. The more extensive negative charge is centred, on average, near the – 8° C level, while the main upper positive charge is still higher and even more diffuse. The negative charge centre is apparently the starting point of the lightning flashes.

It is of some importance to reconcile the deductions of Malan and Schonland and of Wormell concerning the distribution of the negative charge in a thundercloud. In most of the South African storms it appears that the negative charge is distributed in a nearly vertical column which is tapped at progressively higher and higher levels by outwardly-directed positive streamers during successive strokes of a flash to earth. This charge configuration might be expected in a cell containing only one region of strong updraught and one column of precipitation and electric charge. However, if there are more than one such regions separated in space and time throughout the cell, it is possible that a particular centre may become discharged by positive streamers directed outwards from a neighbouring centre which has already passed its charge to earth. Thus, the total charge dissipated in a lightning flash may be drawn from several charge centres of smaller dimensions than the thunderstorm cell and the discharge of a new centre by the next stroke might involve very little change in electric moment or electric field as measured at the ground. Such a mechanism may be responsible for the 75 % of Wormell's records.

(d) *Correlation between Electrical Activity and Meteorological Processes*

Kuettner states that a high precipitation is an indispensable requirement for electrical activity in a cumulonimbus, the central lightning area usually being coincident with the area of highest precipitation intensity. The onset of lightning activity coincides with the appearance of heavy solid precipitation within the cloud.

WORKMAN and REYNOLDS (1950 a) assert that separation of electric charge within the cloud is closely associated with the precipitation mechanisms and does not take place until precipitation processes are well under way; it takes place at temperatures between 0° C and – 15° C, most probably between – 5° C an – 10° C. The first internal flash occurs about 12 minutes after the initial radar echo, which by this time has approached the – 30° C level and started to descend; at the same time precipitation appears at the cloud base. Cloud-to-ground discharges follow within a few minutes. These authors also report that the lightning activity has a periodicity of 25 to 40 minutes corresponding to the active life of a cell.

WORKMAN and HOLZER (1942) report that clouds of greatest vertical depth display the

greatest electrical activity. The vertical motion often appeared to be pulse-like in character, each new surge (or turret) being associated with increasing electric fields at the ground and a new series of lightning flashes.

Measurements of field strength from aircraft made in conjunction with ground radar observations during the Thunderstorm Project showed that, during growth of the cell, the positive field (positive charge above, negative below), became strong in the precipitation area. In the dissipating stage the positive field was replaced by a negative one. A positive charge was often found in the rain core of the cloud near the cloud base. The maximum frequency of lightning preceded the onset of maximum intensity of rainfall at the ground.

(e) *The Electric Moment Destroyed in a Lightning Flash—Rate of Charge Dissipation*

From measurements of the change in the vertical component of the electric field at the ground during a distant lightning flash, one can calculate the electric moment $\delta M = 2H\delta Q$ destroyed, where δQ is the charge neutralised and H is the vertical separation of the main positive and negative charge centres for an internal flash, or the height or the involved charge above ground for a discharge to earth. Wormell (1939, 1953) gives 110 C-km and 130 C-km as the most frequent values for the moments destroyed during internal and cloud-to-ground flashes respectively, in storms investigated at Cambridge. Wilson (1920) gave an earlier mean value of 100 C-km, while Schonland (1928) quotes 90 C-km as the appropriate mean value for South African thunderstorms. Taking a mean value of 110 C-km for all types of flashes, values of H varying from 2 to 3.5 km for cloud-to-ground discharges and up to 5 km for internal flashes, the charges neutralised are calculated to be of the order 10 to 30 coulombs. Workman and Holzer (1942) report that the magnitude of the charge involved in New Mexico storms varies between 10 C and 190 C, the most frequent values lying between 20 C and 50 C. Holzer (1950) states that a multiple-stroke flash which may neutralise about 20 C, very often originates from several charge centres, each of which may contribute from about 3 to 8 coulombs. He gives the average interval between strokes of a cloud-to-ground flash as 0.05 sec.; Wormell gives 0.07 sec. and Schonland 0.03 sec. Taking Allibone and Meek's (1938) mean value for the positive streamer velocity as 2.4×10^6 cm/sec., and the average duration of a stroke as 0.05 sec., we arrive at 1.2 km for the average separation of the charge centres; this is a very reasonable value for the separation of the sub-cells or bubbles in the cloud.

Lightning flashes from a given cell occur on average at intervals of about 20 sec., so that the current dissipated by lightning is of the order 1 amp.

(f) *Recovery of the Electric Field after a Flash; Rate of Charge Generation*

The recovery of the field after the passage of a lightning flash which corresponds to the regeneration of the electric moment in the cloud, is approximately exponential in form and according to Wilson (1929) and Wormell (1939) has, on average, a time constant of about 7 sec. The initial rate of recovery represents the rate at which the electric moment grows when the internal field is small; the slowing down which follows is due to the increased electrical forces on the charged elements tending to oppose their separations as the internal field grows, and by the increased rate of dissipation by charges on the precipitation elements, by point discharge currents and ionic leakage to the upper atmosphere. If we take the charge neutralised in an average flash to be 20 C and the *initial* rate of regeneration as $1/7$ sec.$^{-1}$, the vertical current in the cloud immediately after the discharge turns out to be 3 amps; however, the various leakage factors mentioned above, subsequently restrict the average net charging current to about 1 amp.

The rebuilding of the electric moment, however, implies not only a generation of charge but a vertical separation of charges of opposite sign. If, as is assumed in most theories, charge of one sign is attached to the precipitation particles and that of opposite sign carried upwards on ions or cloud droplets, their rate of vertical separation cannot exceed the rate of fall of the precipitation elements in still air. Now, the initial rate of regeneration of moment, would if it remained constant, replace the whole moment destroyed by the discharge, 110 C-km, in 7 sec. Taking 8 m/sec. as the

fall velocity of the particles, the maximum vertical separation of the charges in this time would be 56 m; this implies that the magnitude of the charges which are separating immediately after discharge is about 1,000 C.

Wilson first suggested that these charges would be distributed through a considerable volume which is in the main electrically neutral, but as separation proceeds through the volume, a positively charged region appears near the top and a negatively charged region near the base. As WORMELL (1953) points out, such a bulk charge of about 1,000 C would be sufficient without replenishment, to supply the charges removed in a considerable number of lightning flashes, so that the primary charging mechanism need not necessarily supply new charge to the region as rapidly as it is being dissipated by a brief spell of lightning activity.

(g) *Summary—The Requirements of a Satisfactory Theory*

The main features of the thunderstorm which have been described in the foregoing paragraphs and with which any theory of charge generation must be consistent are:

(i) The average duration of precipitation and electrical activity from a single cell is about 30 minutes.

(ii) The average electric moment destroyed in a lightning flash is about 110 C-km, the corresponding charge being 20 to 30 C.

(iii) The magnitude of the charge which is being separated immediately after a flash, by virtue of the fall-speed v of the precipitation elements, is of order $8{,}000/v$ coulombs where v is in metres/sec.

(iv) In a large, extensive cumulonimbus this charge is generated and separated in a volume bounded by the $-5°$ C and the $-40°$ C levels and having a typical radius of say, 2 km.

(v) The negative charge is centred near the $-5°$ C isotherm while the main positive charge is situated some kilometres higher up; a subsidiary positive charge may also exist near the cloud base, centred at or below the 0° C level.

(vi) The charge generation and separation processes are closely associated with the development of precipitation, particularly in the solid form (graupel); the precipitation particles must be capable of falling through updraughts of several metres/sec.

(vii) Sufficient charge must be generated and separated to supply the first lightning flash within about 12 to 20 minutes of the appearance of precipitation particles of radar detectable size.

3. The Theories of Charge Generation and Separation

Having reviewed briefly our present knowledge concerning the electrical and meteorological behaviour of a thunderstorm, the two, of course, being intimately related, we are now in a position to examine the various theories of charge generation and separation and determine how far they are consistent with the observed facts.

(a) *Influence Theories*

(i) ELSTER and GEITEL (1913) considered the effects associated with a raindrop falling through a vertical electric field and colliding with smaller cloud droplets lying in its fall-path. The raindrop will be electrically polarised; in a downwardly directed field such as exists in the atmosphere under fine-weather conditions, the lower half of the drop will carry a positive charge and the upper half a negative charge. Elster and Geitel assumed that on collision, the cloud particles would *rebound* from the raindrop and carry away some of the charge from its lower half. Thus, with a positive field, the raindrops would acquire a net negative charge, while further gravitational separation would enhance the original field. Nowadays, this theory appears untenable; the *coalescence* of drops possessing differential rates of fall plays an important part in modern precipitation theory, and there is direct experimental evidence that it takes place with high efficiency when drops of raindrop-size fall through a cloud of droplets of radius about 10 μ (GUNN and HITSCHFELD, 1951).

(ii) *Wilson's Process of Charging by Selective Ion Capture*

Wilson (1929) pointed out that under certain conditions, an electrically polarised raindrop in falling through a cloud of ions or charged cloud droplets, could by a process of selective ion *capture*, acquire a net charge. If the drop falls more rapidly through a downwardly-directed field than the downwardly-moving positive ions, the latter are repelled from the lower half of the drop and deviated to one side, while the negative ions are attracted to it. Hence the drop acquires a net negative charge which tends to augment the pre-existing field. The mathematical theory of the process has been worked out by Whipple and Chalmers (1944) who showed that, if the fall velocity of the raindrop is large compared with the drift velocity of the ions under the existing vertical field, (this will generally be the case if the ions are charged cloud droplets), (α) the final charge acquired by a drop of radius a, independent of its initial charge, in a vertical field of intensity X, is

$$Q_{max} = -3\,(3-2\sqrt{2})\,Xa^2 = -0.52Xa^2 \quad (1)$$

(β) if its initial charge is zero, the initial (i.e. maximum) rate of charging of a drop is

$$\left(\frac{dQ}{dt}\right)_{max} = -3\pi Xa^2\lambda_- \quad (2)$$

where λ_- is the polar conductivity for the large negative ions,
(γ) the time required for the drop to acquire half of its final charge is

$$\tau = 0{,}04/\lambda_- \text{ sec.} \quad (3)$$

As the above mechanism proceeds, the field increases, so that the equilibrium charge towards which the drops are tending is increasing with time. However, we can estimate the magnitude of the maximum charge which can be generated by this process, and the rate of charging.

Let us suppose that the precipitation process has developed to a stage at which the precipitation rate in the active part of the cloud reaches 2.5 cm/hr with a corresponding mean volume drop radius of 1.5 mm and precipitation-water content of 1 g/m^3; the concentration of drops under these conditions will be 70/m^3. Taking the average intensity of the vertical field to be 1,000 V/cm, the maximum charge that can be developed per km^3 by the Wilson process is then 0.9 C. But, we now have to consider whether the drops could approach their equilibrium charge during the life of a thunderstorm cell. There appears to have been no reliable determination of polar conductivity in cloudy air, but if we substitute a conservative value of 4×10^{-6} e.s.u. for λ_- in (3), we find that it would take 10^4 sec. for the drop to acquire half of its maximum charge. Hence, the value of 0.9 C/km^3 is a considerable overestimate of the charge which could be built up by the Wilson process during the life of an active cell, and even so, is much smaller than the value of about 16 C/km^3 required by conditions (iii) and (iv) of Section 2 (g).

As Wormell (1953) points out, the maximum possible rate at which the charging process can proceed, cannot exceed the rate at which ions are being produced in the lower atmosphere, i.e. 10 ions cm^{-3} sec.$^{-1}$, or 6 C-km^{-3}hr^{-1}. But the raindrops sweep out only a fraction of the space in which ions are being produced; in the above example the fraction would be only 3.5×10^{-3}, so that if the raindrops catch all the cloud particles encountered in their fall-paths, the charging rate would be only 2×10^{-2} C-km^{-3} hr^{-1}. This is to be compared with the average rate of 1,000 C in 20 minutes generated in a volume of about 60 km^3, i.e. 50 C-km^{-3}hr^{-1} required by conditions (iii), (iv), (vii).

It therefore appears impossible that the Wilson process can of itself separate the observed charges during the life time of a typical cell. It may well play a minor role in the charge separation process during the later stages when copious ionisation and strong fields have been produced by the primary process. It is almost certainly of importance in determining the magnitude and sign of the charge on precipitation elements reaching the ground after they have fallen through the space-charge blanket existing between cloud base and ground.

(iii) *Wall's Theory*

Wall (1948) does not accept the view that the direction in which the electric field builds up can be controlled by the normal fine-weather field—a fundamental assumption of

Wilson's theory. He also attempts to account for the fact that charge separation occurs mainly at temperatures below 0° C, by suggesting that ice crystals, rather than raindrops, are involved in selective ion capture. The initial polarising field is now attributed to the polar properties of the hexagonal plate-like crystals which, in falling with their principal axes vertical, are assumed to become dipoles, *presumably* with their undersides positively charged. These crystals, originating at temperatures below −10° C and having become polarised by their own internal field, are then assumed to separate the charge in much the same way as proposed by Wilson.

This theory rests on the assumption that ice is polar; it should therefore exhibit piezo- and pyro-electricity; Wall deduced its polar nature, not from direct experimental tests, but from observations of asymmetrical development along the *c* axis of crystals grown from the melt. Experimental tests on crystals from the melt have all failed to detect piezo- and pyro-electricity. Recently, MASON and OWSTON (1952) using very sensitive tests, have failed to detect these effects in asymmetric crystals grown from the vapour; indeed the molecular structure of ice and the randomised motion of the dipoles militates against the lattice possessing a resultant dipole moment. These are serious objections to Wall's theory which, in any case, is subject to the quantitative limitations of the Wilson theory. It appears to have few, if any, redeeming features.

(iv) *Frenkel's Theory*

FRENKEL (1944, 1946, 1947) considers that the electrification of clouds arises primarily from the orientation of the molecular dipoles at the surface of a water drop or ice crystal, giving rise to an electric double-layer with the negative ends of the dipoles directed outwards. By virtue of this surface configuration the drop (or crystal) is supposed to capture negative ions preferentially from an ionised atmosphere. In a state of statistical equilibrium, the drops are assumed to acquire a net negative charge q and a corresponding potential ξ equal to the potential difference across the electric double-layer; thus $q=a\xi$, where a is the droplet radius and $\xi=-0.25$ volt. The corresponding positive charge is left in the air in the form of large ions surrounding the drop. Gravitational separation of the positive ions and negative drops then produces a positive field, the growth of which is opposed by the migration of ions under the field setting up a depolarising current. Frenkel considers that these two effects eventually become balanced to produce a steady electric field, the total current density through the cloud then being zero. The intensity of the equilibrium field can be written

$$X=g\Big/\frac{q}{m}+\frac{\lambda g}{Nqv}=g\Big/\frac{3\xi}{4\pi a^2}+\frac{\lambda g}{Na\xi v} \qquad (4)$$

where m, a and v are respectively the mass, radius and fall velocity relative to the air, of the drop, g the acceleration due to gravity, N the number of drops per unit volume (assumed all of the same size), and λ the total conductivity of cloudy air.

If we take the liquid-water content of the cloud to be 2 g.m^{-3}, $\lambda=4\times10^{-6}$ e.s.u., $\xi=0.25$ V $\simeq 10^{-3}$ e.s.u. we have that, when $a=10\,\mu$, $X=1{,}200$ V/cm. This value is not seriously affected by assuming a higher value of λ, e.g. 3×10^{-5} e.s.u., the average value for the lower *dry* atmosphere at Kew.

The time constant of the field is approximately $3/4\pi\lambda$, i.e. 6×10^{4} sec. or 8×10^{3} sec. depending on which of the above values of λ is adopted. These figures suggest that Frenkel's mechanism, if it occurs, could produce a positive field of several volts/cm in the early, non-precipitating stages of the cloud; measurements by GUNN (1952) suggest that these fields are always less than 10 V/cm.

However, as Frenkel points out, for large drops in strong fields, the capture of ions due to the polarisation charges on the drop is a more important phenomenon. He attributes the acquisition of charge by this latter mechanism merely to the difference between the polar conductivities due to positive and negative ions, the equilibrium charge then being *positive* and of magnitude

$$q^1=\frac{\lambda_+-\lambda_-}{\lambda_++\lambda_-}\cdot Xa^2=0.13\ Xa^2,\ \left(\frac{\lambda_+}{\lambda_-}=1.3\right) \qquad (5)$$

This positive-charging mechanism therefore predominates over the negative charging process described above if $Xa > 6.4\times10^{-3}$. Thus, a drop of radius 100 μ would eventually acquire a positive rather than a negative charge in a field of 200 V/cm, while the

corresponding field for a droplet of 10 μ radius would be 2,000 V/cm. It then appears that while sedimentation of cloud droplets might, perhaps, set up an initial positive field by the Frenkel process, precipitation particles would become positively charged in the fields which exist in thunderclouds and that these, in settling out, would tend to destroy the original field.

Frenkel argues that this influence mechanism does not affect materially his primary charge separation process but may explain the fact that rain from thunderstorms is predominantly positive in sign. Nevertheless, one would expect that, on his picture, the build up of the positive field would reach a maximum in the Cu-congestus stage, before an appreciable fraction of the liquid water becomes transformed into precipitation elements which will, according to *his* influence mechanism, oppose its growth. This is inconsistent with the observation that the development of precipitation is essential to the onset of lightning activity. Moreover, as the fall velocities of cloud particles are so small, the charge which must be separated in order to produce a lightning flash must be correspondingly large. For droplets of $a = 10\,\mu$, for which $v \simeq 1$ cm.sec.$^{-1}$, generation of an electric moment of 110 C-km in 7 sec. would require separation of 8×10^5 C of charge. The maximum negative charge which a 10 μ droplet will acquire by Frenkel's process is 10^{-6} e.s.u.; assuming a concentration of 500 droplets/cm^3, we find that is a volume of 60 km^3 the maximum possible charge would be 10^4 C, but the actual charge built up during the life of the cell will be an order of magnitude less. Thus, quantitatively, Frenkel's theory is incapable of accounting for the rate of charge separation required in a thundercloud. With regard to separation of charge leading to a positive field, the maximum charge predicted by Wilson's theory exceeds that given by Frenkel for drops of $a > 50\,\mu$ in a field of 100 V/cm.

(b) *The Drop-Breaking Theory*

The electrification associated with the rupture of water drops on colliding with a solid surface was first investigated in detail by Lenard (1892). Simpson (1909), in a series of careful experiments in which he largely eliminated this "splashing" or "Lenard" effect, established that breaking of a drop in a strong vertical air jet could also produce a considerable electrification. The results were found to be sensitive to traces of impurity in the water, but, for distilled water the large fragments of the broken drops carried positive charges, while the surrounding air contained ions of both signs with an excess of negative charge. Ruptured drops of diameter about 8 mm produced, on average, a charge of 5.5×10^{-3} e.s.u., i.e. about 2.3×10^{-2} e.s.u./cm^3; with less violent shattering in conditions approximating more closely to those under which a raindrop might break-up in a thundercloud, the charge produced was slightly less -1.5×10^{-2} e.s.u./cm^3.

Zeleny (1933), using highly purified water, found that the rupture of drops in a 20 m.sec.$^{-1}$ horizontal air jet was accompanied by charges of about 2×10^{-2} e.s.u./cm^3. The negative charge communicated to the air increased quite rapidly with increasing velocity of the jet.

Chapman (1952) allowed drops of distilled water of diameter 4 mm to fall into a vertical jet of speed 17.3 m.sec.$^{-1}$. The violent disruptions were accompanied by separation of charge amounting on average to about 0.3 e.s.u. per drop, i.e. 10 e.s.u./cm^3. However, when he allowed two drops to coalesce and the resultant unstable mass to break-up into *large* fragments in a steady upcurrent of 8 m.sec.$^{-1}$, the charge generated was less than one-thousandth of the previous figure, i.e. of the same order of magnitude found by Simpson and by Zeleny.

It then appears, that the charge separated by breaking drops depends markedly on the violence with which they are shattered, i.e. the number of fragments which result. According to Simpson and Zeleny, the more pure the water the higher the charge generated; Chapman, however, found evidence for a slight increase in the charge when solutions of concentration 5×10^{-4} N. were used.

It is generally accepted that falling raindrops cannot exceed a diameter of about 5.5 mm. At this size they become distorted from the spherical, become unstable and break up into several large, and probably many more small fragments. These conclusions are based on the studies of Lenard (1904) who balanced drops of various sizes on vertical air jets of appropriate velocities. Some recent work by Blanchard (1950) has shown that the size at which drops rupture depends largely on the

scale and intensity of the microturbulence in the jet, and that the maximum stable diameter may be greater, or less than 5.5 mm, depending on these factors.

It is likely that a raindrop in falling through an updraught region of a cumulus will encounter small-scale eddies and be subjected to appreciable accelerations, but probably not as violent as those obtaining in Chapman's experiments with the high-speed jet. Even the accelerations in the experiments of Simpson and Zeleny appear severe compared with those which might be experienced by a raindrop in a thundercloud, where, according to the Thunderstorm Project, velocities of sharp-edged gusts rarely exceed 8 m.sec.$^{-1}$.

We shall therefore assume the values quoted by Simpson and by Zeleny of about 2×10^{-2} e.s.u./cm^3 as an upper limit for the charge separated by the rupture of water drops in a cumulonimbus, and enquire whether this could be a significant factor in the generation of thunderstorm electricity.

It is clear that if a positive charge resides on the large fragments of the broken drops and a corresponding negative charge is communicated to the air by ions (which may soon become captured by cloud droplets), gravitational separation will tend to confer a negative polarity on the cloud, i.e. of opposite sign to the observed polarity. It is of interest, however, to determine whether the charges generated by drop-breaking are significant in magnitude compared with those involved in lightning discharges.

We may take 4 gm^{-3} as an average value for the liquid-water content of a large cumulus, and if this is all involved at least once in drop breaking, the charge generated would be 3×10^{-2} C/km^3, assuming Simpson's value of 2.3×10^{-2} e.s u./gm. It is clear, then, that for the process of drop-breaking to be significant in the electrical budget of the thunderstorm, repeated rupture of the same mass of water would be necessary. Now, if one traces the growth of a raindrop by the coalescence process in a cumulus cloud having a base temperature of 10° C, a steady updraught of 8 m.sec.$^{-1}$ and containing the theoretical maximum liquid-water content, one finds that it is theoretically possible for it to reach a diameter of 5 mm before reaching cloud base. If, at this stage, the drop is assumed to break into fragments of radius 1 mm, the *minimum* time taken for each of these to grow again to break-up size by coalescence, is about 4 minutes. This can be seen from the following simplified and approximate calculation. The growth rate of a drop by coalescence is given by

$$da/dt = Ewv/4\varrho \qquad (6)$$

where a, ϱ, E are respectively the radius, density, and collection efficiency of the drop, v its fall-speed relative to the cloud droplets, and w the liquid-water content. Thus assuming E and w to be constant during the growth from $a = 0.1$ cm to 0.25 cm, we have

$$a - a_0 = \frac{Ew}{4\varrho} \int_0^t v\,dt \simeq \frac{Ew}{4\varrho}\, \bar{v} \cdot t \qquad (7)$$

where t is the time required for growth to break-up size. Putting $E = 0.9$, $w = 4 \times 10^{-6}$ g.cm^{-3}, $\varrho = 1$, and $\bar{v}$ the average fall speed during growth = 700 cm.sec^{-1}, t turns out to be 239 sec. Actually, this is an underestimate of the time required, because when there are a considerable number of growing rain-drops all competing for the available cloud droplets, the effective value of w will be less than that assumed here.

We have seen that only about 12 minutes elapses between the appearance of the initial radar echo from a thunderstorm and the first lightning flash, so that there is time for about only three successive ruptures of the same mass of water during this interval. The maximum possible charge which will be generated in 1 km^3 is therefore 9×10^{-2} C, which is two orders of magnitude smaller than that required by (iii) and (iv) of Section 2 (g)[1].

It has been suggested by Simpson and others that the drop-breaking mechanism might account for the appearance of the pocket of positive charge in the base of some thunderclouds, generally in the region of heaviest precipitation. Simpson describes the positive charge as having magnitude about 4 C dis-

[1] It must be pointed out, however, that no experiments have been reported which provide information on the charges liberated by drops breaking in the presence of a strong electric field. In these circumstances the separated charges might be considerably larger than those measured by Simpson and by Zeleny in view of the polarisation charges $3\,Xa^2/4$.

tributed throughout a volume of about 0.5 km^3, i.e. 8 C/km^3. This again is about 100 times larger than we should expect to be generated by the drop-breaking process, so that it appears necessary to find another mechanism to explain the origin of the lower positive charge centre. It may well arise by capture of positive ions by the drops from the upwardly-directed point-discharge current which prevails beneath thunderclouds.

(c) *Simpson's Theory of Charging by Collision of Ice Crystals*

Simpson and Scrase (1937), Simpson (1942) suggested that the main charge structure of a thundercloud could be accounted for by the production of frictional electricity during the collision of ice crystals which were assumed to receive a negative charge, the compensating positive charge being carried upwards on the cloud droplets.

Unfortunately, there is practically no direct information as to the sign and magnitude of the charge released by colliding ice crystals. Pearce and Currie (1949) have eroded a block of snow with an air blast and found the large eroded fragments to carry a negative charge, the air receiving a positive charge. Chalmers (1952) has rubbed two handfuls of snow together and allowed the fragments so produced to fall into a collector. On every occasion a negative charge was recorded, the generation of which he attributed to friction. The results of these experiments, cannot however, be applied quantitatively to the atmospheric problem, and since we can make no reliable estimate of the frequency of collisions between ice particles in a turbulent cloud mass, it is not possible to demonstrate that such a mechanism could generate and separate charge at the required rate.

There is, however, some laboratory evidence to show that when air currents of a few cm/sec. are allowed to flow past a deposit of frost grown by sublimation, small splinters are broken off the delicate dendritic crystals and carry away charges predominantly of one sign, leaving those of opposite sign on the parent crystal. Such a splintering process might well occur in clouds when snowflakes composed of delicately branded crystals collide or, they may be torn off by frictional drag with the air. Findeisen (1940, 1943) found the splinters from a growing deposit to be predominantly negatively charged and the deposit positively charged; with an air stream of 35 cm.sec.$^{-1}$ the rate of charging of the deposit was 4×10^{-16} C/cm^2 sec. Kramer (1948) found a charging rate of the same magnitude and sign in the early stages of a growing frost layer but found that later, the polarity became reversed. Kumm (1951) measured the charges on individual splinters and found positive splinters to be about 7 times as numerous as negative ones, so that the frost deposit acquired a negative charge. The average charge carried per splinter was much the same as found by Findeisen, i.e. about 10^{-15} C.

Let us take Findeisen's value of 4×10^{-16} C cm^{-2} sec.$^{-1}$ for the rate of charging and make a crude estimate of the rate of charge production by splintering in a cloud. We shall assume a frozen-water content af 1 gm^{-3} composed of snowflakes of average mass 1 mg and effective area 1 cm^2, (a high value). The charge generated per second in a volume of 1 km^3 would then be 4×10^{-4} C, i.e. about 0.5 C would be produced over a period of 20 minutes. If the fall-velocity of the flakes is assumed to be 1 m.sec.$^{-1}$, generation of an electric moment of 110 C.km in 7 sec. would require separation of 8,000 C of charge, or about 130 C per km^3. Thus, unless the splintering of ice crystals in the atmosphere is more efficient than in the above laboratory experiments, by at least two orders of magnitude, it cannot play a significant role in the generation of thunderstorm electricity. Furthermore, it is doubtful whether dendritic snow crystals form a major part of the frozen-water content during the active growth stage of the thundercloud, when falling crystals collect large numbers of supercooled droplets which freeze on contact to form pellets of graupel or hail.

(d) *The Dinger-Gunn Effect*

Dinger and Gunn (1946) have shown that when ice containing air melts the air bubbles are released, and upon breaking the surface they transfer to the adjacent air a negative charge, while the melted water retains an equal and opposite positive charge of magnitude 1.25 e.s.u./gm. This process may have relevance during the melting of graupel pellets and snowflakes. It is of the wrong sign, however, to account for the observed polarity of

thunderclouds, but may be partly responsible for the predominance of positive charge associated with steady rain and may, perhaps, contribute to the local positive charge found in the bases of warm thunderclouds. In a cloud where solid precipitation elements in a concentration of 2 gm^{-3} are approaching the 0° C level, a charge of 0.8 $C.km^{-3}$ would be developed according to the results of Dinger and Gunn.

(e) *The Workman-Reynolds Theory*

Workman and Reynolds (1948, 1950 b) have made extensive investigations of the electrical effects associated with the freezing of water and dilute aqueous solutions. They discovered that, during freezing, a potential difference developed across the ice-liquid interface, the sign and magnitude of which depended on the nature and concentration of the solute. For the majority of solutions tested the ice became negative with respect to the liquid, with important exceptions in the case of ammonium salts. The largest potential difference, −232 V, (potential of liquid with respect to ice), was obtained with a 5×10^{-5} N solution of ammonium hydroxide. Sodium chloride and calcium carbonate solutions of concentration 10^{-4} N produced potential differences of +30 V and +20 V respectively, while doubly-distilled water carefully freed of traces of ammonia showed practically no electrical effects. It appears that, during the freezing process, solute ions of one sign are preferentially incorporated into the ice, those of opposite sign being left in excess in the liquid.

Workman and Reynolds have attempted to erect a theory of charge generation and separation in thunderstorms on the basis of these laboratory experiments. The kernel of their arguments is the wet hailstone—an ice pellet which, on reaching a critical size and fall velocity determined by the temperature and liquid-water content of the cloud, commences to collect supercooled cloud droplets at a rate faster than these can freeze, and so acquires a liquid coat. The limiting factor is the rate at which the latent heat of fusion can be dispersed to the environment, the theory of which has been worked out by Ludlam (1950). Workman and Reynolds assume that hailstone will first become wet at temperatures between −10° C and −15° C and that, thereafter, only a fraction of the impinging water will become frozen, the rest being flung off in the form of *small* drops. It is further assumed that at the ice-water interface, negative ions will be preferentially incorporated into the ice, (as in the laboratory experiments with solutions of NaCl and $CaCO_3$), so that the water drops flung-off will carry away a positive charge leaving the hailstone with a net negative charge. Gravitational separation of the negative hailstones and small positive drops will then lead to a charge distribution of the observed polarity. In the non-supercooled region of the cloud, the water shed by the hailstone will carry away its excess negative charge and the authors suggest that these negative drops may be carried up to levels where they may be captured by negative hailstones, whose charge is thereby enhanced. The build up of the electric field thus becomes a cumulative process.

The two main advantages which the authors claim for their theory is that it affords a natural explanation for the centre of the negative charge being located around the −10° C level and that the charges transferred across the ice liquid interface during the laboratory freezing experiments (a maximum value of 9×10^4 e.s.u. per cm^3 of frozen NaCl solution) are of sufficient magnitude to account for the charges appearing in thunderstorms.

The assumption that hailstones will not become wet until they approach the −10° C level may be challenged. For a cloud of given temperature and liquid water content, the temperature at which an ice particle becomes wet depends largely on the density with which it is assumed to grow. Calculation shows that in a cloud with base temperature 10° C, the maximum theoretical water content and a steady updraught of 10 $m.sec.^{-1}$, an ice pellet originating at −5° C and growing with a density of 0.3 will first become wet at −25° C − i.e. 10 1/2 minutes later.

Whether the Workman—Reynolds effect has relevance to thunderstorm electrification will depend upon the contaminants present in the precipitation elements being able to give a positive water-negative ice charge distribution during freezing. Workman and Reynolds (1951) collected small hail pellets from near the 0° C level in an active thunderstorm and found them to contain $CaCO_3$

and NaCl, the concentrations of which were not, however, determined. The electrical effects associated with the re-freezing of the melted particles were erratic. When stored at room temperature, the water became *negative* as freezing began and assumed zero potential at the end of the freezing period. When stored at 0° C before freezing, the water again assumed a *negative* potential when freezing began, but became positive after about 20 sec.; thereafter the potential fell to zero at the end of the freezing period. These erratic effects were attributed to the absorption of CO_2 and its reaction with the calcium carbonate to produce soluble calcium bicarbonate. Certainly the electrical effects obtained with solutions of $CaCO_3$ and $Ca(OH)_2$ were very sensitive to the amounts of dissolved CO_2. For NaCl solutions the charging phenomena were very sensitive to the concentration of salt; while maximum charge separation was obtained with a 10^{-4} N solution, no effect at all was produced when the concentration was increased to 5×10^{-4} N. With doubly-distilled water the water became *negative* with respect to the ice during freezing, an effect which has been confirmed by Gill and Alfrey (1952) Workmann and Reynolds attribute this to the presence of small traces of ammonia.

The fact that the Workman—Reynolds effect appears to be so sensitive to the concentrations of salts and carbon dioxide and to traces of ammonia in the cloud water makes it unattractive as the main mechanism of charge generation in thunderstorms. Also, an ice particle becomes wet only when it has attained a radius of several millimetres; it then acquires a clear coat of ice to form a true hailstone and takes longer to melt than the low-density graupel. This leads us to suppose that if the Workman—Reynolds effect were the most important charge generating mechanism, thunderstorms would generally be accompanied by hail. The observational evidence, although admittedly not well documented, does not show this to be the case.

The cumulative build-up of the electric field in the manner visualised by the authors also seems open to doubt. It seems likely that most of the water accumulated by a wet hailstone will be flung off from the top-side, in the form of large drops rather than as small ones; thus their velocity of separation from the hailstones and the probability of their capture by hailstones at higher levels will be correspondingly reduced. Furthermore, in the presence of a positive field, the separation of liquid water from the negatively polarised upper half of the hailstone will tend to *diminish* the field.

(f) *Charge Separation Associated with the Formation of Rime*

A number of experimenters have, in recent years, reported that when supercooled droplets are allowed to impinge and freeze on an ice surface, the latter acquires a substantial charge. This effect is to be distinguished from that which obtains when non-supercooled water splashes off an ice surface. In the latter case it was shown early on by Faraday and later by Sohncke that the ice becomes positively charged, the rebounding water drops acquiring a negative charge; the same result has been obtained recently by Gill and Alfrey (1952).

Findeisen (1940, 1943) formed a rime layer by spraying water droplets onto a cold metal surface and found that it acquired a positive charge of order 3×10^{-13} C.cm^{-2} sec.$^{-1}$. The charging ceased if the surface became smooth and glassy, or if it became wet.

A very careful re-investigation of these phenomena has been made by Kramer (1948) who found the ice deposit acquired a *negative* charge which varied as the impact velocity of the drops; for a speed of 0.5 m.sec.$^{-1}$ the charging rate was 2×10^{-14} C.cm^{-2} sec.$^{-1}$ Findeisen assumed that the compensating charge was carried away on splinters in much the same way as for his frost deposits, (see Section 3 (c)), and some evidence for the production of charged splinters during riming was obtained by Kramer.

Lueder (1951) made experiments in natural supercooled clouds on a mountain top in order that the contaminants present in the water should be those occurring in nature. The rime was deposited on a slowly rotating metal rod which was enclosed for a part of each revolution by a Faraday cage. Its charge caused a periodic variation in the potential of an electrode. Lueder states that the growing deposit of rime acquired a very strong negative charge, an equal positive charge being communicated to the air, probably on the parts of the drops which were flung off without freezing. The charge generation was more

pronounced at lower temperatures, i.e. the more efficient and rapid the freezing process. It is not, however, easy to deduce the actual magnitude of the rate of charging from these experiments.

MEINHOLD (1951) measured the electric field strength at the surface of the fuselage of an aircraft flying at 80 m.sec.$^{-1}$ through a supercooled Cu-congestus. The deposition of rime was accompanied by a rapid rise in the field strength from about 200 V/m to 5,500 V/m in a sense which showed that the aircraft skin was acquiring a strong negative charge. From the rate of increase of the field intensity Meinhold calculated the rate of charging to be 5×10^{-12} C.cm^{-2} sec.$^{-1}$ and attributed this high rate to the high speed of impact and the rapid freezing of the droplets.

The balance of the evidence from these experiments points to the acquisition of a *negative* charge by a growing layer of rime, the rate of charging being higher the velocity of impact of the drops and the more efficient the freezing process. The outstanding contradiction is provided by Findeisen's experiment in which he claimed the rime deposit acquired a positive charge. Some difficulty may arise in the interpretation of the experimental results because of the complications connected with the rebound of some of the droplets from the ice—a process which appears to communicate a *positive* charge to the ice. It seems important, therefore, to separate the electrical effects associated with the freezing and with the rebound of droplets in these investigations.

In this respect the most satisfactory and conclusive experiments have been carried out by WEICKMANN and aufm KAMPE (1950 and private communication). Their cold body was a metal rod of diameter 5 mm placed in a cold room kept either at $-5°$ C or $-12°$ C. Water droplets of diameters 5 μ to 100 μ were sprayed on to the rod at velocities varying from 5 to 15 m.sec.$^{-1}$ The droplets in the immediate vicinity to the rod were slightly supercooled and the water content of the cloud in this region was about 4 g.m^{-3}. Thus, conditions relevant to graupel pellets or small hailstones falling in a cumulonimbus were fairly well simulated. Singly-distilled water, tap water, weak NaCl solutions and strong solutions of ammonium hydroxide and sodium fluoride were used in different experiments, but in each case the rate of charging of the rod was the same, for a given air velocity. The charge generation increased with the velocity of the air-stream, i.e. the rate of accretion of the rime, and for a velocity of 15 m.sec.$^{-1}$ attained a value of 5×10^{-12} C. cm^{-2}sec.$^{-1}$ The ice deposit on the rod showed the clear and opaque layers characteristic of hailstones, but charging stopped when the ice became wet. When water at temperatures slightly above freezing was sprayed on the rod it acquired a slight *positive* charge.

4. Conclusions

We have seen that all the theories of charge generation and separation which have been advanced during the last forty years, and which have been discussed above, are open to objection on quantitative grounds and/or because they do not fit the known facts about the meteorological and electrical behaviour of thunderstorms as listed in Section 2 (g). The only other mechanism suggested by laboratory experiments and which appears to fit, in a qualitative manner, the observed facts, is the charge generation associated with riming. The onset of lightning activity appears to coincide with the appearance of heavy solid precipitation, especially in the form of graupel. We recall that Malan and Schonland gave evidence for the negatively charged column extending up to, but not beyond the $-40°$ C level; this is consistent with the theory of charge generation accompanying the growth of graupel particles because supercooled droplets may be found at temperatures down to, but not below $-40°$ C. The fact that laboratory experiments show that during the formation of a rime layer, a negative charge is acquired by the ice and presumably an equal positive charge by the air, indicates that the growth and fall-motion of graupel pellets would bring about a charge distribution of the observed polarity.

It remains to be shown, quantitatively, that this process is capable of generating and separating the required quantity of charge in the time suggested by the electric field-change and radar data. This will form the subject of a future paper.[2]

[2] See Mason, B. T. "On The Generation of Charge Associated with Graufel Formation is Thunderstorm. Q. J. Roy. Met. Soc. 79 p. 501. 1953.

REFERENCES

Allibone, T. E., and Meek, J. M., 1938: The development of the spark discharge, *Proc. Roy. Soc.* A., **166**, p. 97.

Blanchard, D. C., 1950: Experiments with water drops and the interaction between them at terminal velocity in air. Project Cirrus. Occas. Report, No. 17.

Byers, H. R., and Braham, R. R., 1950: "The Thunderstorm", Washington, D. C.

Chapman, S., 1950: Hydrometeors and thunderstorm electricity, *Proc. Conf. on Thunderstorm Elect.*, Chicago, p. 149.

— 1952: Thunderstorm electrification studies, Cornell Aero. Lab., Report VC-603-P-1.

Chalmers, J. A., 1952: Electric Charges from Ice Friction, *J. Atmos. and Terr. Phys.*, **2**, p. 337.

Dinger, E. J., and Gunn, R., 1946: Electrical effects associated with a change of state of water, *Terr. Mag. Atmos. Elect.*, **51**, p. 477.

Elster, J., and Geitel, H., 1913: Electric charge of rain, *Phys. Z.*, **14**, p. 1287.

Findeisen, W., 1940: Über die Entstehung der Gewitterelektrizität, *Met. Z.*, **57**, p. 201.

— 1943: Untersuchungen über die Eissplitterbildung an Reifschichten, ibid., **60**, p. 145.

Frenkel, J., 1944: A theory of the fundamental phenomena of atmospheric electricity, *J. Phys. U.S.S.R.*, **8**, p. 285.

— 1946: Influence of water drops on the ionization and electrification of air, ibid., **10**, p. 151.

— 1947: Atmospheric electricity and lightning, *J. Franklin Inst.*, **243**, p. 287.

Gill, E. W. B., and Alfrey, G. F., 1952: Production of electric charge on water drops, *Nature*, **169**, p. 203.

Gunn, K. L. S., and Hitschfeld, W., 1951: A laboratory investigation of the coalescence between large and small water drops, *J. Met.*, **8**, p. 7.

Gunn, R., 1948: Electric field intensity inside natural clouds, *J. App. Phys.*, N. Y., **19**, p. 481.

— 1952: The electrification of cloud droplets in non-precipitating cumuli, *J. Met.* **9**, p. 397.

Holzer, R. E., 1950: Thunderstorms and sferics, *Proc. Conf. on Thund. Elect.*, Chicago, p. 217.

Kramer, C., 1948: Electrische ladingen aan berijpte oppervlakken, *K. Ned. Met. Inst. Med. er Verh.*, A., **54**.

Kuettner, J., 1950: The electrical and meteorological conditions inside thunderclouds, *J. Met.*, **7**, p. 322.

Kumm, A., 1951: Über die Entstehung von elektrischen Ladungen bei Vorgangen in der kristallinen Eisphase, *Arch. Met. Geophys. Biokl.* A, Vienna, **3**, p. 385.

Lenard, P., 1892: Ueber die Electrizität der Wasserfälle, *Ann. d. Phys.*, **46**, p. 584.

— 1904: *Met. Z.*, **39**, p. 249.

Ludlam, F. H., 1950: The composition of coagulation elements in cumulonimbus, *Q. J. Roy. Met. Soc.*, **76**, p. 52.

Lueder, H., 1951: A new electrical effect during the formation of soft hail (Graupel) in natural undercooled mist, *Z. angew. Phys.*, **3**, pp. 247, 289.

Malan, D. J., and Schonland, B. F. J., 151 a: The electrical processes in the intervals between the strokes of a lightning discharge, *Proc. Roy. Soc.*, A, **206**, p. 145.

— 1951 b: The distribution of electricity in thunderclouds, ibid., A, **209**, p. 158.

Mason, B. J., and Owston, P. G., 1952: Ice crystals of spiral form grown from the vapour, *Phil. Mag.*, Ser. 7, **43**, p. 911.

Meinhold, H., 1951: Die elektrische Ladung eines Flugzeuges bei Vereisung in Quellwolken, *Geofisica Pura e Applicata*, **19**, p. 176.

Pearce, D. C., and Currie, B. W., 1949: Some qualitative results on the electrification of snow, *Can. J. Res.*, A, **27**, p. 1.

Schonland, B. F. J., 1928: The polarity of thunderclouds, *Proc. Roy. Soc.*, A, **118**, p. 233.

Simpson, G. C., 1909: On the electricity of rain and its origin in thunderstorms, *Phil. Trans.*, A, **209**, p. 379.

— 1942: The electricity of cloud and rain, *Quart. J. R. Met. Soc.*, **68**, p. 1.

Simpson, G. C., and Robinson, G. D., 1941: The distribution of electricity in thunderclouds-II, *Proc. Roy. Soc.*, A, **177**, p. 281.

Simpson, G. C., and Scrase, F. J., 1937: Distribution of electricity in thunderclouds, ibid., A, **161**, p. 309.

Wall, E., 1948: Das Gewitter, *Wetter und Klima* 1, pp. 7, 65, 193.

Weickmann, H. K., and aufm Kampe, H. J., 1950: Preliminary experimental results concerning charge generation in thunderstorms concurrent with the formation of hailstones, *J. Met.*, **7**, p. 404.

Whipple, F. J. W., and Chalmers, J. A., 1944: On Wilson's theory of the collection of charge by falling drops, *Quart. J. R. Met. Soc.*, **70**, p. 103.

Wilson, C. T. R., 1921: Investigations on lightning discharges and on the electric field of thunderstorms, *Phil. Trans.* A, **221**, p. 73.

— 1929: Some thundercloud problems, *J. Franklin Inst.*, **208**, p. 1.

Workman, E. J., and Holzer, R. E., 1942: The electrical structure of thunderstorms, *N.A.C.A. Tech. Note*, No. 850.

Workman, E. J., Holzer, R. E., and Pelsor, G. T., 1942: The electrical structure of thunderstorms, *N.A.C.A. Tech. Note*, No. 864.

Workman, E. J., and Reynolds, S. E., 1948: A suggested mechanism for the generation of thunderstorm electricity, *Phys. Rev.*, **74**, p. 709.

— 1950 a: Thunderstorm research programme at New Mexico School of Mines, *Proc. Conf. on Thund. Elect.*, Chicago, p. 29.

— 1950 b: Electrical phenomena occurring during the freezing of dilute aqueous solutions and their possible relationship to thunderstorm electricity, *Phys. Rev.*, **78**, p. 254.

— 1951: Thunderstorm electricity, *New Mexico School of Mines*, Final Rep. 1951.

Wormell, T. W., 1939: The effects of thunderstorms and lightning discharges on the earth's electric field, *Phil. Trans.*, A, **238**, p. 249.

— 1953: Atmospheric electricity; some recent trends and problems, *Quart. J. R. Met. Soc.*, **79**, p. 3.

Zeleny, J., 1933: Variation with temperature of the electrification produced in air by the disruption of water drops and its bearing on the prevalence of lightning, *Phys. Rev.*, **44**, p. 837.

The Abundance of O^{18} in Atmospheric Water and Water Vapour

By W. DANSGAARD, Biophysical Laboratory, University of Copenhagen.

(Manuscript received June 10, 1953)

Abstract

Investigations into the O^{18}-abundance in the precipitation from a warm front reveal a distinct process of fractionation explainable by the unequal pressures of the saturated vapours of H_2O^{16} and H_2O^{18}.

An explanation is given of the low O^{18}-abundance in glacial waters.

A method of experimental investigation into the mechanism of the process of precipitation is discussed.

Research upon the abundance in nature of the heavy oxygen isotope, O^{18}, has been carried on persistently for several years. Before World War II the most important method of measurement was by density tests made on water. Of late, however, excellent mass-spectrometers have become available, and these have made it possible through a relatively simple measuring technique to achieve an equally good reproducibility as by the density tests; and it is possible, moreover, by a suitable procedure to obviate the correction for the deuterium content in the water —a not inconsiderable correction, which is lacking in several of the density tests published in the relevant literature.

The O^{18} tests on water, recorded in this paper, were made with a mass-spectrometer of the Nier type (*1*). For technical reasons, e.g., owing to the vacuum, it is not possible to introduce the water directly into the apparatus. It is necessary, therefore, either to electrolyze the water and introduce the oxygen—a process which is not quite satisfactory, because of the undesirable action of the pure oxygen on the filament of the ionic source—or to shake the excess of water with carbon dioxide, as in the tests here under discussion. According to COHN and UREY (*2*), oxygen atoms are exchanged between CO_2 and H_2O, to the effect that equilibrium

$$CO_2^{16} + H_2O^{18} \rightleftharpoons CO^{16}O^{18} + H_2O^{16}$$

is achieved after the lapse of 3 hours. Next, the O^{18}-abundance in the carbon dioxide is measured and made equal to the O^{18}-abundance in the water multiplied by the coefficient of equilibrium of the process stated above, which at 25° C is equal to 1.080. From this the abundance of O^{18} in the water is computed. In similar manner the abundance of O^{17} may be found, though this is rarely of any significance. It is proved that the abundance of the three oxygen isotopes

$$O^{16} : O^{17} : O^{18} = 99.76 : 0.04 : 0.20\ \%,$$

depending to some extent on the origin of the water. Technically it is of importance that one never is faced with the need to measure these absolute values directly but only to determine differences, e.g., between O^{18}-abundances in two different samples of water. The absolute values can be found by determining the difference between the sample and a standard of known O^{18}-abundance. Difference tests on samples with O^{18}-abundance approximating the normal value of 0.20 % show a reproducibility of ± 0.0001 %.

Dole, Vrooman, a.o. (*3, 4, 5*) have determined the relative O^{18}-abundances in atmospheric air and water of various origins. The tests are set out in Table 1, where the O^{18}-abundance in the fresh water from Lake Ontario is made equal to 1.000.

Table 1

	O^{18}-abundance		Ref.
	relative	%	
Water:			
Fresh water, Lake Ontario	1.000	0.1972	(5)
Atmospheric water vapour from above Lake Ontario	0.991	0.1954	(5)
Glacier water, Lake Louise	0.977	0.1927	(5)
Dead Sea water	1.020	0.2011	(5)
Ocean water	1.009	0.1990	(4)
Air:			
Atmospheric oxygen.....	1.033	0.2033	(3)
Atmospheric carbon dioxide	1.040	0.2053	(5)

The variations in O^{18}-abundance, given expression in Table 1, are explainable principally through the fact that the ratio of the pressures of the saturated vapours of H_2O^{16} and H_2O^{18}, p_0^{16} and p_0^{18}, is more than 1. By experiment, Riesenfeld and Chang (*6*) have determined p_0^{16}/p_0^{18} as:

$$\log_{10}(p_0^{16}/p_0^{18}) = 2.74/T - 0.0056 \qquad (1)$$

where T is the absolute temperature. In Fig. 1 (1) is plotted in a graph. At the temperature of 0° C $p_0^{16}/p_0^{18} = 1.01$. Conversely p_0^{18}/p_0^{16} is within the same temperatures approximately 0.99. This means that the O^{18}-abundance in vapour is obtainable ay multiplying with 0.99 the O^{18}-abundance in the water in equilibrium with the vapour. This directly explains,

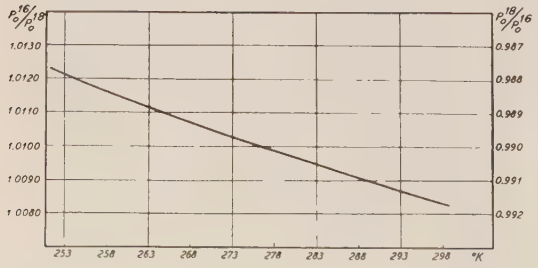

Fig. 1. The ratio of the pressures of the saturated vapours of H_2O^{16} and H_2O^{18}, $p_0{}^{16}/p_0{}^{18}$, plotted against the absolute temperature T.

first, why the O^{18}-abundance in the water vapour above the Lake Ontario is about 1 % less than in the water from the lake proper; second, that in fresh water, mainly a condensation of ocean water vapour, the O^{18}-abundance is about 1 less % than in ocean water; and third, that it is a fact, obviously, that the Dead Sea, where the affluent water is exclusively compensated by the high rate of evaporation, will attain a very high O^{18}-abundance. On the other hand, the low value for the Glacier water is not immediately explainable in a similar way.

Information on precipitation is sparse. Harada and Titani (*7*) have recorded that by observations on rains of long duration the density was higher in the beginning than at the end, and that snow-water is somewhat lighter than rainwater. Riesenfeld and Chang (*8*) explain this phenomenon by equation (1), assuming that the O^{18}-abundance in the snow is equal to the O^{18}-abundance in the vapour, and that the latter value is dependent on the temperature of evaporation only. However, the variations mentioned in this paper with reference to the O^{18}-abundance in the precipitation exceed by several times the magnitudes that can be explained exclusively from the assumptions made by Riesenfeld and Chang.

Teis (*9*) found the following variations in the density of rain falling within the same period:

Time	cc	Δ d(γ/cc)
12^h00—13^h15	75	+ 0.4
13^h15—14^h30	150	− 2.3
14^h30—15^h45	75	− 2.3
15^h45—18^h15	60	− 2.3
18^h15—19^h15	40	− 0.3

Although it is not possible to distinguish between the H^2- and O^{18}-variations the results indicate a decrease in the O^{18}-abundance in the beginning and in contradistinction to the results obtained by Harada and Titani, and increase towards the end of the period.

A certain kind of precipitation frequently occurs at the so-called warm front. So far, no explanation in detail of the mechanism of this process can be given with any certainty. However, in principle, it so occurs that warm and humid air (Fig. 2) flows upwards over

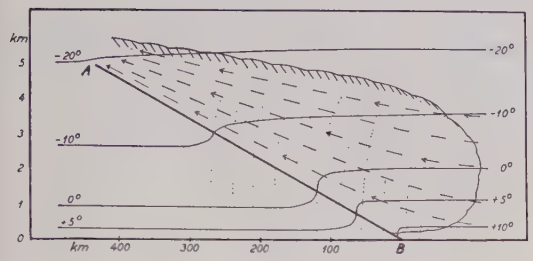

Fig. 2. Vertical section perpendicular to a warm front.

relatively cold air and is chilled so that some of its vapour is condensed. In the case of a cold front the cold air glides forward under the warm and humid air, which is carried aloft and chilled so that some of its vapour is condensed.

On June 22nd, 1952, a very strong warm front passed over the city of Copenhagen. In advance, some showers had fallen, and a cold front followed immediately upon the passage of the warm front. In the upper part of Fig. 3, plotted along the horizontal axis, are shown the atmospherie conditions prevailing at those times and in those places where the rainwater samples used in the present study were gathered. In the lower part of Fig. 3 the sections of the horizontal line indicate the time intervals within which precipitation occurred. The horizontal line-sections are set out above the time-axis at levels corresponding to the percentage excess of O^{18} in the precipitation in question compared with a certain standard. It will be seen that the rain showers which preceded the warm front show an excess of O^{18} of about 0.0023 %, whereas the rain from the upper part of the warm front is considerably lighter. Through the front (proceeding to the right in the figure) the O^{18}-abundance of the precipitation (hereinafter designated a_p) increases, and the rain falling at the point where the warm air commenced its upward motion is heavier even than the preceding showers of rain. On the arrival of the cold front a similar phenomenon occurs. However, because of the violent turbulence developed here, the conditions are so complicated that quantitative discussion is out of the question.

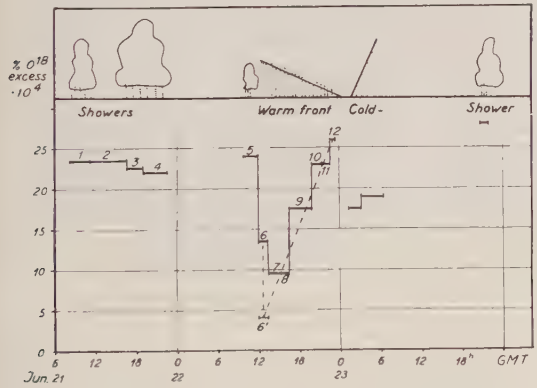

Fig. 3. The upper part shows weather conditions and structure of the atmosphere at the place and time of collections of rainwater for analysis. The horizontal line-sections in lower part of the figure indicate the time intervals during which precipitation occured. These sections are placed above the time-axis at distances which correspond to the percentage excess of O^{18} in the corresponding rainwater sample as compared with a certain standard.

Following the movement of the air upwards through the front, the drop in a_p (to the left in the figure) can be qualitatively explained through equation (1): The first rain, precipitated after the upward motion of the air had begun, according to (1), has a higher O^{18}-abundance than the vapour from which it was condensed. Hence, the remaining vapour has become lighter and the rain condensed therefrom is consequently lighter again than the first rain, and so on. There is, however, a slight increase in a_p in the rain originating from the topmost layers of the warm front. This might possibly be attributed to the fact that this rain had been subject to vigorous evaporation during the relatively long fall through the cold air.

This fact also goes to explain qualitatively the low figure for O^{18}-abundance in the glacier water, Table 1, as it may be assumed that this water exclusively came from high altitudes above the ocean surface, thus corresponding to the topmost part of the warm front.

This interpretation seems to be more likely than an earlier statement made in the literature where the low O^{18}-abundance is ascribed to an isotopic fractionation assumed to take place in the melting of the ice during which "the O^{16}-rich molecules, being the most energetic of the possible isotopic combinations, would be prevalent in the early fractions of the liquid phase" (SILVERMAN (*10*)). Regardless of the fractionation that may occur during the first part of the melting the water, for a

considerable period of time, must average an O^{18}-abundance equal to or higher than that of the precipitation, since accumulation of H_2O^{18} can not take place. The only reason possible for any difference between these two values must be ascribable to evaporation which would cause the O^{18}-abundance in the melting water to rise above that of the ice and the precipitation.

The explanation put forward in this paper find support in measurements of the O^{18}-abundance in six chunks of ice from Greenland glaciers. These chunks of ice, picked up from the sea, originated from the inland ice-cap, where the precipitation presumably falls at temperatures down to $-50°$C. The O^{18}-abundances relative to that of fresh water from lake Ontario were found be in the vicinity of 0.977 to 0.984 in good agreement with the value of glacial water given in Table 1. The ice investigated was taken from the central part of the chunks, which should preclude any possibility of exchange with sea water. Such exchange, otherwise, would contribute to an increase in O^{18}-abundance, which would also take place in the event of evaporation. Hence, the cause of the extremely low values must be looked for, exclusively, in the very great loss of moisture occurring in the air previous to the formation of the precipitation involved.

Before attempting a quantitative explanation of these conditions, it is necessary to consider more closely the mechanism of the warm front process: In the process of condensation primarily cloud droplets of diameter 10 μ are formed. From these droplets and/or from the vapour, rain drops of diameter 1 mm are formed. Observations indicate that at least in our latitudes precipitation is not likely to occur until the clouds have reached an altitude where the topmost part is at a temperature below $-10°$ C. Consequently, Bergeron (*11*) has assumed that at this temperature some ice-crystals are formed which, on account of the supersaturation of the surrounding vapour, would rapidly increase in size at the expense of the water droplets and in consequence drop down. There are, however, rain-clouds which do not extend above the 0°-isotherm, showing that rain drops can be formed in other ways than from ice-crystal-nuclei. Findeisen (*12*) and Langmuir (*13*) have investigated the possibility of producing rain drops through collisions of cloud droplets. If the droplets are not of equal size they are likely to collide in falling because of their differing velocities. It is probable, however, that a certain minimum size is required for a collision to result in the merging of two drops.

With regard to the first mentioned theory Houghton (*14*) has calculated that the time required for an ice-crystal of diameter 20 μ tc grow by sublimation to a diameter of only 200 μ would be 5 to 10 minutes in the most favourable circumstances, and that it would require several hours for its growth to the size of a rain drop (diameter 1 mm). However, the same investigator (*15*) has also calculated the time required for a droplet of diameter 30 μ to grow exclusively by collision in air containing 20 μ-droplets of the order of 1 g/m³. The result shows that 105 min. are required for the droplet to grow frow 30 μ to 20 μ,0 and only 18 min. to grow from 200 μ t theo diameter of 1 mm. From these facts Houghton concludes that it is most likely that the process of sublimation predominates in the beginning, and that the process of collision gradually assumes a greater role as the droplet or the crystal increases in growth. Since the volume increases directly with the third power of the diameter it may be concluded, further, that the greater part of the volume of water which reaches the ground as rain is formed by the process of collision.

On this basis, a picture of the formation of precipitation of the warm front, in best agreement with our present knowledge, may be drawn. Thus, AB in Fig. 2 represents the boundary between the warm air and the cold air, the warm air crossing from the right side upwards to the left side. When the cloud is chilled to slightly below the dew point (the humidity being about 102 %), the formation of cloud droplets begins. Apart from a very slow settling velocity due to gravity the cloud droplets will follow the course of the air. During the following upwards glide an increase in the number of cloud droplets occurs as a result of the continued cooling of the vapour, while a decrease in number occurs because some of the droplets either evaporate on to, or collide with, the heavier particles falling from above (ice-crystals, or else water drops). Most of the

precipitating particles develop near the $-10°$ isotherm. At that level ice-crystals are formed which during the downward drop increase in size; to begin with mainly owing to diffusion and sublimation of the vapour which is highly super-saturated relative to ice. Later, when the particles have grown considerably, their further increase is mainly due to collisions with the surrounding cloud droplets. When the cloud is dense a rain drop may grow to such an extent that it becomes unstable and splits up into two or more drops. If the air below the boundary is relatively dry, a considerable evaporation of the rain drops will take place after their departure from the cloud.

On factor of importance to the O^{18}-abundance (a_p) in the rain is the relationship between the cloud droplets and the surrounding water vapour. On the surface of the droplet evaporation and condensation are constantly going on. These two processes mutually maintain equilibrium, if the size of the droplet remains constant. At all events, however, they will cause an exchange of water molecules between the vapour and the droplet. If this exchange is extremely rapid, the O^{18}-abundance in the droplet must correspond to that in the surrounding vapour. Whereas if the exchange is extremely slow the O^{18}-abundance in the droplet will correspond with that of the vapour at the place where the droplet was formed, i.e., because of the oblique movement of the droplet, at a considerably lower level of the front. In reality the exchange goes on at a final, probably not very high, rate and consequently a precipitating particle while falling will accumulate cloud drops with an O^{18}-abundance corresponding to that of the vapour which is still at a lower level than the precipitating particle. Fig. 4 shows hypothetical tracks of particles falling through a cloud. Owing to the fact that the tracks are diverted by the wind, especially while the precipitant particle is small, the lines drawn are not vertical. The curve *d* represent the course to be taken by certain precipitating particle in order to acquire the same O^{18}-abundance as that of an actual particle, supposing the exchange between the cloud droplets and the vapour to be complete and immediate. Thus the rain collected at *C* has followed the track of *c*, while its O^{18}-abundance is representative of the H_2O^{18}-value of the cloud along the track of *d*.

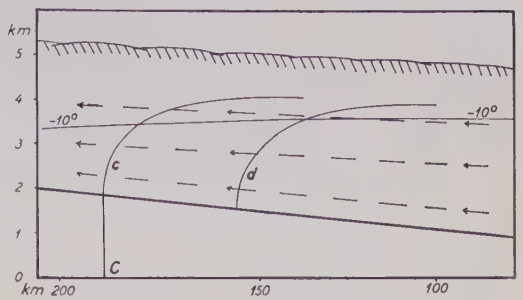

Fig. 4. Imaginary tracks of precipitant particles falling through a cloud.

In this connection it may be worth while to mention a method which, at any rate in principle, might permit us to determine what proportion of the precipitation is due to condensation and what proportion is due to collisions with cloud drops. At a certain locality in the cloud the O^{18}-abundance of the cloud droplets, the vapour and the rain drops are designated a_c, a_v, and a_p, respectively. Then a_c, according to the above, will be bigger than $1.010 \cdot a_v$ at 0° C. If the precipitation is formed exclusively through collisions, a_p will be equal to a_c. If a_p is less than a_c, the fraction, x, due to the condensation of vapour along the track, can be determined by the equation:

$$\left.\begin{aligned} & a_p = x \cdot 1.010 \cdot a_v + (1-x)a_c, \\ \text{or} \quad & x = \frac{a_p - a_c}{1.010 \cdot a_v - a_c} \end{aligned}\right\} \qquad (2)$$

Hitherto, technical difficulties by collecting separately water from cloud droplets, vapour and precipitant perticles have impeded an experimental determination of x.

Since, inter alia, x in equation (2) is unknown, a quantitative determination expressive of a_p is not possible. It is possible to solve the problem only by assuming that the distance between the tracks of *c* and *d* (Fig. 4) is 0. If so, the expression for a_p will be a function, first, of the O^{18}-abundance in the vapour before the upward glide starts ($a_p°$); second, of the average temperature

$$T_0 = \frac{1}{Q}\int t \cdot dq$$

along the track of the first released precipitating particle (t being the temperature of the small element of water and water vapour, dq, taken up by the particle in an infinitesimal section of its track, and Q being the total volume absorbed); and, third, of the corresponding temperature, T, along the track of the observed precipitation. Leaving out of consideration the assumption of the distance between c and d being 0, an expression for a_p may be deduced to give correct values for variations in the a_p along the front, if

1. in each of the tracks of precipitation in the cloud the air in rising from d to c is chilled in equal degree;
2. no evaporation takes place from the drop during its fall from the cloud to the ground.

1. presumably is satisfied in sufficiently close approximation, while 2. rarely or never is realized. Since the evaporation increases with the distance from cloud to ground, the observed difference will be less than the computed value. Hence the expression renders the maximum value for variations in a_p.

With the partial pressures of H_2O^{18} and H_2O^{16} termed p^{18} and p^{16}, Raoult's Law of equilibrium between vapour and cloud droplets makes

$$\left.\begin{aligned} p^{18} &= \frac{a_c}{100}\cdot p_0^{18} \\ \text{and} \qquad p^{16} &= \frac{100-a_c}{100}\cdot p_0^{16} \end{aligned}\right\} \qquad (3)$$

where p_0^{18} and p_0^{16} represent the vapour pressures of pure H_2O^{18} and pure H_2O^{16} respectively, and where the index, c, may be changed into p on the supposition that the part played by the process of collision is considerably greater than the part played by the condensation process.

Hence the O^{18}-abundance in vapour is

$$a_v = \frac{p^{18}}{p^{16}+p^{18}}\cdot 100$$

and after inserting (3)

$$\left.\begin{aligned} a_v &= \frac{a_p\cdot p_0^{18}}{(100-a_p)p_0^{16}+a_p p_0^{18}}\cdot 100 = \\ &= \frac{100}{\left(\frac{100}{a_p}-1\right)\frac{p_0^{16}}{p_0^{18}}+1} \end{aligned}\right\} \qquad (4)$$

whence

$$\frac{100}{a_v}-1=\left(\frac{100}{a_p}-1\right)\frac{p_0^{16}}{p_0^{18}}$$

and

$$a_p = \frac{100}{\left(\frac{100}{a_v}-1\right)\frac{p_0^{18}}{p_0^{16}}+1}\ \% \qquad (5)$$

Within the interval $258 < T < 293$ equation (1) may be approximated by the straight line

$$\frac{p_0^{16}}{p_0^{18}} = 1.03139 - 7.80\cdot 10^{-5}\cdot T \qquad (6)$$

Next re-calculating (5) we get

$$a_p = \frac{100}{\left(\frac{100}{a_v}-1+\frac{p_0^{16}}{p_0^{18}}\right)\cdot\frac{p_0^{18}}{p_0^{16}}} =$$

$$= \frac{100}{100+\left(\frac{p_0^{16}}{p_0^{18}}-1\right)a_v}\cdot a^v\frac{p_0^{16}}{p_0^{18}}$$

$$a_p \cong \frac{100}{100.002}\cdot a_v\frac{p_0^{16}}{p_0^{18}} = 0.99998\cdot a_v\frac{p_0^{16}}{p_0^{18}}$$

whence

$$a_p = (1.03137 - 7.80\cdot 10^{-5}T)a_v \qquad (7)$$

With A representing the total volume of H_2O^{18} in the M g of water vapour contained in one m³ of saturated air, we have

$$A = \frac{20}{18}\cdot\frac{Ma_v}{100}\ \text{g}$$

and

$$dA = \frac{20}{1800}(M\cdot da_v + a_v\cdot dM) \qquad (8)$$

However, dA being equal also to the condensed quantity of H_2O^{18}, we get

$$\left.\begin{aligned} dA &= \frac{20}{1800}a_p dM = \frac{20}{1800}\cdot \\ &\cdot(1.03137 - 7.80\cdot 10^{-5}T)a_v dM \end{aligned}\right\} \qquad (9)$$

From (8) and (9) we get

$$Mda_v + a_v dM = (1.03137 - 7.80\cdot 10^{-5}T)\,a_v dM,$$

whence

$$Mda_v = (0.03137 - 7.80\cdot 10^{-5}T)a_v dM =$$
$$= (c_1 - c_2 T)\,a_v\,dM,$$

and

$$\frac{da_v}{a_v} = (c_1 - c_2 T)\frac{dM}{M} \qquad (10)$$

Since M is equal to 100^3 times the density of saturated vapour or

$$M = 100^3 \frac{18}{29} 0.001293 \frac{273}{T} \frac{E}{760} = 288 \frac{E}{T} \qquad (11)$$

where E represents the pressure of saturated vapour in mm Hg at $T°$ K, we get

$$dM = 288\left(\frac{dE}{T} - \frac{E}{T^2}dT\right) = \frac{288}{T^2}(TdE - EdT) \qquad (12)$$

By Clapeyron's formula

$$dE = \frac{LdT}{T(v_1 - v_2)} \qquad (13)$$

where v_1 and v_2 respectively represent the volume of 1 g water in the vapour phase and in the liquid phase, while L represents the heat of vaporisation. Since $v_2 \ll v_1$ and

$$v_1 = \frac{1}{18}\frac{RT}{E}$$

(13) may be written

$$dE = \frac{18L}{RT^2} EdT$$

which inserted in (12) gives

$$dM = \frac{288}{T^2}\left(\frac{18L}{RT} - 1\right)EdT \qquad (14)$$

and from (10) together with (11) and (14) we get

$$\frac{da_v}{a_v} = (c_1 - c_2 T)\left(\frac{18L}{RT^2} - \frac{1}{T}\right)dT \qquad (15)$$

L however is dependent on T. In the interval $258 < T < 293$ we may with good approximation put

$$L = 745.7 - 0.550\ T = (c_3 - c_4 T) \text{ cal/g.}$$

Thereby (15) is transformed into

$$\frac{da_v}{a_v} = (c_1 - c_2 T)\left[\frac{18c_3}{RT^2} - \left(\frac{18c_4}{R} + 1\right)\frac{1}{T}\right]dT$$

or

$$\frac{da_v}{a_v} = \left\{c_1 c_2 \frac{18}{R}\frac{1}{T_2} - \left(\frac{18}{R}(c_1 c_4 + c_2 c_3) + c_1\right)\frac{1}{T} + \right.$$
$$\left. + \left(\frac{18c_4}{R} + 1\right)c_2\right\} dT = \left(C_1\frac{1}{T^2} - C_2\frac{1}{T} + C_3\right)dT$$

By integration of this expression from a_v^0 to a_v, respectively from T_0 to T, we get

$$\ln\frac{a_v}{a_v^0} = C_1\left(\frac{1}{T_0} - \frac{1}{T}\right) + C_2 \ln\frac{T_0}{T} + C_3(T - T_0)$$

or

$$\frac{a_v}{a_v^0} = e^{\frac{C_1}{T_0}} \cdot T_0^{C_2} \cdot e^{-C_3 T_0} \cdot e^{-\frac{C_1}{T}} \cdot T^{-C_2} \cdot e^{C_3 T}$$

whence

$$a_v = K \cdot e^{-\frac{C_1}{T}} \cdot T^{-C_2} \cdot e^{C_3 T} \qquad (16)$$

Finally from (7) and (16) we get

$$\log a_p = \log(1 + c_1 - c_2 T) + \log K - C_2 \log T +$$
$$+ \left(C_3 T - \frac{C_1}{T}\right)0.43429 \qquad (17)$$

From this formula (17) a_p can be determined as a function of T when once the constants have been calculated from the meteorological facts of the problem under consideration.

Based upon the Nier value, 0.2039 % for the O^{18}-abundance in atmospheric oxygen (*16*), we obtain the values shown in the third column of Table 1; thus from column 2 $0.2039\frac{1.009}{1{,}033} = 0.1990$ % for ocean water, and for vapour from ocean water, $0.1990 \cdot \cdot 0.991 = 0.1972$ %. However, because of the variation with temperature of p_0^{16}/p_0^{18}, the latter quantity to some extent depends on this variable factor. In equation (3) substituting 0 for c and regarding a_0 as the O^{18}-abundance in ocean water, equation (3) becomes valid for the partial pressures respectively of H_2O^{18} and H_2O^{16}; and substituting 0 for p in (4) this equation becomes valid for vapour from ocean water. Upon the insertion of $a_0 = 0.1990$ % and the elimination of less significant terms, we get

$$a_v = 0.1990\frac{p_0^{18}}{p_0^{16}} \text{ \%} \qquad (18)$$

Table 2 shows a_v at various vaporisation temperatures:

Table 2

t °C.	T °K	a_v %
0	273	0.1970_1
6	279	0.1970_9
13	286	0.1971_9
19	292	0.1972_7
25	298	0.1973_5
		mean 0.1972

It will be seen that a_v varies only slightly with the temperature of the sea, and if we assume the evaporation from the oceans to be $a_v = 0.1972$ %, no great error is committed.

For the warm front earlier discussed we insert in equation (17) $T_0 = 285°$ K, $a_v^0 = 0.1972$ %, corresponding to the conditions existing in the warm air at the beginning of the upward motion taken together with the values introduced in the computation, viz:

$$c_1 = 0.03137$$
$$c_2 = 7.80 \cdot 10^{-5} \text{ grad}^{-1}$$
$$c_3 = 745.7 \text{ cal/gram.}$$
$$c_4 = 0.550 \text{ cal/gram.grad.}$$
$$R = 1.9864 \text{ cal/grad.mol.}$$

and further the values derived therefrom: K, C_1, C_2 and C_3, and we get

$$\log a_p = \log (1.03137 - 7.80 \cdot 10^{-5} T) + 1.44555 - \\ - 0.76066 \log T + (4.92 \cdot 10^{-4} T - 225.89/T) \cdot \\ \cdot 0.43429 \qquad (19)$$

The variation of a_p with T is shown graphically in Fig. 5.

The altitude of the warm front, whereby is understood the distance from the ground to the topmost level of the boundary from which precipitation reaches the ground, most likely was 3.5 to 4 km in the instance mentioned. At that altitude the temperature must have been in the vicinity of -7 to $-11°$ C, assuming a saturation adiabatic rate extending upward (along the front) from an elevation of 200 m and a temperature of $+12°$ C at that level. According to Fig. 5, a fall in temperature from $+12°$ C to -7 or $-11°$ C should cause a maximum change in a_p from 0.1990 % to 0.1966 or 0.1960 %; hence, between 0.0024 or 0.0030 %; which is in satisfactory agreement with the measured value in Fig. 3: 0.0016_5 %, especially considering the fact that in the calculation the evaporation from the rain drops in falling from the cloud to the ground was not included. Drawing a straight line in Fig. 3, through the levels of collections of rain, Nos 12 to 7, we get, by a line intersecting No. 6 vertically, the value for the O^{18} excess at No. 6, $+0.0004$ %, to some extent corrected for evaporation. Thus, the measured a_p change is corrected to 0.0022 %, per cent which is in good agreement with the calculated value for the maximum change in a_p, viz: 0.0024 to 0.0030 %.

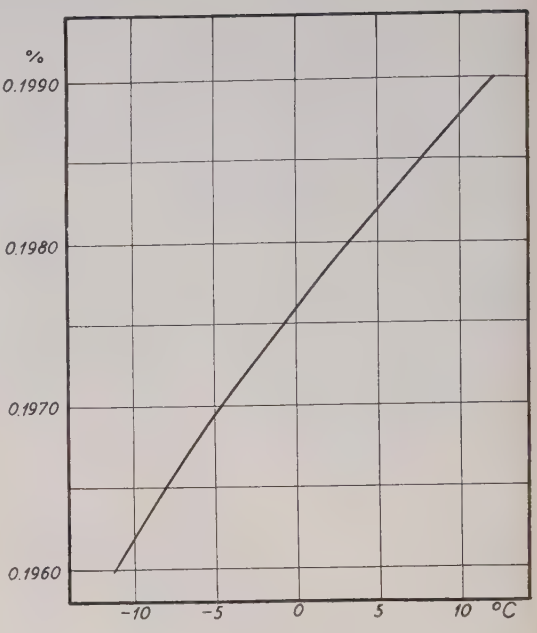

Fig. 5. The calculated variation of the O^{18}-abundance of precipitation plotted against the temperature of condensation.

However, the measured absolute values of a_p differ considerably from the values calculated here. In the warm front here discussed the a_p was found to vary between 0.1976 and 0.1959_5 %; whereas the a_p according to the calculations should have changed from 0.1990 to about 0.1963 %.

A reason for this is that the circulatory process of the water in nature is far from being so ideal as assumed in the above. Thus a_v^0 is not solely dependent on T_0 but also on the pre-history of the air. For example, the air may have absorbed some of its water vapour over solid ground, i.e., from fresh water of an O^{18}-abundance about 0.0018 % lower than in ocean water. In air of this description a_v will be less than supposed in the case discussed in the above. However, if maritime air only is considered deviations of this nature should be of slight importance.

More important is the fact that air rarely is chilled so much that the absolute humidity practically becomes to. This means that the general circulatory process, which consists of the following three processes:

1. Saturated air at T_0 (with a_v^0 as stated in Table 2) will liberate rain by cooling to $T°$;
2. The air is again heated to $T_0°$;
3. The air is saturated with water vapour at $T_0°$;

will alter the a_v considerably, bacause the a_v remaining in the air after process 1. will be less than a_0^0. When the air in process 3. has absorbed a certain quantity of water vapour of O^{18}-abundance a_v^0, the a_v for the total quantity of vapour must also be less than a_v^0.

Such a fall in a_v naturally cannot proceed indefinitely. Since the air continually passes through circulatory processes, an equilibrium has been established where the final a_v on an average is just so much below the values stated in Table 2 that the decrease in a_v during process 1. is balanced by the increase in a_v during process 3. The final mean value of a_v is dependent on the climatic and geographic conditions.

A third reason for the disagreement in the absolute values is, no doubt, the fact that the warm air in question had given off moisture before starting the upward movement at Copenhagen.

However, the significant part of this investigation is that these considerations have no effect on the agreement between the computed and the measured, corrected *changes* in a_p. Actually, the insertion in (17) of a value for a_v^0 differing 0.0014 ‰, from the value earlier used makes no essential difference in the calculated a_p changes.

Further investigations into these problems will be discussed in a later paper.

REFERENCES

1. *Symposium*, 1948: Preparation and measurements of isotopic tracers, Ann. Arbor.
2. Cohn, M., and H. C. Urey, 1938: Oxygen exchange reactions of organic compounds and water, *J. Am. Chem. Soc.*, **60**, 679.
3. Dole, M., 1935: The relative atomic weight of oxygen in water and air. Ibid., **57**, 2731.
4. Green, C. H., and R. J. Voskuyl, 1936: Explanation of the relatively large concentration of O^{18} in the atmosphere. Ibid., **58**, 693.
5. Vrooman, R. H., 1948: M. Sc. Thesis, Mc Master Univ., Canada.
6. Riesenfeld, E. H., und T. L. Chang, 1936: Dampfdruck, Siedepunkt und Verdampfungswärme von HDO und H_2O^{18}. *Z. phys. Chem.*, B. 33, 127.
7. Harada, M, and T. Titani, 1935: Isotopic composition of rain and snow water. *Chem. Soc. Japan*, Bull. 10, 206 and 263.
8. Riesenfeld, E. H., und T. L. Chang, 1936: Über den Gehalt an HDO und H_2O^{18} in Regen und Schnee. *Ber. deut. Chem, Ges.*, **69**, 1305.
9. Teis, R. V., 1939: Isotopic composition of rain water. Akad. Nauk., SSSR, Doklady, **23**, 674.
10. Silverman, S. R., 1951: The isotopic geology of oxygen. *Geochim. et Cosmochim. Acta*, **2**, 26.
11. Bergeron, T., 1933: On the physics of clouds and precipitation. Proc., 2, 156. Int. geod. geophys. Un., fifth general assembly, Lisbon.
12. Findeisen, W., 1930: Messungen der Grösse und Anzahl der Nebeltropfen zum Studium der Koagulation in homogenen Nebel. *Beitr. Geophys.*, **35**, 295.
13. Langmuir, I., 1948: The production of rain by a chain reaction in cumulus clouds at temperatures about freezing. *J. Meteor.*, **5**, 175.
14. Houghton, H. G., 1951: On the physics of clouds and precipitation. Comp. of Meteor., p. 176, Boston, Mass.
15. Houghton, H. G., 1951: On the physics of clouds and precipitation. Comp. of Meteor., p. 176, Boston,
16. Houghton, H. G., 1950: A preliminary quantitative analysis of precipitation mecanisms. *J. Meteor.*, **7**, 363.
17. Nier, A. O., 1950: A redetermination of the relative abundances of the isotopes of C, N, O, A, and K.

A Note on the Chemical Composition of Rainwater

By W. A. MORDY, Honolulu, T. H.

(Manuscript received June 21, 1953)

Abstract

A limited number of observations of nitrogen, sodium and chloride in rainwater made in Hawaii are presented. Because of frequent and high rainfall, calculations of the annual amounts of nitrogen received in various Island localities are rather large. In one storm nitrogen was brought down by rainfall at a nearly constant rate although rainfall intensity varied considerably.

In general, the concentrations of these elements in Hawaiian rains agree with observations in other oceanic areas.

In view of the current interest in atmospheric nitrogen, Dr C. G. Rossby recently asked me to submit to the readers of Tellus some observations of nitrogen and other chemical constituents in rainwater in Hawaii.

During March and April 1953, several samples of rainwater were collected and analyzed for nitrogen content. Total nitrogen (ammonia and nitrate) was determined by distillation in the presence of alkali and Devarda's alloy, reducing the nitrate to ammonia. Ammonia in the distillate was nesslerized and the color was measured on an Evelyn photo-electric colorimeter.

The results of these determinations are shown in Table 1. It appears that these figures

Table 1

Date	Time[1]	Elapsed Time	Rate of Collection	Rainfall Intensity	Volume of Sample	Total Rain for Day	Total N [2] NH_4-NO_3-N	N/min	Na [3]	Cl [4]
		min	cm^3/min	mm/h	cm^3	cm	mg/l	g/min	mg/l	mg/l
3/11/53	9: 34—9: 37	3	220	13.2	660		.16	35.2		
	9: 38 3 4									
	9: 43 1/2	4—3/4	97	5.9	460	1.19	.11	10.6		
3/27/53	14: 24—14: 27	3	188	11.3	566	.47	.08	15.1		
4/22/53	14: 45—15: 10	25	38	1.8	740		.51	15.1	2.8	4.8
	15: 12—15: 43	31	23	1.4	715		.39	9.0	1.4	3.0
	15: 44—15: 55	11	65	3.9	720		.10	6,6	.6	.6
	16: 08—16: 25	17	35	2.1	591		.24	8.4		
	16: 28—17: 30	62	11	.7	707	.35	.66	7.5	2.0	2.0
							Av=.28			

[1] Hawaiin Standard Time=150th Meridian Time.
[2] Nitrogen Determined by Distillation and Colorimetry.
[3] Sodium Determined by Flame Photometer.
[4] Chloride Determined by Titration.

Published with the approval of the Director as Technical Paper No. 218 of the Pineapple Institute of Hawaii.

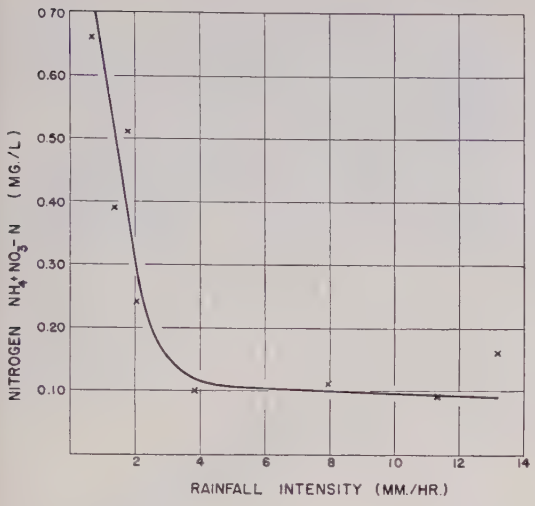

Fig. 1. Relationship of rainfall intensity to rainwater nitrogen content for 8 samples of rainwater collected in Honolulu for March 11 to April 22, 1953.

are in good agreement with the figures found elsewhere in ocean climates, ERIKSSON (1952). They are somewhat lower than the figures that ÅNGSTRÖM (1952) indicated should be found for rainfall from tropical air masses, and the relationship which he suggests concerning the decrease in the rate of collection of nitrogen as the rainfall endures, is not borne out in the one test of it here on April 22 where five consecutive samples were obtained.

An inverse relationship between nitrogen content and rainfall intensity appears to exist in these data. Only one observation, the first on March 11, 1953, lies away from the line sketched in on the scatter diagram, Fig. 1. If the nitrogen is absorbed by the rainwater in a washing action of the rain an inverse relationship might be expected. Such a relationship also might be expected to show better in these data from Hawaii due to the nature of the rainfall. These samples were of orographic rainfall collected at the meteorological observatory on top of the Hawaiian Sugar Planters' Association Experiment Station 4 miles (6 km) leeward from the crest of the Koolau Mountains, Fig. 2. Because the rainfall was orographic it can be considered essentially stationary with new air pouring into the rainy zone with the speed of the wind.

Fig. 2. Location of meteorological observatory Experiment Station of Hawaiian Sugar Planters' Association, where rainwater samples were collected. Rainwater was collected orographic rainfall 4 miles (6 km) leeward from the crest of the Koolau Mountains.

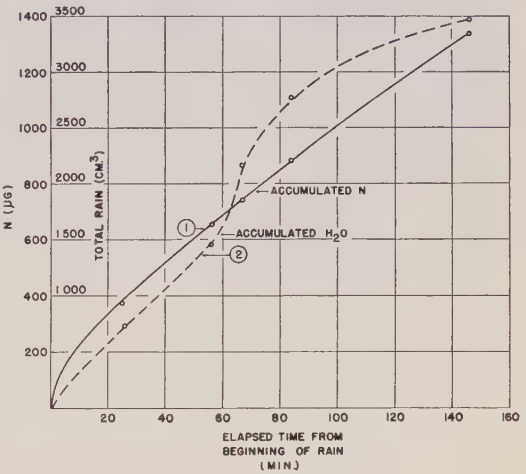

Fig. 3. Rate of accumulation of nitrogen (curve 1) with the accumulation of rainwater (curve 2), on April 22, 1953. The rate of accumulation of nitrogen per unit time appears to be quite constant, while the rate of accumulation of rainwater as a result of changes in rainfall intensity is quite different.

If the air contains only a fixed amount of nitrogen which can be brought down by the rain, then the rainwater from the higher intensity rains will contain less nitrogen per unit volume of water than the lower intensity rain. Such reasoning would also require, of course, that the washing efficiency of high and low intensity rains be nearly the same.

The amount of nitrogen accumulated in the rainwater per unit time has been examined with this reasoning in mind. In Fig. 3 are graphs of the accumulated nitrogen and the

accumulated rainfall after a given elapsed time from the beginning of the rainfall. It is interesting to see that the rate of nitrogen accumulation (slope of curve 1) seems fairly steady for a two hour period, while the rate of rainfall (curve 2) accumulation varies significantly. This is interpreted by the author, somewhat intuitively, to mean that the nitrogen exists as a limited supply in a given volume of the atmosphere and is almost completely brought down from the air through which the rain falls.

A further point of interest lies in the relationship between the nitrogen and sodium or chloride determinations. Sodium and chloride determinations have been made on a number of rainfall samples in cloud physics studies during the past year. Variations in the latter elements have been accounted for by postulating the role the sea salt particles in the atmosphere play in the formation of raindrops, (Woodcock 1951, Blanchard 1952). It is interesting therefore to compare the amounts of nitrogen with the sodium and chloride determinations to determine:

1. If the nitrogen in the rainwater could be directly from the sea as it has been reasoned the salt is;
2. If the nitrogen and salt exist as particles in the air which might be washed down rather than the salt being the nucleus for raindrops.

If the nitrogen and sea salt get into the rainwater by the same route from the sea, then the ratio of salt to nitrogen should be relatively the same in rain and sea water or at least the amounts of nitrogen and chlorides should be strongly correlated. This is not the case since the nitrogen to chloride ratios in the rainwater exceeds roughly 1,000 times the nitrogen to chloride ratio in sea water (Sverdrup 1946).

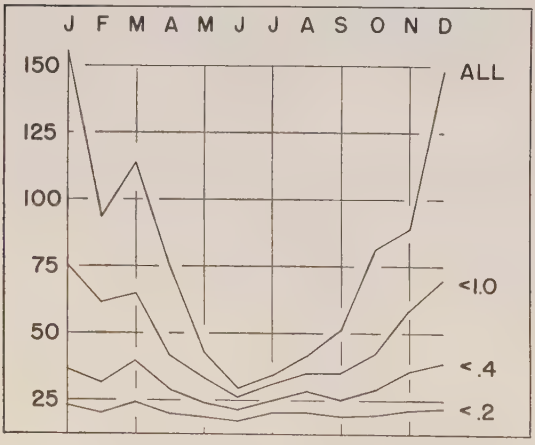

Fig. 4. The amount of rain at the Honolulu Weather Bureau office for the years 1909 to 1949 inclusive, which resulted from rains of 0.2 in. (0.51 cm) or less, 0.4 in. (1.02 cm) or less, 1 in. (2.54 cm) or less per day, and the total rain received for the 39 year period by months. Rains of less than an inch per day account for more than half the total rainfall.

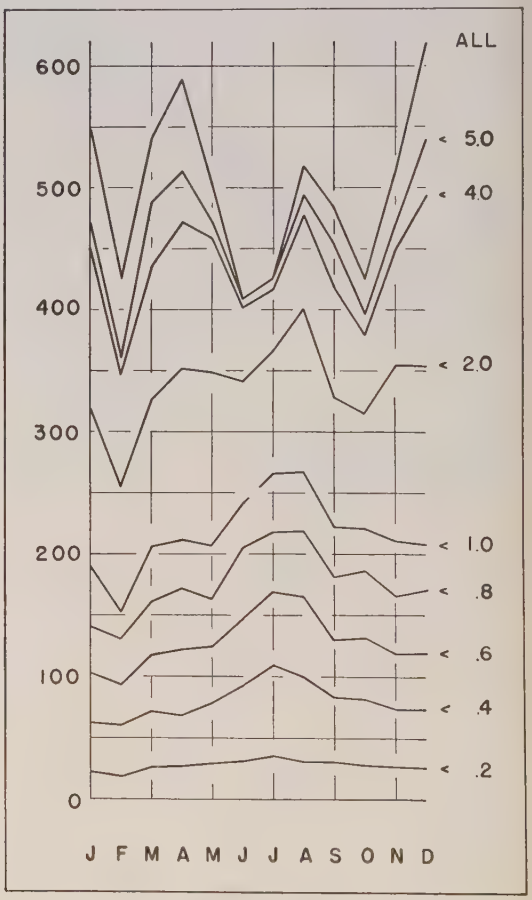

Fig. 5. Rainfall at Nuuanu Dam No. 4 (average rainfall 150 in.) which has resulted from rains of various amounts per day. Rains smaller than 1 in. (2.54 cm) per day count for approximately half of the total rainfall.

Secondly, if the nitrogen and salt were part of the same particles, or separate particles subject to the washing action of the rain the ratio of nitrogen to salt in the different rainfall samples taken within relatively short periods of time should be fairly constant. In the four April 22 cases in Table 2 where this comparison can be made, this is not the case.

The amount of nitrogen which arrives in the soil as a result of rainfall is a main point of interest. In view of the apparent inverse relationship between rainfall intensity and nitrogen content, some rough calculations can be performed which are likely to be conservative, since the rainfall was in each case heavier than the median rainfall and similarly of greater intensity.

To perform these calculations it is helpful to look first at monthly frequency distributions of two rainfall stations, the Honolulu U.S. Weather Bureau office with 30 inches (76 cm) average annual rainfall, and Nuuanu Dam No. 4 with 150 inches (381 cm) average annual rainfall, on the Island of Oahu. These distributions are different from the usual representation of such data in that they show the amount of the total rainwater which is received by each category of rainfall (Figs 5, 6). It can be seen that daily rains which are one inch or less comprise over half the total rainfall for the thirty inch station, and rains of one inch or less similarly comprise over half the total rainfall at the 150 inch station.

In another study the author has examined the rainfall from a number of such stations and found that in general the increase in rainfall in the wetter areas of the island is due to increased frequency of smaller rains particularly, although of course the frequency of all intensities of rain is greater.

These statements are intended to help show that if we calculate nitrogen arriving on the surface of the land by using the figures from the graph in Fig. 1 or by using the average nitrogen figure of .28 from Table 1, we are likely to arrive at a result somewhat less than the actual, the *average* nitrogen/unit vol. figure producing the lower value of the two for nitrogen per unit area.

Using the average value of nitrogen/unit vol. from Table 1, the results obtained were:

Table 2

Average Rainfall		Calculated Kg N/Ha/year
Inches	cm	
30	76.2	2
100	254	7
200	508	14
400	1 016	28
600	1 524	43

Later, more meaningful calculations can be made when more data have been assembled showing the relationship of nitrogen to raindrop size, rainfall intensity, and daily rainfall.

However, in lieu of these calculations it is interesting to examine some unpublished observations of monthly amounts of nitrogen in rain water made here at the HSPA Experiment Station (38 inches annual rainfall) and the HSPA Manoa Arboretum (160 inches annual rainfall), Fig. 2, by L. R. Smith in 1935—36. These data are shown in Table 3.

The methods which Smith used in his determinations are subject to some criticism. 1) The use of zinc in his alkaline distillation was likely to reduce some of the nitrate present to ammonia. The ammonia values therefore may be too high. 2) No provision was made to remove chlorides. In the presence of chlorides and upon the addition of concentrated sulphuric acid in the phenol-disulfonic acid reagent, nitrate may have been lost by reduction to gaseous nitric oxide. Nitrate values may then be too low. The magnitude of the gain in ammonia and the loss in nitrate is of course speculative. Assuming that these errors are compensatory, then the total nitrogen values may not be too greatly in error. It can be seen that the estimates of nitrogen from the average determinations is low for the Makiki case and high for the Manoa station.

As a final point of discussion, one factor stands out in Eriksson's table of values of nitrogen determinations for various parts of the world. This is the near uniformity of the low values which have been obtained in isolated oceanic regions. There appears to be little difference between areas of frequent storms where electrical discharges would not be uncommon and areas such as Hawaii where a thunderstorm or lightning discharge is very

Table 3

1936—1937	Manoa Arboretum		Rainfall	Total N for Month	Makiki Experiment station		Rainfall	Total N for Month
	NH_3N	NO_3N			NH_3N	NO_3N		
	Kg/Ha	Kg/Ha	Cm	Kg/Ha	Kg/Ha	Kg/Ha	Cm	Kg/Ha
September	.14	.27	53.59	.41	.28	.05	7.01	.33
October	.53	.25	52.83	.79	.23	.15	29.26	.37
November	.97	—	19.33	.97	.15	.06	6.99	.20
December	.19	.14	52.02	.33	.89	.09	17.73	.98
Januari	.55	.36	70.28	.92	.21	.21	21.36	.43
February	—	—	41.63	—	.80	.23	18.85	1.03
		Total 5 months		3.42		Total 6 months		3.34

infrequent. Although the proportion of nitrogen in the rainwater is fairly constant from one ocean area to another, the amount and frequency of rainfall, of course, is very different. Hence the distribution of nitrogen brought down by the rainfall over different parts of the world should be very uneven indeed.

A continuing program of nitrogen observations is planned to attempt to relate nitrogen with drop size, rainfall intensity, character, and the general weather synopsis.

Acknowlegment

The author is indebted to Mr H. Y. Young for the chemical analyses of the rainwater and Mr T. Hayashi who collected the rainwater samples.

REFERENCES

Ångström, A., and Högberg, L., 1952: On the content of nitrogen (NH_4N & NO_3N) in atmospheric precipitation. *Tellus* **4**, *31—42*.

Blanchard, D. C., 1952: Sea-salt nuclei studies. Part II —Precipitation studies, periodic status, report No. 4, *Woods Hole Oceanographic Institution*.

Eriksson, E., 1952: Composition of atmospheric precipitation. I and II. *Tellus* **4**, *215—323, 280—303*.

Sverdrup, H. V., Johnson, M. W., and Fleming, R. H., 1946: The Oceans, 176.

Woodcock, A. H., 1951: Atmospheric salt particles and raindrops, *Journal of Meteorology* **9**, 200—212.

On the Production of Mean Zonal Currents in the Atmosphere by Large Disturbances

By HSIAO-LAN KUO, Massachusetts Institute of Technology[1]

Manuscript received July 22, 1952. Revised manuscript received June 2, 1953

Abstract

The problem of the production of mean zonal currents by large-scale horizontal disturbances in the atmosphere is attacked by computation of time-tendencies from the vorticity equation. It is shown that the earth's rotation, acting through the variable Coriolis parameter, generally produces a mean northward transport of westerly momentum, with the maximum transport occurring south of the middle of the zonal belt occupied by the disturbances, and therefore creating mean westerly and easterly currents in the central and outer parts respectively. Its effect on the disturbance may either be a damping or an amplification, depending on the asymmetry of the mean flow profile.

Six different mean flow profiles have been investigated to determine the nature of the interaction between a disturbance and the mean flow. For three profiles with inflection points, the interaction depends upon the wave length of the disturbance. If the wave length is longer than a critical value, an amplifying effect on the disturbance is produced accompanied by a divergence of westerly momentum in the region of maximum mean flow, and if shorter, a damping effect with a convergence of westerly momentum. On the other hand, the interaction produces only a damping effect for three mean flow profiles without inflection point.

Since the zonal currents in the atmosphere are seldom very strong and not far from symmetrical, the total effect of the earth's rotation and of the mean flow leads to horizontal damping, in which the contrast in the mean flow at different latitudes is increased and a mean northward transport of westerly momentum is produced. This is in qualitative agreement with observations, indicating that these factors are of real importance in the development and maintenance of the mean zonal flow.

1. Introduction

In previous studies, the author has discussed the mechanism of the mean meridional transport of westerly momentum by large-scale atmospheric disturbances (Kuo, 1951 a, 1951 b), based on the properties of solutions of the linearized vorticity equation for horizontal, inviscid, barotropic, non-divergent flow. This will again be our subject. Although vertical motion and baroclinicity in the atmosphere are of paramount importance in some other aspects of the meteorological problem, it is believed that the omission of such factors does not significantly distort the average interactions between the purely horizontal components of the large-scale disturbances on the one hand and the mean flow and the earth's rotation on the other, as can be demonstrated by integrating the equations along the vertical with respect to pressure, or by comparing the simple vorticity equation with the general differential equation for quasi-geostrophic flow. In previous studies,

[1] The research reported in this document has been made possible through support and sponsorship extended by the Geophysics Research Division of the AF Cambridge Research Labs, AMC, U.S. Air Force, under Contract No. AF 19—122—153. It is published for technical information only and does not represent recommendations or conclusions of the sponsoring agency.

the classical eigenvalue (perturbation) method was used, where the disturbances are assumed to be harmonic both in the coordinate x and in time t, so that each fundamental harmonic is represented by a function of the type $f(y)\exp(ik(x-ct))$. The problem is then to find the permissible values of c (the eigenvalues) and the function $f(y)$ (the eigenfunction) for different wave numbers k and a given mean flow profile $U(y)$. Using this method it was possible to find some general properties of the disturbances related to the nature of the mean flow without actually solving the eigenvalue problem for each k and U. It was shown that if the absolute vorticity of the mean zonal flow has extreme values in the zone considered, and increases with latitude where the mean zonal velocity U is large and decreases with latitude where the mean zonal velocity U is small, the linear vorticity equation permits solutions with non-vanishing real exponential time factor (c is complex). In this case, disturbances of wave length shorter than a certain value will decrease exponentially with time and are therefore "damped"[1], and those longer than the critical wave length will increase exponentially, i.e., "amplify". The effect of the damped shorter disturbances is, in the mean, to transport zonal westerly momentum from regions of weaker to regions of stronger mean zonal flow, thereby accentuating the contrast in the existing zonal flow, leading to the development of a sharper jet type mean flow profile. The effect of the amplifying disturbances is in the reverse direction, flattening the existing mean flow profile.

If, on the other hand, the absolute vorticity of the mean flow does not have an extreme value, then no such eigenvalues exist for the inviscid vorticity equation. The failure of the eigenvalue method for this case is due to the assumption of a particular harmonic time dependence, which is a very restrictive assumption. If the problem is one relating merely to the stability or instability of steady mean flows which can be established in a real fluid, it is natural to take viscosity into consideration, whereupon the difficulty is removed and definite results can again be obtained by the eigenvalue method. Thus in the case mentioned above, most of the small disturbances will be damped in a flow of very high Reynolds number.

However, the inclusion of viscosity seems somewhat artificial when treating the large-scale motions of the atmosphere, since the Reynolds number is very large and the motion of a nonviscous fluid should also remain determinate. Furthermore, although a mean zonal current almost always exists, large disturbances are also invariably present; a purely zonal steady state flow has rarely been observed. Thus, in considering the production of zonal motions by large disturbances, we are confronted by an inherently nonlinear process, therefore, the question of the validity of the perturbation method arises in addition to the difficulties in its application mentioned above. Furthermore, in discussing this process, we are less concerned with the stability or instability of the existing mean flow, which are difficult to define when the disturbances are finite, than with the effects of the interactions between the disturbances and the mean flow or the earth's rotation. In view of these difficulties confronting the perturbation method, it becomes most desirable to approach this problem by another method.

The method to be used in the present investigation is to assume the existance of a mean flow and of certain disturbances and to compute the subsequent changes from the nonlinear vorticity equation. This method is similar to the one used by TAYLOR and GREEN (1937) in their study of the production of small eddies. The same method has also been used by PLATZMANN (1952) in a recent paper. In principle, the general solution corresponding to a given initial condition can be found by repeating the process and expanding the quantities in a Taylor's series in t. However, there is the question of convergence of the series, and it is found that the labor involved in obtaining the higher derivatives becomes prohibitive even for very simple initial disturbances. We must therefore be satisfied with only one or two terms in the expansion. But since we are not particularly interested in the

[1] The term "damped" and "amplified" are used, as in the previous investigations on horizontal non-divergent motions, merely to describe the interactions between the horizontal disturbances and the mean flow or the earth's rotation; they need not be identified with actual changes of any disturbance in the atmosphere, since these disturbances may be produced by the factors that have been neglected.

instantaneous rate of change, but in the end effect of the interaction, the question arises as to whether the single term represents only a transient effect.

Still another difficulty arises in the general interpretation of the results obtained from a specific model. Since the behavior of a disturbance is directly and continuously reflected in the form of the disturbance, the result obtained for any one disturbance is valid only for that disturbance. This difficulty is absent in some measure in the eigenvalue solutions, as both the time dependence of the solutions and the forms of the fundamental modes of the disturbances are determined by the eigenvalues and the eigenfunctions, so that all effects can be attributed to the character of the mean flow and to the scale of the disturbance. This is precisely what we would like to do in our present study. We must therefore attempt to eliminate those effects that are the result of the particular form of the initial disturbance.

One way of eliminating the effects that depend mainly on the initial form of the disturbance is to consider arbitrary or random disturbances, which may be expressed as a Fourier series in x and y. So far as the effect of earth's rotation is concerned, we are able to extend the results to the general initial disturbance and demonstrate that whenever the disturbance is not represented by the exactly neutral solution of the vorticity equation, it always produces a mean northward transport of zonal momentum in almost all parts of the belt (northern hemisphere) except near the northern boundary, where a reverse transport may occur. On the other hand, no such generalization is possible regarding the interaction between the disturbance and the mean flow, which actually depends both on the form of the disturbance and on the type of mean flow, and therefore may change direction. We therefore choose only one simple initial wave-disturbance for the study of this effect, which initially does not produce a mean momentum transport. However, we shall take it to be different from the exactly neutral disturbances if such disturbances exist, either by taking a different amplitude function or by taking an arbitrary wave length so that some change will be produced later. Since all these initial changes are produced by the linear terms of the vorticity equation, the results obtained should be comparable with those obtained from the linear vorticity equation, at least qualitatively. It should be emphatically remarked that as no energy source is included in the simple vorticity equation, we merely assume the existence of an arbitrary disturbance rather than to identify it as given by the neutral solutions of this equation.

2. The production of mean zonal currents on a rotating earth.

Let us assume that in the atmosphere there exist disturbances at the initial moment, presumably produced through some external processes such as differential heating or the release of potential energy but which are now left to be controlled by the simple vorticity equation for nondivergent, barotropic, horizontal flow.

For motions over a spherical earth this controlling equation may be written

$$\frac{\partial \zeta}{\partial t} + \frac{u}{R\cos\varphi}\frac{\partial \zeta}{\partial \lambda} + \frac{v}{R}\frac{\partial}{\partial \varphi}(\zeta + f) = 0 \quad (2.1)$$

where λ and φ are the longitude and latitude, $f = 2\omega \sin\varphi$ is the Coriolis parameter, R the radius of the earth, u and v are the linear west—east and south—north velocity components and ζ is the vertical component of the vorticity of the motion, respectively. For this motion, a stream function ψ can be introduced, defined by

$$\left.\begin{aligned} u = R\dot{\lambda}\cos\varphi &= -R\frac{\partial \psi}{\partial \varphi}, \\ v\cos\varphi = R\dot{\varphi}\cos\varphi &= R\frac{\partial \psi}{\partial \lambda} \end{aligned}\right\} \quad (2.2)$$

where $\dot{\lambda}$ and $\dot{\Phi}$ are the velocity components in angular measure. In terms of this stream function and the new independent variable $\eta = \sin\varphi$, the vorticity equation (2.1) takes the symmetrical form

$$\frac{\partial \nabla^2\psi}{\partial t} = \frac{\partial \psi}{\partial \eta}\frac{\partial \nabla^2\psi}{\partial \lambda} - \frac{\partial \psi}{\partial \lambda}\frac{\partial (\nabla^2\psi + f)}{\partial \eta} \quad (2.3)$$

where the symbol ∇^2 denotes the two-dimensional Laplacian operator in spherical coordinates and $\nabla^2\psi$ is proportional to the relative vorticity,

$$\nabla^2\psi \equiv \frac{1}{\cos^2\varphi}\frac{\partial^2\psi}{\partial\lambda^2} + \frac{\partial}{\partial\eta}\left[(1-\eta^2)\frac{\partial\psi}{\partial\eta}\right] \equiv R^2\zeta \tag{2.4}$$

To avoid complications, we at first study the simple initial disturbance with only one wave-component and north—south trough- and ridgelines, such that no mean momentum transfer is produced at the initial moment, and then extend the treatment to the more general disturbance with several wave-components and with tilted troughs and ridges, i.e., to the most general disturbance represented by

$$\psi = \sum_{m=0}^{\infty} H_m(\eta, t)e^{im\lambda} \tag{2.5}$$

where H is generally complex.

Since the amplitude of the waves varies, we shall now consider the proper boundary conditions that should be applied to the motion.

From symmetry considerations, it seems natural to assume that there is no momentum flux across the equator, which can be satisfied by requiring either u or v to be zero. We shall assume v is to vanish, which requires the vanishing of the amplitude functions identically along the equator. We note that the parts of the north—south velocity from the wave-components with m larger than 1 must be zero at the pole, since the corresponding components of the stream function are symmetric about this point. For the component $m=1$, the corresponding stream function is not symmetric about the pole, and there is one stream line which cuts through this point, therefore v is finite. This represents a single vortex centered off the pole. Therefore, we must require that the Fourier-component of v with $m=1$ to be finite and all the other components with $m \geq 2$ to vanish at the pole, if this point is to be included in the region of consideration. This requires the functions $(1-\eta^2)^{-\frac{1}{2}} H_m(\eta, t)$ to be finite for $m=1$ and to be zero for all $m \geq 2$. In this section, we shall concentrate on the effect of the earth's rotation, and therefore assume that there is no basic current.

a. *A simple wave disturbance.* We first discuss the motion given by

$$\psi_0 = aF_m(\eta)\sin m\lambda \tag{2.6}$$

where $F_m(\eta)$ satisfies the boundary conditions. Substituting in (2.3), we get

$$\nabla^2\frac{\partial\psi}{\partial t} = -2\omega maF(\eta)\cos m\lambda + \frac{ma^2}{2}w(\eta)\sin 2m\lambda \tag{2.7}$$

where

$$w(\eta) \equiv \frac{dF}{\partial\eta}\frac{\partial}{\partial\eta}\left[(1-\eta^2)\frac{dF}{d\eta}\right] - F\frac{d^2}{d\eta^2}\left[(1-\eta^2)\frac{dF}{d\eta}\right] + \frac{2m^2}{(1-\eta^2)^2}\eta F^2$$

Therefore, the solution $\frac{\partial\psi}{\partial t}$ must be of the following form

$$\frac{\partial\varphi}{\partial t} = 2\omega ma\gamma(\eta)\cos m\lambda + \frac{ma^2}{2}Z(\eta)\sin 2m\lambda \tag{2.8}$$

where γ and Z satisfy the differential equations

$$\frac{d}{d\eta}\left[(1-\eta^2)\frac{d\gamma}{d\eta}\right] - \frac{m^2}{1-\eta^2}\gamma = -F \tag{2.9 a}$$

$$\frac{d}{d\eta}\left[(1-\eta^2)\frac{dZ}{d\eta}\right] - \frac{4m^2}{1-\eta^2}Z = W \tag{2.9 b}$$

and the boundary conditions

$$\left.\begin{aligned}(1-\eta^2)^{-\frac{1}{2}}\gamma = 0,\ (1-\eta^2)^{-\frac{1}{2}}Z = 0\\ \text{for } \eta = 0 \text{ and } \eta = 1\end{aligned}\right\} \tag{2.9 c}$$

Substituting the solution (2.8) in the expression for $\frac{\partial(\overline{uv})}{\partial t}$ we find

$$\left.\begin{aligned}\frac{\partial(\overline{uv})}{\partial t} = -R^2\left(\overline{\frac{\partial\psi}{\partial\eta}\frac{\partial^2\psi}{\partial t\partial\lambda}} + \overline{\frac{\partial\psi}{\partial\lambda}\frac{\partial^2\psi}{\partial t\partial\eta}}\right) =\\ = \frac{R^2m^2a^2}{2}\left[\gamma\frac{dF}{d\eta} - F\frac{d\gamma}{d\eta}\right]\end{aligned}\right\} \tag{2.10}$$

where the bars denote averages around the latitude circles. It is seen that $\frac{\partial(\overline{uv})}{\partial t}$ depends only on γ and F, that is, depends upon the interaction between the disturbance and earth's rotation, as represented by the term $v\frac{df}{Rd\varphi}$ in eq. (2.1). Since Z does not contribute to $\frac{\partial(\overline{uv})}{dt}$, we shall find γ only. In order to deal

with an arbitrary F, it is convenient to use Green's method, writing γ in the form

$$\gamma = \int_0^1 G(\eta, \xi) F(\xi) d\xi \qquad (2.11)$$

where G is the Green's function, satisfying the homogeneous part of (2.9 a) and the boundary conditions and has a jump of the first derivative for $\eta = \xi$. It is given by

$$G(\eta, \xi) = \frac{1}{2m}\left(\frac{1-\xi}{1+\xi}\right)^{\frac{m}{2}}\left[\left(\frac{1+\eta}{1-\eta}\right)^{\frac{m}{2}} - \left(\frac{1-\eta}{1+\eta}\right)^{\frac{m}{2}}\right] \quad \text{for } \eta \leq \xi$$

$$= \frac{1}{2m}\left(\frac{1-\eta}{1+\eta}\right)^{\frac{m}{2}}\left[\left(\frac{1+\xi}{1-\xi}\right)^{\frac{m}{2}} - \left(\frac{1-\xi}{1+\xi}\right)^{\frac{m}{2}}\right] \quad \text{for } \eta \geq \xi \qquad (2.12)$$

Because of the particular form of the Laplacian operator (2.4), it is sometimes convenient to express $F_m(\eta)$ in terms of spherical harmonics. It is evident that any sum or product of the functions

$$F(\eta) = a p_n^{n-1}(\eta) = a_1 \eta (1-\eta^2)^{\frac{n-1}{2}} \qquad (2.13)$$

satisfies our boundary conditions. For simplicity, we shall simply take (2.13) as the amplitude function of the initial disturbance (2.6), and leave the more general case for treatment in section (c). Substituting in (2.11) and then in (2.10), we find

$$\frac{\partial(\overline{uv})}{\partial t} = \frac{R^2 a^2 m^2 \omega}{2}(1-\eta^2)^{\frac{n-3}{2}} \cdot \left\{(1 + m\eta - n\eta^2) \cdot \left(\frac{1-\eta}{1+\eta}\right)^{\frac{m}{2}}\left[\int_0^{\eta}\left(\frac{1+\xi}{1-\xi}\right)^{\frac{m}{2}} p_n^{n-1}(\xi) d\xi - \int_0^1 \left(\frac{1-\xi}{1+\xi}\right)^{\frac{m}{2}} p_n^{n-1}(\xi) d\xi\right] + (1 - m\eta - n\eta^2) \cdot \left(\frac{1+\eta}{1-\eta}\right)^{\frac{m}{2}} \int_{\eta}^1 \left(\frac{1-\xi}{1+\xi}\right)^{\frac{m}{2}} p_n^{n-1}(\xi) d\xi\right\} \qquad (2.14)$$

It may be mentioned that disturbances with their relative vorticity proportional to the stream function, i.e., $\triangle^2 \psi = -K\psi$, are exactly neutral. For these disturbances, w and therefore also Z are identically zero and γ is a constant multiple of the initial amplitude function which is given by $p_n^m(\eta)$. These disturbances merely rotate around the pole without change of shape, and no mean transport of momentum is produced by them at any time.[1] Thus the case with $m = n-1$ belongs to this group of exactly neutral disturbances. We note that if we take a sum or product of the functions of eq. (2.13) as the amplitude function, no disturbance could be exactly neutral.

For all values of $m \neq n-1$, (2.14) gives a positive $\frac{\partial \overline{uv}}{\partial t}$ at every point. It increases from zero at the equator to a positive maximum somewhere south of $\varphi = 45°$ and decreases to zero toward the pole. The value of this function for $m=4$ and $n=3$, when divided by the constant factor $4\bar{v}^2 U/D$ to make it non-dimensional, is represented by the dotted curve in Fig. 1.

Similar results may be obtained for disturbances with amplitude functions different from that given by (2.13), and it is found that if the maximum is stronger, then a slight southward transport in the region near the pole will occur, which also appears to be verified observationally.

b. A single vortex. As has been mentioned before, a requirement of $v=0$ at the pole is not justified for the motion of a single vortex centered off the pole, or a wave motion of $m=1$. Since this motion is also of some interest, we shall analyze its effect on the mean momentum transfer. As the motion represented by $p_2^1(\eta)\sin\lambda$ is exactly neutral, we shall take a different amplitude function. The simplest initial disturbance which satisfies the conditions that $v=0$ at the equator and gives a finite v at the pole and which is not exactly neutral is

$$\psi_0 = a\eta^2(1-\eta^2)^{\frac{1}{2}} \sin\lambda \qquad (2.15)$$

Substituting in (2.10) we find

$$\frac{\partial(\overline{uv})}{\partial t} = \frac{R^2 a^2}{60}\frac{\omega\eta}{1+\eta}\left\{\left(2 + \frac{1}{2}\eta - 3\eta^2\right) \cdot$$

[1] For discussions of these exactly neutral disturbances see Neamtan (1946) and other papers.

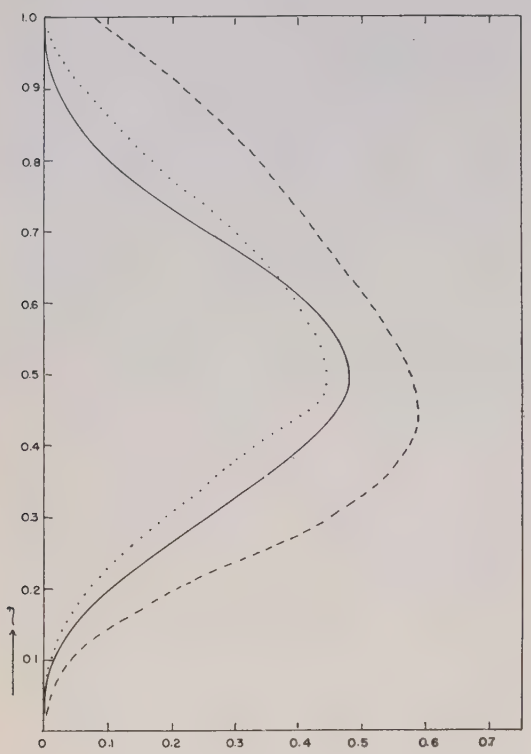

Fig. 1. Theoretical distribution of $\overline{uv}$, dashed curve corresponds to two sets of disturbances for profile (b), shifted a disturbance D/3. Full curve is that given by (3.3a) and the dotted curve is given by (2.14).

$$\cdot (10\eta^3 + 15\eta^4 + 6\eta^5 - 1) + \left(2 - \frac{1}{2}\eta - 3\eta^2\right) \cdot$$

$$\cdot (1+\eta)(1+\eta+\eta^2 - 9\eta^3 - 9\eta^4)\Big\} \quad (2.16)$$

which is also positive for all values of η, and has its maximum around 45°.

c. *Disturbances limited between two parallels of latitude.* Although the preceding results are obtained under the assumption that v vanishes identically at the equator and at the pole but not at any other latitudes, similar results will be obtained whenever the amplitude of the disturbance varies with latitude, which may be considered as determined by the supply of energy to the disturbances in the atmosphere. Thus we shall investigate the disturbances that are limited to some other belt, and demand the vanishing of v along two latitude circles φ_1 and φ_2. To satisfy these boundary conditions for unspecified positions of these parallels, it is more convenient to use the new coordinate system

$$x = \lambda, \; y = \log(\tan\varphi + \sec\varphi) \qquad (2.17)$$

Then, after multiplying by $\cos^2\varphi$, the vorticity equation (2.3) becomes

$$\left.\begin{aligned} \frac{\partial}{\partial t}\left(\frac{\partial^2\psi}{\partial x^2} + \frac{\partial^2\psi}{\partial y^2}\right) = &-2\omega \operatorname{sech}^2 y \frac{\partial\psi}{\partial x} + \\ &+ \frac{\partial\psi}{\partial y}\frac{\partial \nabla^2\psi}{\partial x} - \frac{\partial\psi}{\partial x}\frac{\partial \nabla^2\psi}{\partial y} \end{aligned}\right\} \quad (2.18)$$

It is seen that the Laplacian operator on the left side has the same form as in Cartesian coordinates. The symmetry of the last two terms on the right has been preserved by using the operator ∇^2 given by (2.4). We note that the earth rotation term takes the form

$$2\omega \cos^2\Phi \frac{\partial\psi}{\partial x} = 2\omega \sec h^2 y \frac{\partial\psi}{\partial x}$$

in this equation. The origin of y can be changed to latitude φ_1, by changing $\operatorname{sech}^2 y$ into $\operatorname{sech}^2(y+y_1)$. Then the boundary conditions will be $v=0$ for $y=0$ and $y=y_2$, corresponding to φ_1 and φ_2. We also assume the initial disturbance to be a single wave of the type (2.6). Then $\dfrac{\partial\psi}{\partial t}$ takes the same form (2.8), while now γ satisfies the differential equation

$$\frac{d^2\gamma}{\partial y^2} - m^2\gamma = -F(y)\operatorname{sec} h^2(y+y_1) = -R(y) \quad (2.19)$$

Both γ and F should vanish at $y=0$ and $y=y_2$. Here we assume y_2 to be finite, i.e., $\varphi_2 < 90°$. Since Z does not contribute to the change of the mean momentum transfer, we shall not discuss it.

We shall now specify the amplitude variations by assuming that F has its maximum near the latitude $y=y_2/2$. Thus we put

$$F(y) = A(y)\sum_{n=1}^{N} b_n \Theta^n$$

where $\Theta = \sin\dfrac{\pi y}{y_2}$ and $A(y)$ is a monotone function of y. Each term of F has its maximum near $y=y_2/2$ and satisfies the boundary conditions. As the term in the vorticity equation is linear in ψ, the effect of the disturbance with this amplitude function is similar to that given by a single term of it. Therefore we shall

simply put F to be proportional to Θ^n. To simplify the integration, we take $A(\gamma)=cs^2(\gamma+\gamma_1)$, so that $R(\gamma)=\Theta^n$. Then γ is given by

$$\gamma=\sum_{r=1}^{n}c_r\Theta^r+C_0\left(1-\frac{csm(\gamma-\gamma_{2/2})}{cs\dfrac{\mu\pi}{2}}\right) \quad (2.20)$$

where $\mu=\dfrac{m\gamma_2}{\pi}$ and cs stands for the hyperbolic cosine, and the coefficients are given by

$$c_{n-2l}=\left(\frac{\gamma_2}{\pi}\right)^2\cdot\frac{1}{n^2+\mu^2}\cdot\frac{1}{(n-2)^2+\mu^2}\cdots$$

$$\frac{1}{(n-2l)+\mu^2}\frac{n!}{(n-2l)!}$$

$$c_{n-2l-1}=0$$

When n is even, c_0 is given by the upper expression by putting $2l=n$; when n is odd, $c_0=0$.

Substituting γ in the expression for $\dfrac{\partial\overline{uv}}{\partial t}$ we find

$$\cos^4\varphi\frac{\partial\overline{uv}}{\partial t}=R^2m^2a^2\omega(M_1+M_2) \quad (2.21)$$

where

$$M_1\equiv\Theta^{n-1}\left\{\frac{\pi}{\gamma_2}\cos\frac{\pi\gamma}{\gamma_2}\sum_{r=1}^{n}(n-r)c_r\Theta^r+\frac{co}{cs\dfrac{\mu\pi}{2}}\cdot\right.$$

$$\cdot\left[\frac{n\pi}{\gamma_2}\cos\frac{\pi\gamma}{\gamma_2}\left(cs\frac{\mu\pi}{2}-csm(\gamma-\frac{1}{2}\gamma_2)\right)+\right.$$

$$\left.\left.+m\Theta Snm\left(\gamma-\frac{1}{2}\gamma_2\right)\right]\right\}$$

$$M_2\equiv 2\sin\varphi\Theta^n\gamma \quad (2.22)$$

Similar results are obtained if we choose $A=1$; then M_2 will be larger. It can be shown that M_1 is positive for $\gamma<\gamma_2/2$ and negative for $\gamma>\gamma_2/2$, therefore, has the effect of producing a westerly current in the central part of the belt and easterly currents in the outer parts. On the other hand M_2 is positive for all γ and has its maximum near $\gamma=\gamma_2/2$, therefore produces a westerly current north of this latitude and an easterly current to the south. It can also be seen that for smaller values of n, M_2 is much larger than M_1. For example, M_1 disappears when $n=1$. As n increases, or as the maximum of the amplitude becomes more pronounced, M_1 becomes larger than M_2. The sum of these two terms gives a northward transport of momentum for almost all γ except near the northern boundary, where a reverse transport may result if M_1 is larger than M_2. The value of the transfer corresponding to $n=1$ ($M_1=0$), with the factors sin φ and cos φ omitted, is plotted in Fig. 1, as the fully drawn curve. The case for $n>1$ is something like those given by the curves b, c, or d in Fig. 9.

These examples show that whenever the disturbance is not exactly neutral, the interaction between it and the earth's rotation produces a northward transport of momentum, except at very high latitudes where a reverse transport may occur. The maximum transport always occurs somewhere south of the midpoint of the belt in northern hemisphere. Figuratively, it may be said that this interaction tends to tilt the trough- and ridge-lines in a SE—NE direction in almost the entire region except near the northern boundary where they may take a SE—NW direction.

d. Disturbances with more wave-components. We now discuss the disturbance represented by

$$\psi_0=a_lF_l(\eta)\sin l\lambda+a_mF_m(\eta)\sin m\lambda \quad (2.23)$$

where l and m are different integers. Substituting in (2.3) it can be seen that $\dfrac{\partial\psi}{\partial t}$ must take the form

$$\frac{\partial\psi}{\partial t}=2\omega la_l\gamma_l(\eta)\cos l\lambda+2\omega ma_m\gamma_m(\eta)\cos m\lambda+$$

$$+Z_l(\eta)\sin 2l\lambda+Z_m(\eta)\sin 2m\lambda+Z_3(\eta)\sin$$

$$(m+l)\lambda+Z_4(\eta)\sin(m-l)\lambda \quad (2.24)$$

The Z-terms are new wave-components while γ's satisfy eq. (2.9 a) or (2.19) with the proper F-function on the right. Substituting in the expression for $\dfrac{\partial\overline{uv}}{dt}$, we get

$$\left.\begin{aligned}\frac{\partial(\overline{uv})}{\partial t}&=R^2l^2a^2{}_l\omega\left(\gamma_l\frac{dF_l}{d\eta}-F_l\frac{d\gamma_l}{dy}\right)+\\&+R^2m^2a^2{}_m\omega\left(\gamma_m\frac{dF_m}{d\eta}-F_m\frac{d\gamma_m}{d\eta}\right)\end{aligned}\right\} \quad (2.25)$$

It is seen that each wave-component produces its own momentum transfer because of the earth's rotation, if it is not exactly neutral. Thus the results obtained before can be extended to disturbances with any number of wave components.

e. Initial disturbances with tilted troughs. If this effect of the earth's rotation is always in the same direction regardless of the initial tilt of the disturbances, then we may say that it is not a temporary effect. Thus we shall consider the initial disturbance

$$\psi_0 = a_1 F_1(\eta) \sin m\lambda + a_2 F_2(\eta) \cos m\lambda \quad (2.26)$$

with $F_1 \neq kF_2$. For this disturbance, $\frac{\partial \psi}{\partial t}$ takes the form

$$\frac{\partial \psi}{\partial t} = 2m\lambda[a_1\gamma_1(\eta) \cos m\lambda - a_2\gamma_2(\omega) \sin m\lambda] + \\ + Z_1 \sin 2m\lambda + Z_2 \cos 2m\lambda + Z_3$$

in which γ_1 and γ_2 satisfy eq. (2.19), with the proper F. Substituting in (2.10) we find

$$\frac{1}{R^2 m^2 \omega} \frac{\partial \overline{uv}}{\partial t} = a_1^2 \left(\gamma_1 \frac{dF_1}{d\eta} - F_1 \frac{d\gamma_1}{d\eta} \right) + \\ + a_2^2 \left(\gamma_2 \frac{dF_2}{d\eta} - F_2 \frac{d\gamma_2}{d\eta} \right)$$

Since γ_2 is related to F_2 in the same way as γ_1 is related to F_1, we see that both the sine and the cosine components produce an increase of the transport irrespective of the initial transport. Thus our result also applies to the most general disturbance given by (2.5), and the effect will persist.

3. Modification of the mean zonal current

Let us now assume that there exists a mean zonal current $U = u(y)$ and study its interaction with the disturbance. Writing the streamfunction as $\overline{\psi}(y) + \psi(x, y, t)$ and u for $-\frac{1}{R \cos^2 \varphi} \frac{\partial \overline{\psi}}{\partial y}$, it can be seen that the terms in (2.18) depending on the mean flow are given by $-u\frac{\partial \nabla^2 \psi}{\partial x} + \frac{\partial \psi}{\partial x}\frac{\partial}{\partial y}\left(\frac{\partial u}{\partial y} - 2 \sin \varphi u\right)$, where ∇^2 now stands for the operator $\frac{\partial^2}{\partial x^2} + \frac{\partial^2}{\partial y^2}$. In the following, we shall neglect the term $2 \sin \varphi \cdot u$ and the variation of $\cos \varphi$ in the nonlinear terms, and consider the coordinates x, y as has been multiplied by R. Equation (2.18) then beeomes

$$\left.\begin{aligned} \frac{\partial \nabla^2 \psi}{dt} = &- u\frac{\partial \nabla^2 \psi}{\partial x} - (f' - u'')\frac{\partial \psi}{\partial x} + \\ &+ \frac{1}{\cos^2 \varphi}\left(\frac{\partial \psi}{\partial y}\frac{\partial \nabla^2 \psi}{\partial x} - \frac{\partial \psi}{\partial x}\frac{\partial \nabla^2 \psi}{\partial y}\right) \end{aligned}\right\} \quad (3.1)$$

where the primes denote differentiation with respect to y. This equation has the same form as the equation for plane motion, except for f'. Since it is only an approximation to (2.18), we may still take f' as given by $\frac{2\omega}{R} \cos^2 \varphi$. In what follows we shall investigate the interactions between different mean currents and the initial disturbance

$$\psi_0 = a \sin ly \sin kx \quad (3.2)$$

where $l = \pi/D$ and D is the width of the belt. As the general effect of earth's rotation is independent of the presence of the mean zonal current and is already known, we shall find only its expression for this disturbance, by putting $f' = \frac{\omega}{R}(1 + \cos 2\varphi) = \frac{\omega}{R}(1 + \alpha \cos ly)$, with $\alpha < 1$. The increase of the mean momentum transfer produced by this effect is then equal to

$$\frac{\partial \overline{uv}}{dt} = \frac{\alpha\omega}{2R}\frac{k^2 a^2}{l}\frac{1}{\mu^2 + 4} \sin^3 ly \quad (3.3\text{ a})$$

which is positive everywhere and is very similar to that given by (2.14). It may be noted that if the amplitude of the disturbance is the nth power of $\sin ly$, then an antisymmetric part will also be present in this $\frac{\partial \overline{uv}}{\partial t}$, which originates from the constant part of f' and is given by M_1 of (2.22). From (3.3 a) we find

$$\frac{\partial^2 u}{\partial t^2} = -\frac{3\alpha\omega}{R}\frac{k^2 a^2}{4(\mu^2 + 4)} \sin ly \sin 2ly \quad (3.3\text{ b})$$

These quantities may be added to the corresponding changes due to the mean current.

For the particular disturbance (3.2), the nonlinear terms on the right side of (3.1)

disappear and the solution $\frac{\partial \psi}{\partial t}$ takes on the form

$$\frac{\partial \psi}{\partial t} = ak\gamma(y) \cos kx$$

where γ is to satisfy

$$\gamma'' - k^2\gamma = [(k^2 + l^2)u + u'' - f'] \sin ly \quad (3.4)$$

and the conditions $\gamma(0) = \gamma(D) = 0$.

The rate of increase of the mean momentum transfer is given by

$$\frac{\partial(\overline{uv})}{dt} = \frac{a^2k^2}{2}(l\gamma \cos ly - \gamma' \sin ly) \quad (3.5)$$

From this we get the second derivative of the mean zonal current

$$\frac{\partial^2 u}{\partial t^2} = -\frac{\partial^2(\overline{uv})}{\partial y \partial t} = \frac{a^2k^2}{2} \sin ly(\gamma'' + l^2\gamma) \quad (3.6)$$

Since the present problem is related to the stability of the mean flow, we may also write down the energy equation for the mean flow. Since $u_t = 0$ initially, $E_t = 0$ and

$$E_{tt} = \int_0^D u u_{tt} dy \quad (3.7)$$

Thus the disturbance might be said to be "amplified" when E_{tt} is negative, "damped" when E_{tt} is positive and neutral when E_{tt} is zero. All these quantities are related to each other and their determination depends upon the solution of the vorticity equation. However, it can be shown that u_{tt} not only occur in E_{tt}, but also in the higher derivatives. This can be seen from the increment of the kinetic energy of the mean flow relative to its initial value,

$$\left.\begin{aligned} \triangle E = \frac{1}{2}\int_0^D (U^2 - U_0^2)dy = \\ = \int_D^0 U_0 \triangle U dy + \frac{1}{2}\int_D^0 (\triangle U)^2 dy \end{aligned}\right\} \quad (3.8)$$

If $\triangle U$ is identified with $\frac{1}{2}t^2\overline{U}_{tt}$, it can be shown that the first term corresponds to $\frac{1}{2}t^2\overline{E}_{tt}$ in the Taylor expension of $\overline{E}$ and the second term corresponds to $\frac{1}{4!}t^4\frac{\partial^4 E}{\partial t^4}$. Thus, even when all the higher derivatives of U are zero, $\frac{\partial^4 E}{\partial t^4}$ is still different from zero. Since this term is positive if $\triangle u$ is not identically equal to zero, it represents a damping effect upon the disturbance. Thus, E_{tt} as a measure of the initial rate of amplification or damping of the disturbance generally underestimates the damping effect and overestimates the amplifying effect as compared to the information given by U_{tt}.

4. The mean zonal flow $U = U_0 + (U_m - U_0) \sin^2 ly$

Let us discuss this symmetrical mean zonal flow. In the expression U_m is the maximum value of U at the axis of the flow. The profile has two inflection points (where $U'' = 0$) midway between the axis of the flow and the walls, and also critical points (where $u'' = f'$) if U_m is higher than a certain value. According to the previous investigation (Kuo, 1949), the inviscid linear vorticity equation will yield solutions with positive and negative real exponential time factors, so that there exist amplified and damped disturbances in the strict sense. We shall discuss this case in some detail to find whether the present method will also give comparable results.

When this expression for the mean flow is substituted into (3.4), the function Y can be found by simple integration. Thus we find with the part depending on f' omitted

$$\left.\begin{aligned} 4\gamma = \frac{k^2 - 3l^2}{k^2 + 9l^2} A \sin 3ly - \\ - \frac{(3k^2 - l^2)A + 4(k^2 + l^2)u_0}{k^2 + l^2} \sin ly \end{aligned}\right\} \quad (4.1)$$

The second time derivative of the mean flow, expressed in non-dimensional form, is then given by

$$U_{tt} = -\frac{k^2a^2\pi^2 A(\mu^2 - 3)}{(\mu^2 + 9)D^2} \sin ly \sin 3ly \quad (4.2)$$

where $\mu = k/l$ and A is used as an abbreviation for $U_m - U_0$.

From (4.2) it may be seen that the interaction

between the disturbance and the mean flow increases the mean flow in the central part of the zonal band from $ly = 60°$ to $ly = 120°$ and decreases the mean flow in the rest of the band if the wavelength $L = 2\pi/k$ of the disturbance is shorter than $2D/\sqrt{3}$. The change in the mean flow is in the reverse direction if the wavelength is longer than this critical value.

When U_{tt} and the initial mean flow U are substituted into (3.6) we find

$$\frac{4D}{a^2(k^2+l^2)A^2}E_{tt} = \frac{\pi^2}{2}\frac{(\mu^2-3)\mu^2}{(\mu^2+1)(\mu^2+9)} \quad (4.3)$$

Since $a^2(k^2+l^2)/4$ is the average disturbance kinetic energy per unit area, this equation with a minus sign expresses the normalized second time rate of change of kinetic energy of the perturbation. From (4.3) it will be seen that the wave length $L = 2D/\sqrt{3}$ is the neutral wave length which separates the longer amplifying disturbances from the damping shorter disturbances. It may be noted that this rate of change has a maximum negative value ($= -0.496\, A^2/D^2$) for the wave length $L = 2.1\, D$ so that this disturbance may be termed the most unstable disturbance. In a flow of $U_m = 20$ m sec^{-1}, of width $D = 5 \times 10^6$ m, the most unstable disturbance will increase in energy by but 2.96 % during the first day. However, if the mean flow is stronger and contained in a narrower belt, the change may be very rapid. Thus in a flow of $U_m = 50$ m sec^{-1} of width $D = 2 \times 10^6$ m, this most unstable disturbance will double its energy during the first day. It will also be noted that the earth's rotation does not contribute to E_{tt} with this symmetric mean flow profile.

5. The higher time derivatives of the mean flow

As the kinetic energy of both the mean flow and the disturbance is finite for a finite disturbance, there must be an upper limit to the energy attainable by the disturbance when it is amplified or by the mean flow when the disturbance is damped. Whether this limit is actually attained and the rate of approach to the limit depends not only upon U_{tt} or E_{tt}, but upon higher derivatives as well. Thus, a discussion of the higher derivatives in one case is of interest.

Generally, in order to find $\frac{\partial^n u}{\partial t^n}$, it is necessary to compute all the time derivatives of ψ up to the order $(n-1)$ which while possible in principle, would require an undue amount of labor if n is large. Since $\frac{\partial^3 u}{\partial t^3}$ is zero initially let us find only $\frac{\partial^4 u}{\partial t^4}$ for the mean flow discussed in the preceding section. For simplicity, we shall take f' as a constant ($= \beta$) and put U_0 equal to zero. Then the fourth derivative is given by

$$\frac{4(\mu^2+9)^2D^2}{k^4a^2(\mu^2-3)A^3\pi^2}\frac{\partial^4 u}{\partial t^4} =$$

$$= \left\{\frac{(\mu^2+9-2\beta')(3\mu^2-1-4\beta') - (\mu^2-3)(\mu^2+5)}{2(\mu^2+1)} - \right.$$

$$- \frac{(\mu^2+9-2\beta')^2}{2(\mu^2+9)} - \frac{(\mu^2+9)(3\mu^2-1-4\beta')^2}{8(\mu^2+1)^2} -$$

$$\left. - \frac{(\mu^2+5)(\mu^2+21)}{8(\mu^2+25)} + \frac{a^2l^2(4\mu^4-35\mu^2-207)}{(\mu^2+4)A^2}\right\} \times$$

$$\times (\cos 4ly - \cos 2ly) + \frac{3(\mu^2+5)(\mu^2+9)}{4(\mu^2+25)} \cdot$$

$$\cdot \left\{\frac{\mu^2+9-2\beta'}{\mu^2+9} + \frac{\mu^2+25-2\beta'}{\mu^2+25} - \frac{3\mu-1-4\beta'}{\mu^2+1} - \right.$$

$$- \frac{4a^2l^2(2\mu^4-7\mu^2-69)}{(\mu^2+5)(\mu^2+4)A^2} \times (\cos 6ly - \cos 4ly) +$$

$$\left. + \frac{3(\mu^2-3)(\mu^2+5)}{4(\mu^2+25)} \times (\cos 8ly - \cos 2ly)\right. \quad (5.1)$$

in which $\mu = k/l$ and $\beta' = \beta/l^2A$. The expression (5.1) is too complex to discuss generally. However, there are a few points worthy of mention. It may be noted that for the disturbance with $\mu^2 = 3$, these derivatives are zero so that the disturbance is neutral at least up to $\frac{\partial^4 u}{\partial t^4}$ and $\frac{\partial^4 E}{\partial t^4}$. The factor A comes into this equation raised to a higher power than in the expression for U_{tt}, so the influence of the higher derivative is much higher with a stronger mean flow than with a weaker one. Computation shows that this fourth derivative generally has a sign opposite to that of U_{tt}, indicating that the time required by the system to reach the limiting condition is longer than that estimated from U_{tt}, or the change may

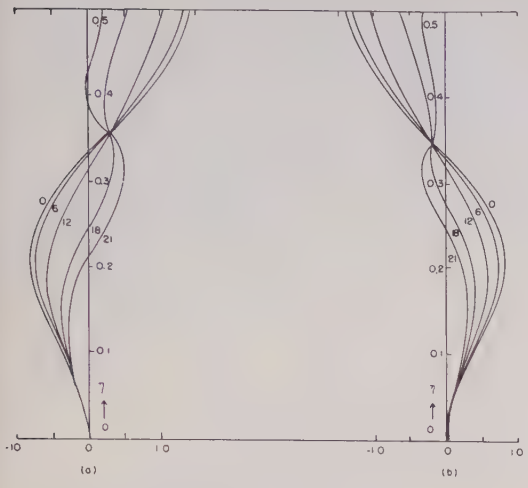

Fig. 2. The variations of U_{tt} for the profile $U = A \sin^2 ly$, with $A = 20$ m sec^{-1}. (a) is for the damping disturbance $\mu^2 = 5$, (b) for the amplifying disturbance $\mu^2 = 1.5$.

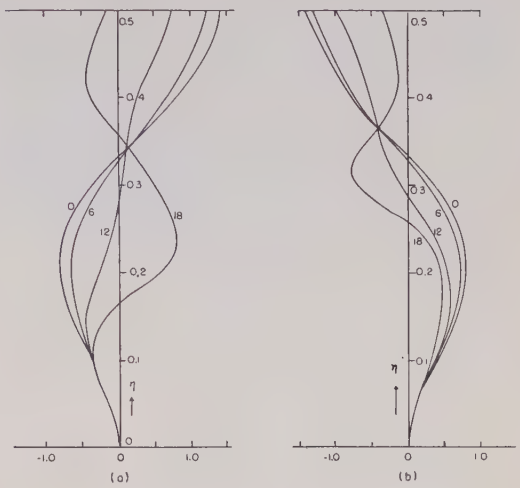

Fig. 3. The same as Fig. 2, with $A = 50$ m sec^{-1}.

be reversed. Since $\dfrac{\partial^4 u}{\partial t^4}$ is proportional to k^4, its effect must be small for disturbances of long wavelength.

To illustrate the effect of this fourth derivative, a few computed rates of change of the mean flow U_{tt} are shown in Figures 2 and 3, expressed in units of $a^2k^2AD^{-2}$. Since the term containing α in (4.2) is neglected, the change is a symmetrical function of y so that only half of the flow is plotted. Figure 2 shows the effects of a relatively weak mean zonal flow ($A = 20$ m sec^{-1}) and Figure 3 shows the effect of a stronger mean flow ($A = 50$ m sec^{-1}). These examples show that the parabolic extrapolation $\bar{u} - \bar{u}_0 = \dfrac{t^2}{2} u_{tt}$ cannot be used for time intervals longer than 24 hours.

To estimate the order of magnitude of the interaction between the disturbance and the mean flow, we may take the example plotted in Figure 2 a, which is for the damped disturbance with $\mu^2 = 5$, $al = 10$ m sec^{-1}, $A = 20$ m sec^{-1}, and $D = 5 \times 10^6$ m. Taking the mean value of U_t for a time interval of one day, we find an increase of the mean zonal flow of about $2m$ sec^{-1} in the middle of the stream and a decrease in the outer parts. These changes are of the same order of magnitude as those produced by the earth's rotation.

As mentioned above, the disturbance with $\mu^2 = 3$ is neutral at least up to $\dfrac{\partial^4 u}{\partial t^4}$ or $\dfrac{\partial^4 E}{\partial t^4}$. Since it is very difficult to find the higher derivatives, it appears desirable to examine the exactly neutral disturbance from another point of view, if one can be found. For the present case, let us consider the total stream function

$$\left.\begin{aligned} \varphi = -\left(U_0 + \frac{A}{2}\right) y + \frac{A}{2l} \sin 2ly + \\ + a \sin k(x - ct) \sin ly \end{aligned}\right\} \quad (5.2)$$

which represents a system of alternating cyclonic and anticyclonic vortices embedded in a sine-curve mean zonal flow, propagated with a phase velocity c without changing shape, and therefore is exactly neutral. At $t = 0$, this reduces to the initial motion we have been discussing. In order that this stream function satisfy the vorticity equation (3.1) with $f' = \beta$, the wave number k and the phase velocity c must satisfy the following relations:

$$k^2 = 3l^2 \quad (5.3\,a)$$

$$c = U_0 + \frac{A}{2} - \frac{\beta}{k^2 + l^2} \quad (5.3b)$$

It is seen that the wavelength and phase velocity of this neutral disturbance are determined by the mean zonal current and the width of the belt, so that it cannot be con-

sidered as representing a continuous spectrum of neutral disturbances unless A is zero, or unless the mean flow is uniform. For the latter case, the condition (5.3 a) is unnecessary.

Since the stream function (5.2) reduces to the initial flow we have discussed, it may be concluded that the disturbance of the type (3.2) with $\mu^2=3$ is exactly neutral for this mean zonal flow if the variable part in f' is neglected.

6. The mean currents $U=U_m \sin ly$ and $U=U_m \sin^4 ly$

The simple sine profile $U=U_m \sin ly$ has no inflection point within the walls, therefore is stable for small disturbances according to the linear theory. With this mean flow, the solution Y of (3.4) is

$$\gamma=\frac{2U_m}{\mu^2+4}\left[\frac{Snk\gamma+Snk(D-\gamma)}{SnkD}-1-\frac{\mu^2}{2}\sin^2 ly\right] \tag{6.1}$$

Substituting into (3.6), we obtain

$$\frac{D^2U_{tt}}{k^2a^2U_m}=\frac{\pi^2(\mu^2+1)}{\mu^2+4}\cdot$$

$$\cdot\sin ly\left[\frac{Snk\gamma+Snk(D-\gamma)}{SnkD}-1+\frac{3\mu^2\sin^2 ly}{2(\mu^2+1)}\right] \tag{6.2}$$

It may be seen that for any wavelength, this expression is positive in the central part of the zonal belt and negative in the outer part, indicating that the interaction between the disturbance and the mean flow is to accentuate the mean flow while the disturbance is damped. In this case, the energy integral E_{tt} is given by

$$\frac{4D}{a^2(k^2+l^2)U_m^2}E_{tt}=$$

$$=\frac{4\pi^2\mu^2}{\mu^2+4}\left[\frac{4}{\mu(\mu^2+4)\pi}\tanh\frac{\mu\pi}{2}+\frac{9\mu^2}{16(\mu^2+1)}-\frac{1}{2}\right] \tag{6.3}$$

which is positive for all values of k, indicating that all the disturbances of type (3.2) are damped.

To find whether this is really the case, we might try to find an exactly neutral disturbance in this mean zonal flow. The only disturbance that can propagate with a constant phase velocity without change of shape is the one

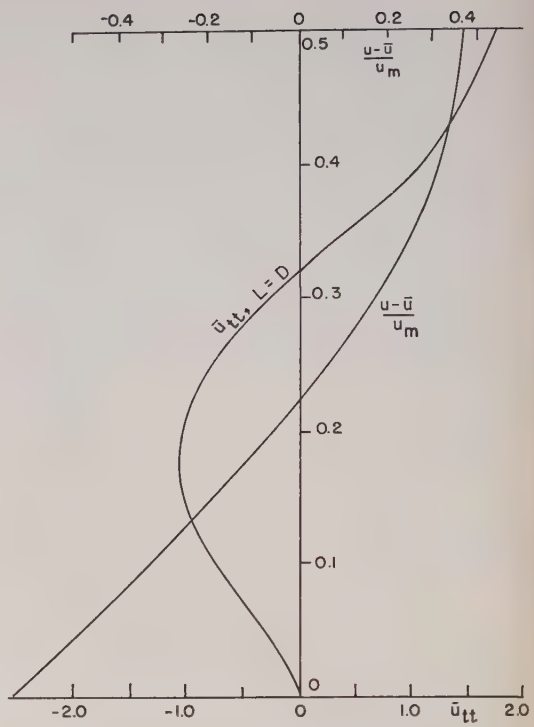

Fig. 4. The distribution of U_{tt} for the mean flow $U=U_m \sin ly$.

of $k=0$, that is, only an infinitely long disturbance can remain exactly neutral and perfectly periodic. Since it has been shown that disturbances of finite wavelengths are damped, it must be concluded that all disturbances of the type (3.2) must be damped in this mean flow. This is in agrement with the result of the linear theory.

The change of the mean zonal flow produced by the interaction between the disturbance and the mean flow, with $L=D$, is given by the curve U_{tt} in Figure 4, while the other curve represents the initial mean flow expressed as the ratio $(U-\bar{U})/U_m$, where U_m is the maximum and $\bar{U}$ the average value. From these two curves, it may be seen that the kinetic energy of the mean flow is increasing and the disturbance is being damped. For a disturbance with $L=D$, the relative second derivative of the kinetic energy given by (6.3) is equal to $0.5776\ U_m^2/D^2$, so that for $U_m=20$ m sec^{-1} and $L=D=5\times10^6$ m (about 45 degrees of latitude) the kinetic energy changes by 3.45 % during the first day.

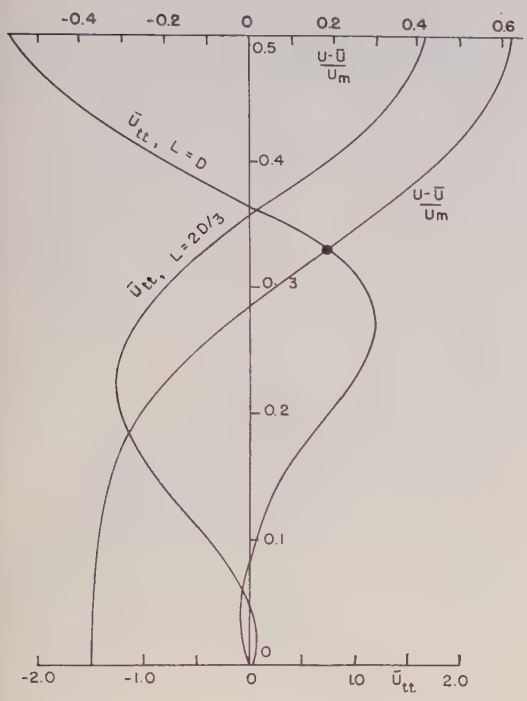

Fig. 5. The distribution of U_{tt} for the mean flow $U = U_m \sin^4 ly$.

As a further example of a sine-curve profile, we consider the mean flow $U = U_m \sin^4 ly$, which has two inflection points at $y = D/3$ and $y = 2D/3$, and therefore may yield both amplifying and damping disturbances according to the linear theory. It can be found that for this profile U_{tt} and E_{tt} are given respectively by

$$\frac{D^2 U_{tt}}{k^2 a^2 U_m} = \frac{\pi^2}{4} \sin ly \cdot$$

$$\cdot \left[\frac{3(\mu^2 - 15)}{\mu^2 + 25} \sin 5ly - \frac{5\mu^2 - 27}{\mu^2 + 9} \sin 3ly \right] \cdot$$

$$\frac{4D}{a^2(k^2 + l^2) U_m^2} E_{tt} = \frac{\pi^2}{32} \mu^2 \frac{7\mu^4 + 118\mu^2 - 945}{(\mu^2 + 1)(\mu^2 + 9)(\mu^2 + 25)} \qquad (6.5)$$

According to E_{tt}, the disturbance with wavelengths longer than 0.8322 D are amplified and those shorter than this value are damped. The most unstable disturbance is the one with $L = 1.7\, D$, for which the energy integral has the value -0.5. The changes of the mean flow produced by the interaction with the disturbances with $L = D$ (amplified) and $L = 2\, D/3$ (damped) are shown in Figure 5.

7. The polynomial profiles

If the mean zonal wind exhibits a profile of the third degree

$$U = a_0 + a_1 y + A_2 y^2 + a_3 y^3 \qquad (7.1)$$

and a disturbance has the form (3.2), the solution of Y in (3.4) is

$$\left. \begin{aligned} v = -\left[U + \frac{2(\mu^2 - 1)}{(\mu^2 + 1)^2} \frac{D^2}{\pi^2} U'' \right] \sin ly - \\ - \frac{2l}{k^2 + l^2} G(y) \cos ly - \frac{2l}{k^2 + l^2} \frac{1}{Snk D} \cdot \\ \cdot [G(D) Snky - G(0) Snk(D - y)] \end{aligned} \right\} \qquad (7.2)$$

where $G(y) = U'(y) + \frac{3k^2 - l^2}{(k^2 + l^2)^2} U'''(y)$. We shall apply this solution to three particular cases:

a. The constant shearing flow $U = U' y$ (Plane Couette flow), where U' is a constant. Since the profile has no inflection point, according to the linear theory, it is stable for small disturbances. In our development,

$$\left. \begin{aligned} \frac{D^2 U_{tt}}{k^2 a^2 U_m} = -\frac{\pi}{2} \sin 2ly + \frac{\pi}{Sn\mu\pi} \cdot \\ \cdot [Sn\pi\mu(1 - \eta) - Sn\mu\pi\eta] \sin \pi\eta \end{aligned} \right\} \qquad (7.3)$$

where $U_m = U' D$, the maximum value of U, $\eta = y/D$ and $\mu = k/l$. Then the energy integral E_{tt} is given by

$$\frac{4DE_{tt}}{a^2(k^2 + l^2) U_m^2} = \frac{\mu^2}{(\mu^2 + 1)^3} \cdot \left[(\mu^2 + 1)(\mu^2 - 3) + \right.$$

$$\left. + \frac{16}{\pi} \mu \coth \frac{\mu\pi}{2} \right] + \frac{4\alpha D^2 \mu^2}{3(\mu^2 + 1)(\mu^2 + 4) U_m} \qquad (7.4)$$

which is positive for all values of μ, indicating that all disturbances are damped. In (7.3) it will be seen that if U' is positive, the effect is to increase the zonal wind in the northern half of the belt and to decrease it in the southern half, the same direction of change as that produced by the earth's rotation. It will be noted that with this profile α also enters into the energy integral E_{tt}, increasing the kinetic energy of the mean flow. Since this profile is of small interest, no numerical example will be given.

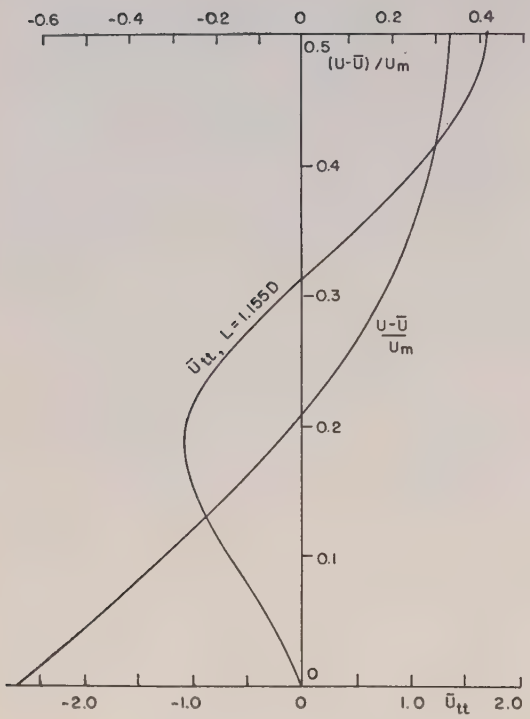

Fig. 6. The distribution of U_{tt} for the mean flow $U = 4U_m\eta\,(1-\eta)$.

b. The parabolic profile $U=4U_m\eta(1-\eta)$ (Poiseuille flow). According to the linear theory, this form of profile is also stable for small disturbance, since U'' is equal to $-8\,U_m/D^2$ and there is no inflection point in the profile. From (7.2) we find

$$\frac{DU_{tt}}{k^2a^2U_m} = -2\pi(1-2\eta)\sin 2\pi\eta + \frac{4(\mu^2-3)}{\mu^2+1}\cdot$$
$$\cdot\sin^2\pi\eta + \frac{4\pi\sin\pi\eta}{Sn\mu\pi}\left[Sn\mu\pi(1-\eta) + Sn\mu\pi\eta\right] \tag{7.5}$$

The energy integral E_{tt} is given by

$$\frac{4DE_{tt}}{a^2(k^2+l^2)U_m^2} = \frac{16}{3}\left(1-\frac{6}{\pi^2}\right)\frac{\mu^2}{\mu^2+1} - \frac{64\mu^2}{3(\mu^2+1)^2}\cdot$$
$$\cdot\left(1+\frac{3}{\pi^2}\right) - \frac{256}{\pi^2}\frac{\mu^2(3\mu^2-1)}{(\mu^2+1)^4} +$$
$$+\frac{256\,\mu^3}{\pi(\mu^2+1)^3}\tanh\frac{\mu\pi}{2} \tag{7.6}$$

which is positive for all values of μ, so that all disturbances of the type (3.2) are damped.

The distribution of U_{tt} produced by the interaction between the disturbance and the mean flow, given by (7.5), is represented in Figure 6 for $L=1.155\,D$. The relative second derivative of the energy of the disturbance given by (7.6) is $0.4875\;U_m^2/D^2$ for a disturbance of this wave length. It may be noted that this case is quite similar to that of the simple sine curve profile discussed in section 6.

c. The profile $u=27\,u_m\eta^2(1-\eta)/4$. This is an unsymmetric mean flow profile which has only one point of inflection, at $y=D/3$, as is shown in Figure 7a by the curve marked $(U-\bar{U})/U_m$. The perturbation theory shows that if the effect of the earth's rotation is neglected, or if the mean flow is strong, both damped and amplified disturbances exist, separated by a neutral disturbance. Because of the presence of a singularity in the linear vorticity equation, even the neutral disturbance is difficult to obtain, making it most desirable to study this case from the present point of view.

With this profile, we find

$$\frac{D^2U_{tt}}{k^2a^2U_m} = -\frac{27\pi}{8}\left[\eta(2-3\eta) - \frac{6}{\pi^2}\frac{3\mu^2-1}{(\mu^2+1)^2}\right]\cdot$$
$$\cdot\sin 2\pi\eta - \frac{27}{4}\frac{\mu^2-3}{\mu^2+1}(1-3\eta)\sin^2\pi\eta +$$
$$+\frac{27\pi}{4}\frac{\sin\pi\eta}{Sn\mu\pi}\left\{Sn\mu\pi\eta + \frac{6}{\pi^2}\frac{3\mu^2-1}{(\mu^2+1)^2}\cdot\right.$$
$$\left.\cdot\left[Sn\mu\pi\eta - Sn\mu\pi(1-\eta)\right]\right\} \tag{7.7}$$

The energy integral is given by

$$\frac{4D}{k^2a^2U_m^2}\frac{\pi^2}{3^7}E_{tt} = -\frac{1}{16}\left(1-\frac{15}{2\pi^2}\right) + \frac{(\mu^2-1)\pi^2}{360(\mu^2+1)}\cdot$$
$$\cdot\left[1+\frac{15}{2\pi^2}\left(1-\frac{9}{2\pi^2}\right)\right] - \frac{3\mu^2-1}{3(\mu^2+1)^3}\cdot$$
$$\cdot\left[1+\frac{9(\mu^2+1)}{16\pi^2}\right] - \frac{3}{\pi^2}\frac{(3\mu^2-1)^2}{(\mu^2+1)^5} + \frac{\mu\pi}{6(\mu^2+1)^2}\cdot$$
$$\cdot\left[1+\frac{6(3\mu^2-1)}{\pi^2(\mu^2+1)^2}\right]\coth\mu\pi + \frac{\mu(3\mu^2-1)}{\pi(\mu^2+1)^4}\cdot$$
$$\cdot\operatorname{csch}\mu\pi + \frac{2}{\pi}\frac{\mu^2-1}{(\mu^2+1)^4}\left[1+\frac{12(3\mu^2-1)}{\pi^2(\mu^2+1)^2}\right]\cdot$$
$$\cdot\coth\frac{\mu\pi}{2} + \frac{\alpha\omega D^2}{3^6R(\mu^2+4)}\left(\frac{40}{\pi}-3\right) \tag{7.8}$$

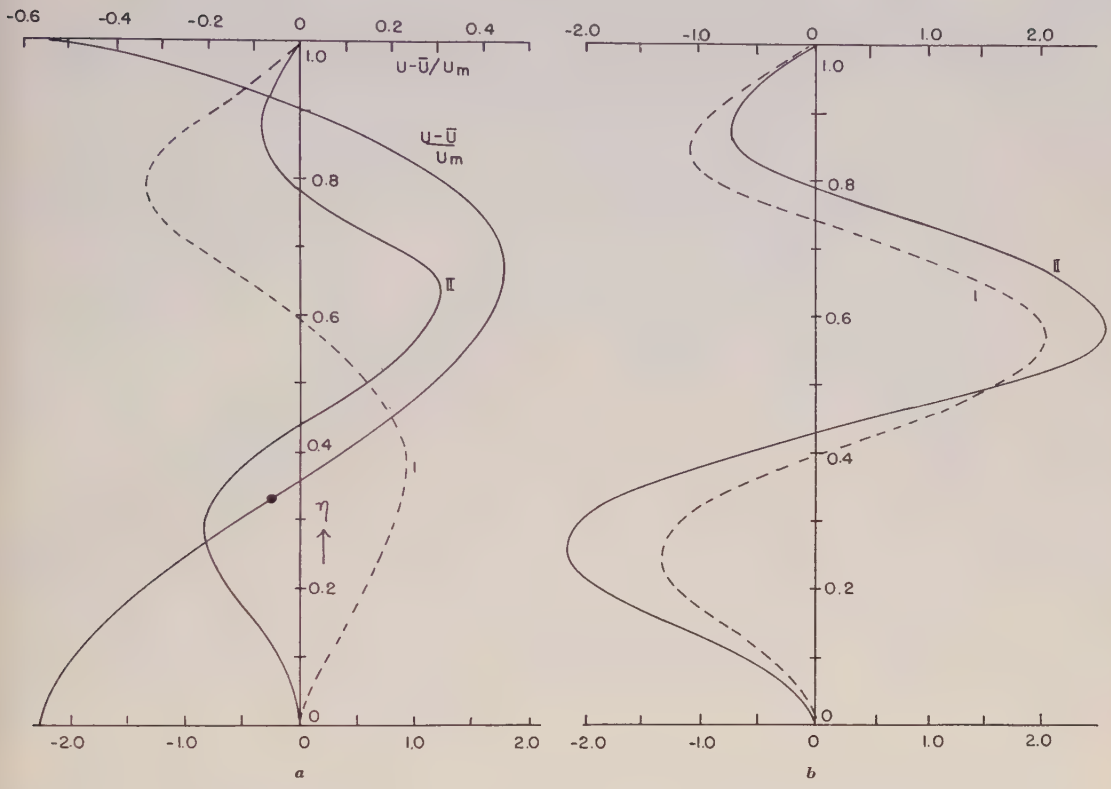

Fig. 7. The distribution of U_{tt} for the mean flow $U = 27U_m\eta^2(1-\eta)/4$.
(a) is for the longer disturbance $L = 3.464D$, (b) for $L = D$. The curves 1 represents the results when the earth rotation factor ω is neglected, curves 2, when the effect of ω is included.

It will be noted that the parameter ω of the earth's rotation enters into the last term of this energy integral because of the lack of symmetry of the mean flow. This term is always positive and therefore represents a damping effect.

Two examples worked out for this mean flow are plotted in Figures 7 a and 7 b. Figure 7 a is for a longer disturbance of $L = 3.464\ D$ and Figure 7 b is for a shorter disturbance of $L = D$. To demonstrate the relative importance of the mean flow and of the earth's rotation, the quantity $D^2U_{tt}/k^2a^2U_m$ has been computed both without and with the part given by (3.3 b). The results are represented by the curves 1 and 2 respectively. Curve 1 in Figure 7 a shows that when this part is neglected, the interaction between a long disturbance and the mean flow diminishes the mean flow in the northern part of the flow where U is relatively high, and increases the mean flow in the southern part where U is relatively low, and so abstracts kinetic energy from the mean flow and flattens it. The relative second derivative of the kinetic energy of the disturbance is $-0.1062\ U_m^2/D^2$. When the effect of the earth's rotation is included, this amplifying effect may be reversed. Thus, with $D = 5 \times 10^6 m$, $\frac{\alpha\omega}{R} = 1.0 \times 10^{-11}\ \mathrm{m}^{-1}\ \mathrm{sec}^{-1}$, and $U_m = 20$ m sec^{-1}, the last term on the right side of (7.8) is equal to 0.2308, so that the total relative second derivative of the kinetic energy is now equal to $0.1246\ U_m^2/D^2$. The corresponding modification of the mean flow is shown by curve 2 of Figure 7 a, which shows a general accentuation of the contrast of the mean flow for different zones.

For the shorter disturbance with $L = D$, both the mean flow and that of the earth's rotation have a damping effect so that the inclusion of the term with ω only magnifies the damping

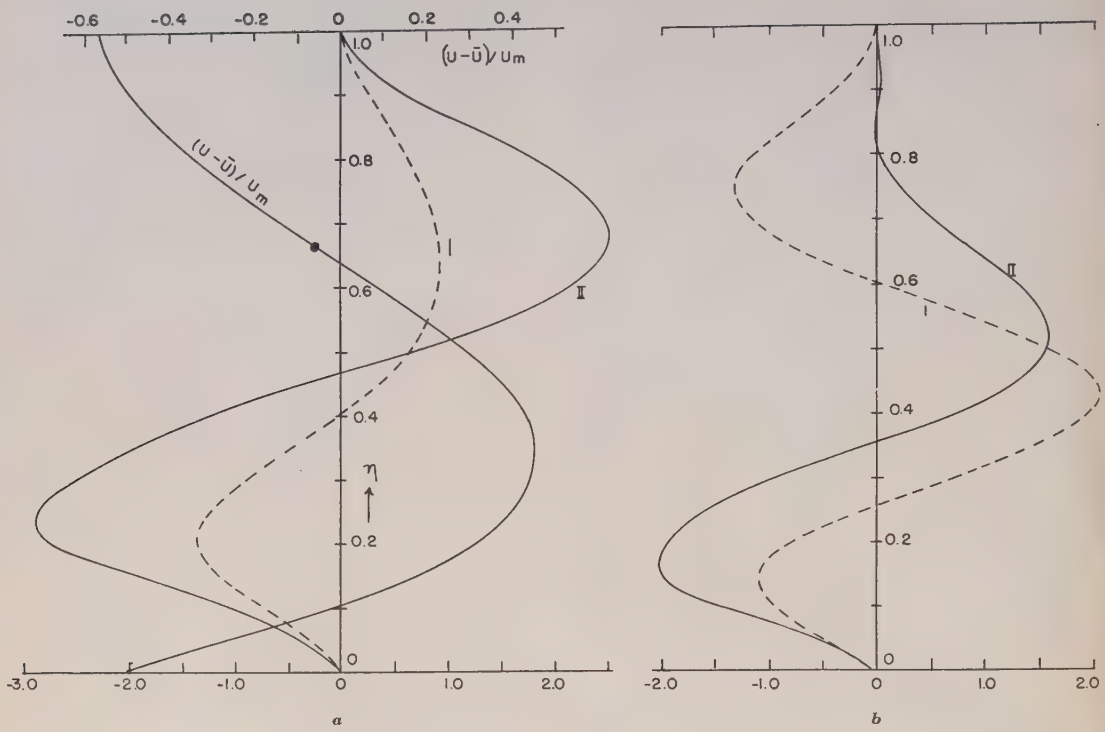

Fig. 8. Same as Fig. 7 for the mean flow $U = 27U_m\eta\ (1-\eta)^2/4$.

effect, as indicated by the curves 1 and 2 of Figure 7 b. The relative second derivative of the kinetic energy of the disturbance is 0.6955 U_m^2/D^2 without the parameter ω and 1.0955 U_m^2/D^2 with this parameter of the earth's rotation.

It should be pointed out that the earth's rotation may have an amplifying effect if the mean flow is unsymmetrical and is stronger in the southern part of the flow and weaker in the northern. To demonstrate this, let us take the mean flow $U = \frac{27U_m}{4}\eta(1-\eta)^2$ which is the image of the profile (c) about the line $\eta = \frac{1}{2}$. The change of mean flow is obtained by replacing η in (7.7) by $1-\eta$. Figures 8 a and 8 b show the result of this substitution for $L = 3.464\ D$ and $L = D$ respectively. The energy integral is obtained from (7.8) by changing the sign of the last term containing the factor ω. For these disturbances, the energy integral including the last term is -0.337 and 0.295 respectively.

8. The mean meridional transfer of zonal momentum

The mean transfer of zonal momentum produced by the large scale atmospheric disturbances has been investigated by a number of workers in recent years, and its meridional distribution is now roughly known. It will be most interesting, then to compare the theoretical results with that obtained from observational material.

In this section we shall discuss the mean momentum transfer corresponding to the disturbance (3.2) and the mean flow profiles (a) $U = U_m \sin^2 ly$, (b) $U = U_m \sin ly$, (c) $U = 27\ U_m\eta^2(1-\eta)/4$ and (d) $U = U_m \sin^4 ly$. For these four mean flow profiles, the rate of increase of the mean meridional transport of zonal momentum is given by the following equations:

$$\frac{D}{a^2k^2U_m}\frac{\partial\overline{uv}}{\partial t} = \frac{(\mu^2-3)\pi}{8(\mu^2+9)}(2\sin 2\pi\eta - \sin 4\pi\eta) \qquad (8.1)$$

$$\frac{D}{a^2k^2U_m}\frac{\partial\overline{uv}}{\partial t}=\frac{\pi}{\mu^2+4}\cos\pi\eta\cdot$$
$$\cdot\left\{\frac{\sinh\mu\pi\eta+\sinh\mu\pi(1-\eta)}{\sinh\mu\pi}-\right.$$
$$-\frac{\mu\tan\pi\eta\,[\operatorname{csch}\mu\pi\eta-\operatorname{csch}\mu\pi(1-\eta)]}{\sinh\mu\pi}-$$
$$\left.-1+\frac{\mu^2}{2}\sin^2\pi\eta\right\} \qquad (8.2)$$

$$\frac{D}{a^2k^2U_m}\frac{\partial\overline{uv}}{\partial t}=\frac{27}{4}\frac{1}{\mu^2+1}\frac{1}{\sinh\mu\pi}\cdot$$
$$\cdot\left\{\mu\sin\pi\eta\cosh\mu\pi\eta-\cos\pi\eta\sinh\mu\pi\eta+\right.$$
$$+\frac{6(3\mu^2-1)}{(\mu^2+1)^2\pi^2}[\mu\sin\pi\eta(\cosh\mu\pi\eta+$$
$$+\cosh\mu\pi(1-\eta))-\cos\pi\eta\cdot$$
$$\left.\cdot(\sinh\mu\pi\eta-\sinh\mu\pi(1-\eta))\right\}+\frac{27\eta(2-3\eta)}{16}\cdot$$
$$\cdot\left(\frac{\mu^2-3}{\mu^2+1}-\cos2\pi\eta\right)-\frac{81}{4(\mu^2+1)^3\pi^2}\cdot$$
$$\cdot[(\mu^4-1)\cos2\pi\eta-\mu^4+6\mu^2-1]-$$
$$-\frac{27(1-3\eta)}{4(\mu^2+1)\pi}\sin2\pi\eta \qquad (8.3)$$

$$\frac{D}{a^2k^2U_m}\frac{\partial\overline{uv}}{\partial t}=\frac{\pi}{16}\frac{\mu^2-15}{\mu^2+25}\sin6\pi\eta-$$
$$-\frac{\pi}{4}\frac{\mu^4+10\mu^2-135}{(\mu^2+9)(\mu^2+25)}\sin4\pi\eta+ \qquad (8.4)$$
$$+\frac{\pi}{16}\frac{5\mu^2-27}{\mu^2+9}\sin2\pi\eta$$

To each of these we should add the transport produced by earth's rotation, given by (3.3 a). For the mean flow profiles (a), (c), and (d), the nature of this interaction depends upon the wave length of the disturbance. However, since the mean zonal flow in the atmosphere is generally not very strong, this interaction represents in the mean a horizontally damping effect on the large atmospheric disturbances, therefore we shall only discuss the damped disturbances with $L=D$ for (a), (b), and (c) and $L=2\,D/3$ for (d). It may also be pointed out that for these large-scale disturbances, this average meridional distribution of the transfer is not much effected by the occasional presence

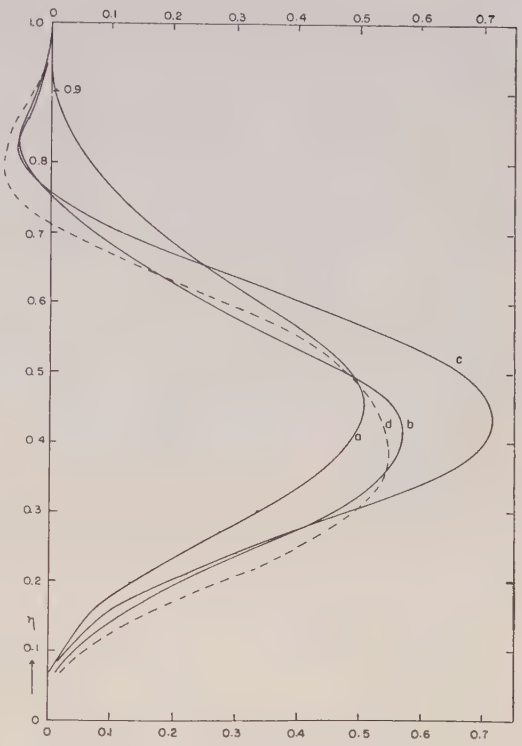

Fig. 9. Theoretical distributions of $\overline{uv}$ for the mean flow profiles (a), (b), (c), and (d).

of amplifying disturbances, as it is determined largely by the earth rotation effect. Taking $D=6.6\times10^6$ m, $\frac{\alpha\omega}{R}=1.1\times10^{-11}\,\mathrm{m^{-1}\ sec^{-1}}$ and $U_m=20$ m sec^{-1}, the nondimensional rates of increase of the mean momentum transfer given by these equations are as represented by the curves (a), (b), (c), and (d) in Figure 9. Similar transports can be produced by earth rotation alone, if the disturbance is more concentrated as have been discussed before.

Since the mean transfer of zonal momentum is initially zero for the type of motion we are considering, we may take the rates of change as representative of the actual transfer and compare them with the results obtained from observations.

In Figure 10, the curve 1 is the six months average (January through June, 1950) total meridional transport of zonal momentum across unit length of the latitude circle, from earth's surface to the 100 mb level, based on

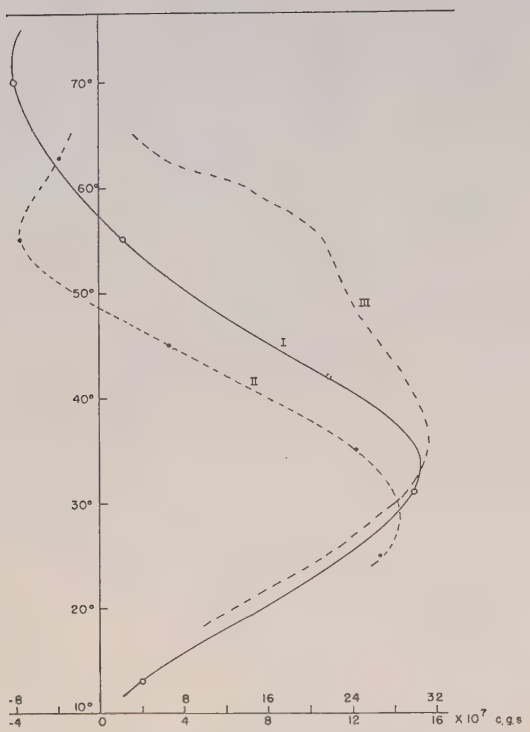

Fig. 10. Observed distribution of $\overline{uv}$: I, 6 months average (January through June, 1950). Hemispherical. II, February 1949, American Continent. II, January 1949, Hemispherical.

the results obtained by Starr and White from actual wind studies along the latitude circles 13° N, 31° N, 42° N, 55° N and 70° N (Starr and White, 1951; 1952 a; 1952 b; and unpublished computations). Curve 2 is the average total transport over the American Continent in February, 1949 (Starr, 1951), and Curve 3 is obtained from Mintz's (1951) results of geostrophic transport for January, 1949. The units for the two curves 2 and 3 are twice as large as for the curve 1. If we put the maximum point of the curves in Figure 9 at the maximum points of the Curves 1 and 2 of Figure 10, it can be seen that they are in rough agreement. The magnitude of the transfer represented by the curves in Figure 9 is also correct if we take the mean north—south velocity to be about 5 to 7 m sec^{-1}, and let the increase take place for a period of one day. For the month of January, 1949, Mintz's mean geostrophic zonal wind profile indicates that two jet streams of westerly current were present, a stronger one around 30° N and a weaker one around 50° N. This suggests that the curve 3 in Figure 10 may be interpreted by superimposing two sets of disturbances with the one having a smaller intensity shifted about 20 latitudinal degrees to the north. Thus, if we take the curve b in Figure 9 and add another one with an intensity equal to two-thirds of that of b and shifted a distance equal to $D/3$ toward north, we get the dashed curve in Figure 1. It is seen that this curve fits the curve 3 in Figure 10 nicely. The momentum transfer produced by the interaction between the disturbance and earth's rotation alone without any mean flow, is also shown in Figure 1 by the full curve.

9. Summary and Conclusions

The problem of the production of mean zonal flow by atmopheric disturbances is attacked by the computation of tendencies. The investigation shows that the effect of the earth's rotation is always to produce a mean northward transport of westerly momentum and a tilt of the troughs and ridges in the SW—NE direction over almost all the regions except near the northern boundary, with the maximum transport and maximum tilting occurring south of the mid-point between the two latitudinal walls assumed. This interaction may either be a damping effect or an amplifying effect for the disturbance, depending on the asymmetry of the existing mean flow profile. For the symmetric mean flow profiles, this process always results in a slow damping of the disturbance, and appears in the fourth time derivative of the mean flow energy. From the nature and distribution of this effect, it would appear that it must have some bearing on the meridional distribution of the mean northward transfer of zonal momentum observed in the atmosphere.

In regard to the interaction between the disturbance and the mean flow, the six examples examined indicate that the presence or absence of an inflection point in the mean flow profile is an important and decisive factor, so far as the particular disturbance is concerned. Thus, in the three cases in which U'' is of one sign throughout, all disturbances of the type discussed are damped, while in the cases in which U'' changes its sign, both damped and amplified disturbances exist. The disturbances

of wavelength longer than a critical wavelength abstract kinetic energy from the mean flow and flatten the profile, and are therefore amplified, while disturbances of shorter wavelength are damped, accentuating the mean flow. The three sinecurve profiles discussed above also indicate that the range of the amplifying wavelength increases as the inflection point of the profile moves away from the boundaries.

Since the mean zonal current in the atmosphere is generally not very strong, the interaction between the disturbance and the mean flow generally represents a horizontal damping process similar to the effect of earth's rotation, while the possible instability of the horizontal motion associated with a stronger mean zonal current happens only occasionally.

To compare our theoretical results with observational facts, the meridional distribution of the mean northward transfer of zonal momentum are computed by this method for four different mean velocity profiles. These examples show that the effects of earth's rotation and that of the mean flow are of the same order of magnitude for the large-scale atmospheric motions. When taken together, the combined effect is to produce a mean northward transport of zonal momentum corresponding to a general SW—NE orientation of the troughs and ridges in almost all parts of the belt except a possible reversal near the northern boundary. It is shown that if the mean north—south velocity is about 5 m sec^{-1} and the increase of these transports takes place for a period of one day, then the computed transports agree roughly with the results obtained from observational material, indicating that the processes discussed are of real importance for the development of the mean zonal current.

REFERENCES

Kuo, H. L., 1949: Dynamic instability of two-dimensional nondivergent flow in a barotropic atmosphere. *J. Meteor.*, **6**, 105—122.

— 1950: The motion of atmospheric vortices and the general circulation. *J. Meteor.*, **7**, 247—258.

— 1951 a: Vorticity transfer as related to the development of the general circulation. *J. Meteor.*, **8**, 307—315.

— 1951 b: Dynamical aspects of the general circulation and the stability of zonal flow. *Tellus*, **3**, 268—284.

Mintz, Yale, 1951: The geostrophic poleward flux of angular momentum in the month of January 1949. *Tellus*, **3**, 195—200.

Neamtan, S. M., 1946: The motion of harmonic waves in the atmosphere. *J. Meteor.*, **3**, 53—56.

Platzman, George W., 1952: The increase or decrease of mean-flow energy in large-scale horizontal flow in the atmosphere. *J. Meteor.*, **9**, 347—358.

Starr, Victor P., 1951: A note on the eddy transport of angular momentum. *Quart. J. R. Met. Soc.*, **77**, 44—50.

Starr, Victor P., and White, R. M., 1951: A hemispherical study of the atmospheric angular momentum balance. *Quart. J. R. Met. Soc.*, **77**, 215—225.

— 1952 a: Note on the seasonal variation of the meridional flux of angular momentum. *Quart. J. R. Met. Soc.*, **78**, 62—69.

— 1952 b: Meridional flux of angular momentum in the tropics. *Tellus*, **4**, 118—125.

Taylor, G. I., and Green, A. E., 1937: Mechanism of the production of small eddies from large ones. *Proc. Roy. Soc.*, A. 158, 499—521.

Note Concerning the Nature of the Large-Scale Eddies in the Atmosphere

By VICTOR P. STARR, Massachusetts Institute of Technology, Cambridge, Mass.

(Manuscript received August 10, 1953)

Abstract

The rate of generation of kinetic energy of mean zonal motions by the large-scale horizontal eddies in the atmosphere is computed from three independent sets of hemispheric wind data. The results are larger than certain analogous dissipation estimates would require. Meteorological implications of the material are discussed.

General discussion

The aim of this brief article is to discuss further, with the aid of new additional data, some essential properties of the large-scale horizontal eddies in the atmosphere, which are involved in their relation to the mean zonal motions present. The particular physical principle to be reviewed has been treated previously mainly by my colleague Dr. H. L. Kuo (1950, 1951 a, 1953) both theoretically and observationally, although it appears that certain additional remarks and graphic illustrations might be of value, since some residual misunderstandings seem to be prevalent.

The mean zonal motions (i. e., averaged with respect to longitude) of the atmosphere may be pictured as comprising a large vortex about the polar axis in which the angular velocity is a function of elevation, latitude and time. As an example the solid curve in (a) of the figure gives the distribution with latitude of this angular velocity relative to the earth, averaged also with respect to pressure in the vertical from 150 to 900 mb and with respect to time over the six-month period January to June 1950 inclusive (N. H.). Most of what is to be said concerning this profile can be made to apply equally to an instantaneous profile at some given level. One may now ask what the effect of genuine lateral friction alone on such a flow might be. Quite obviously the effect of such viscosity would be to retard the zones of most rapid rotation and to increase the angular velocity of the less rapidly rotating ones, so as to cause the whole to assume a more nearly uniform angular velocity. That is to say, lateral friction would cause a flow of angular momentum northward and also southward away from the zone of most rapid rotation.

One may inquire next as to whether the large-scale eddies in the atmosphere act upon the mean zonal motions in a manner analogous to friction and hence may be regarded as merely giving rise to an eddy viscosity. This is outstandingly not the case, for according to any compilation of data at all adequate for the purpose (and there are a number of such independent ones now available) there exists a strong northward eddy transport of angular momentum to the south of the jet of westerlies (N. H.) and therefore *a fortiori* to the south of the zone of maximum angular velocity, on the average. This is exactly contrary to a frictional effect and would be compatible only with a negative virtual viscosity coefficient, if it were desirable even to use such terminology. The mere existence of this state of affairs is in itself most remarkable and by no means to be

lightly dismissed, for regardless of further considerations it is a manifestation of a fundamental process which requires explanation ultimately. The associated angular momentum transport by eddies is given by the dashed line in (a) of Fig. 1.

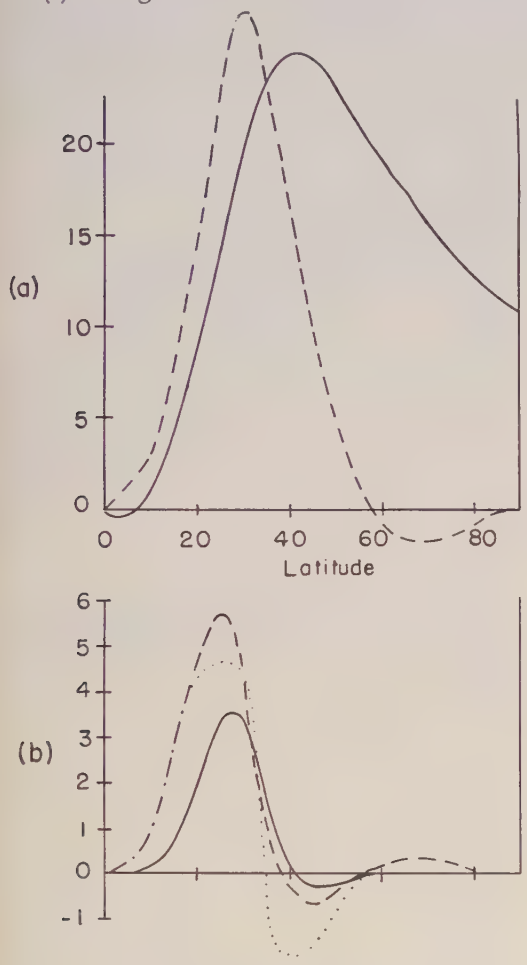

Fig. 1. Relative angular velocity in 10^{-7} sec^{-1} as function of latitude given by full curve in (a). Total angular momentum transport by eddies in 10^{25} c.g.s. units given by dashed curve in (a). Production of zonal kinetic energy using mean wind and total transport (full curve), using 300 mb wind and transport (dashed curve) and using 200 mb wind and transport (dotted curve) shown in (b) in terms of arbitrary units.

Kinetic energy considerations

It is convenient and instructive to study these effects of the eddies upon the *kinetic energy* of the mean zonal motions. Considering the northern hemisphere as acting independently, the net influence on this total kinetic energy is to increase it, if the (positive) action to the south predominates and to decrease it if conditions are the reverse. The rate of production may be written as

$$2\pi r^2 \int\int \varrho [u'v'] \cos^2 \Phi \frac{\partial}{\partial \Phi}\left(\frac{[u]}{r \cos \Phi}\right) d\Phi dz \quad (1)$$

if small approximations such as the horizontal uniformity of density are allowed in the definition of mean zonal kinetic energy. The notation is that of STARR and WHITE (1951, 1952), u, v, being eastward and northward wind components, ϱ density, r earth's radius, Φ latitude, z elevation, the square brackets denoting averaging along complete latitude circles, and the primes indicating deviations from such averages. This expression may either be set up directly from a consideration of the work done by net forces due to the eddy stresses on elementary rings of air, or it may be obtained by writing the proper form of the balance equation for zonal kinetic energy as done, for example, by KUO (1951 a).

Data and computations

Among the available data for investigating expression (1) the following may be listed.

(1) The first six months of the year 1950 already referred to. These data are based upon (daily) actual wind observations similar to those of Starr and White in the references already given, for Latitudes 13°, 31°, 42°, 55°, and 70° N. The integrand of (1) evaluated from the six-month averages of $[u]$ and $[u'v']$ is given for the 300 and 200-mb levels by the dashed and dotted lines respectively in (b) of the figure. The full line results from using the vertical pressure averages of wind and eddy transport (i.e., corresponding to the curves given in (a) already discussed). Since in (b) the area under each curve measures the production of zonal kinetic energy, it is to be noted that in each case this area is positive by a wide margin.

(2) The second six months of the year 1950. These data are exactly analogous to those for the first six months and were treated in the same way. The integrands (not shown) were again positive without question, i.e., do not represent small differences between large quantities.

(3) One month of data (Jan. 1949) published by MINTZ (1951). These represent geostrophic evaluations obtained by punched card methods. As in the case of the curves (b), here also there is no ambiguity as to the sign of the areas beneath the curves (not shown) in all three instances.

Using the vertically averaged winds and transports the data (1) give 4.2×10^{20} ergs per second for the production over the hemisphere. The data (2) give 4.6×10^{20} units. Data (3) give 10.5×10^{20} units. These magnitudes are to be compared with appropriately defined and properly estimated measures of the dissipation. When the vertical averages are used one deals essentially with the kinetic energy of the mean rotation of the atmosphere, and the dissipation becomes merely the work done against the zonal component of ground stresses in virtue of this mean relative rotation, save for minor other effects. Further discussion of this subject is given by STARR and WHITE (1953). The zonal ground stresses may be obtained in the form of empirical climatological estimates as given by PRIESTLEY (1951), for example. The stresses deduced from the angular momentum balance considerations for the particular period in question as calculated for example by MINTZ (1951) would not give an independent check for the present purpose. Use of Priestley's stresses with the data (1) gives 3.6×10^{20} units for the hemisphere. The data (2) give 1.9×10^{20} units, while data (3) give 4.0×10^{20} units.

If the angular velocity curve in (a) of the figure is assumed to be representative of the entire depth of the atmosphere, we may compute from it the corresponding kinetic energy of mean rotation for the northern hemisphere, which turns out to be about 6.8×10^{26} ergs. Upon appeal to the figure given for the mean rate of production from data (1), it is seen that this amount is normally generated in about 19 days. The corresponding period for data (2) is 12 days and for data (3) it is 17 days. Presumably if the production were suddenly to cease while the dissipation were to maintain its normal rate, the motions of the air here involved would be abolished in about two weeks.

Discussion of results

Relegating certain further technical matters and qualifying remarks to the next section, we may enumerate certain important inferences which may be drawn from the general character of the results, if these latter are correct in main outline, as seems most probable. These are:

1. The large disturbances in the atmosphere produce kinetic energy of mean zonal motions, and not the reverse as has been with few exceptions generally supposed in the past.

2. Since the magnitudes of this generation are of the order of the estimated dissipation, and could regenerate the motions involved in about two weeks, it may be stated that any theory for the general circulation of the atmosphere which omits this effect is crucially deficient, lacking an essential correspondence to reality, however interesting it may otherwise be.

3. Through the years there has been current in meteorology an assortment of general circulation theories which do not presuppose this action of the eddies. The singular sterility and lack of promise which have characterized these can perhaps be ascribed largely to the shortcoming under discussion.

4. It is increasingly clear that a valid formal theory of the general circulation showing how the incoming radiational energy supply results in the observed motions (rather than others) will probably be evolved only slowly because of its inherent complexity.

The problem of the mean zonal motions and the large-scale disturbances is one and inseparable, because of the now demonstrated interdependence of these circulations; hence there exists a natural and direct connection to such other modern developments as those in cyclone theory and similar topics, which latter will first have to be not only better understood but also fitted into the more general picture. For the time being it may be necessary to content oneself with the theoretical examination of only portions or phases of the total process. Indeed much of what now may appear as composed of separate and distinct subjects in theoretical meteorology must ultimately form a coordinated and harmonious whole, displaying in true light the proper and natural relationships among these parts.

5. The theoretical efforts of my esteemed friend Dr. H. L. KUO may be mentioned specifically as an example of what has just been said (see KUO, 1950, 1951 b, 1953). These

studies are directed toward the elucidation of the transformation of eddy kinetic energy into mean zonal kinetic energy through the application of the vorticity equation. This procedure may be interpreted also as an effort to apply the general principles, if not the specific techniques, used in what is now called numerical forecasting to the problem of the general circulation. It is to be noted that in this connection, and also from the general results stated in this paper, the seat of the kinetic energy processes is placed in the cyclonic and anticyclonic systems in the atmosphere, which directly or indirectly account for the continued replenishment of the eddy kinetic energy.

6. It may with profit be again contemplated that the positive nature of the production process as measured from data is not contingent upon the attainment of some petty accuracy, but is at once fixed by very gross aspects of the zonal-wind and angular momentum transport profiles. The end result could, in fact, hardly be otherwise if the maximum northward angular momentum transport is found in the vicinity of the mean latitude of the jet stream.

7. Most of the so-to-speak simple theories of the general circulation start from the assumption that the mean zonal motions are maintained by mean meridional circulations. From time to time thinking men have expressed dissatisfaction with such a framework to various degrees, e. g., JEFFREYS (1926), ROSSBY (1947, 1949), although the direct measurement of the mean meridional circulations cannot be carried out with great enough confidence for a direct refutation which would be reliable. Once, however, very extensive independent compilations of data consistently point to the existence of a sufficiently potent alternative, it is quite unscientific to concentrate merely on the older approach. The writer's opinion in this regard does not exclude the possibility that sufficiently extensive observational studies may show that mean meridional circulations perform certain other important functions, or even modify to some extent the eddy-produced zonal flows. In any case it would be highly improper not to give recognition to those indications and suggestions deriving most clearly and unambiguously from purely objective data as already expounded.

Critique and further computations

During the course of the work performed a number of added questions and matters of thoroughness were examined and treated in much greater detail than can be fully entered into for the purpose of this note. Some critical statements and results of corresponding checks in some instances may nevertheless be made for purposes of better orientation.

1. The use of vertical averages for the zonal wind profile is a rather specialized device which introduces valuable simplifications, but general interest still demands that the results be compared with what would be obtained from calculations at individual levels which are then integrated vertically as a final step. Such alternative figures were calculated giving for data (1) 3.9×10^{20}, for data (2) 5.5×10^{20}, and for data (3) 9.8×10^{20} erg sec^{-1}.

2. A second check carried out was to calculate the production using a vertically integrated zonal-wind profile but applying the technique to the instantaneous daily conditions, the long term mean being then formed by averaging the daily figures for the production.

By this procedure an opportunity is also afforded to compute confidence limits defined as twice the standard error of the mean of the daily values, indicating roughly the 95 per cent confidence range. The data (1) were subjected to such a treatment, although at the time this work was done the observations for 70° N latitude had as yet not been tabulated and hence were not included. The figure obtained was $(4.5 \pm 1.0) \times 10^{20}$ erg sec^{-1}.

3. A still further elaboration consists of the use of the analysis by levels, not with the long period averages, but with instantaneous daily data. The long term mean may then again be formed by averaging the daily production figures. The data (1) with the 70° N latitude circle omitted were used also for this purpose. The figure which resulted was 9.8×10^{20} erg sec^{-1}.

4. In the computations it was arbitrarily assumed that $[u]$ and $[u'v']$ are zero at the equator. What the exact values of the momentum transport are at the equator is not known, but the use of more proper negative values of $[u]$ would tend to increase the anticyclonic wind shear immediately to the north where the transport is positive and hence would probably increase the production.

5. Selectivity in the availability of wind observations favoring lower speeds probably leads to an underestimate of the production. It is to be noted that the integrand of expression (1) involves a triple product of quantities in the nature of wind velocity components, hence underestimates of the latter could produce a larger percentual underestimate here than in such quantities as, for example, the kinetic energy itself.

6. It should be most carefully observed that if the effect of the eddy processes on the mean zonal kinetic energy is studied for a narrower belt of latitude, terms representing the meridional transport of this energy across the bounding latitudes should be considered, and the mere adjustment of the limits of integration in (1) does not provide for this requirement. In the case of the whole hemisphere it is doubtful, however, that such a transport across the equator is anything more than a slight correction, which is here neglected (and would necessarily vanish for the entire atmosphere).

7. The surface zonal stresses given by Priestley are according to most proper interpretation values for the oceans. Doubtless the extensive land masses present in the northern hemisphere give rise to larger such stresses as suggested by the angular momentum convergence study of Mintz (1951), thus helping to bridge the great disparity found here between the eddy production and the dissipation of the energy of mean rotation.

8. The expression (1) is actually nothing more than the spherical polar form of the corresponding term in the familiar theory of Osborn Reynolds (1895) concerning the nature of eddy processes. A review of this material is given also by Lamb (1932) in his textbook on hydrodynamics. Indications of the importance of the process here measured by expression (1) have been obtained also by Blackadar (1950) and by Van Mieghem (1953).

REFERENCES

Blackadar, A. K., 1950: Transformation of energy by the large scale eddy stress in the atmosphere. *Meteorological Papers*, **1**, 3, New York University, College of Engineering, New York, 39 p.

Jeffreys, H., 1926: On the dynamics of geostrophic winds. *Quart. J. R. Meteor. Soc.*, **52**, 85—104.

Kuo, H. L., 1950: The motion of atmospheric vortices and the general circulation. *J. Meteor.*, **7**, 247—258.

— 1951 a: A note on the kinetic energy balance of the zonal wind systems. *Tellus*, **3**, 205—207.

— 1951 b: Dynamical aspects of the general circulation and the stability of zonal flow. *Tellus*, **3**, 268—284.

— 1953: On the production of mean zonal currents in the atmosphere by large disturbances. *Tellus* **5**, 475—493.

Lamb, H., 1932: *Hydrodynamics*. 6th ed., Camb. Univ. Press, 738 p.

Mintz, Y., 1951: The geostrophic poleward flux of angular momentum in the month January 1949. *Tellus*, **3**, 195—200.

Priestley, C. H. B., 1951: A survey of the stress between the ocean and atmosphere. *Austr. J. Sci. Res.*, Series A, **4**, 315—328.

Reynolds, O., 1895: On the dynamical theory of incompressible viscous fluids and the determination of the criterion. *Phil. Trans. Roy. Soc. London* (*A*), 186, 123—164.

Rossby, C.-G., 1947: On the distribution of angular velocity in gaseous envelopes under the influence of large-scale horizontal mixing processes. *Bull. Amer. Meteor. Soc.*, **28**, 53—68.

— 1949: On the nature of the general circulation of the lower atmosphere. *The atmosphere of the earth and planets*, G. P. Kuiper, editor. Univ. of Chicago Press.

Starr, V. P., and White, R. M., 1951: A hemispheric study of the atmospheric angular momentum balance. *Quart. J. R. Meteor. Soc.*, **77**, 215—225.

— 1952: Meridional flux of angular momentum in the tropics. *Tellus*, **4**, 118—125.

— 1953: The maintenance of the mean rotation of the atmosphere. (Unpublished)

Van Mieghem, J., 1953: Energy conversions in the atmosphere on the scale of the general circulation. *Tellus*, **5**, 334—351.

Zur numerischen Wettervorhersage mittels Relaxationsmethode unter Einbeziehung barokliner Effekte. II[1]

K. HINKELMANN, Deutscher Wetterdienst, Bad Kissingen

(Manuscript received January 20, 1953)

II. Lösungsmethoden

Es sollen 2 Lösungsverfahren kurz behandelt werden, die zur Berechnung der im Abschn. III. gezeigten Lösungen benutzt wurden. Jedoch sind auch andere Lösungsverfahren anwendbar.[2]

1.) Relaxationsmethode nach R. Southwell:

Zur Lösung des Differenzengleichungssystems (16), in welchem die obere und untere Randbedingung (7, 8) bereits enthalten sind, ist besonders -ür Handberechnungen die Relaxationsmethode von Southwell geeignet.

Man geht bei diesem Lösungsverfahren von einem an sich beliebigen bequemen Lösungsansatz, im allgemeinen von $\overset{0}{\tau} = 0$ (Lösung nullter Näherung) aus. Dano geben die rechten Seiten von (16) den Fehler R an, um den die Gleichungen durch den Ansatz $\overset{0}{\tau} = 0$ nicht erfüllt sind. Diesen Fehler bezeichnet man allgemein als Residuum.

Durch schrittweise Verbesserung des τ-Feldes versucht man, das Residuum gleichmäßig im gesamten Gitterfeld gegen 0 konvergieren zu lassen.

Als erste Nährung $\overset{1}{\tau}$ benutzt man gewöhnlich

$$\overset{1}{\tau}_k = \delta\overset{0}{\tau}_k = A_k h_k \quad \text{mit} \quad A_k = \frac{1}{4 + \alpha_{k+} + \alpha_{k-}}$$

In diesem Falle ist das zum Ansatz $\tau = 0$ gehörige Residuum R mit dem inhomogenen Term der Gleichungen (16) identich. Da die Gleichungen (16) einen Funktionswert τ_k^{ij} mit den Funktionswerten $\tau_k^{i\pm1,j}$, $\tau_k^{i,j\pm1}$, $\tau_{k\pm1}^{ij}$ funktionell verkoppeln, bewirkt eine Änderung $\delta\tau_k^{ij}$ eine Änderung des Residuums nicht nur im Aufpunkt $\mathbf{r}_k^{ij}$ selbst, sondern auch in den je um eine Maschenweite vom Aufpunkt entfernten Nachbarpunkten.

Im vorliegenden Falle ergibt eine Änderung $\delta\tau_k^{ij}$ folgende Änderungen der Residuen.

$$\delta R_k^{ij} = -A_k^{ij}\,\delta\tau_k^{ij};\quad \delta R_k^{i\pm1,j} = \delta R_k^{i,j\pm1} = \delta\tau_k^{ij} \quad (18\text{ a})$$

$$\delta R_{k+1}^{ij} - \alpha_{k+1-}^{ij}\delta\tau_k^{ij};\quad \delta R_{k-1}^{ij} = \alpha_{k-1+}^{ij}\delta\tau_k^{ij} \quad (18\text{ b})$$

wie man sich leicht klarmacht, wenn man den Gitterpunkten $\mathbf{r}_k^{ij}$, $\mathbf{r}_k^{i\pm1,j}$, $\mathbf{r}_k^{i,j\pm1}$, $\mathbf{r}_{k\pm1}^{ij}$ die zugehörigen Gleichungen (16) zuordnet. Anstelle von (18 b) liefert jedoch entsprechend Gleichung (16 b) eine Änderung

$\delta\tau_k^{ij}$ im Punkte $k = {}^1/_2$ die Residualänderungen $\delta R_{k+1}^{ij} = \alpha_{k+1-}^{ij}\delta\tau_k^{ij}$; $\delta R_{k-\frac{1}{2}}^{ij} = 0$ und analog Gleichung (16 c) eine Änderung

$\delta\tau_k^{ij}$ im Punkte $k = n - {}^1/_2$ die Residualänderungen

$$\delta R_{k-1}^{ij} = \alpha_{k-1+}^{ij}\,\delta\tau_k^{ij};\quad \delta R_{k+\frac{1}{2}=n}^{ij} = 0$$

Die durch eine Änderung von $\delta\tau$ entstehende neue R-Verteilung kann wiederum zur Verbesserung der τ-Werte benutzt werden, entsprechend erhält man als zweite Näherung $\overset{2}{\tau} = \overset{1}{\tau} + \delta\overset{1}{\tau}$; mit $\delta\overset{1}{\tau} = \overset{1}{R}A$ und gem. obigem Schema (18) neue Residuen $\overset{2}{R}$ usw.

Die obige Annahme $\delta\overset{l}{\tau}_k^{ij} = A_k^{ij}\,\overset{l}{R}_k^{ij}$ bewirkt also gerade, daß das Residuum in Punkte $(\mathbf{r}_k^{ij})$ exakt verschwindet. Allerdings wird durch

[1] Continued from Vol. 5, No. 3.

[2] z. Bsp. die Verwendung des modernisierten Gaußschen Algorithmus, vgl. dazu die Berichte Nr. 5, 6 des Instituts für Praktische Mathematik, Darmstadt.

Verfügung über die τ-Werte in der Nachbarschaft von $(\mathbf{r}_k^{ij})$ wiederum ein $R_{k\cdot}^{ij}$ erzeugt.

Beim Relaxieren muß deshalb angestrebt werden, die Änderung von τ im Aufpunkt $(\mathbf{r}_k^{ij})$ und in den Nachbarpunkten so abzustimmen, daß R_k^{ij} erst durch die vom Aufpunkt und von den Nachbarpunkten herrührenden Änderungen möglichst klein wird.

Eine schnellere Konvergenz wird z. B. erreicht, wenn man anstelle der Abschätzung $\overset{l}{\delta\tau}_k = A_k \overset{l}{R}_k$ die dem Lösungswert näherkommende Abschätzung

$$\overset{l}{\delta\tau}_k = A_k \overset{l}{R}_k + A_k(\sum A_k^{i'j'} \overset{l}{R}_k^{i'j'} + \alpha_{k+} A_{k+1} \overset{l}{R}_{k+1} + + \alpha_{k-} A_{k-1} \overset{l}{R}_{k-1}) \qquad (19)$$

benutzt, vgl. dazu die Operatorenmethode in Abschn. II, 2

Jedoch braucht man sich bei Handberechnung nicht an ein starres Schema für die Verbesserung der τ-Werte zu halten. Durch geschicktes Schätzen der Funktionswerte τ bzw. deren Zuschläge zur vorangehenden Schätzung unter Berücksichtigung möglichst vieler Residualwerte in der Nähe des Schätzpunktes kann der Lösungsprozeß u. U. erheblich beschleunigt werden.

Als Resultat erhält man schließlich $\tau = \sum_{l=0}^{N} \overset{l}{\delta\tau}$, wobei der Prozeß abgebrochen werden kann, wenn N einem Residualfeld entspricht, das den Genauigkeitsansprüchen genügt, d. h. dessen Residualwerte R sich innerhalb der Fehlergrenzen der inhomogenen Terme h halten.

Die Behandlung der seitlichen Randnachbarpunkte richtet sich nach den speziellen seitlichen Randbedingungen. Im Falle, daß die τ-Werte auf den seitlichen Randflächen vorgegeben werden, erübrigt sich selbstverständlich eine Residualwertkontrolle für die seitlichen Randpunkte.

2. Operatorenlösungsmethode.

Mit etwa dem gleichen Rechenaufwand kann die Lösung von (16) auch durch Anwendung der Operatorenlösungsmethode herbeigeführt werden, wie sie z. Bsp. für die zweidimensional barotrope Vorticity-Gleichung von R. FJØRTOFT (1952) — vgl. Gl. (16)′ — benutzt wird. Gleichung (16 a)

$$\tau_k - A_k (\sum \tau_k^{i'j'} + \alpha_{k+} \tau_{k+1} + \alpha_{k-} \tau_{k-1} = A_k h_k$$

schreibt sich, wenn folgender Mittelbildungsoperator

$$D \equiv A\,(\sum\nolimits_{k}^{i'j'} + \alpha_{k+\,\cdots\,k+1} + \alpha_{k-\,\cdots\,k-1})$$

eingeführt wird:

$(1 - D)\,\tau = Ah$ mit der formalen Lösung

$$\tau = \frac{1}{1 - D} Ah \qquad (20\,a)$$

Unter der Voraussetzung, daß die Koeffizienten der Iterierten von D hinreichend rasch nach o konvergieren — ob diese Voraussetzung zutrifft, muß die Lösungsfolge erweisen — ist

$$\tau = (1 + D + D^2 + \ldots + D^l \ldots +)\,Ah = \sum_{l=0}^{\infty} D^l Ah \qquad (20\,b)$$

Wir setzen abkürzend $\overset{l}{\delta\tau} = D^l Ah$; dann ist

$$\tau = \sum_{l=0}^{\infty} \overset{l}{\delta\tau} \text{ und } \overset{l+1}{\delta\tau} = D\,(\overset{l}{\delta\tau})$$

Man erhält damit:

$$\overset{0}{\delta\tau}_k = A_k h_k$$

$$\overset{l+1}{\delta\tau}_k = D_k\,(\overset{l}{\delta\tau}) = A_k\,(\sum \overset{l}{\delta\tau}_k^{i'j'} + + \alpha_{k+} \overset{l}{\delta\tau}_{k+1} + \alpha_{k-} \overset{l}{\delta\tau}_{k-1})$$

Naturgemäß konvergiert dieses Operatorenlösungsverfahren ebenso rasch wie der Relaxationsprozeß, wenn man sich bei letzterem bei der »Schätzung« der τ-Werte starr an das Schema (18) hält.

Eine raschere Konvergenz wird durch folgende Entwicklung bei etwas veränderter Bedeutung der $\overset{l}{\delta\tau}$ erreicht:

$$\overset{0}{\delta\tau} = (1 + D)\,Ah$$

$$\overset{1}{\delta\tau} = D^2\,(1 + D)\,Ah = D^2\,(\overset{0}{\delta\tau})$$

$$\overset{l+1}{\delta\tau} = D^2(\overset{l}{\delta\tau})$$

Als Lösung erhält man wiederum

$$\tau = \sum_{e=0}^{\infty} \overset{l}{\delta\tau} \qquad (21)$$

Das Lösungsverfahren erfordert die Bestimmung des Operators D^2. Durch Anwendung von D_k auf $D_k \psi = A_k\,(\sum \psi_k^{i'j'} + \alpha_{k+} \psi_{k+1} + + \alpha_{k-} \psi_{k-1})$ erhält man

$$[A_k^{-1}(D_k)^2\psi]^{ij} = \sum A_k^{i'j'}\left(\sum \psi_k^{i'j'} + \alpha_{k+}^{ij}\psi_{k+1}^{ij} + \right.$$
$$+ \alpha_{k-}^{ij}\psi_{k-1}^{ij}) + \alpha_{k+}A_{k+1}\left(\sum \psi_{k+1}^{i'j'} + \alpha_{k+1+}\psi_{k+2} + \right.$$
$$\left. + \alpha_{k+1-}\psi_k\right) + \alpha_{k-}A_{k-1}\left(\sum \psi_{k-1}^{i'j'} + \alpha_{k-1+}\psi_k + \right.$$
$$\left. + \alpha_{k-1-}\psi_{k-2}\right)$$

und nach Zusammenfassen von ψ-Werten gleicher Gitterpunkte.

$$[A^{-1}D^2\psi]_k^{ij} = \left(\sum A_k^{i'j'} + A_{k+1}^{ij}\alpha_{k+}^{ij}\alpha_{k+1-}^{ij} + \right.$$
$$\left. + A_{k-1}^{ij}\alpha_{k-}^{ij}\alpha_{k-1+}^{ij}\right)\psi_k^{ij} + A_k^{i+1,j}\psi_k^{i+2,j} +$$
$$+ A_k^{i-1,j}\psi_k^{i-2,j} + A_k^{i,j+1}\psi_k^{i,j+2} + A_k^{i,j-1}\psi_k^{i,j-2} +$$
$$+ \left(A_k^{i+1,j} + A_k^{i,j+1}\right)\psi_k^{i+1,j+1} + \left(A_k^{i+1,j} + \right.$$
$$\left. + A_k^{i,j-1}\right)\psi_k^{i+1,j-1} + \left(A^{i-1,j} + A_k^{i,j+1}\right)\psi_k^{i-1,j+1} +$$
$$+ \left(A_k^{i-1,j} + A_k^{i,j-1}\right)\psi_k^{i-1,j-1} + A_{k+1}^{i,j}\alpha_{k+}^{i,j}\alpha_{k+1+}^{i,j}\psi_{k+2}^{i,i} +$$
$$+ A_{k-1}^{i,j}\alpha_{k-}^{ij}\alpha_{k-1-}^{ij}\psi_{k-2}^{i,j} + \sum\left(A_k^{i',j'}\alpha_{k+}^{i',j'} + \right.$$
$$\left. + A_{k+1}^{i,j}\alpha_{k+}^{i,j}\right)\psi_{k+1}^{i'j'} + \sum\left(A_k^{i'j'}\alpha_{k-}^{i'j'} + A_{k-1}^{i,j}\alpha_{k-}^{i,j}\right)\psi_{k-1}^{i,j'}$$

Beim Übergang von $\delta^{l}\tau$ auf $\delta^{l+1}\tau$ zur Verbesserung der Lösungsfunktion mittels der Folge (21) gehen zur Bestimmung von $\delta^{l+1}\tau$ bereits 18 dem Aufpunkt benachbarte $^{l}\tau$-Werte ein. Allgemein führt die Entwicklung $\tau_k = (1 + D + D^2 + \ldots)_k$ Ah, die alle h-Werte des Raumgitters in dem betrachteten Integrationsgebiet erfaßt, auf die Bestimmung der lösenden Kerngitterfunktion des Differenzengleichungssystems im Punkte $\mathbf{r}_k^{ij}$, dargestellt durch die Koeffizienten der h-Gitterwerte. s. III.

Die Berücksichtigung der Randbedingungen erfolgt dabei automatisch, wenn der Operator D an den Randnachbarpunkten entsprechend den Koeffizienten von (16 b, c) definiert wird.

Praktische Rechenversuche mit Hilfe der Relaxations- oder Operatorenlösungsmethode ergaben, daß bei willkürlicher Streuung der inhomogenen Terme, wie das bei tatsächlichen Wettersituationen auftritt, etwa 5—10 Relaxationen bzw. Operatorenschritte für jeden Gitterpunkt durchzuführen sind, bis eine ausreichende Genauigkeit der Lösungsfunktion τ erreicht wird.

Eine wesentlich schnellere Konvergenz wäre sicherlich herbeizuführen, wenn mit Hilfe von Einfluß- oder Greenschen Funktionen eine wenn auch grobe Vorschätzung des Tendenzfeldes τ durchgeführt werden könnte.

Unglücklicherweise hängen jedoch die Koeffizienten des Differentialausdrucks in 16 wegen der darin vorkommenden σ, η-Terme ebenfalls wie die inhomogenen Glieder der rechten Seite von (16) von der zu behandelnden Wettersituation ab.

Um eine Vorstellung zu vermitteln, mit welch unterschiedlichem Gewicht inhomogenes Feld h und Koeffizientenfeld α des Differentialausdrucks die Lösung beeinflussen, sollen die Gleichungen (16) hinsichtlich der von z und inneren Ableitungen von z abhängigen Größen linearisiert werden:

Wir machen für das stationäre Grundfeld (überstrichene Größen) folgenden Ansatz:

$$\bar{z} = L(p)\cdot\gamma + l(p);\ \text{dann ist}$$
$$\bar{\eta} = f;\ \text{weiterhin sei } f_x \approx 0$$

Für das Störungsfeld z'; $z = \bar{z} + z'$, sollen keine einschränkenden Annahmen gemacht werden. Linearisierung der Koeffizienten der Vorticity-Gleichung:

$$\Delta\tau - \frac{f}{m^2 g}\eta^2\left(\frac{\omega}{\eta}\right)_p = -J(z,\eta)$$

ergibt wegen $\bar{\omega} = \bar{\tau} = 0$

$$\Delta\tau' - \frac{f}{m^2 g}\bar{\eta}\,\omega_p = \Delta\tau - \frac{f^2}{m^2 g}\omega_p =$$
$$= -J(\bar{z},\eta') - J(z',f) \qquad (22)$$

Linearisierung der Koeffizienten des I. Hauptsatzes (6) mit

$$\frac{dq}{dt} = 0;\ \omega = -\frac{g}{\sigma}(\tau_p + Q) =$$
$$= -\frac{g}{\sigma}\left[\tau_p - \frac{gm^2}{f}J(z_p, z)\right]$$

ergibt wegen $\overline{Q} = J(\bar{z}_p, \bar{z}) = 0$

$$\omega' = -\frac{g}{\sigma}(\tau_p' + Q') \text{ mit} \qquad (23)$$

$$Q' = \frac{g}{f}m^2(\bar{z}_{py}z_x' - z_{px}'\bar{z}_y) = \frac{m^2}{f}\frac{R}{p}(T_x'\bar{z}_y - \bar{T}_{y\sim x}')$$

$$\bar{\sigma} = \frac{g}{\varkappa p}\bar{z}_p + g\bar{z}_{pp},$$

worin wegen der speziellen Wahl des Grundzustandes die Akzente auch fortgelassen werden können.

Elimination von ω aus (22) und (23) und Ersetzen der τ und ω enthaltenden Differentialausdrücke durch entsprechende Differenzenausdrücke ergibt anstelle (16a)

$$(4+\alpha_{k+}+\alpha_{k-})\,\tau_k - \alpha_{k+}\,\tau_{k+1} - \alpha_{k-}\tau_{k-1} -$$
$$-\sum \tau_k^{i'j'} = h_k^{ij} = \mu^2 J_k(\bar{z},\eta') + \mu^2 J_k(z',f) +$$
$$+\nu\,(\alpha_{k+}\,Q_{k+\frac{1}{2}} - \alpha_{k-}\,Q_{k-\frac{1}{2}}) \text{ mit}$$
$$\alpha_{k\pm} = \frac{f^2}{m^2}\frac{\mu^2}{\nu^2}\frac{1}{\bar{\sigma}_{k\pm\frac{1}{2}}} \quad \text{für } 1 < k < n-1 \quad (24)$$

und (16b) und (16c) analoge Gleichungen für $k = {}^1/_2$ und $k = n - {}^1/_2$.

Nach Linearisierung treten in dem Differenzenoperator von τ d. h. auf der linken Seite von Gleichung (24), keine Störgrößen mehr auf. Das legt den Schluß nahe, daß man auch mit einem α-Feld eines Grundzustandes, der von der speziellen Wetterlage unabhängig ist, noch zu einer vernünftigen Lösung gelangen kann. Die Tatsache, daß jetzt wegen $\bar{\eta} = f$

$$\alpha_{k\pm} = \alpha_{k\pm1,\mp}$$

läßt weiterhin vermuten, daß auch der vertikale Vorticitytransport $\omega\eta$ einen geringeren Einfluß auf die Lösung ausübt als der Divergenzausdruck $\eta\omega_p$.

Wir werden also berechtigt sein, uns zumindest einen Überblick über den vermutlichen Lösungsverlauf zu verschaffen unter Zugrundelegung eines von den speziellen Topografien unabhängigen Koeffizientenfeldes α.

Dies hat den entscheidenden Vorteil, daß man mit Greenschen Standardfunktionen G ohne einen Iterationsprozeß zu einer Näherungslösung τ, ω gelangen kann, wobei bei einer nur von p abhängigen Standardatmosphäre diese Greenschen Funktionen sogar weitgehend invariant gegen Koordinatenverschiebung in x, y sein werden, zumindest in hinreichendem Abstand von der seitlichen Begrenzungsfläche.

Mit Hilfe solcher ebenfalls mit Hilfe der Relaxations- oder Operatorenlösungsmethode gewinnbarer Funktionen G kann man sich durch eine einmalige Integration bzw. Summation die zu dem Standard-α-Feld gehörige Lösung eines beliebigen Feldes inhomogener Terme verschaffen, die als Vorschätzung der Lösung des aktuellen α-Feldes betrachtet wird.

Nach Auswechseln der α-Koeffizienten erhält man sicherlich nach wenigen Relaxations- bzw. Operatorenschritten eine dem variablen α-Feld zugeordnete Lösung, wenn mit der mit Hilfe Greenscher Funktionen gewonnenen Näherungslösung begonnen wird.

III. Anwendungen

Die Fig. 4—13 geben einige Einflußfunktionen für verschiedene Lagen des Quellpunktes wieder: Wir wollen unter einer Einflußgitterfunktion I $(\mathbf{r}', \mathbf{r})$ eine Lösungsfunktion τ verstehen, die in allen inneren Gitterpunkten die Differenzengleichungen (16a—c) mit $h_k^{ij} \equiv 0$ erfüllt, mit Ausnahme des Quellpunktes $\mathbf{r}'(_{k'}^{i'j'})$, wo $h_{k'}^{i'j'} \neq 0$ sei. Entsprechend lassen sich Einflußfunktionen I als Lösungsfunktion der Gln. (16) definieren, wo im Quellpunkt $\mathbf{r}'$ nur entweder der Vorticitytransport $\mu^2 J(z,\eta)$ oder die thermische Quantität Q von Null verschieden ist.

Im Falle $\mu^2 J(z,\eta) \neq 0$, $Q = 0$ für $\mathbf{r} = \mathbf{r}'$ ist

$$h_{k'}^{i'j'} = \mu^2 J_{k'}^{i'j'}(z,\eta)$$
und $h = 0$ für $\mathbf{r} \neq \mathbf{r}'$

Im Falle $Q \neq 0, \mu^2 J(z,\eta) = 0$ für $\mathbf{r} = \mathbf{r}'$ ist

$$h_{k'+\frac{1}{2}}^{i'j'} = -\alpha_{k'+\frac{1}{2},-}^{i'j'}\,\nu Q_{k'}^{i'j'};\quad h_{k'-\frac{1}{2}}^{i'j'} = +\alpha_{k'-\frac{1}{2},+}^{i'j'}\,\nu\,Q_{k'}^{i'j'}$$
und $h = 0$ für $\mathbf{r} \neq \mathbf{r}_{k'\pm\frac{1}{2}}^{i'j'}$

Ein »punktförmiger« Term Q_k^{ij} kann demnach in seiner Wirkung auf das Lösungsfeld durch einen Dipol im Vorticitytransport:

$$\mu^2 J(z,\eta)_{k'\pm\frac{1}{2}}^{i'j'} = \mp\alpha_{k'\pm\frac{1}{2},\mp}^{i'j'}\,\nu Q_{k'}^{i'j'}$$

ersetzt werden.

Setz man für die inhomogenen Bestandteile im Quellpunkt einen Einheitswert an, so hängen die Einflußfunktionen lediglich vom Koeffizientengitterfeld des Differenzenoperators nach (16) ab. Gewählt wurde im Quellpunkt für $\mu^2 J(z,\eta)$ bzw. aus Dimensionsgründen für

$$pQ = \frac{R}{g}\left(\frac{1}{c_p}\frac{dq}{dt} - \mathbf{v}\cdot\nabla T\right) =$$
$$= \frac{R}{g}\left(\frac{1}{c_p}\frac{dq}{dt} + \frac{m^2 g}{f}J(T,z)\right)$$

der Wert von 100 Einheiten [m. std^{-1}]

Da die Differentialgleichungen (5, 6) in τ, ω bzw. die Differenzengleichungen (16) in τ linear sind, gilt das Superpositionsprinzip. D. h. bei beliebiger Verteilung der inhomogenen Terme gibt die auf h angewandte Einflußfunktion $I(\mathbf{r}, \mathbf{r}')$ im Punkte $\mathbf{r}(_k^{ij})$ den Anteil des Lö-

sungswertes τ in % des inhomogenen Terms h im Punkte $\mathbf{r}\binom{i,j}{k}$ an. Zur Berechnung der in der Fig. 4—13 dargestellten Einflußfunktionen wurde ein α-Koeffizientengitterfeld einer Standardatmosphäre zugrundegelegt mit einer von x, y unabhängigen z- und damit T-Verteilung mit folgenden Daten:

$$T\Big|_{\substack{z=0\\ p=1000\text{ mb}}} = 283{,}2°; \frac{\partial T}{\partial z} = -6° \text{km}^{-1} \text{ für } p \geqq 225 \text{ mb};$$

$$\frac{\partial T}{\partial z} = 0 \text{ für } p \leqq 225 \text{ mb};$$

als Maschenweite wurde $\mu = 300$ km, $\nu = 50$ mb gewählt.[1]

Wegen der automatisch durch (16a—c) erfüllten kinematischen Randbedingungen einerseits und der Abhängigkeit der Koeffizienten α von p, x, y hängt selbstverständlich der Verlauf der Einflußfunktion I $(\mathbf{r}', \mathbf{r})$ wesentlich von der Lage des Quellpunktes $\mathbf{r}'$ ab.

Wegen der relativ geringen Variabilität von α mit x, y gegenüber der Abhängigkeit von p wird die Einflußfunktion jedoch weitgehend invariant gegenüber einer horizontalen Verschiebung des Quellpunktes $\mathbf{r}'$ sein, zumindest soweit der Quellpunkt noch hinreichend weit vom seitlichen Rand entfernt ist. Wir wollen uns deshalb bei der Berechnung von Einflußfunktionen auf eine Quellpunktslage im mittlerer Breite (φ' in etwa 50° geogr. Breite) beschränken und lediglich die p'-Koordinate des Quellpunktes variieren.

In den Fig. 4—13 sind einige derartige Einflußfunktionen in einem den Quellpunkt in $\varphi' = 51°$ enthaltenden Meridionalschnitt $x =$ const.[2] wiedergegeben, wobei einmal $\mu^2 J(z, \eta) = 100$ Einheiten in den Quellpunkten

$p' = 975, 725, 475, 275, 75$ mb resp.

und einmal $pQ = 100$ Einheiten in den Quellpunkten

$p' = 950, 700, 500, 300, 100$ mb resp.

angesetzt wurde.

Obwohl Lösungen von (16) naturgemäß nur Gitterfunktionen mit definierten Werten an den Gitterpunkten allein liefern können, wurde in den Abbildungen aus Gründen der Anschaulichkeit eine durch Interpolation gewonnene kontinuierliche Darstellungsweise gewählt.

Da jeder Gitterpunkt ein Volumelement $\mu^2\nu$ repräsentiert, so approximiert das τ-Feld der Fig. 4—13 demnach übergreifende räumliche Mittelwerte der Lösungsfunktion τ der Differentialgln. (5—6)

$$\tau_{\text{Differenzengl.}} \approx \frac{1}{\mu^2\nu} \int_{x-\frac{\mu}{2}}^{x+\frac{\mu}{2}} \int_{y-\frac{\mu}{2}}^{y+\frac{\mu}{2}} \int_{p-\frac{\nu}{2}}^{p+\frac{\nu}{2}} \tau_{\text{Differentialgl.}}\, dx\,dy\,dp$$

Der Differentialausdruck $L[\tau]$, den man durch Elimination von ω aus (5, 6) gewinnt, ergibt sich zu

$$L[\tau] = \triangle \tau + f\eta^2 \left(\frac{\tau_p}{\sigma\eta}\right)_p$$

Dieser wegen $\frac{\eta}{\sigma} > 0$ elliptische Differentialausdruck ist dann selbstadjungiert[3], wenn $\eta_p = 0$,

[3] Liegt eine (elliptische) Differentialgleichung der Form

$$L[u] = \sum_{i,j=1}^{3} a_{ij}\, u_{x_i x_j} + \sum_{i=1}^{3} a_i\, u_{x_i} + a_0\, u = h;\ a_{ij}, a_i, a_0, h = \text{Funktionen von } x_1, x_2, x_3$$

vor, so wird der Differentialausdruck $L[u]$ dann als selbstadjungiert bezeichnet, wenn gilt:

$$L[u] = \sum_{i,j=1}^{3} (a_{ij} u)_{x_i x_j} - \sum_{i=1}^{3} (a_i u)_{x_i} + a_0\, u$$

Für einen selbstadjungierten (elliptischen) Differentialausdruck läßt sich dann die Lösung in der Form darstellen:

$$u(x_1, x_2, x_3) = -\int u(s)\, G_n\, ds +$$

$$+ \iiint G(x_1', x_2', x_3'; x_1, x_2, x_3)\, h(x_1', x_2', x_3')\, dx_1' dx_2' dx_3',$$

wobei das erste Integral über den Rand des Integrationsgebietes, das 2. Integral über den Integrationsraum zu erstrecken ist. Der Kern G wird als Greensche Funktion bezeichnet und genügt der Symmetrieeigenschaft

[1] Bei einer stereographischen Projektion mit $\varphi_0 = 60°$ erhält man für die Vertikalsäule in einer Breite von $\varphi \approx 51°$ folgende Werte für die dimensionlose Größe α:

$p =$	1 000	950	900	850	800	750	700	650	600	550	500	450	400	350	300	250	200	150	100	50
$\alpha =$	0,25	41,6	37,7	33,9	30,4	27,0	23,8	20,8	18,0	15,3	12,9	10,6	8,6	6,7	5,1	3,6	0,92	0,52	0,23	0,06

wobei wegen $\eta = f$ $\alpha_{k\pm} = \alpha_{k\pm 1, \mp}$ ist.

[2] Der Verlauf der Einflußfunktionen ist nahezu rotationssymmetrisch.

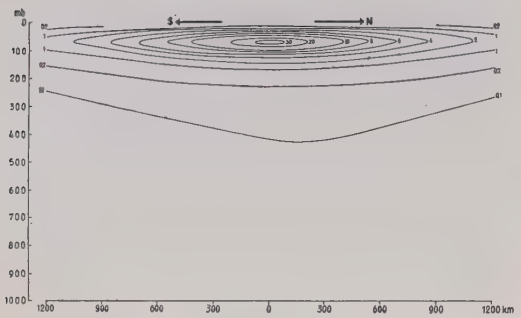

Fig. 8.

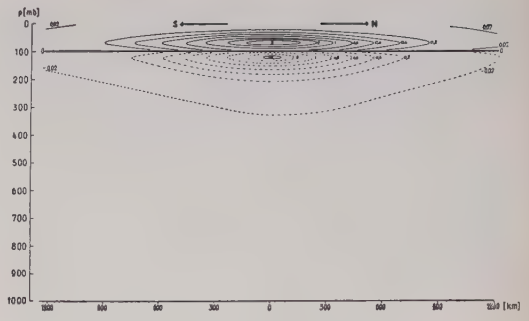

Fig. 13.

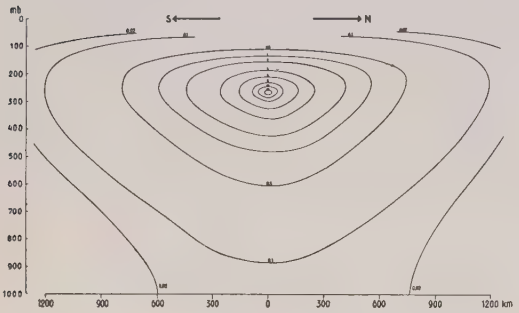

Fig. 7.

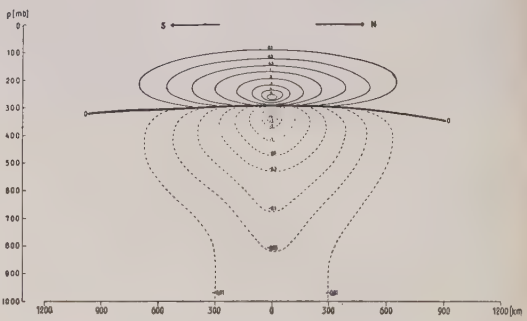

Fig. 12.

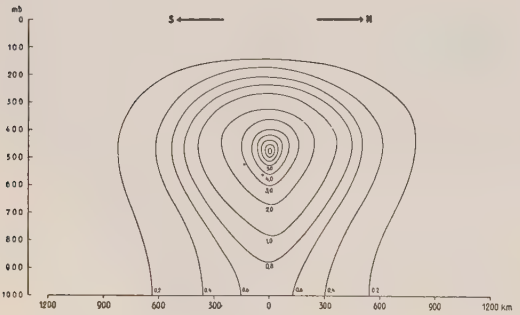

Fig. 6.

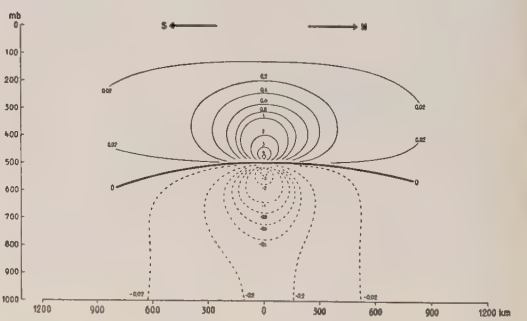

Fig. 11.

$$G(x'_1, x'_2, x'_3; x_1, x_2, x_3) = G(x_1, x_2, x_3; x'_1, x'_2, x'_3)$$

Im Falle, daß die Randwerte $u(s)$ verschwinden, verschwindet das Randintegral.

Die Lösung des Differenzengleichungssystems läßt sich dann analog zu

$$u^{ij}_{k} = \sum G^{i'j'}_{k'};\ {}^{ij}_{k}\, h\, {}^{i'j'}_{k'}$$

darstellen und die Einflußgitterfunktion $I(\mathbf{r}, \mathbf{r}')$ wegen der Symmetrie unmittelbar als Greensche Funktion interpretieren.

was wegen $\eta = f$ im Falle der gewählten Standardatmosphäre erfüllt ist.

Im vorliegenden Fall verschwinden die Randwerte τ an den Grenzflächen $p = 0$ und $p = p^{\star} = 1\,000$ mb jedoch nicht notwendigerweise, so daß auch die Symmetrie der Einflußfunktion geringfügig gestört ist. Analytisch kommt dieser Sachverhalt in der unterschiedlichen Form der Koeffizienten des Differenzenoperators der Gl. (16) für Randnachbarpunkte und die übri-

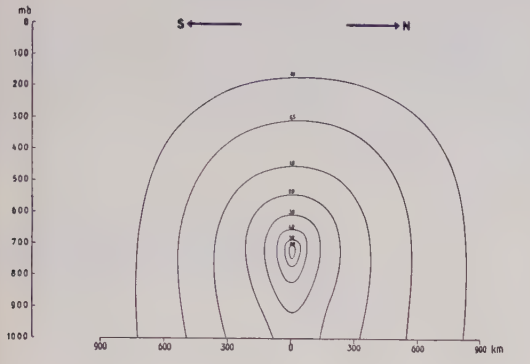

Fig. 5.

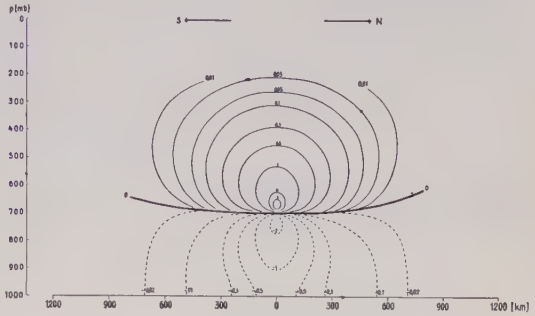

Fig. 10.

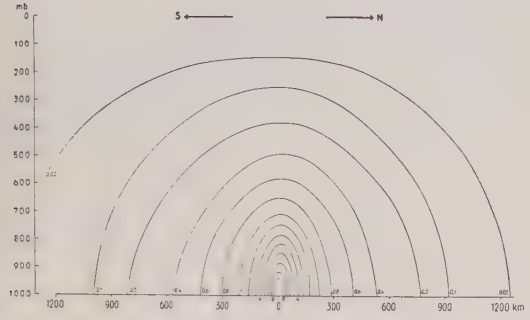

Fig. 4.

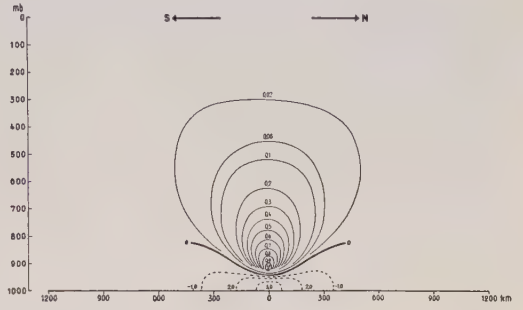

Fig. 9.

Fig. 4—8. Einflußfunktion $\tau \left[\frac{\text{dm}}{\text{Std}}\right]$ mit einem nichtverschwindenen dynamischen Jacobiausdruck $\mu^2 J^{i'j'}_{k'}(z,\eta) = 100 \left[\frac{\text{dm}}{\text{Std}}\right]$ im Störpunkt $\mathbf{r}'$ in $\varphi' \approx 51°$ Breite und $p' = 975$ mb (Fig. 4), 725 mb (Fig. 5), 475 mb (Fig. 6), 275 mb (Fig. 7), 75 mb (Fig. 8). $T_z = -6°/\text{km}$ in der Troposphäre; $\eta = f$.

Fig. 9—13. Einflußfunktionen $\tau \left[\frac{\text{dm}}{\text{Std}}\right]$ mit einem nichtverschwindenden Jacobiausdruck $(pQ)^{i'j'}_{k'} = 100 \left[\frac{\text{dm}}{\text{Std}}\right]$ entspricht einem Wert $\left(\frac{1}{c_p}\frac{dq}{dt} - \mathbf{v}\cdot\nabla T\right)^{i'j'}_{k'} = 3{,}42 \left[\frac{°K}{\text{Std}}\right]$ im Störpunkt $\mathbf{r}'$ in $\varphi' \approx 51°$ Breite und $p' = 950$ mb (Fig 9), 700 mb (Fig. 10), 500 mb (Fig. 11), 300 mb (Fig. 12), 100 mb (Fig. 13). $T_z = -6°/\text{km}$ in der Troposphäre, $\eta = f$.

gen inneren Gitterpunkte zum Ausdruck. Auch im Falle der Asymmetrie von I, was insbesondere für $\eta_p \neq 0$ gilt, kann man jedoch stets wegen der Gültigkeit des Superpositionsprinzips bei durch die α gegebenem Differenzenausdruck eine lösende Funktion G aus den Einflußfunktionen sich so zusammensetzen, daß

$$\tau^{ij}_{k} = \sum G^{ij\ i'j'}_{k\ k'}\ h^{i'i'}_{k'},$$

Summation über alle inneren Gitterpunkte. Man findet $G^{ij\ i'j'}_{k\ k'} = I^{i'j'}_{k'}$. Das bedeutet, daß vor Aufstellung der Greenschen Funktion oder besser des lösenden Kerns G die Einflußfunktionen für sämtliche Innenpunkte zu berechnen sind.

Jedoch wird ein derartiger lösender Gitterkern G bei Behandlung aktueller Wettersituationen, also bei beliebiger Anordnung der α und h-Werte, nur dann mit Vorteil zu benutzen sein, wenn sich erweist, daß auch eine Lösung mit einem von der speziellen Wetterlage unabhängigen Differenzenausdruck (seitlicher Mittelwert) die tatsächliche Lösung approximiert.

Man wird in diesem Falle diese Approximation als erste Näherung im Relaxations- bzw. Operatorenverfahren zur Abkürzung des Lösungsprozesses mit dem aktuellen Differenzenoperator verwenden können.

Liegt eine Lösung τ vor, so gewinnt man durch Differenzenprozesse das Feld der Vertikalgeschwindigkeit aus (17)

$$\omega_k = \frac{g}{\nu\sigma_k}\left(\tau_{k+\frac{1}{2}} - \tau_{k-\frac{1}{2}} + \nu Q_k\right)$$

und das Tendenzfeld der Temperatur sowie die horizontale Divergenz aus den beiden folgenden Betimmungsgleichungen:

$$(T_t)_k = -\frac{p_k}{\nu}\frac{g}{R}\left(\tau_{k+\frac{1}{2}} - \tau_{k-\frac{1}{2}}\right)$$

$$-\nu\,(\mathrm{Div}\,\mathbf{v})_k = \omega_{k+\frac{1}{2}} - \omega_{k-\frac{1}{2}}$$

Für Quellpunkte in Tropopausennähe sind diese letzten 3 Felder für ein $\mu^2 J(z,\eta) = 100$ (m/Std.) in $p' = 275$ mb bzw. $p\,Q = 100$ (m/Std.) im Quellpunkt $p' = 300$ mb in den Fig. 14—19 dargestellt worden.

Die Einflußfunktionen lassen unmittelbar die Flächen gleichen Einflußgewichts und die praktische Einflußreichweite einer Störung in Form einer Vorticity-Advektion bzw. eines pQ-Wertes im Quellpunkt ablesen.

Sie vermitteln andererseits auch einen Einblick in den atmosphärischen Mechanismus, wie er durch die definierten Störquellen ausgelöst wird. Insbesondere liefern die zugehörigen Lösungsfelder eine quantitative Vorstellung von dem atmosphärischen Kompensationsmechanismus.

Der Annahme quasistatisch verlaufender Prozesse liegt zwar die physikalische Conception unendlicher Signalgeschwindigkeit zugrunde, d. h. es existiert ein starrer Übertragungsmechanismus sowohl zwischen horizontal als auch vertikal benachbarten Gitterpunkten, der eine zeitlose Beeinflußung durch eine Störquelle auf den meteorologischen Zustand eines beliebig weit davon entfernten Gitterpunktes zuläßt.

So enthält z. B. die Tendenzgleichung in der aus der Kontinuitätsgleichung $\omega_p = -\mathrm{Div}\,\mathbf{v}$ und oberen und unteren Randbedingung ableitbaren Form

$$\tau^\star = -\frac{1}{g\varrho^\star}\int_0^p \mathrm{Div}\,\mathbf{v}\,dp + M$$

die physikalische Aussage, daß eine Massenanhäufung in einer Schicht dp eine nicht von deren Entfernung vom Erdboden abhängige Tendenz am Boden hervorruft. Wegen der integralen Abhängigkeit muß jedoch stets die Möglichkeit unterstellt werden, daß eine Divergenz der einen Schicht in ihrer Wirkung auf den Bodendruck durch entsprechende Vorgänge in Schichten darüber oder darunter kompensiert wird, wobei a priori nichts darüber ausgesagt werden kann, ob derartige Massendivergenzen willkürlich über die Vertikalsäule verteilt sein können, oder ob funktionelle Beziehungen zwischen diesen Größen verschiedener Schichten bestehen.

Die synoptische Erfahrung erweist jedenfalls, daß allgemein das Kompensationsprinzip sowohl in der Form

$$\left|\int_0^{p^\star} \mathrm{Div}\,\mathbf{v}\,dp\right| \ll \int_0^p |\mathrm{Div}\,\mathbf{v}|\,dp$$

als auch in der Form

$$\left|\int_0^{p^\star} T_t\,d\ln p\right| \ll \int_0^{p^\star} |T_t|\,d\ln p \text{ gilt;}$$

was auf eine Korrelation zwischen den Integranden innerhalb der betrachteten Vertikalsäule schließen läßt.

Beide Quantitäten — Div $\mathbf{v}$, T_t — sind den Topographien eines Termins nicht zu entnehmen, zumindest nicht vollständig. Ableitbar aus simultanen aerologischen Meßdaten ist lediglich ein gewisser Beitrag, nämlich die ersten Terme der rechten Seiten folgender Bestimmungsgleichungen für Div $\mathbf{v}$ und T_t:

$$\eta\,\mathrm{Div}\,\mathbf{v} = -\mathbf{v}\cdot\nabla\eta - A;$$

$$A = \eta_t + \omega\eta_p = \left(\frac{\partial}{\partial t} + \omega\frac{\partial}{\partial p}\right)\frac{q}{f}\Delta Z$$

$$T_t = -\mathbf{v}\cdot\nabla T + B_1;\quad B_1 = \left(\frac{d}{dt} - \omega\frac{\partial}{\partial p}\right)T$$

$$T_t = \frac{g}{R}pQ + B_2;\quad B_2 = \frac{p}{R}\sigma\omega \;^1$$

also die horizontalen Transporte der Vorticity und der Temperatur, bzw. mit der einschränkenden Annahme über die Kenntnis von $\frac{dq}{dt}$ die

[1] Man erhält diese Formulierung für T_t aus dem 1. Hauptsatz in der Form:

$\frac{dT}{dt} = \frac{1}{c_p}\frac{dq}{dt} + \frac{kT}{p}\frac{dp}{dt} = T_t + \mathbf{v}\cdot\nabla T + \omega T_p$. Dann ist

$$T_t = \frac{1}{cp}\frac{dq}{dt} - \mathbf{v}\cdot\nabla T - \omega T_p + \omega\frac{kT}{p} = \frac{gpQ}{R} + \frac{p}{R}\sigma\omega$$

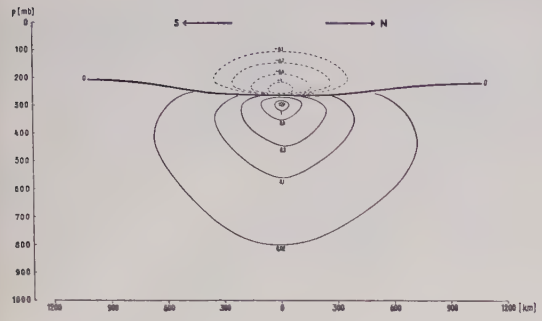

Fig. 14.

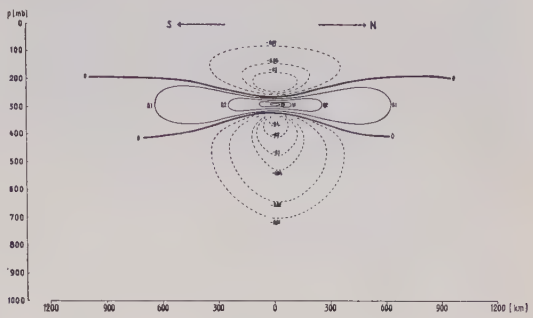

Fig. 17.

Fig. 14—16. Zur Einflußfunktion τ der Fig. 7 zugehöriges Temperaturänderungsfeld $T_t \left[\frac{^\circ K}{\text{Std}}\right]$ (Fig. 14); Vertikalgeschwindigkeitsfeld $-\omega \left[\frac{\text{mb}}{\text{Std}}\right]$ (Fig. 15) und Feld der horizontalen Massendivergenz $-\nu$ Div $\mathbf{v}$ $\left[\frac{\text{mb}}{\text{Std}}\right]$ (Fig. 16).

Fig. 17—19. Zur Einflußfunktion τ der Fig. 12 zugehöriges Temperaturänderungsfeld $T_t \left[\frac{^\circ K}{\text{Std}}\right]$ (Fig. 17)' Vertikalgeschwindigkeitsfeld $-\omega \left[\frac{\text{mb}}{\text{Std}}\right]$ (Fig. 18) und Feld der horizontalen Massendivergenz $-\nu$ Div $\mathbf{v}$ $\left[\frac{\text{mb}}{\text{Std}}\right]$ (Fig. 19).

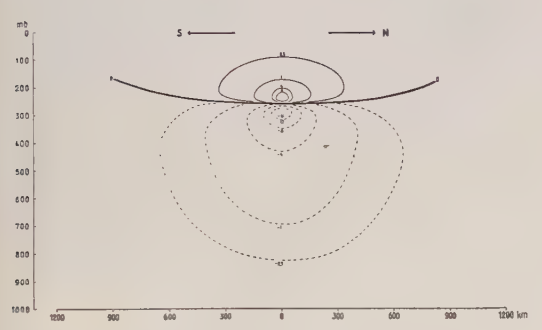

Fig. 15.

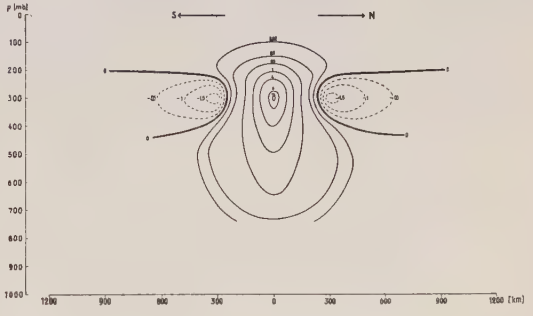

Fig. 18.

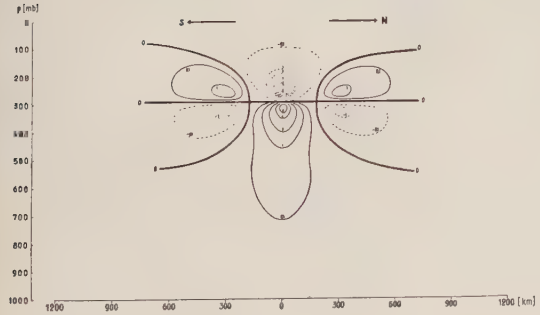

Fig. 16.

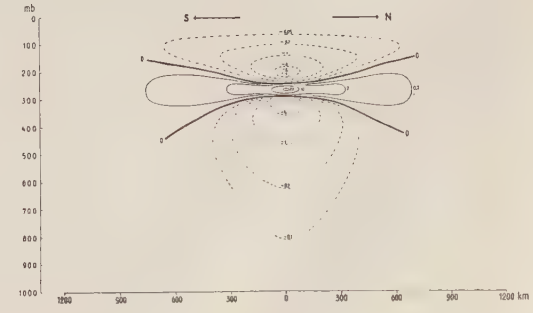

Fig. 19.

Größe Q; während die weiteren Beiträge A bzw. B_1, B_2 zum Divergenz- und Temperaturtendenzausdruck nur durch die Rechnung bestimmt werden können.

Man könnte annehmen, daß die Kompensation dadurch zustande kommt, daß

$$\left|\int_0^{p^*} \mathbf{v}\cdot\nabla\eta\, dp\right| \ll \int_0^{p^*} |\mathbf{v}\cdot\nabla\eta|\, dp \text{ und dass}$$

$$\left|\int_0^{p^*} Q dp\right| \ll \int_0^{p^*} |Q dp| \text{ bzw.}$$

$$\left|\int_0^{p^*} \mathbf{v}\cdot\nabla T d\ln p\right| \leqslant \int_0^{p^*} |\mathbf{v}\cdot\nabla T|\, d\ln p \quad (25)$$

Jedoch dürfte eine solche Annahme physikalisch nicht begründbar sein. Eine physikalische Erklärungsmöglichkeit für die Kompensation würde darin bestehen, daß gezeigt werden kann daß auch bei einer völlig beliebigen vertikalen Verteilung der Transportgrößen, also im ungünstigen Falle bei Gleichheit der rechten und linken Seiten obiger Ungleichungen, noch eine Kompensation stattfindet, also (25) oder zumindest

$$\left|\int_0^{p^*} \mathrm{Div}\,\mathbf{v}\, dp\right| \ll \left|\int_0^{p^*} \mathbf{v}\cdot\nabla\eta\, dp\right| \text{ und}$$

$$\left|\int_0^{p^*} T_t d\ln p\right| \ll \left|\int_0^{p^*} \mathbf{v}\cdot\nabla T d\ln p\right| \text{ bzw. } \frac{g}{R}\left|\int_0^{p^*} Q dp\right| \text{ gilt.}$$

Eine derartige Kompensation käme dadurch zustande, daß die Advektionsgrößen $\mathbf{v}\cdot\nabla\eta$, $\mathbf{v}\cdot\nabla T$ bzw. $J(z,\eta)$, Q, die wir als primäre Divergenzen bzw. Temperaturtendenzen bezeichnen wollen, *automatisch* sekundäre Divergenzen und lokale Temperaturveränderungen A, B_1, B_2 im Quellpunkt selbst und in dessen Umgebung hervorrufen in einer Weise, daß sekundäre Felder A, B und primäre Quellen ($J(z,\eta)$, Q) sich weitgehend kompensieren, ein Mechanismus, den man als automatische Kompensation bezeichnen könnte.

Gerade diesen Sachverhalt bringen aber die Einflußfunktionen zum Ausdruck, wie man leicht den Meridionalschnitten der Fig. 14—19 sowie den Bilanzen innerhalb der den Quellpunkt enthaltenden Vertikalsäule entnimmt, die in Fig. 20, 21 dargestellt sind.

Man entnimmt diesen Bilanzdiagrammen unmittelbar, daß primäre Divergenzen und Temperaturtendenzen an einer bestimmten Stelle $\mathbf{r}'$ des Raumes sekundäre Divergenz- bzw. Temperaturänderungseffekte am Quellpunkt $\mathbf{r}'$ selbst sowie in dessen Nachbarschaft auslösen, die einmal den primären Vorgang am Quellpunkt selbst abzuschwächen suchen und sich mit den primären Effekten soweit kompensieren, daß die Lösungsfelder aller met. Größen mit zunehmendem horizontalen und vertikalen Abstand vom Quellpunkt rasch abklingen, wobei noch das Ausmaß der Kompensation wesentlich von den Stabilitätsverhältnissen in der Atmosphäre abhängt[1].

Bei Abänderung der Stabilitätsverhältnisse σ und η werden die Einfluß- und damit Greenschen Funktionen insofern modifiziert, als niedrige η-Werte einen stärkeren »Durchgriff« des Einflusses in horizontaler Richtung, niedrige σ bzw. s-Werte (hohe statische Labilität) einen stärkeren »Durchgriff« in vertikaler Richtung auf Kosten der anderen Koordinaten bewirken, wobei die Gewichtsverteilung vorwiegend durch die Kombination $\frac{\eta}{\sigma}$ des α-Koeffizienten bestimmt wird.

Als Beispiel zeigt Fig. 22 die zu Fig. 6 analoge Einflußfunktion, unter Zugrundelegung eines Temperaturgradienten von 9°/km anstelle von 6°/km in der Troposphäre, die eine merkliche Bevorzugung der vertikalen Koordinate anzeigt. Wie man sich diesen automatischen Kompensationsmechanismus physikalisch vorzustellen hat, sei kurz qualitativ erläutert, wobei das zeitliche Nebeneinander des quasistatischen Vorganges notwendigerweise in ein zeitliches Nacheinander eines nicht quasistatischen Prozesses aufgelöst werden muß. Im Falle einer

[1] Wegen empirischer Untersuchungen über den Kopplungsmechanismus advektiver und konvektiver Temperaturänderungen vgl. Craddock (1951) und W. Regula (1952).

Fig. 20. Einflußfunktion der Höhentendenz τ $\left[\frac{\mathrm{m}}{\mathrm{Std}}\right]$, der Vertikalgeschwindigkeit ω $\left[\frac{\mathrm{mb}}{\mathrm{Std}}\right]$, der Temperaturänderung T_t $\left[\frac{^\circ K}{\mathrm{Std}}\right]$ und der horizontalen Massendivergenz $-\nu\,\mathrm{Div}\,\mathbf{v}$ $\left[\frac{\mathrm{mb}}{\mathrm{Std}}\right]$ innerhalb der den Störpunkt enthaltenden Vertikalsäule, ausgelöst durch einen nichtverschwindeden Jacobi-Ausdruck $\mu^2 J^{i'j'}_{k'}(z,\eta) = 100$ $\left[\frac{\mathrm{m}}{\mathrm{Std}}\right]$ im Störpunkt $\mathbf{r}'$ mit $\varphi' \approx 51°$ Breite und $p' =$ $= 75$ mb (obere Reihe), 475 mb (mittlere Reihe), 975 mb (untere Reihe).

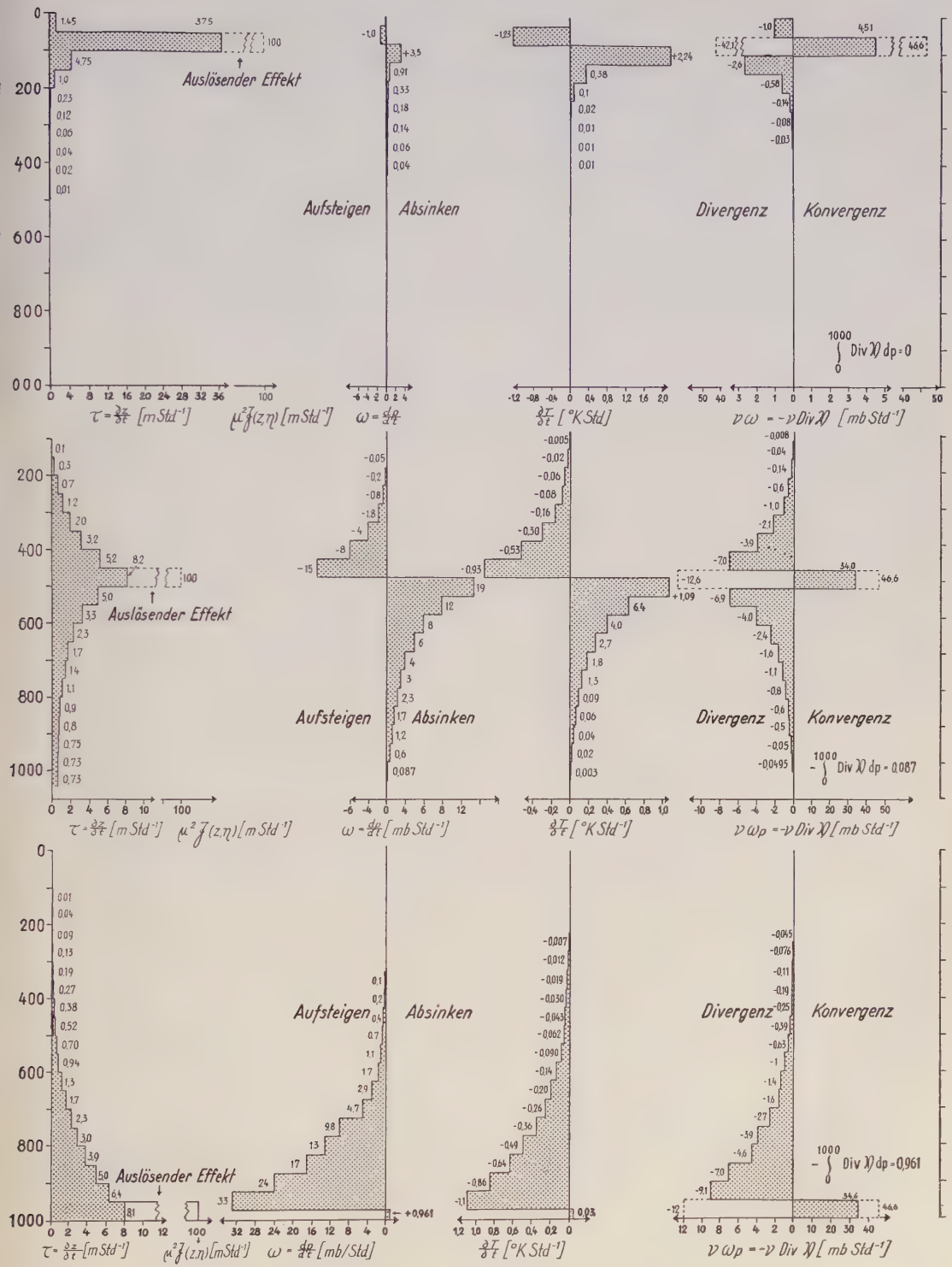
Auslösender Effekt
Aufsteigen
Absinken
Divergenz
Konvergenz
Auslösender Effekt
Aufsteigen
Absinken
Divergenz
Konvergenz
Auslösender Effekt
Aufsteigen
Absinken
Divergenz
Konvergenz

Fig. 20.

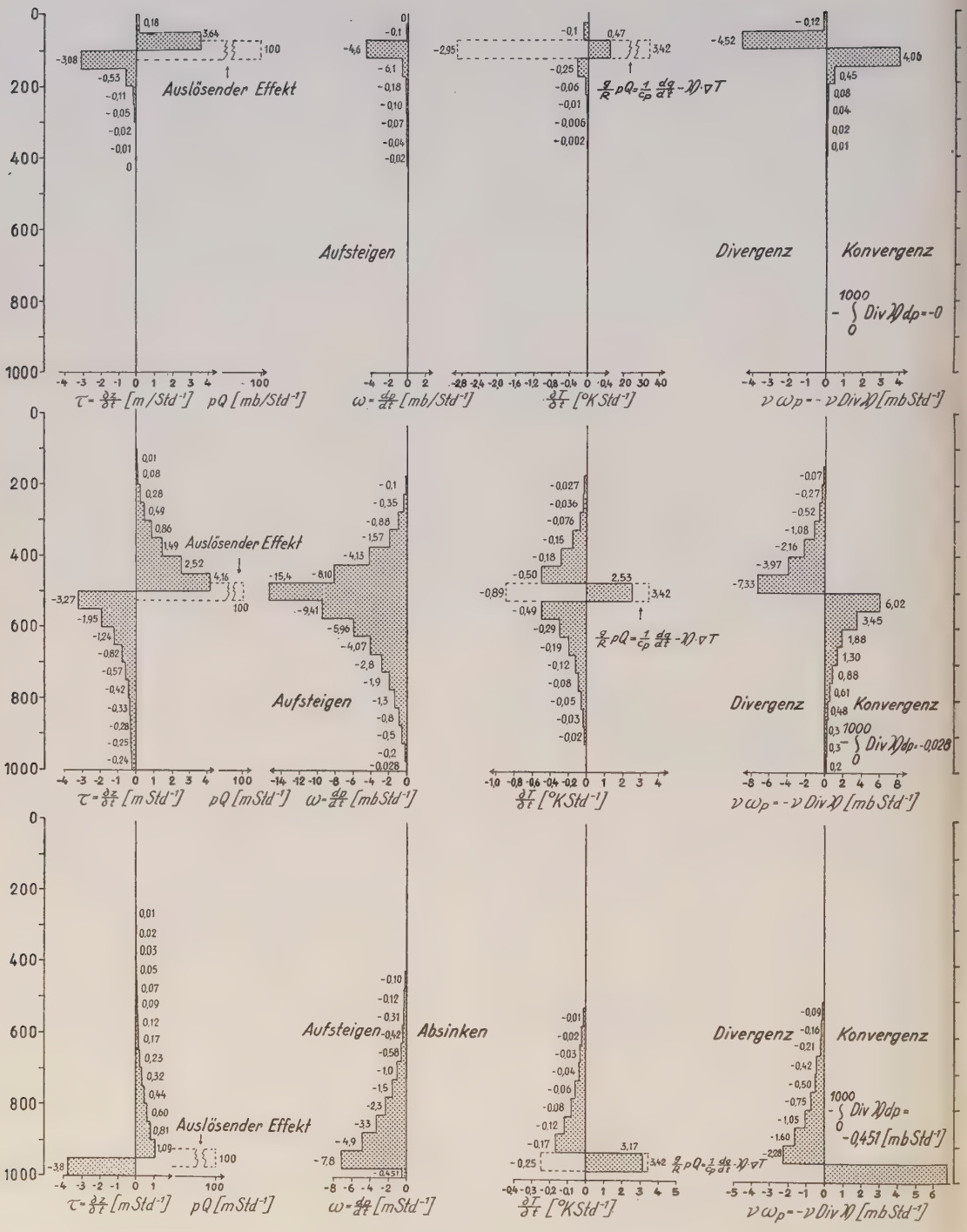
Auslösender Effekt
Aufsteigen
Divergenz
Konvergenz
Absinken
$\tau = \frac{\partial z}{\partial t}$ [m/Std^{-1}]
pQ [mb/Std^{-1}]
$\omega = \frac{dp}{dt}$ [mb/Std^{-1}]
$\frac{\partial T}{\partial t}$ [°K Std^{-1}]
$\nu\,\omega_p = -\nu\,\mathrm{Div}\,\mathfrak{V}$ [mb Std^{-1}]
$\frac{g}{R}pQ = \frac{1}{c_p}\frac{dq}{dt} - \mathfrak{V}\cdot\nabla T$
$-\int_0^{1000} \mathrm{Div}\,\mathfrak{V}\,dp = -0$
$-\int_0^{1000} \mathrm{Div}\,\mathfrak{V}\,dp = -0{,}028$
$-\int_0^{1000} \mathrm{Div}\,\mathfrak{V}\,dp = -0{,}451$ [mb Std^{-1}]
pQ [mStd^{-1}]
$\omega = \frac{dp}{dt}$ [mStd^{-1}]
$\frac{\partial T}{\partial t}$ [°K Std^{-1}]
$\nu\,\omega_p = -\nu\,\mathrm{Div}\,\mathfrak{V}$ [mb Std^{-1}]

Fig. 21.

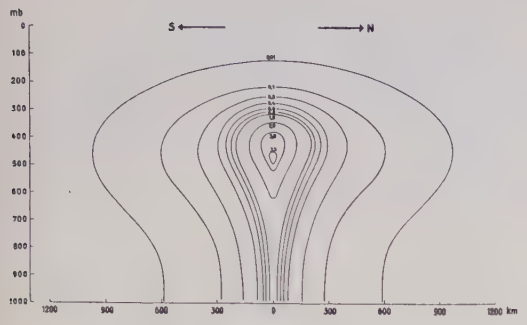

Fig. 22. Einflußfunktion $\tau \left[\frac{\mathrm{dm}}{\mathrm{Std}}\right]$ mit einem nichtverschwindenden Jacobi-Ausdruck $\mu^2 J_{k'}^{i'j'}(z, \eta) = 100 \left[\frac{\mathrm{dm}}{\mathrm{Std}}\right]$ im Störpunkt $\mathbf{r}'$ mit $\varphi' \approx 51°$ Breite und $p' = 475$ mb bei hoher Labilität in der Troposphäre: $T_z = -9°/\mathrm{km}$, $\eta = f$.

positiven Störquelle $J(z, \eta) > 0$ (primäre Konvergenz) entsteht vorerst im Störpunkt selbst eine horizontale Massenkonvergenz, die wegen der geringen Kompressibilität der Luft aus Kontinuitätsgründen eine vertikale Massendivergenz erzeugt mit aufsteigender Luft oberhalb und mit absinkender Luft unterhalb des Quellpunktes. Unterhalb des Quellpunktniveaus wird wegen des Massenzuflusses im Quellpunkt positive Drucktendenz erzeugt, oberhalb des Quellpunkts infolge der positiven Vertikalkomponente $\frac{dz}{dt} > 0$ ebenfalls eine positive Drucktendenz, d. h. die Niveauflächen heben sich in der gesamten Störpunktsvertikalsäule relativ zur Umgebung an. Diese Anhebung bewirkt wegen der Trägheit des Windes, der nur mit einer gewissen Verzögerung dem ansteigenden Gradientfeld sich anpassen kann, in allen Niveaus der Quellpunktssäule wegen Überwiegens der Gradientkraft über die Corioliskraft ein Ausströmen, d. h. Divergenzen, die sich mit der primären Konvergenz im Quellpunkt weitgehend kompensieren. Temperaturmäßig gleicht sich das infolge des Aufwindes entstehende Abkühlungsgebiet oberhalb mit dem infolge des Absinkens erzeugten Erwärmungsgebiet unterhalb des Störniveaus (bei stabiler Schicht) in seiner Wirkung auf den Bodendruck ebenfalls weitgehend aus, siehe Fig. 7, 14—16.

Im Falle einer positiven Q-Störquelle findet vorerst infolge der Expansion ein Aufsteigen der Luft mit konvektiver Abkühlung und positiver Tendenz $\tau > o$ oberhalb des Quellpunktes statt; das mit diesem Druckanstieg verbundene Massendefizit führt zu einem Druckfall unterhalb des Quellpunktniveaus und damit zu Konvergenzen mit aus Kontinuitätsgründen aufsteigenden Komponenten und konvektiver Abkühlung. In der gesamten Vertikalsäule findet demnach konvektive Abkühlung statt, die die primäre Erwärmung im Quellpunkt selbst weitgehend kompensiert. Die ausgelösten Massendivergenzen mit entgegengesetzten Vorzeichen unterhalb und oberhalb des Quellpunkts kompensieren sich gleichfalls weitgehend in ihrer Wirkung auf die Bodendrucktendenz (vgl. Fig. 12, 17—19). Die exakten quantitativen simultanen Vorgänge in der zugrundegelegten Standardatmosphäre zeigen die Fig. 20 und 21 für die betrachtete Störpunktssäule mit p' in Bodennähe, im mittleren Niveau und in der Stratosphäre. Soweit die der Berechnung zugrundeliegenden Gesetzmäßigkeiten (16) die atmosphärischen Vorgänge adäquat beschreiben, muß aus den Lösungsergebnissen geschlossen werden, daß in der Atmosphäre trotz der Annahme quasistatischer Vorgänge und unendlicher Signalgeschwindigkeiten doch ein Nahewirkungsprinzip gültig ist[1].

Das bedeutet, daß in praxi eine Quellpunktsstörung im oben definierten Sinne Deformationsfelder der meteorologischen Feldgrößen auslöst, die räumlich rasch mit wachsender Distanz vom Quellpunkt abklingen und daß ande-

Fig. 21. Einflußfunktion der Höhentendenz $\tau \left[\frac{\mathrm{m}}{\mathrm{Std}}\right]$, der Vertikalgeschwindigkeit $\omega \left[\frac{\mathrm{mb}}{\mathrm{Std}}\right]$, der Temperaturänderung $T_t \left[\frac{°K}{\mathrm{Std}}\right]$ und der horizontalen Massendivergenz $-\nu \operatorname{Div} \mathbf{v} \left[\frac{\mathrm{mb}}{\mathrm{Std}}\right]$ innerhalb der den Störpunkt enthaltenden Vertikalsäule, ausgelöst durch einen nichtverschwindenden thermischen Ausdruck $(pQ)_{k'}^{i'j'} = 100 \left[\frac{\mathrm{m}}{\mathrm{Std}}\right]$, entspricht einem Wert $\left(\frac{1}{c_p}\frac{dq}{dt} - \mathbf{v} \cdot \nabla T\right)_{k'}^{i'j'} = 3{,}42 \left[\frac{°K}{\mathrm{Std}}\right]$ im Störpunkt $\mathbf{r}'$ mit $p' \approx 51°$ Breite und $p' = 100$ mb (obere Reihe), 500 mb (mittlere Reihe), 950 mb (untere Reihe).

[1] Vergleiche dazu die Betrachtung von CHARNEY (1949) über die Gruppen-Geschwindigkeiten mit analogen Ergebnissen.

rerseits die Ursachen für eine beobachtete Deformation in einem bestimmten Punkte ebenfalls in unmittelbarer Umgebung derselben ihren Sitz haben müssen. Man muß natürlich berücksichtigen, daß mit zunehmendem Abstand r vom betrachteten Aufpunkt auch die Anzahl der beitragenden Gitterpunkte mit r^2 anwächst, so daß trotz abnehmenden Einflußgewichts des Einzelpunktes der Einfluß weit entfernter Flächen den Einfluß der Nachbarpunkte überdecken kann.

Jedoch ist zu bedenken, daß mit zunehmender Entfernung auch die Verteilung der inhomogenen Terme in zunehmendem Maße auf den Flächen gleichen Einflußgewichts die Form willkürlicher oder zufälliger Belegungen annehmen werden, so daß sich die einzelnen Gitterpunkte der Einflußfläche weitgehend in ihrer Wirkung auf den Lösungswert des Aufpunktes gegenseitig auslöschen.

Für die während des Herbstsemesters 1951 empfangenen wertvollen Anregungen und Ratschläge für die Abfassung der Arbeit sei den Angehörigen des Instituts für Meteorologie, Stockholm, besonders Prof. Rossby, Dr. Eliassen und Dr. Bolin herzlich gedankt.

LITERATURVERZEICHNIS

Bolin, B., Charney, J. G., 1951: Numerical tendency computations from the barotropic vorticity equation. *Tellus* **3**, 4, 248—257.

Charney, J. G., 1948: On the scale of atmospheric motion *Geof. publ. XVII* **2**.

Charney, J. G. 1949: On a physical basis for numerical prediction of largescale motions in the atmosphere. *J. meteor.* **6**, 6, 371—385.

Charney, J. G., Eliassen, A., 1949: A numerical method predicting the perturbations of the middle latitude westerlies. *Tellus* **2**, 38—54.

Charney, J. G., Fjørtoft, R., v. Neumann, J., 1950: Numerical integration of the barotropic vorticity equation. *Tellus* **4**, 237—254.

Craddock, J. M., 1951: Advective temperature change in the 1000—700 mb and 700—500 mb layers. *Quart. J. Roy. Meteor. Soc.* **77**, 317

Eady, E. T., 1952: Note on weather computing and the so-called $2^1/_2$-dimensionel model. *Tellus* **4**, 3, 157—167.

Eliassen, A., 1948: The quasistatic equations of motion with pressure as independent variable. *Geof. publ. XVII*, **3**.

Eliassen, A., 1952: Simplified dynamic models of the atmosphere, designed for the purpose of numerical weather prediction. *Tellus* **4**, 3, 145—156.

Fjørtoft, R., 1952: On a numerical method of integrating the barotropic vorticity equation. *Tellus* **4**, 3, 179—194.

Hinkelmann, K., 1951: Der Mechanismus des meteorologischen Lärmes. *Tellus* **3**, 4, 285—296.

Hinkelmann, K., Essenwanger, O., Reymann, G., Wippermann, F., 1952: Physikalisch-mathematische Grundlagen der numerischen Integration in einer baroklinen Atmosphäre. *Ber. d. Dt. Wetterdinnstes i. d. US-Zone Nr.* **38**, 416—428.

Kleinschmidt, E. jun. 1951: Über Aufbau und Entstehung von Zyklonen, III. Teil. *Met. Rdsch.* **4**, 5/6, 89—96.

Philipps, H., 1939: Die Abweichung vom geostrophischen Wind. *Meteor. Z.* **56**, 460—483.

Phillips, N., 1951: A simple three-dimensional model for the study of largescale extratropical flow patterns. *J. Meteor.* **8**, 6, 381—394.

Regula, W., 1952: Advektive und nichtadvektive Vorgänge im Bereich einer Zyklone als Funktion von Raum und Zeit. *Ber. d. Dt Wd. i. d. US-Zone* **38**, 36—41.

Rossby, C. G. and collaborators 1939: Relation between variations in the intensity of the zonal circulation of the atmosphere and the displacements of the semipermanent centers of action. *J. Marin. Res.* **2**, 1, 38—55

Rossby, C. G., 1949: On a mechanism for the release of potential energy in the atmosphere. *J. Meteor.* **6**, 163—180.

Sawyer J. S., Bushby F. H., 1951: Note on the numerical integration of the equations of Meteorological dynamics. *Tellus* **3**, 4, 201—203.

Staff Members, University of Stockholm 1952: Preliminary report on the prognostic value of barotropic models in the forecasting of 500 mb height changes. *Tellus* **4**, 1; 21—30.

Stümke, H. 1950: Theorie der Weiterentwicklung von stabilen atmosphärischen Druckfeldern. *Met. Rdsch.*, **3**, 241—243; **4**, 7—13.

Stümke, H., 1953: Differentialgleichungen der schwingungsfreien Weiterentwicklung von schwachen, mittleren und starken Störungen in der Erdatmosphäre und ähnlichen rotierenden Systemen. i. Druck.

Sutcliffe, R. C., 1947: A contribution to the problem of development. *Quart. J. R. meteor. Soc.* **73**, 370—383.

A Power Law Representation of the Heat Transfer in the Lowest 100 metres of the Atmosphere

By R. FROST, Meteorological Office, London

(Manuscript received March 16, 1953)

Abstract

On the assumptions that the flux of heat in the air is governed by an interchange coefficient which can be represented by a simple power law of the height above the surface, that the flux of heat in the ground is by molecular processes and that during the daylight hours the variation of temperature can be represented by a sine function, the phase angle of the diurnal temperature wave is calculated and is shewn to be in good agreement with observations. The phase angle of the annual temperature wave is also discussed.

Calculations of K_H the coefficient of eddy conductivity of heat and of its mode of variation with height in unstable conditions suggest that it is approximately equal to K_M the coefficient of eddy viscosity.

1. Introduction

Despite the fact that the mean temperature distribution within the lowest 100 metres of the atmosphere has been described in considerable detail in a series of geophysical memoirs (JOHNSON, 1929; BEST, 1935; FLOWER, 1936; JOHNSON and HEYWOOD, 1938; BEST, KNIGHTING, PEDLOW and STORMONTH, 1950) the theoretical conclusions from these observations have been conflicting, partly owing to the complexity of the problem and lack of any clear cut picture of the physical processes involved in the mechanism of heat transfer, and partly to the effects of the different topography of the stations.

In most discussions of heat transfer in the atmosphere (cf. SUTTON, 1949), it has been assumed that molecular conduction is negligible, except within the lowest cm or so above the surface, that radiation may be neglected and that, at least in the mid period of the day, convection is mainly responsible for the transfer of heat in the vertical, although there is disagreement as to the roles played by 'free convection' due to buoyancy effects and 'forced convection' due to frictional turbulence. On the other hand, RIDER and ROBINSON (1951) have stated that in the lowest two metres above the ground the absorption of long wave radiation by the air is at least comparable in effect with convection.

In view, therefore, of the uncertainty as to the mechanism of heat transfer, Richardson's direct approach, which avoids the necessity of making any assumptions as to the nature of that mechanism, has been adopted in this paper.

RICHARDSON (1919) defined K the coefficient of eddy diffusivity for any transferable property χ of the atmosphere by

$$\frac{D\chi}{Dt} = \frac{\partial}{\partial z}\left\{K\frac{\partial \chi}{\partial z}\right\} \qquad 1.00$$

where the only limitation imposed upon χ is that χ must represent some property which is unchanged by transfer to a different level.

Whilst the coefficient K in this equation was originally called the coefficient of eddy diffusivity, this interpretation is not essential and if in heat transfer part of the temperature change at any level is due to factors other than eddy motion, equation 1.00 can still be used to represent the whole of the observed variation, although in this case K is a composite diffusion coefficient which takes into account all the causative factors.

It is evident that K as defined in this manner may be a function of χ and z and hence may vary from property to property if the transferable property under consideration influences the motion. Comparison of values of K for various transferable properties computed by means of this equation thus affords some evidence as to whether, as has been suggested by various writers on turbulent motion from Reynolds onwards, the transfer of heat momentum and water vapour is affected by the same mechanism.

In the case of controlled wind tunnel experiments PASQUILL (1942) found that the coefficients of eddy diffusivity and momentum were practically identical, but in a second paper (1949) dealing with the diffusion of water vapour in the lowest two metres above the surface he concluded that whilst under stable conditions there was equality between the coefficients of eddy diffusivity for water vapour and heat, in unstable conditions the latter was substantially greater.

RIDER and ROBINSON (1951) however questioned Pasquill's conclusions, and by a further series of measurements within the lowest two metres above the surface shewed that the wind and temperature profiles in nearly all cases had the same form and established a strong probability that the coefficients of eddy viscosity, eddy diffusivity and eddy conductivity were approximately equal under all circumstances.

2. The present position of K_H

It has been noted by many writers that near the ground the diurnal variation of temperature can be represented approximately by a sine wave of period 24 hours, whilst at great heights it is negligible. If therefore, horizontal advection can be neglected the problem of heat transfer in the lowest atmosphere reduces to the problem of obtaining a solution of

$$\frac{\partial \Theta}{\partial t} = \frac{\partial}{\partial z}\left\{K_H \frac{\partial \Theta}{\partial z}\right\} \qquad 2.00$$

where Θ is the potential temperature of the air at a height z above the surface at a time t, subject to the boundary conditions

$$\Theta = \Theta_0 + a \sin qt \quad \text{when } z \to 0 \qquad 2.01$$

$$\Theta = \Theta_0 \quad \text{when } z \to \infty \qquad 2.02$$

where $q = \dfrac{2\pi}{24 \times 60 \times 60} = 7.3 \times 10^{-5}$,

and a is a constant.

The solution of 2.00 which fits these conditions with K_H = a constant was given by G. I. TAYLOR (1915), and is

$$\Theta = \Theta_0 + a \sin (qt - bz) \exp - bz \qquad 2.03$$

where $b^2 = \dfrac{q}{2K_H}$

Thus on the assumption that K_H = a constant, the lag in the time of maximum temperature with height should be a linear function of the height above the surface.

BEST (1935) however, from a very careful set of measurements between 2.5 cm and 17 m above the surface, found that the lag varied very closely as $z^{0.2}$ whilst calculations, which he made on the assumption that K_H could be treated as a constant over certain shallow layers of the atmosphere, indicated that K_H increased with height according to the power law

$$K_H = \text{const. } z^{1.8} \qquad 2.04$$

so that the assumption that K_H is a constant is clearly unacceptable. Subsequently however COWLING and WHITE (1941) showed that methods which assumed that K_H could be regarded as independent of height through even a shallow layer led to erroneous results and could give values of K_H which were not even correct as regards order of magnitude. Values of K_H, which they computed by a variety of methods, indicated that K_H increased very rapidly with height above the surface, the rate of increase being greater by day than by night, and it was shewn by the present writer (1948) that their values of K_H under

night inversion conditions could be fitted very closely by a simple power law $K_H = \text{const.}\ z^{2/3}$.

In the case of momentum transfer it has been shewn by many writers, including the present writer (1948), that K_M can be represented by a power law of the form

$$K_M = cz^{1-m} \qquad 2.05$$

where the index m always lies between 0 and 1 and varies from a value of about $\frac{1}{7}$ under adiabatic conditions in the daytime to a value of between $\frac{1}{3}$ and $\frac{1}{2}$ under night inversion conditions, so that under inversion conditions the modes of variation with height of K_M and K_H are approximately the same. Under unstable conditions however the evidence from Leafield (JOHNSON and HEYWOOD, 1938) and Rye (BEST and OTHERS, 1950) is conflicting.

SUTTON (1948) from an examination of the Leafield data found that in the hours around noon on a clear summer day $\frac{\partial \Theta}{\partial t}$ became approximately constant with height and time above 1.2 m, and by making certain assumptions as to the amount of heat convected from the surface and assuming that the horizontal flux of heat in the mid hours of the day was negligible (cf. however section 4) concluded that the variation with height of the vertical flux of heat could be ignored below about 100 m. By plotting log $\frac{\partial \Theta}{\partial z}$ against log z, Sutton found that over the limited range from 7 m to 45 m $\frac{\partial \Theta}{\partial z}$ could be closely represented by const. $z^{-1.75}$, so that on the assumption that the vertical flux of heat was constant over this height interval it followed that over the same range

$$K_H = \text{const.}\ z^{1.75} \qquad 2.06$$

Sutton therefore argued that as the direct application of the solution of 2.00 with $K_H = \text{const.}\ z^{1-m}$, where m was a small positive fraction < 1, to the case of heat transfer in the hottest hours of the day led to results which were not in agreement with observations, then the mechanism responsible for heat transfer must differ from that for momentum transfer and suggested that this was due to buoyancy forces.

On the other hand KNIGHTING and BEST (1950), in a discussion of the Rye data, whilst making the assumption that $\frac{\partial \Theta}{\partial t}$ was approximately constant and $= A$ in the mid hours of a hot summer day, made no assumptions as to the constancy with height of the vertical flux of heat, and by integrating 2.00 when $K_H = cz^{1-m}$ obtained

$$\Theta = \frac{Az^{1+m}}{c(1+m)} + \frac{Bz^m}{cm} + C \qquad 2.07$$

where A, B and C are constants. By fitting this equation to a series of observations of potential temperature at four heights between 1.1 m and 106.7 m and eliminating A, B and C, they derived the following equation for m, i.e.

$$\begin{vmatrix} \Theta_4 - \Theta_1 & z_4^{1+m} - z_1^{1+m} & z_4^m - z_1^m \\ \Theta_3 - \Theta_1 & z_3^{1+m} - z_1^{1+m} & z_3^m - z_1^m \\ \Theta_2 - \Theta_1 & z_2^{1+m} - z_1^{1+m} & z_2^m - z_1^m \end{vmatrix} = 0 \qquad 2.08$$

and by solving this equation graphically, found a value of $m = 0.45$. It will be noted that the value of m obtained in this manner is independent of $A = \frac{\partial \Theta}{\partial t}$, providing that A is a constant $\neq 0$, but that the values of c and B depend upon the values of m and A.

Unlike the negative value of m derived by SUTTON (1948) from the Leafield data on the assumption that the first term on the right hand side of 2.07 could be neglected in comparison with the second, this value of m lies within the possible range of values derived from considerations of momentum transfer, although differing considerably from that appropriate to an unstable lapse rate. An examination of the Rye temperature data on clear summer days however shews that $\frac{\partial \Theta}{\partial t}$ falls from about 4.5×10^{-4}° F. sec^{-1} at 1030 to about 1.0×10^{-4} ° F. sec^{-1} at 1230, so that calculations of m from small differences of potential temperature at Rye based upon the assumption of constancy of $\frac{\partial \Theta}{\partial t}$ must accordingly be suspect.

When the value of m was recomputed from the Leafield summer data using the observa-

tions at the four heights 12.4 m, 30.5 m, 57.4 m and 87.7 m, using the method suggested by KNIGHTING and BEST (1950), it was found that the potential temperatures over the period 1000 G.M.T. to 1300 G.M.T. could be fitted very closely with a value of $m = \frac{1}{7}$.

With this value of m together with the value of $A = 3.3 \times 10^{-4}$ °F sec^{-1} found by SUTTON (1948), the values of c and B calculated from 2.07 are 22 and -3.1 respectively, so that the Leafield observations yield

$$K_H = 22\, z^{6/7} \qquad 2.09$$

For comparison the observed values of the differences of potential temperature over various height intervals on a clear summer day and values calculated from

$$\Theta - \Theta^{12.4} = \frac{3.3 \times 10^{-4}}{22 \times 8/7}\{z^{8/7} - 1240^{8/7}\} - \frac{3.1}{22 \times 1/7}\{z^{1/7} - 1240^{1/7}\} \qquad 2.10$$

are shewn in Table I.

The potential temperatures used are means from 1000 G.M.T. to 1300 G.M.T. so that each entry in the second row of Table I represents the mean of about 30 observations.

Table I. Observed and computed differences of potential temperature.

Height interval in m	30.5—12.4	57.4—12.4	87.7—12.4
Observed differences in °F.	—0.31	—0.46	—0.52
Calculated differences in °F	—0.30	—0.46	—0.52

The expression for K_M derived by the present writer (1948) was

$$K_M = m\, z_0^{2m} V_h h^{-m} z^{1-m} \qquad 2.11$$

where V_h was the velocity measured at a standard height h above the surface, z_0 was a parameter characteristic of the degree of roughness of the surface and m was a thermal parameter.

The mean value of V_h during the period 1000 G.M.T. to 1300 G.M.T. on clear summer days at Leafield at a height of 12.7 m was 4.2 m sec^{-1} and whilst the value of z_0 over the grass covered surface is not known, it is unlikely to be widely different from the value of $z_0 = 2.6$ cm. found by a variety of methods for the rolling grassland of Salisbury Plain. With this value of z_0 and a value of $m = \frac{1}{7}$, which was derived from velocity profiles measured near the surface under unstable conditions,

$$K_M = 28.4\, z^{6/7} \qquad 2.12$$

Thus whilst with small differences of potential temperature, such as those in Table I, the possibility of observational error cannot be excluded, it would seem that, contrary to Sutton's conclusions, the Leafield observations in the hottest hours of a clear summer day and at heights greater than 1.2 m are not inconsistent with predictions made from the heat transfer equation when $K_H = cz^{1-m}$ where m has a value of approximately $\frac{1}{7}$, and where c is of the same order of magnitude as $mz_0^{2m} V_h h^{-m}$.

KNIGHTING (1950), in a mathematical discussion of the heat transfer equation, shewed that if any experimental results were analysed by means of solutions obtained from 2.00 and this led to values of m which were negative, then the solutions were not applicable, or alternatively, if the experiments resulted in values of m which were negative, no use having been made of any solutions, then equation 2.00 was invalid and could not be used to represent the equation.

In this connection, it is perhaps not without interest to note that if Sutton's negative value of m is used to calculate c from 2.07 using the Leafield observations at 12.4 m, 30.5 m, and 87.7 m, then $c = -5 \times 10^{-2}$ so that K_H is negative which is physically impossible.

KÖHLER (1932), on the assumptions that near the ground the diurnal variation of temperature could be represented by a sine wave of period 24 hours and that K_H could be represented by cz^{1-m} where c and m were constants, obtained a solution of 2.00 in terms of Bessel Functions of an imaginary argument and from this solution derived formulae which could be used for comparison with observations near the ground. With the aid of these formula Köhler computed the variation of the amplitude with height for various values of c and m over the height range from the surface

to about 30 metres and by comparing JOHNSON's (1929) measurements at Porton of the mean amplitudes at heights of 1.2 m, 7.1 m and 17.1 m with curves derived from these computations for $m=\frac{1}{7}$, found that a close fit was obtained with

$$K_H = 13.8z^{6/7}$$

BEST (1935) who employed formula 12 of Köhler's paper in order to discuss the variations of the lag with height of the time of maximum temperature found that for large values of z the lag tended to a law

$$\text{lag} = \text{const.}\ z^{\frac{1+m}{2}} \qquad 2.13$$

and by comparing this with his empirical result obtained a negative value of $m=-0.6$ which is incompatible with values derived from the momentum theory.

Later however, Best (Meteorological Magazine, November 1935) concluded that the assumption that formula 12 could be used for heights as low as those considered in his paper (1935) was not justified and that the deduction that $m=-0.6$ was invalid.

If therefore we exclude Sutton's conclusions, which appear to be open to some criticism, it appears that the Leafield observations both at night-time and in the daytime are not inconsistent with predictions made from solutions of the heat transfer equation on the assumption that $K_H=\text{const.}\ K_M$.

In the following sections, where the consequences of this assumption are examined in more detail, it is shewn that the predicted values are also in very close agreement with observations at Ismailia and at Kew.

3. The diurnal temperature wave at the earth's surface

It was shewn by the present writer (1948) that $K_M=\text{a const.}\ z^{1-m}$, where m is a function of $\frac{\partial\Theta}{\partial z}$ varying from a value of about $\frac{1}{2}$ to $\frac{1}{3}$ in the early hours of the morning to a value of about $\frac{1}{7}$ or less at midday and the Leafield observations suggest that a similar expression holds for K_H. Such a consideration in the case of heat transfer however renders equation 2.00 quite unmanageable, but since the variation of m during the daylight hours is slight the solution of 2.00 with $m=$ a const. can be used to discuss the temperature changes during this period. We thus require a solution of

$$\frac{\partial\Theta}{\partial t} = c\frac{\partial}{\partial z}\left\{z^{1-m}\frac{\partial\Theta}{\partial z}\right\} \qquad 3.00$$

where c is independent of t and z subject to

$$\left.\begin{aligned}\Theta &= \Theta_0 + a\sin qt \quad \text{when } z\to 0\\ \Theta &= \Theta_0 \qquad\qquad \text{when } z\to\infty\end{aligned}\right\} \qquad 3.01$$

where a is the amplitude of the diurnal temperature wave at the surface and

$$q = \frac{2\pi}{24\times 60\times 60} = 7.3\times 10^{-5}$$

Writing

$$\xi = \frac{z^{1+m}q}{(1+m)c} \qquad 3.02$$

and

$$\Theta = \Theta_0 + (\exp iqt)\cdot f(\xi) \qquad 3.03$$

in 3.00 gives

$$(1+m)\xi\frac{\partial^2 f}{\partial\xi^2} + \frac{\partial f}{\partial\xi} - if = 0 \qquad 3.04$$

The solution of this equation was given by the present writer (1948), and substituting this in 3.03 and selecting the real part, the solution of 3.00 which fits the required boundary conditions is readily found to be

$$\Theta = \Theta_0 + a\varphi(\xi)\sin qt - a\psi(\xi)\cos qt \qquad 3.05$$

where

$$\begin{aligned}\varphi(\xi) = &\left\{-\frac{\xi^2}{\underline{|}2(2+m)} + \frac{\xi^4}{\underline{|}4(2+m)(3+2m)(4+3m)} - \cdots\right\} -\\ &- C\xi^{\frac{m}{1+m}}\left\{1 - \frac{\xi^2}{\underline{|}2(1+2m)(2+3m)} + \cdots\right\} +\\ &+ D\xi^{\frac{m}{1+m}}\left\{\frac{\xi}{1+2m} - \cdots\right\}\end{aligned} \qquad 3.06$$

and

$$\left.\begin{aligned}\psi(\xi) = &-\left\{\xi - \frac{\xi^3}{\underline{|3}(2+m)(3+2m)} + \ldots\right\} + \\ &+ D\xi^{\frac{m}{m+1}}\left\{1 - \frac{\xi^2}{\underline{|2}(1+2m)(2+3m)} + \ldots\right\} + \\ &+ C\xi^{\frac{m}{1+m}} \cdot \\ &\cdot\left\{\frac{\xi}{1+2m} - \frac{\xi^3}{\underline{|3}(1+2m)(2+3m)(3+4m)} + \ldots\right\}\end{aligned}\right| \quad 3.07$$

and C and D are functions of m which were tabulated loc. cit. for various values of m and whose values for $m=\frac{1}{7}$ are 1.1161 and 0.2221 respectively. Theoretical expressions for C and D derived by A. F. Crossley are given in an appendix to this paper, and it can be seen from equations 6.24 and 6.25 of the appendix that

$$\left.\begin{aligned}C &= \frac{\Gamma(2-n)}{\Gamma(1+n)}(1-n)^{-(1-n)}\cos\frac{n\pi}{2}, \quad \& \\ D &= \frac{\Gamma(2-n)}{\Gamma(1+n)}(1-n)^{-(1-n)}\sin\frac{n\pi}{2}\end{aligned}\right| \quad 3.08$$

where

$$n = \frac{m}{1+m} \quad 3.09$$

so that

$$\sqrt{C^2+D^2} = \frac{\Gamma(2-n)}{\Gamma(1+n)}(1-n)^{-(1-n)} \quad 3.10$$

and

$$\frac{D}{C} = \tan\frac{n\pi}{2} = \tan\frac{m}{m+1}\cdot\frac{\pi}{2} \quad 3.11$$

Equation 3.05 may be written

$$\Theta = \Theta_0 + a\chi(\xi)\sin(qt-\lambda) \quad 3.12$$

where

$$\tan\lambda = \frac{\psi(\xi)}{\varphi(\xi)}, \ \& \ \chi(\xi) = \sqrt{\psi^2(\xi)+\varphi^2(\xi)} \quad 3.13$$

and these functions are tabulated and utilized in the following section. It can be seen from 3.12, 3.13, 3.06 and 3.07 that very near the surface the lag with height of the time of maximum temperature is given by

$$\lambda = \tan^{-1}\frac{\psi(\xi)}{\varphi(\xi)} = \tan^{-1}\frac{D\xi^{\frac{m}{m+1}}}{1 - C\xi^{\frac{m}{m+1}}} = \text{const.}\ \xi^{\frac{m}{m+1}}$$

approximately = const. z^m 3.14 whilst at great heights, from the asymptotic expansion cf. 2.13 the lag is given by

$$\text{lag} = \text{const.}\ z^{\frac{1+m}{2}} \quad 3.15$$

Thus with $m=\frac{1}{7}$ the lag varies as $z^{\frac{1}{7}}$ near the surface and as $z^{\frac{4}{7}}$ at great heights so that it is not altogether surprising that Best's (1935) comparison of Köhler's asymptotic solution for great heights with observations near the surface gave misleading results.

The time of maximum temperature at the surface can be obtained from a consideration of the fluxes of heat in the air and ground as follows. The convective flux of heat $C(0)$ from the surface

$$= Lt_{z\to 0} - c_p\varrho c z^{1-m}\frac{\partial\Theta}{\partial z} \quad 3.16$$

and hence from 3.02, 3.05, 3.06, 3.07 and 3.08

$$\left.\begin{aligned}C(0) &= mc_p\varrho ca\left[\frac{q}{c(1+m)}\right]^{\frac{m}{m+1}} \\ &\quad \{C\sin qt + D\cos qt\}\end{aligned}\right| \quad 3.17$$

$$= mc_p\varrho ca\left[\frac{q}{c(1+m)}\right]^{\frac{m}{m+1}}\sqrt{C^2+D^2}\sin(qt+\alpha) \quad 3.18$$

where

$$\alpha = \tan^{-1}\frac{D}{C} \quad 3.19$$

but from 3.11

$$\frac{D}{C} = \tan\frac{m}{m+1}\cdot\frac{\pi}{2}$$

and hence

$$\alpha = \frac{m}{m+1}\cdot\frac{\pi}{2} \quad 3.20$$

Thus the convective flux of heat from the surface can be represented by a sine wave and

is a maximum at a time t before the time of maximum temperature given by

$$t = \frac{m}{m+1} \cdot \frac{\pi}{2} \cdot \frac{24}{2\pi} = \frac{6m}{m+1} \text{ hours} \qquad 3.21$$

and it will be noted that this phase difference is a function of m only and is independent of the wind speed, amplitude of the diurnal wave of temperature or nature of the surface.

The flux of heat in the ground may be derived by means of a similar analysis, with k_1, the coefficient of thermal diffusivity of the soil, replacing $K_H = cz^{1-m}$, the coefficient of eddy diffusivity of the air. The corresponding solutions may be derived very simply by writing $m = 1$ in 3.16 and replacing c_p (the specific heat of the air) by c_1 (the specific heat of the soil), ϱ (the density of the air) by ϱ_1 (the density of the soil) and c by k_1 (the coefficient of thermal diffusivity) whenever they occur in equations 3.17 et sequitur.

Hence the ground flux of heat $G(0)$ is given by

$$G(0) = c_1\varrho_1 k_1 a\left(\frac{q}{2k_1}\right)^{1/2}\sqrt{C_1^2 + D_1^2}\,\sin\,(qt + \alpha_1) \qquad 3.22$$

where from 3.10 and 3.20

$$\sqrt{C_1^2 + D_1^2} = \sqrt{2} \text{ and } \alpha_1 = \frac{\pi}{4} \qquad 3.23$$

and thus

$$G(0) = c_1\varrho_1 k_1^{1/2} a q^{1/2} \sin\left(qt + \frac{\pi}{4}\right) \qquad 3.24$$

Thus the ground flux of heat can be represented by a sine wave and is a maximum at a time t before the time of surface maximum temperature given by

$$t = \frac{\pi}{4} \cdot \frac{24}{2\pi} = 3 \text{ hours} \qquad 3.25$$

and again it can be seen that this phase difference is independent of the amplitude of the diurnal temperature wave, nature of soil etc.

This result was first obtained by SCHMIDT (1925) who also, on the assumption of a constant coefficient of eddy diffusivity in the air, found that the ground flux of heat was in phase with the convective flux of heat.

Now the heat balance equation on the assumption that there are no horizontal gradients of temperature and water vapour is

$$C(0) + E(0) + R(0) + G(0) = 0 \qquad 3.26$$

where $C(0)$ is the convective flux of sensible heat at the surface, $E(0)$ is the convective flux of latent heat, $R(0)$ is the net radiative flux of heat and $G(0)$ is the flux of heat into the ground. Fluxes directed away from the surface are considered positive.

Over a desert surface it may be assumed that $E(0)$ is zero, and hence

$$R(0) = -C(0) - G(0) \qquad 3.27$$

and $\therefore$

$$\left.\begin{aligned} R(0) = &- mc_p\varrho ca\left[\frac{q}{c(1+m)}\right]^{\frac{m}{m+1}}\sqrt{C^2 + D^2}\,\cdot \\ &\cdot \sin\left(qt + \frac{m}{m+1}\cdot\frac{\pi}{2}\right) - c_1\varrho_1 k_1^{1/2} a q^{1/2} \sin\left(qt + \frac{\pi}{4}\right) \end{aligned}\right\} \qquad 3.28$$

$$\equiv A \sin\,(qt + \gamma) \qquad 3.29$$

where

$$\left.\begin{aligned} A = a\sqrt{\;} &\left\{m^2 c_p^2 \varrho^2 c^2\left[\frac{q}{c(1+m)}\right]^{\frac{2m}{m+1}}(C^2 + D^2) + \right. \\ &+ c_1^2\varrho_1^2 k_1 q + 2mc_p\varrho c\left[\frac{q}{c(1+m)}\right]^{\frac{m}{m+1}}\cdot \\ &\left.\cdot\sqrt{C^2 + D^2}\varrho_1 c_1 k_1^{1/2} q^{1/2} \cos\frac{\pi}{4}\left(\frac{1-m}{1+m}\right)\right\} \end{aligned}\right\} \qquad 3.30$$

and

$$\left.\begin{aligned} \tan\gamma = &\frac{mc_p\varrho c\left[\frac{q}{c(1+m)}\right]^{\frac{m}{m+1}}\sqrt{C^2 + D^2}\,\cdot}{mc_p\varrho c\left[\frac{q}{c(1+m)}\right]^{\frac{m}{m+1}}\sqrt{C^2 + D^2}\,\cdot} \\ &\cdot \sin\frac{m}{m+1}\cdot\frac{\pi}{2} + c_1\varrho_1 k_1^{1/2} q^{1/2}\sin\frac{\pi}{4} \\ &\cdot \cos\frac{m}{m+1}\cdot\frac{\pi}{2} + c_1\varrho_1 k_1^{1/2} q^{1/2}\cos\frac{\pi}{4} \end{aligned}\right\} \qquad 3.31$$

Thus the net radiative flux of heat at the surface $R(0)$ is also represented by a sine wave which is out of phase with the temperature wave.

The net radiative flux of heat on a clear day is however a maximum at local noon, and hence the time of maximum temperature at the surface occurs at a time $12+t$ hours where

$$t = \gamma \times \frac{2\pi}{360} \times \frac{24}{2\pi} = \frac{\gamma}{15} \text{ hours} \qquad 3.32$$

where γ is given by 3.31.
It can be seen from 3.31 that γ must lie between $-\frac{m}{m+1} \cdot \frac{\pi}{2}$ and $\frac{\pi}{4}$ and hence over the desert it follows that the time of maximum must occur not earlier than $\frac{6m}{m+1}$ hours and not later than 3 hours after local noon, the actual time depending upon the relative magnitudes of the convective and ground fluxes of heat, but being independent of the amplitude of the diurnal wave of temperature. With K_H const. with height, $m=1$ so that the time of maximum would always occur 3 hours after local noon. If $K_H \propto K_M$, so that $c \propto m z_0^{2m} V_h h^{-m}$, then an increase in wind speed, or to a lesser extent an increase of the surface roughness, should result in an earlier time of maximum.

Over a grass covered surface from which evaporation is taking place the effect of the flux of water into the air is difficult to assess directly. According to BOWEN (1926) however, the ratio between the flux of latent heat and sensible heat is constant for any given surface and may be obtained from simultaneous measurements of humidity and temperature at two heights, and although it is not possible to prove this theoretically, RIDER and ROBINSON (1951), who calculated values of Bowen's ratio μ near the surface on clear summer days at Kew, found that μ was constant with height and shewed little variation from day to day. If therefore the fluxes of sensible and latent heat are in phase, equations 3.27 to 3.31 can still be used with $(1+\mu)$ $C(0)$ replacing $C(0)$ over a grass surface. Hence if the other variables remain unaltered, the time of maximum will be earlier over a grass surface from which evaporation is taking place than over a dry surface, but it will still occur between the limits of $\frac{6m}{m+1}$ and 3 hours after local noon.

4. Comparison with observations

As this theory depends upon the fundamental assumption that there is no horizontal flux of heat, it does not appear possible to use the results from either Rye or Leafield other than qualitatively.

The station at Rye for example, is only 5 km from the sea and is affected by sea breezes especially on clear summer days, and the irregularities in the mean temperature curve for such days make it impossible to determine the time of maximum with any degree of confidence. Furthermore an examination of the individual daily records, from which the mean curve is constructed, shews that on many occasions in the hours around midday the temperature instead of rising is falling at all heights, so that any theory which depends upon the simple propagation of a sine wave upwards from the surface is clearly incapable of explaining the observed vertical thermal structure at Rye on such occasions.

Leafield on the other hand, although free of complications such as a sea breeze, is situated on a spur of the Cotswold Hills with a rapid fall of 100 m in 3 km to the north and a fall of the same amount in about 4 km to the south, and the meteorological observations at Leafield have been found to be unrepresentative of conditions over more level sites. JOHNSON and HEYWOOD (1938) for example, list several anomalies in the meteorological elements at Leafield on clear summer days and ascribe them to the fact that during the hottest hours of the day, the surface air at Leafield mainly consists of air which has come from the relatively great height of about 100 m above the lower ground to the north and south of the spur.

The desert site at Ismailia however is singularly free from topographical defects except in the summer months when it is sometimes affected by a slight 'sea breeze' from Lake Timsah 3 km to the south east, and hence the observations from here, and mainly those on clear December days (FLOWER, 1936) have been utilised to test out the theory.

Now from 3.18 the maximum value of $C(0)$ with $m=\frac{1}{7}$ is

$$C(0) = \frac{1}{7} \times \frac{1}{4} \times \frac{1}{800} \times c^{7/8} \times a \times \left. \times \left(\frac{7.3 \times 10^{-5}}{8/7} \right)^{1/8} \times 1.138 \right\}$$

$$= ac^{7/8} \times 1.520 \times 10^{-5} \text{ g cal. cm}^{-2} \text{ sec}^{-1} \quad 4.00$$

where a is the amplitude of the diurnal temperature wave at the surface, and from 3.21 $C(0)$ is a maximum 45 minutes before the time of maximum at the surface.

Similarly, using the values of c_1, ϱ_1 and k_1 for Ismailia given by FLOWER (1936) i.e., $c_1 = 0.19$, $\varrho_1 = 2.63$ and $k_1 = 10^{-2}$ the maximum value of $G(0)$ is from 3.22

$$G(0) = 0.19 \times 2.63 \times 0.1 \times a \times (7.3 \times 10^{-5})^{1/2}$$

$$= a \times 4.05 \times 10^{-4} \text{ g cal. cm}^{-2} \text{ sec.}^{-1} \quad 4.01$$

and hence from 3.30 the maximum value of $R(0)$ is

$$R(0) = a\left[(4.05)^2 + c^{7/4}(0.1520)^2 + 2 \times 4.05 \times \right.$$

$$\left. \times 0.1520 \times c^{7/8} \cos \frac{3\pi}{16} \right] \quad 4.02$$

whilst from 3.31

$$\tan\gamma = \frac{c^{7/8} \times 0.1520 \sin \frac{\pi}{16} + 4.05 \sin \frac{\pi}{4}}{c^{7/8} \times 0.1520 \cos \frac{\pi}{16} + 4.05 \cos \frac{\pi}{4}} \quad 4.03$$

Whilst at Ismailia there appear to be no direct observations of $R(0)$, $C(0)$ or $G(0)$ which can be used to calculate c and a, $R(0)$ and $G(0)$ can be estimated with a reasonable degree of confidence.

Thus on a clear December day the maximum downward flux of short wave radiation at Ismailia may be taken as approximately 140×10^{-4} gram cal. cm^{-2} sec^{-1} and the albedo of the desert surface may be taken as approximately 20 %. The former value is based on American observations in California and is supported by observations at Kew Observatory made when the solar elevation is the same as that at Ismailia, whilst the latter is based upon mesasurements by Ångström and observations from American aircraft at high levels over Death Valley, California (1951). The incoming long wave radiation of atmospheric origin, using Flower's data of temperature and vapour pressure, is about 75 gram cal.cm^{-2} sec^{-1} whilst the outward long wave radiation from a desert surface at a temperature of 300° A is about 112×10^{-4} gramcal.cm^{-2}sec^{-1}. Hence the net radiative flux of heat, which Dr G. D. Robinson of Kew Observatory, to whom I am indebted for this estimate, considers may possibly be in error by as much as 10%, is 75×10^{-4} gram cal.cm^{-2}sec^{-1}.

Dr Robinson has also drawn my attention to unpublished measurements of the ground flux of heat in arid soil in Palestine by Ashbel which give $G(0) = 50 \times 10^{-4}$ gramcal.cm^{-2}sec^{-1} and by W. Swinbank in semi-desert soil near Melbourne which also give values of $G(0)$ of about 50×10^{-4} gramcal.cm^{-2}sec.$^{-1}$.

With a value of $G(0) = 50 \times 10^{-4}$ gram cal.cm^{-2}sec^{-1}, the amplitude a of the diurnal wave at the surface is, from 4.01, 12.4° C. With this value of $a = 12.4°$ C and a value of $R(0) = 75 \times 10^{-4}$ gram cal.cm^{-2}sec^{-1} the value of c from $4.02 = 21.9$, whilst from 4.00 with $c = 21.9$ and $a = 12.4°$ C, $C(0) = 28.4 \times 10^{-4}$ gramcal.cm^{-2}sec^{-1}.

Whilst there is some uncertainty as to the value of $C(0)$ at midday, the above value is in accordance with the usual concept of its value, and it is of interest to note that the value of c is very nearly the same as that derived from the Leafield observations in the hottest hours around noon on a clear summer day with similar wind speeds.

With this value of $c = 21.9$ from 4.03,

$$\tan\gamma = \frac{2.27 \sin \frac{\pi}{16} + 4.05 \sin \frac{\pi}{4}}{2.27 \cos \frac{\pi}{16} + 4.05 \cos \frac{\pi}{4}} = \tan 33°17' \quad 4.04$$

and hence the time of maximum temperature at the surface at Ismailia on clear December days should occur $33\frac{17}{60} \times \frac{24 \times 60}{360} = 133$ minutes after the time of local noon, i.e. at 1413 local time.

The values of $\chi(\xi)$ and λ from 3.06, 3.07, and 3.13 with $m = \frac{1}{7}$ for selected values of ξ are shewn in Table II.

Table II. Values of $\chi(\xi)$ and λ when $m=\frac{1}{7}$.

ξ	10^{-5}	10^{-4}	10^{-3}	10^{-2}	5×10^{-2}	10^{-1}
$\chi(\xi)$	.737	.650	.537	.391	.272	.224
λ	3°55′	5°55′	9°32′	17°42′	29°01′	35°55′

The lag in the time of maximum temperature in minutes from equation 3.12 is $\frac{\lambda\times24\times60}{360}=4\lambda$, and hence from 3.02 using the value of $c=21.9$, Table III shewing the amplitude and lag at various heights can be constructed.

Table III. Percentage amplitude and lag in minutes at various heights.

Height	3.07 cm	22.04 cm	1.65 m	12.40 m	50.78 m	92.94 m
Percentage Amplitude	73.7	65.0	53.7	39.1	27.2	22.4
Lag in minutes.....	16	24	38	71	116	144

Table IV shews the time of maximum temperature at four heights above the surface as determined by Flower from the December clear day observations and those derived from Table III together with the time of maximum temperature at the surface i.e. 1413 hours, and it can be seen that the agreement between the two sets of times is remarkably close.

Table IV. Times of maximum temperature at various heights.

Height in m	1.1	16.2	46.4	61.0
Observed times...	1447	1524	1605	1623
Calculated times..	1447	1530	1605	1616

It is of interest to note that in view of the doubtful accuracy of determining times of maximum temperature at various heights from smooth curves drawn through mean hourly values, Flower (1936) carried out a harmonic analysis of the variation of temperature at each height and determined the time of maximum from the phase angle of the diurnal harmonic.

Flower also calculated the times of occurrence of the maximum temperature at each of the four heights for each month of the year and, noting that the time of maximum especially at a height of 1.1 m varied very closely with the equation of time, suggested that the variation of temperature at the surface was equal to the equation of time. It will be seen that provided the variations in the mean monthly fluxes of convective heat are small, this follows from the fact that the radiative flux of heat is a maximum at local noon.

If, as might be expected by analogy with momentum transfer, c is proportional to the mean wind speed measured at some standard height, then the effect of the wind speed upon the time of maximum temperature can readily be determined. The value of c in 4.03 was determined at a time when the mean wind speed at a height of 15.2 m was 3.8 m sec^{-1} and hence if the other factors remain unchanged the values of γ over a desert surface are, from 4.04, given by

$$\tan\gamma=\frac{2.27\left(\frac{V}{3.8}\right)^{7/8}\sin\frac{\pi}{16}+4.05\sin\frac{\pi}{4}}{2.27\left(\frac{V}{3.8}\right)^{7/8}\cos\frac{\pi}{16}+4.05\cos\frac{\pi}{4}} \quad 4.05$$

so that an increase in the wind speed results in an earlier time of maximum.

The values of γ and the corresponding times of maximum temperature for various values of V_h are given in Table V.

Table V. Variation with wind speed of time of maximum temperature over the desert.

Wind speed at 15.2 m in m. sec.$^{-1}$	0	2½	5	7½	10
γ.....	45°	36°19′	31°21′	28°34′	26°10′
Time of maximum at surface.....	1500	1425	1406	1354	1345
Time of maximum at 1.1 m.....	—	1504	1439	1425	1414
Time of maximum at 16.2 m.....	—	1556	1519	1459	1445
Time of maximum at 46.4 m.....	—	1635	1548	1523	1507
Time of maximum at 61.0 m.....	—	1646	1558	1532	1515

There are unfortunately no observations in the Ismailia report (1936) which can be used to check this dependence of the time of maximum upon the wind speed, but that at least the order of magnitude of the effect is correct can be seen from tables given by JOHNSON and HEYWOOD (1938) shewing the times of maximum at various heights at Leafield in summer for various wind speeds.

Table VI.

Wind speed at 12.7 m in m. sec.$^{-1}$	2.5	4.2	7.5
Time of maximum at 1.2 m	1505	1455	1430
" " " " 12.4 m	1546	1535	1500
" " " " 30.5 m	1600	1550	1512
" " " " 57.4 m	1616	1606	1522

A curious feature of the Leafield observations, which has no counterpart in either the Rye or Ismailia observations, is the fact that on clear summer days at Leafield the times of maximum temperature at all heights occur very nearly an hour later than the corresponding times of maximum on a mean June day, and in fact occur outside the theoretical times of maximum based on the assumption of very light winds and a very high value of the thermal conductivity. This is consistent with other anomalous features of the Leafield observations on clear summer days noted by JOHNSON and HEYWOOD (1938) and lends support to their suggestion that these were due to advection and lateral mixing.

As already stated, the value of V_h at Ismailia at a height of 15.2 m during the midday hours was 3.8 m, and assuming that the parameter z_0 for Ismailia is of the same order of magnitude as that for the rolling downland of Salisbury Plain, then K_M with $m=\frac{1}{7}$ is given by

$$\left.\begin{aligned} K_M &= \frac{1}{7}(2.6)^{2/7}\frac{380}{(1520)^{1/7}}z^{6/7} \\ &= 25.6z^{6/7} \end{aligned}\right\} \qquad 4.06$$

whereas with $m=\frac{1}{7}$

$$K_H = 21.9z^{6/7} \qquad 4.07$$

which also lends some support to the suggestion that $K_H = \text{const.}\ K_M$ where the constant is approximately unity.

From 3.05, 3.06, 3.07 and 3.08, it can be seen that around midday and within a few metres of the ground Θ is given to a good degree of approximation by

$$\Theta = \Theta_0 + a\sin qt - a\xi^{\frac{m}{m+1}}(C\sin qt + D\cos qt) \qquad 4.08$$

so that from 3.02 and 3.11

$$\left.\begin{aligned} \Theta = \Theta_0 + a\sin qt - az^m\left[\frac{q}{(m+1)c}\right]^{\frac{m}{m+1}}\cdot \\ \cdot\sqrt{C^2+D^2}\sin\left(qt+\frac{m}{m+1}\cdot\frac{\pi}{2}\right) \end{aligned}\right\} \qquad 4.09$$

and hence near the surface

$$\Theta = \Theta_g - \beta z^m \qquad 4.10$$

where Θ_g is the value of Θ at the surface and

$$\beta = a\left[\frac{q}{(m+1)c}\right]^{\frac{m}{m+1}}\sqrt{C^2+D^2}\sin\left(qt+\frac{m}{m+1}\cdot\frac{\pi}{2}\right) \qquad 4.11$$

It follows therefore that if K_H and K_M are represented by similar power laws then the temperature and velocity profiles near the ground should be the same, and conversely that if the temperature and velocity profiles near the ground are the same then K_M and K_H are represented by similar laws.

NOW RIDER and ROBINSON (1951), from observations at Kew Observatory, shewed that when the winds and temperatures measured at several heights between 10 cm and 200 cm were superposed with adjustment for scale, so that the profiles as drawn by hand coincided at 25 cm and 100 cm, the wind and velocity profiles in nearly all cases had the same form.

Table VII shews the velocities from 25 cm to 200 cm for all unstable cases which they listed for clear summer days at Kew 1949 at times between 1100 and 1400 G.M.T. reduced to a standard velocity of 200 cmsec^{-1} at a height of 2.02 m. The wind velocities are mean values over a 30 minute period which the authors considered was sufficiently long to give smooth mean profiles and suffi-

Table VII. Velocities near the surface at Kew on clear sunny days.

Case No.	1	2	3	4	5	6	7	8	9	10	1/9th law
Date	18/6	20/6	20/6	21/6	21/6	23/6	23/6	24/6	1/7	1/7	$200\left(\frac{z}{202}\right)^{1/9}$
Height \ Time in cm.	1121	1121	1410	1110	1400	1103	1432	1419	1122	1428	—
25	159	161	158	152	150	155	153	163	158	156	159
37	162	165	166	163	166	165	163	173	148	161	166
58	173	177	171	174	174	173	175	179	168	173	170
76	176	180	179	178	177	179	180	176	171	175	179
102	187	187	189	188	185	188	186	189	184	185	185
202	200	200	200	200	200	200	200	200	200	200	200

ciently short to exclude the effects of the diurnal variation. For comparison the velocities computed from the simple power law $V=200\left(\frac{z}{202}\right)^{1/9}$ which gives a closer fit than a $\frac{1}{7}$th law are also tabulated.

It can be seen that over this height range the observed velocities can be represented reasonably closely by a simple power law where the index $m=\frac{1}{9}$, and hence since the ve ocity and temperature profiles when adjusted for scale coincide, it follows that over this height range the temperature data can be represented by

$$\Theta=\Theta_g-\beta z^{1/9} \qquad 4.12$$

where Θ is the value of Θ at the surface, and where

$$\beta=\frac{V_{202}}{(202)^{1/9}}\cdot\frac{\Theta_{25}-\Theta_{202}}{V_{202}-V_{25}} \qquad 4.13$$

The values of β in °F. cm$^{-1/9}$ for the above occasions have been computed and are listed in Table VIII.

Table VIII. Values of β on clear summer days.

Case No.	1	2	3	4	5	6	7	8	9	10
β.....	6.3	5.8	5.3	5.6	5.0	6.1	4.2	5.8	5.9	4.9

The mean value of β from Table VIII is 5.5, and hence near the surface where Θ is given by 4.12

$$K_H=cz^{8/9} \qquad 4.14$$

The convective flux of heat at the surface is thus

$$C(0)=Lt_{z\to 0}-K_H\varrho c_p\frac{\partial\Theta}{\partial z}$$

$$=c\times\frac{1}{4}\times\frac{1}{800}\times 5.5\times\frac{1}{9}\times\frac{5}{9}$$

$$=1.06\times 10^{-4}\times c \text{ gram cal. cm}^{-2}\text{ sec}^{-1} \qquad 4.15$$

The mean value of $C(0)$ for the occasions listed in Table VII and computed by Rider and Robinson from the heat balance equation is $C(0)=37.3\times 10^{-4}$ gram cal. cm^{-2} sec^{-1} 4.16

and hence from 4.15 and 4.16

$$c=35$$

This value of c is subject to some uncertainty, as the computations of $C(0)$ from the heat balance equation depend upon the fundamental assumption that there is no horizontal flux of heat, and in view of the topography at Kew it is possible that this does not hold. Thus Rider and Robinson (1951) noted that the temperature fluctuations which they observed near the ground appeared to be inconsistent with this assumption, whilst values of $C(0)$ computed by Lander and Robinson (1952) from simultaneous observations of wind and temperature fluctuations were consistently only about $\frac{1}{2}$ to $\frac{1}{3}$ the values computed from the heat balance equation, so that the value of c lies somewhere between about 12 and 35.

Now the mean value of V_h at 2.02 m for these observations was about 3 m. sec^{-1} and with a value of $m=\frac{1}{9}$ and a value of $z_0=2.6$ cm, the value of $K_M=22.9z^{8/9}$. Whether

however this value of z_0 is approximately true for Kew is uncertain, for whilst the actual observations were made over a surface of level grass which was kept mown to an average length of 1 to 2 cm, this grass surface was surrounded by a solid fence about 1.5 m high which was about 50 m away at the nearest point, whilst in some directions there were very large trees and buildings, including the observatory itself which was on rising ground to the north west of the site. In view of the uncertainty of both c and z_0, all that can be said with any degree of confidence is that under unstable conditions the modes of variation of K_H and K_M at Kew are the same, with $m=\frac{1}{9}$ approximately, whilst the observed values of the convective heat flux are not inconsistent with those predicted on the assumption that $K_H=\text{const.}\ K_M$, where the constant of proportionality is approximately unity.

The general agreement between the observed and calculated values at Leafield, Ismailia and Kew suggest that, except perhaps in the lowest few cm, the mechanism for heat transfer is the same as that for momentum transfer and that the coefficients of eddy viscosity and eddy conductivity are approximately the same.

5. The annual temperature wave

The results of the previous sections can be used with slight modification to discuss the annual variation of temperature. For example during the summer months at Ismailia the annual variation of temperature can be closely represented by a single sine wave of period one year. Similarly during the period May to September the average monthly lapse rate of potential temperature between 1.1 m and 61 m is positive, i.e. the potential temperature decreases with height so that during this period the index m can be assumed to be approximately constant and equal to about $^1/_7$.

The solution of 3.00 with $m=^1/_7$ will therefore be utilized to discuss the variation in the date of occurrence of the maximum air temperature at Ismailia.

The phase lag of the annual temperature wave against the annual convective flux wave is from 3.20 given by

$$\alpha=\frac{m}{m+1}\cdot\frac{\pi}{2} \qquad 5.00$$

and since for annual values $q_a=\frac{q}{365}$, the convective flux of heat from the surface is a maximum at a time t_1 before the time of maximum temperature at the surface given by

$$\left.\begin{aligned} t_1&=\frac{m}{m+1}\cdot\frac{\pi}{2}\cdot\frac{12}{2\pi}\\ &=\frac{3}{8}\text{ months}\\ &=11^1/_4\text{ days approximately}\end{aligned}\right\} \qquad 5.01$$

The phase lag of the annual temperature wave against the annual ground flux wave is from 3.23 given by

$$\alpha_1=\frac{\pi}{4}$$

and hence

$$\left.\begin{aligned} t_2&=\frac{\pi}{4}\times\frac{12}{2\pi}\\ &=1^1/_2\text{ months}\end{aligned}\right\} \qquad 5.02$$

and it will be noted that, as in the case of the diurnal wave, these times are independent of the amplitude of the annual temperature wave and of the physical properties of the air and soil, etc.

The phase lag of the annual temperature wave against the net radiative flux wave is given by 3.31 with q_a replacing q. Thus using the same values of the soil constants at Ismailia as in 4.01 and the same value of c, the time interval from 4.03 is

$$\left.\begin{aligned} t_3&=33^\circ 17'\times\frac{2\pi}{360}\times\frac{12}{2\pi}\\ &=33\text{ days}\end{aligned}\right\} \qquad 5.03$$

Now from 3.12, the lag in days at various heights is $\frac{\lambda\times 365}{360}=\lambda$ approximately, whilst from 3.02, assuming that c does not increase with the increased time over which the means are now taken, the heights corresponding to the specified values of ξ in Table III have to be multiplied by $(365)^{7/8}$.

The dates of maximum air temperature

Table IX. Dates of maximum air temperature at Ismailia at various heights.

Height in m	1.1	16.2	46.4	61.0
Observed date of maximum.....	July 10th	July 29th	July 30th	July 31st
Calculated date of maximum.....	July 26th	July 28/29	July 30th	July 30/31

from Flower's (1936) harmonic analysis of the monthly mean temperatures at 4 heights, during the period October, 1931 to October, 1932, together with those derived by the present theory for the same heights, are given in Table IX.

The agreement between the observed and predicted dates is very good except at 1.1 m where Flower's date of maximum, in the light of his values at greater heights, appears to be somewhat early, and suggests that c is independent of the period over which means are taken.

It is possible that this discrepancy is due to the limited period over which means are taken, or it may be that the present theory has oversimplified the problem of the annual temperature wave.

Acknowledgment: I am indebted to the Director of the Meteorological Office for permission to publish this paper.

6. Appendix by A. F. Crossley, M. A.

Equation 13 (FROST, 1948) c.f. also 3.04 of the present paper, is

$$(1+m)\xi\frac{\partial^2 W}{\partial \xi^2}+\frac{\partial W}{\partial \xi}-iW=0 \qquad 6.00$$

Substituting

$$W=y\xi^{\frac{m}{2}} \text{ and } x=2(1-n)^{1/2}e^{-\frac{i\pi}{4}}\xi^{1/2} \qquad 6.01$$

where

$$n=\frac{m}{1+m} \qquad 6.02$$

gives

$$\frac{\partial^2 y}{\partial x^2}+\frac{1}{x}\frac{\partial y}{\partial x}+\left(1-\frac{n^2}{x^2}\right)y=0 \qquad 6.03$$

which is Bessel's equation of order n

Since $0 \leqslant m \leqslant 1$ 6.04

therefore $0 \leqslant n \leqslant 1/2$ 6.05

so that (except for $n=0$) $y=J_n(x)$ and $y=J_{-n}(x)$ are independent solutions of 6.03 and hence

$$W_1=\xi^{\frac{n}{2}}J_{-n}(x), \text{ and } W_2=\xi^{\frac{n}{2}}J_n(x) \qquad 6.06$$

are independent solutions of 6.00.
Now

$$J_n(x)=\frac{x^n}{2^n\Gamma(1+n)}\left\{1-\frac{x^2}{2^2(1+n)}+\frac{x^4}{2^4\underline{|2}(1+n)(2+n)}-\ldots\right\} \qquad 6.07$$

and hence the two solutions of 6.00 are

$$W_1=\xi^{n/2}J_{-n}(x)=\frac{(1-n)^{-n/2}e^{\frac{in\pi}{4}}}{\Gamma(1-n)}\cdot\left\{1+i\xi+\frac{i^2\xi^2}{\underline{|2}(2+m)}+\ldots\right\} \qquad 6.08$$

and

$$W_2=\xi^{n/2}J_n(x)=\frac{(1-n)^{n/2}e^{-\frac{in\pi}{4}}}{\Gamma(1+n)}\cdot\left\{1+\frac{i\xi}{1+2m}+\frac{i^2\xi^2}{\underline{|2}(1+2m)(2+3m)}+\ldots\right\} \qquad 6.09$$

Except for the constant factors these solutions coincide with equations 17 and 18 (FROST 1948). We require asymptotic expressions for the two series which (following Frost) we separate into their real and imaginary parts. Thus

$$f_1(\xi)+if_2(\xi)=\Gamma(1-n)e^{-\frac{in\pi}{4}}(1-n)^{n/2}\xi^{n/2}J_{-n}(x) \qquad 6.10$$

and

$$f_3(\xi)+if_4(\xi)=\Gamma(1+n)e^{\frac{in\pi}{4}}(1-n)^{-n/2}\xi^{n/2}J_n(x) \qquad 6.11$$

Now from 6.01 amp $x=-\frac{\pi}{4}$, and the corresponding asymptotic expression for $J_n(x)$ is (GRAY, MATTHEWS and MACROBERT, Bessel Functions, p. 61)

$$J_n(x) \to \left(\frac{2}{\pi x}\right)^{1/2} \cos\left(x - \frac{\pi}{4} - \frac{n\pi}{2}\right) \quad 6.12$$

$$= \frac{e^{\frac{i\pi}{8}} \xi^{-\frac{1}{4}}}{\pi^{1/2}(1-n)^{1/4}} \cdot \cdot \cos\left\{2^{1/2}(1-n)^{1/2}(1-i)\xi^{1/2} - \frac{\pi}{4} - \frac{n\pi}{2}\right\} \quad 6.13$$

or putting

$$\alpha = \frac{\pi}{4} + \frac{n\pi}{2} \text{ and } u = \{2(1-n)\xi\}^{1/2} \quad 6.14$$

$$J_n(x) \to \frac{e^{\frac{i\pi}{8}} \xi^{-\frac{1}{4}}}{\pi^{1/2}(1-n)^{1/4}} \cdot \cdot \{\cos(u-\alpha)\cos h\, u + i \sin(u-\alpha) \sin h\, u\} \quad 6.15$$

$$\to \frac{\xi^{-\frac{1}{4}} e^u}{2\pi^{\frac{1}{2}}(1-n)^{\frac{1}{4}}} \cdot e^{i\left(u - \frac{\pi}{8} - \frac{n\pi}{2}\right)} \quad 6.16$$

Similarly

$$J_{-n}(x) \to \frac{\xi^{-\frac{1}{4}} e^u}{2\pi^{\frac{1}{2}}(1-n)^{\frac{1}{4}}} \cdot e^{i\left(u - \frac{\pi}{8} + \frac{n\pi}{2}\right)} \quad 6.17$$

Therefore

$$f_1(\xi) + i f_2(\xi) \to \cdot \frac{\Gamma(1-n) \cdot (1-n)^{-\frac{(1-2n)}{4}} \xi^{\frac{2n-1}{4}} e^{i\left(u - \frac{\pi}{8} + \frac{n\pi}{4}\right)}}{2\pi^{\frac{1}{2}}} \quad 6.18$$

and

$$f_3(\xi) + i f_4(\xi) \to \cdot \frac{\Gamma(1+n)(1-n)^{-\frac{(1+2n)}{4}} \xi^{\frac{(2n-1)}{4}} e^{i\left(u - \frac{\pi}{8} - \frac{n\pi}{4}\right)}}{2\pi^{\frac{1}{2}}} \quad 6.19$$

Equations 26 and 27 (Frost, 1948) therefore become

$$0 = -\varrho_0 G_0 \Gamma(1-n)(1-n)^{-\frac{(1-2n)}{4}} \cdot \cdot \cos\left(u - \frac{\pi}{8} + \frac{n\pi}{4}\right) + \Gamma(1+n)(1-n)^{-\frac{(1+2n)}{4}} \cdot \cdot \left\{C \cos\left(u - \frac{\pi}{8} - \frac{n\pi}{4}\right) - D \sin\left(u - \frac{\pi}{8} - \frac{n\pi}{4}\right)\right\} \quad 6.20$$

and

$$0 = -\varrho_0 G_0 \Gamma(1-n)(1-n)^{-\frac{(1-2n)}{4}} \cdot \cdot \sin\left(u - \frac{\pi}{8} + \frac{n\pi}{4}\right) + \Gamma(1+n)(1-n)^{-\frac{(1+2n)}{4}} \cdot \cdot \left\{D \cos\left(u - \frac{\pi}{8} - \frac{n\pi}{4}\right) + C \sin\left(u - \frac{\pi}{8} - \frac{n\pi}{4}\right)\right\} \quad 6.21$$

whence

$$C \cos\left(u - \frac{\pi}{8} - \frac{n\pi}{4}\right) - D \sin\left(u - \frac{\pi}{8} - \frac{n\pi}{4}\right) = = \varrho_0 G_0 \frac{\Gamma(1-n)}{\Gamma(1+n)}(1-n)^n \cos\left(u - \frac{\pi}{8} + \frac{n\pi}{4}\right) \quad 6.22$$

$$C \sin\left(u - \frac{\pi}{8} - \frac{n\pi}{4}\right) + D \cos\left(u - \frac{\pi}{8} - \frac{n\pi}{4}\right) = = \varrho_0 G_0 \frac{\Gamma(1-n)}{\Gamma(1+n)}(1-n)^n \sin\left(u - \frac{\pi}{8} + \frac{n\pi}{4}\right) \quad 6.23$$

whence

$$C = \varrho_0 G_0 \frac{\Gamma(1-n)}{\Gamma(1+n)}(1-n)^n \cos\frac{n\pi}{2} \quad 6.24$$

and

$$D = \varrho_0 G_0 \frac{\Gamma(1-n)}{\Gamma(1+n)}(1-n)^n \sin\frac{n\pi}{2} \quad 6.25$$

These forms are suitable for computation. The figures in Table II (Frost 1948) are confirmed (apart from some minor differences in the fourth place of decimals).
Also

$$\tan\psi_0 = \frac{D}{C} = \tan\frac{n\pi}{2} \quad 6.26$$

$$\therefore \psi_0 = \frac{n\pi}{2} = \frac{m}{m+1} \cdot \frac{\pi}{2} \quad 6.27$$

which confirms equation 30 (Frost 1948).

REFERENCES

Best, A. C., 1935. Transfer of Heat and Momentum in the Lowest Layers of the Atmosphere. *Geophys. Mem.* London, No. 65.

—, Knighting, E., Pedlow, R. H. and Stormonth, K., 1950. "Temperature and Humidity Gradients in the First 100 metres over South-East England." *Geophys. Mem.* London, No. 85.

Bowen, I. S., 1926. The Ratio of Heat Losses by Conduction and by Evaporation from any Water Surface. *Phys. Rev.* **27**, pp. 779—787.

Cowling, T. G. and White, A., 1941. The Eddy Diffusivity and Temperature of the Lower Layers of the Atmosphere. *Quart. J. R. Met. Soc.* London, **67**, No. 291, pp. 276—283.

Flower, W. D., 1936. An investigation into the variation of the lapse rate in the atmosphere near the ground at Ismailia, Egypt. *Geophys. Mem.* London, No. 71.

Frost, R., 1948. Atmospheric Turbulence. *Quart. J. R. Met. Soc.* London, **74**, 321, pp. 316—338.

Johnson, N. K., 1929. A Study of the Vertical Gradient of Temperature in the Atmosphere near the Ground. *Geophys. Mem.* London, No. 46.

— and Heywood, G. S. P., 1938. An investigation of the lapse rate of temperature in the lowest 100 metres of the atmosphere. *Geophys. Mem.* London, No. 77.

Knighting, E., 1950. On the equation of diffusion in the atmosphere. *Meteorological Research Paper No. 598, Air Ministry*, London.

— 1951. A Particular Solution of the Power Law Diffusion Equation. *Meteorological Research Paper, No. 609, Air Ministry*, London.

Knighting, E. and Best, A. C., 1950. The Treatment of Atmospheric Turbulence in M.R.P. 546. *Meteorological Research Paper, No. 582, Air Ministry*, London.

Köhler, H., 1932. Ein kurzes Studium des Austausches auf Grund des Potenzgesetzes. *Beitr. Phys. frei, Atm.* Bd 19, s. 91—104.

Lander, A. J. and Robinson, G. D., 1952. Some observations of the small scale fluctuations of wind and temperature near the ground. *Meteorological Research Paper, No. 740, Air Ministry*, London.

Pasquill, F., 1943. Evaporation from a Plane, Free-liquid Surface in a Turbulent Air Stream. *Proc. Roy. Soc.* (*A*), **182**, pp. 75—95.

— 1949. Eddy Diffusion of Water Vapour and Heat near the Ground. *Proc. Roy. Soc.* (*A*), **198**, pp. 116—140.

Richardson, L. F., 1919. Atmospheric Stirring measured by Precipitation. *Proc. Roy. Soc.* (*A*), **96**, p. 9.

Rider, N. E. and Robinson, G. D., 1951. A study of the transfer of heat and water vapour above a surface of short grass. *Quart. J. R. Met. Soc.* London, **77**, 333, pp. 375—401.

Schmidt, W., 1925. Der Massenaustausch in freier Luft und verwandte Erscheinungen. (Probl. Kosm. Phys., Bd. 7) Hamburg. Henri Grand.

Smithsonian Meteorological Tables, 1951, 6th Edition, Washington, pp. 442—443.

Sutton, O. G., 1949. Atmospheric Turbulence, London, Methuen.

— 1948. Convection in the Atmosphere near the Ground. *Quart. J. R. Met. Soc.* London, **74**, pp. 13—30.

Taylor, G. I., 1915. Eddy Motion in the Atmosphere. *Phil. Trans. Roy. Soc.* (*A*), **215**, p. 1.

A Remark on the Energy Transport from a Warm River Surface into Cold Air

By A. NYBERG and L. RAAB, Swedish Meteorological and Hydrological Institute

(Manuscript received September 10, 1953)

Abstract

Temperature measurements in very cold air above an open river surface indicate that in spite of very high temperature lapse rate (temperature of river, in the 2 cm, 10 cm, and 12 m levels are + 0.5, — 14.0, — 15.3, and — 18.0° C respectively), the eddy conductivity is of the same order of magnitude as in extremely stable conditions (e. g. above a snow surface during nocturnal cooling).

The vertical transfer of energy in the atmosphere is due to vertical variations in the mean kinetic energy (vertical velocity shear caused by friction or other effects) or due to vertical statical instability (thermal convection). The transport through a horizontal surface of unit area can be expressed as $-c_p A_z \frac{\partial \Theta}{\partial z}$ where c_p is the heat capacity of air at constant pressure, A_z the eddy conductivity and $\frac{\partial \Theta}{\partial z}$ the lapse rate of potential temperature. The eddy conductivity is a function of the lapse rate. In stable conditions the dynamical turbulence is damped whereas in unstable conditions there is a tendency for convection cells to form. In unstable conditions the thermal convection is generally supposed to be the dominating factor. When in an air layer the density increases with height auto-convection is expected to set in, i.e. the colder upper air should break through to the bottom of the layer and the warm air rise to the top of the layer. This condition is reached when the lapse rate amounts to 3.4°/100 m.

Some measurements, recently made at the river Indalsälven near Östersund in central Sweden, seem to indicate, that considerable thermal convection does not start as soon as the lapse rate 3.4° in 100 m is reached.

Fig. 1 shows the location of measurements and the estimated prevailing wind. The surface of the river is not frozen due to the

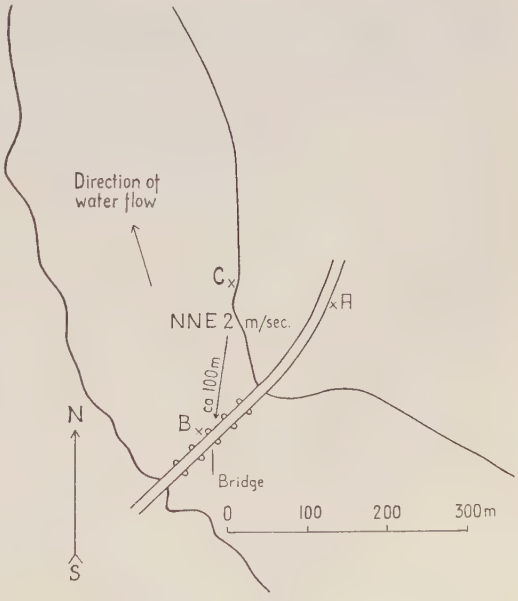

Fig. 1. Observational site.

regulation of the water flow system for the water power industry. The water from the lake Storsjön which is covered by a sheet of ice almost half a meter thick has a temperature of about +0.5° C when leaving the lake. The flow in the river is so rapid that no ice cover is formed until more than 2 km from the lake even at air temperatures of −20° C.

The measurements on 12 February 1953 were made at the point A on land 100 m on the windward side of the river and at the point B on the bridge over the river.

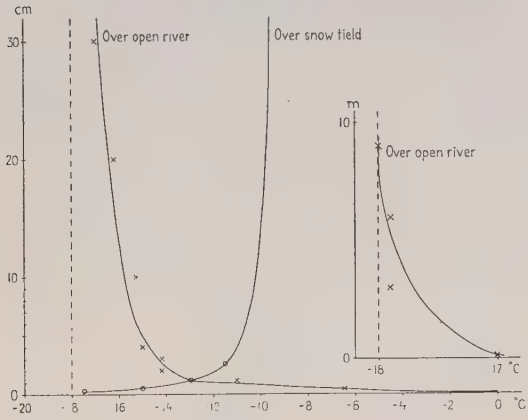

Fig. 2. Temperature height curves in the two cases refered to in the text.

Fig. 2 shows the observed temperature profile. (In fig. 2 is also shown the temperature curve obtained at an extremely stable situation, see NYBERG (1939). The values are given also in Table 1 which in addition shows some values obtained on 11 February at a point C over the river 2 m from the shore. See fig. 1. The instrument used here was a direct indicating resistance thermometer with three thermistors (Western Electric 14 A) coupled to a standard ohmmeter circuit. The thermistors were mounted equally spaced on a 6 m bamboostick. The measurements on the 6 m high bridge (point B in Fig. 1) were made by directing the bamboostick down to the water surface and touching the water surface with the top thermistor. The bamboostick was then successively raised and the temperature variation followed. The height above the water surface was measured with an estimated absolute accuracy of 5 mm. The accuracy of the height difference was about 2 mm.

From these measurements approximate values of the vertical eddy conductivity may be derived under certain assumptions.

Consider a horisontal surface of unit area in the level z. The vertical energy transport through the surface due to eddy motion is in unit time

$$-c_p \cdot A_z \frac{\partial \Theta}{\partial z}$$

Let this surface move with the horizontal wind u_z in the x-direction during the time t_1.

The total vertical eddy transport of energy through the area is then

$$-\int_0^{t_1} c_p A_z \frac{\partial \Theta}{\partial z}\, dt$$

Assuming at first that the horizontal wind u_z is independent of z this energy transport is equal to the increase in energy in a vertical air column above the surface from the level z to the top of the atmosphere. We did estimate the wind in the level 6 m being about 2 m/sec but no measurements took place. However, it is clear from similar cases that the wind must have increased with height roughly at a logaritmic rate. (The wind profile must be fairly complicated in the lowest centimeter layer as the speed of the water flow is as high as about half a meter per second.) The column in which the energy has been stored above the level z_1, is then not vertical but in a twodimensional picture forms an area between the curves $u_z t_1$ and $u_z t_1 + \frac{u_z}{u_{z_1}}$

The temperature increase from A ($t=0$) to B ($t=t_1$) in the level z is $\triangle T_z$. Then we have

$$-\int_0^{t_1} c_p A_z \frac{\partial \Theta}{\partial z}\, dt = \int_{z_1}^{\infty} c_p \varrho \triangle T_z \cdot \frac{u_z}{u_{z_1}}\, dz$$

The data available are not sufficient for a direct computation of A_z from this equation. We therefore make the following simplifications. At first we put ϱ equal to the constant value $1.2 \cdot 10^{-3}$ g/cm^3. We further assume that A_z is independent of time, that $\frac{\partial \Theta}{\partial z}$ is equal to zero at $t=0$ and that $\frac{\partial \Theta}{\partial z}$ has a measured value at $x=x_1$.

Table I

Height above water surface	Profile A	Profile B	Profile C	$\frac{\Delta T}{T_B - T_A}$	$\int_{z_1}^{\infty} \Delta T_z \cdot u_z \cdot dz$	$\frac{\partial \Theta}{\partial z}$	A_z
1,200 cm	— 17.9	— 18.0		(— 0.1)			
900	— 18.1	— 18.0		(0.1)			
600	— 17.8	— 17.9	— 16.5	0.05	20	0.02°/m	1.2
400				0.25	80	0.10°/m	1.0
300		— 17.6	— 16.6	0.4	150	0.18°/m	1.0
200					245	0.24°/m	1.2
50					415	1.04°/m	0.34
30		— 17.0		1.0	445	4.5°/m	0.18
20		— 16.3		1.7	470	8.5°/m	0.12
10		— 15.3		2.7	505	16 °/m	0.072
4		— 15.0		3.0	525	0.4°/cm	0.048
3		— 14.2	— 16.0	3.8	530	0.65°/cm	0.030
2.5		— 14.7		3.3	532	1.4°/cm	0.018
2		— 14.2		3.8	533	2.0°/cm	0.013
1.5		— 13.5		4.5	534	2.6°/cm	0.011
1		— 11.0		7.0	536	5.5°/cm	0.006
0.5		— 6.5	— 14.0	11.5	539	11.0°/cm	0.0035
0		± 0.0		18.0	541		

$x = x_1 \cong 100$ m at $z = 6$ m corresponds to $t = t_1$. We now assume that $\frac{\partial \Theta}{\partial z}$ and T at the time t_1 in each level has the value measured at $x = x_1$ in that level. We then get the following estimates of A_z at different levels. $t_1 = 50$ sec. See Table I. From the measurements at C we can see that $\frac{\partial \Theta}{\partial z}$ in the lowest levels rapidly approaches the values at $x = x_1$ but in higher levels this is not the case. The values of A_z in the lowest layers must be considered more reliable than the values in the uppermost levels.

According to Exner $A_z = \frac{C}{3.4 \cdot 10^{-4} + \frac{\partial \Theta}{\partial z}}$.

This is an empirical law valid in certain cases. However, if the absolute value of the lapse rate is greater than $3.4 \cdot 10^{-4}$ it is obviously not valid.

Sverdrup, see LETTAU (1938), gives the expression

$$A_z = \frac{A_z^i}{(1 + \beta Ri)}$$

where A_z^i is the eddy conductivity at indifferent stratification, β is a constant and Ri is the Richardson number

$$Ri = \frac{\frac{g}{\varrho} \cdot \frac{\partial \Theta}{\partial z}}{\left(\frac{\partial u}{\partial z}\right)^2}$$

Ri is negative over the warm water surface and the absolute value is so large that A_z gets unlimited. Thus even Sverdrup's formula does not hold.

Jeffreys, see BRUNT (1944), p. 244, has given another criterion on the greatest possible gradient. If the actual lapse rate is large compared with the dry adiabatic lapse rate, the condition is:

$$-\frac{\partial T}{\partial z} < \frac{27\pi^4 A^2 T}{4gh^4 \varrho^2}$$

Here g is the acceleration of gravity and h is the thickness of the layer.

The formula is valid in a homogeneous free layer with $\frac{\partial T}{\partial z}$ and A constant throughout the layer. The formula is thus not directly applicable when there is a great variation with height of the two quantities $\frac{\partial T}{\partial z}$ and A. However mean values of $\frac{\partial T}{\partial z}$ and A in the layer considered have been used here.

The formula is valid for a layer with free upper and lower boundaries. In our case the

lower boundary is the water surface and the constant $\frac{27\pi^4}{4}$ should be replaced by the constant 1,100.

Applying the formula for three different thicknesses of the bottom layer we obtain:

Table II

h cm	A_{mean} cgs	$\frac{\partial T}{\partial z}_{\text{mean}}$ °/cm	$\frac{1{,}100A^2T}{gh^4\varrho^2}$ °/cm
2	0.01	7	1,000
20	0.07	0.8	5
50	0.08	0.34	1.2

From Table II we see that the actual lapse rate never reaches the critical value at which convection starts, according to Jeffreys' formula. The discrepancy between the theoretical and actual gradients may be due the above described limitations of Jeffreys' formula.

Studies of cold air outbreaks over warm water by G. I. Taylor and others, see BRUNT, p. 228 (1944), have given values of A_z amounting to 50 – 100 cgs in the lowest 300 m deep layers whereas values of A_z amounting to 1 – 3 cgs have been obtained in a similar layer when warm air flows over cold water. That is to say A is about 50 times larger in slightly unstable conditions than in slightly stable conditions.

We have obtained about the same low values of A in extremely cold air over a very warm water as NYBERG (1939) found at extremely stable conditions. Nyberg found in his group 6 and 7, which had the same winds as in this case, $A_{10} = 29 \cdot 10^{-4}$ and $37 \cdot 10^{-4}$ cgs. Here A_{10} is equal to $60 \cdot 10^{-4}$ cgs. The value of the molecular heat transport coefficient corresponding to A is $\frac{\lambda}{c_p} = 2 \cdot 10^{-4}$ cgs and this value of A_z is reached at about the level 1 mm over the snow field and at a level less than half a mm over the water.

Our suggestion is that the air over the warm water is not in a very unstable state and that A_z is a function of time, or of x, that is to say that convection cells do not start on too small a scale. They have to have a considerable space dimension. An observation of a Swedish glider pilot Mr Söderholm indicates that a length of a warm bay of about half a km is needed to get warm bubbles that can be used by gliders.

REFERENCES

BRUNT, D., 1944. Phys. and Dyn. Meteorology. Cambridge.

LETTAU, H., 1939. Atmosphärische Turbulenz. Leipzig.

NYBERG, A., 1939. Temperature measurements in an air layer very close to a snow surface. *Medd. Stat. Met. Hydr. Anst.* Series of papers no. 27.

Letters to the Editor

Remarks on »Electron Microscope Study of Cloud and Fog Nuclei»

Dear Sir,

We have read with considerable interest the paper by S. Ogiwara and T. Okita on an »Electron Microscope Study of Cloud and Fog Nuclei» in the August 1952 issue of this Journal, and feel obliged to write this letter because of questions concerning certain observations and conclusions made by the authors.

A. Because the studies were made on only 75 fog droplets, we feel that any results are inconclusive because of the difficulties in obtaining a representative sample from so few droplets.

B. The conclusions on changes in form drawn from the electron microphotographs shown in the paper are questionable. The authors state that particles in Figures 1, 2, 3, 4, 6, and 7 did not change their from after electron bombardment and wetting, while 10, 11, 12, and 13 changed. Inspection of the pictures shows no appreciable change in any of the particles. The slight differences seen in comparing the microphotographs appear due to a change in the focus of the already poorly focussed electron microscope and perhaps slight aging of the collodian film. These apparent changes appear just as noticeable in the »unchanged» pictures.

C. Because of the growth of a droplet which had no visible nucleus in its center, and the fact that hygroscopicity changed when external particle shape did not; it is felt that the particles investigated were not the nuclei concerned with droplet formation and the true nuclei were too small to be observed with these optical-electron microscope techniques.

D. The investigation of a so-called sulfuric acid droplet in the electron microscope and the finding that it did not change after electron bombardment is improbable. Sulfuric acid, in spite of its low vapor pressure, will evaporate quite rapidly at the low pressures in the electron microscope. Even if it were possible to focus an electron beam on the droplet, the increased temperature due to bombardment with the electron beam would hasten its evaporation.

E. The statement that sea salt does not change after bombardment with the electron beam in the microscope is contrary to our finding, using the RCA electron microscope. When we observed sea salt crystals in our electron microscope the change from a contrasting opaque material to a transparent crystal was quite spectacular.

We feel that these discrepancies between our findings and those of the authors should be brought before the public so that other interested readers can help clarify some of these disputed points.

Cambridge, March 26th 1953

S. J. Birstein

Geophysics Research Directorate
Air Force Cambridge Research Centre
Air Research and Development Command

Reply

Dear Sir,

We thank Dr Birstein for his discussion of our study which was done when we were at Sendai. We studied the nature and origin of condensation nuclei and concluded that the greater part of cloud and fog nuclei are composed of both hygroscopic and non-hygroscopic substances which originate in combustion and that sea-spray was not a significant source of condensation nuclei. It was also shown that the greater part of the hygroscopic substances contained in the nuclei were not pure sulphuric acid.

Dr Birstein asked us some questions mainly on the techniques of electron microphotographing. We should like to make the following statements:

A. It is clear that in order to obtain any quantitative results, for instance regarding the size distribution of nuclei, the number of droplets which were observed by us was too small. We only studied the nature and origin of the nuclei in which case our samples may be of interest.

B. In fig. (13) filmy substances are observed as if they flew out from the upper part of the large, well-defined dark particle, though it is not so distinct in the reproduction owing to the contraction of the photograph.

However the change in fig. (11) appears due to the poorly focussed electron microscope as Dr Birstein states. In the other figures, namely (2), (4), and (6), such changes are not perceptible. Therefore the original statement should be revised as follows. "Most nuclei retained their original form after wetting, in some nuclei which retained their hygroscopic nature, however, the filmy substance changed its form."

C. Only one cloud sample was obtained in which no nuclei were found neither by the optical nor by the electron microscope. We do not know what kind of nucleus the droplet contained. It may be such a small volatile particle that it has evaporated perfectly by the electron bombardment.

From the theory and the current opinion on condensation, however, it is unreasonable to consider that most nuclei are too small to be detected in the electron microscope.

D. Before we made our observations we had the same opinion as Dr Birstein. However, observations yielded a different result. Through observation of a fuming sulphuric acid droplet by electron microscope we found that the droplet did not change when the intensity of bombardment was about the same as when microphotographing the nuclei. When the intensity became strong or when the time of bombardment was long enough, the droplet evaporated and left a honey-comb-formed image on the collodion film.

E. In the previous paper we only inferred the change of hygroscopicity but not the change of transparency of sea-salt.

We think that Dr Birstein's finding with regard to E is a very interesting and important contribution to our knowledge of nuclei in the atmosphere.

S. Ōgiwara

Institute of Low Temperature Science, Hokkaidō University, Sapporo, Japan

and

T. Ōkita

Geophysical Institute, Asahigawa Branch, Hokkaidō Educational University, Asahigawa, Japan

INDEX

Italics indicate titles of articles and shorter contributions. Asterisks indicate notes and correspondence.

Activities of Institute of Meteorology, University of Stockholm, note on, 420.
Aerosole, Rolle der, Junge, 1.
ALFVÉN, H.: *Identification of Sunspots*, 423.
ÁRNASON, G.: *A Baroclinic Model of the Atmosphere Applicable to the Problem of Numerical Forecasting in Three Dimensions.* II, 386.
Atmospheric water, O^{18} in, Dansgaard, 461.

*BERSON, F. A.: *Letter to the Editor*, 107.
BERGGREN, R.: *On Temperature Frequency Distribution in the Free Atmosphere and a Proposed Model for Frontal Analysis*, 95.
BEST, A. C.: *The Relative Humidity in Radiation Fog*, 32.
*BIRSTEIN, S. J.: *Remarks on Electron Microscope Study of Cloud and Fog Nuclei*, 533.
Blocking Situation, vertical motion and vorticity budget in, Eliassen and Hubert, 196.
BOLIN, B.: *Multiple-Parameter Models of the Atmosphere for Numerical Forecasting Purposes*, 207.
*BOLIN, B.: *Meteorological Conference in Helsingfors, Finland, May, 18—22 1953*, 315.
BOLIN, B.: *The Adjustment of a Non-balanced Velocity Field towards Geostrophic Equilibrium in a Stratified Fluid*, 373.
BOWEN, E. G.: *A new Method of Studying the Fine Structure of Air Movements in the Free Atmosphere*, 36.
BRUNBERG, E. Å.: *Experimental Determination of Electron Orbits in the Field of a Magnetic Dipole.* I, II. 135, 269.
BÅTH, M.: *Comparison of Microseisms in Greenland, Iceland and Scandinavia*, 109.

CARSON, J. E.: *Structure of Wind Field and Variations of Vorticity in a Summer Situation*, 321.
Charge generation in thunderstorms, Mason, 446.
*CHARNEY, J.: *Reply*, 108.
Chronology, ocean floor, Kullenberg, 302.
Circulation, general atmospheric, Wallén, 157.
CLAPP, PH. F.: *Application of Barotropic Tendency Equation to Medium-Range Forecasting*, 80.
Cloud, forms, Schaefer, 27.
Cloud, nuclei, letters to the editor, 533.
Clay, ocean floor, Kullenberg, 302.
Clear days at total eclipse, expectancy of, Lindholm, 101.
*Conference, meteorological, Bolin, 315.
Currents, equatorial ocean, Jerlov, 308.
Cyclone, formation of, Riehl and Teweles, 66; *Nyberg, 316; *Riehl, 317.
Cyclone, tropical, Syōno, 179.

DANSGAARD, W.: *The Abundance of O^{18} in Atmospheric Water and Water Vapour*, 461.
DATTNER, A.: *Experimental Determination of Electron Orbits in the Field of a Magnetic Dipole.* II, 269.
DEFAY, R.: *Sur la formation des germes de condensation et de solidification autour d'un noyau solide insoluble*, 293.
Deformation, fields of pressure, Petterssen 231; Vuorela, 413.
Deposition of clay, Kullenberg, 302.
Dipole, magnetic, Brunberg 135; Brunberg and Dattner, 269.
Dissolved matter in sea water, Jerlov, 59.
Disturbances, atmospheric, Lorenz, 238; Kuo, 475.
DUFOUR, L.: *Sur la formation des germes de condensation et de solidification autour d'un noyau solide insoluble*, 293.

Eclipse, total, Lindholm, 101.
Eddies, large-scale atmospheric, Starr, 494.
Electrification of snow, Norinder and Siksna, 260.
Electron orbits, Brunberg 135; 269.
ELIASSEN, A.: *Computation of Vertical Motion and Vorticity Budget in a Blocking Situation*, 196.

Energy, kinetic; Fjørtoft, 225.
Energy, transport from river surface, Nyberg and Raab, 529.
Equilibrium, geostrophic, Bolin, 373.

Field, pressure, Petterssen, 231; Vuorela, 413.
Field, velocity, Bolin, 373.
Field, wind, Newton and Carson, 321; Mohri, 340; Hollmann and Reuter, 408.
Field, magnetic, Brunberg, 135; 269.
Fine structure of air movements, Warner and Bowen, 36.
FJØRTOFT, R.: *On the Changes in the Spectral Distribution of Kinetic Energy for Twodimensional, Nondivergent Flow*, 225.
Flow, divergent, Fjørtoft, 225.
Flow, mean, Lorenz, 238.
Flow, stratified, Long, 42.
Fluid, stratified, Long, 42; Bolin, 373.
Fog, radiation, Best, 32,
Fog, nuclei, letters to the editor, 533.
*Forecasting, numerical, Bolin, 207; Hinkelmann, 251; Árnason, 386.
Forecasting, medium-range, Clapp, 80.
Frequency distribution of temperature, Berggren, 95.
FROST, R.: *A Power Law Representation of the Heat Transfer in the Lowest 100 metres of the Atmosphere*, 513.

General circulation, changes over Sweden, Wallén, 157.
Germes de condensation, Dufour and Defay, 293.
Geostrophic equilibrium, Bolin, 373.
Greenland microseisms, Båth, 109.

Heat transfer, Frost, 513.
HINKELMANN, K.: *Zur numerischen Wettervorhersage mittels Relaxationsmethode unter Einbeziehung barokliner Effekte I and II*, 251, 499.
HOLLMANN, G.: *Über die Genauigkeit verschiedener Approximationen der horizontalen Windkomponenten*, 408.
HUBERT, W. E.: *Computation of Vertical Motion and Vorticity Budget in a Blocking Situation*, 196.
HUBERT, W. E.: *A Case Study of Variations in Structure and Circulation about Westerly Jet Streams over Europe*, 359.
Humidity in fog, Best, 32.

Iceland, microseisms, Båth, 109.
*Institute of meteorology, University of Stockholm, note on activities, 421.

JERLOV, N. G.: *Influence of Suspended and Dissolved Matter on the Transparency of Sea Water*, 59.
JERLOV, N. G.: *The Tyndall Effect of Uniform Minerogenic Suspensions*, 306.
JERLOV, N. G.: *Studies of the Equatorial Currents in the Pacific*, 308.
Jet stream, Schaefer, 27; Hubert, 359.
JUNGE, CHR.: *Die Rolle der Aerosole und der gasförmigen Beimengungen der Luft in Spurenstoffhaushalt der Troposphäre*, 1.

Kinetic energy, Fjørtoft, 225.
KULLENBERG, B.: *Absolute Chronology of Deep-Sea Sediments and the Deposition of Clay on the Ocean Floor*, 302.
KULLENBERG, B.: *The Tyndall Effect of Uniform Minerogenic Suspensions*, 306.
KUO, H. L.: *On the Production of Mean Zonal Currents in the Atmosphere by Large Disturbances*, 475.

LINDHOLM, F.: *Expretancy of Clear Days in the Central Zone of Total Eclipse of the Sun June 30, 1954, in Sweden*, 101.
LONG, R. R.: *Some Aspects of the Flow of Stratified Fluids. I. A Theoretical Investigation*, 42.
LORENZ, E. N.: *The Interaction between a Mean Flow and Random Disturbances*, 238.

Magnetic dipole, Brunberg 135; 269.
MASON, B. J.: *A Critical Examination of Theories of Charge Generation in Thunderstorms*, 446.
Mean flow, Lorenz, 238; Kuo, 475.
Medium-range forecasting, Clapp, 80.
Microseisms, Båth, 109.
Minerogenic suspensions, Jerlov and Kullenberg, 306.
Model, frontal analysis, Berggren, 95.
Models, atmospheric, Bolin, 207; Smebye, 219; Árnason, 386.
MOHRI, K.: *On the Fields of Wind and Temperature over Japan and Adjacent Waters during Winter of 1950—1951*, 340.
MORDY, W.: *A Note on the Chemical Composition of Rainwater*, 470.

NEWTON, C. W.: *Structure of Wind Field and Variations of Vorticity in a Summer Situation*, 321.
Non-balanced velocity field, Bolin, 373.
Non-divergent flow, Fjørtoft, 225.
NORINDER, H.: *On the Electrification of Snow*, 260.
Numerical forecasting, Bolin, 207; Hinkelmann, 251 and 499; Árnason, 386.
NYBERG, A.: *A Remark on the Energy Transport from a Warm River Surface into Cold Air*, 529.

O^{18} in atmospheric water, Dansgaard, 461.
Ocean floor, Kullenberg, 302.
Ocean currents, equatorial, Jerlov, 308.
*Ogiwara, S.: *Remarks on Electron Microscope Study of Cloud and Fog Nuclei*, 534.

Parametric atmospheric model, Smebye, 219.
Petterssen, S.: *On the Relation between Vorticity, Deformation and Divergence and the Configuration of the Pressure Field*, 231.
Power law of heat transport, Frost.
Precipitation, composition, Dansgaard, 461; Mordy, 470.

Raab, L.: *A Remark on the Energy Transport from a Warm River Surface into Cold River*, 529.
Radiation fog, Best, 32.
Rain water, composition of, Dansgaard, 461; Mordy, 470.
Random disturbances, atmospheric, Lorenz, 238.
Relaxationsmethode, Hinkelmann, 251 and 499.
Reuter, H.: *Über die Genauigkeit verschiedener Approximationen der horizontalen Windkomponenten*, 408.
Riehl, H.: *A Further Study on the Relation between the Jet Stream and Cyclone Formation*, 66.

Schaefer, V. J.: *Cloud Forms of the Jet Stream*, 27.
Sea water, transparency of, Jerlov, 49 and 306.
Siksna, R.: *On the Electrification of Snow*, 260.
Smebye, S. J.: *Tendency Computations with a Continuous Parametric Atmospheric Model*, 219.
Snow, electrification of, Norinder and Siksna, 260.
Spurenstoffhaushalt, Junge, 1.
Stability problem, note on, Starr, 105.
Starr, V. P.: *Note on the Classic Stability Problem*, 105.
Starr, V.: *Note Concerning the Nature of the Large-scale Eddies in the Atmosphere*, 494.
Summer temperature, variability of, Wallén, 157.
Sunspots, Alfvén, 423.
Suspended matter in sea water, Jerlov, 59; Jerlov and Kullenberg, 306.
Syōno, S.: *On the Formation of Tropical Cyclones*, 179.

Tendencey equation, barotropic, Clapp, 80.
Teweles, S.: *A Further Study on the Relation between the Jet Stream and Cyclone Formation*, 66.
Thunderstorms, charge generation in, Mason, 446.
Tyndall effect, Jerlov and Kullenberg, 306.

*University of Stockholm, Institute of Meteorology, investigations conducted 1952—53, 421.
*University of Stockholm, Institute of Meteorology, activities, note on, 420.

Wallén, C. C.: *Variability of Summer Temperature in Sweden and its Connection with Changes in the General Circulation*, 157.
Water vapour, O^{18} in, Dansgaard.
Warner, J.: *A New Method of Studying the Fine Structure of Air Movements in the Free Atmosphere*, 36.
Vertical motion, Eliassen and Hubert, 196.
Wind field, Newton and Carson, 321; Mohri, 340; Hubert, 359; Bolin, 373; Hollmann and Reuter, 408.
Vorticity, Eliassen and Hubert, 196; Petterssen, 231; Newton and Carson, 321.
Vuorela, L. A.: *A Synoptic Study of Deformation Fields*, 413.